

University of Alberta

Hexokinase 1 attenuates type II death receptor-induced apoptosis.

by

Anja Schindler

A thesis submitted to the Faculty of Graduate Studies and Research
in partial fulfillment of the requirements for the degree of

Doctor of Philosophy

in

Immunology

Medical Microbiology and Immunology

©Anja Schindler

Fall 2013

Edmonton, Alberta

Permission is hereby granted to the University of Alberta Libraries to reproduce single copies of this thesis and to lend or sell such copies for private, scholarly or scientific research purposes only. Where the thesis is converted to, or otherwise made available in digital form, the University of Alberta will advise potential users of the thesis of these terms.

The author reserves all other publication and other rights in association with the copyright in the thesis and, except as herein before provided, neither the thesis nor any substantial portion thereof may be printed or otherwise reproduced in any material form whatsoever without the author's prior written permission.

*To my husband Guy-Armel and my son Menelik, who are a constant source of
joy and inspiration*

ABSTRACT

Deregulated TNF signaling with elevated or decreased levels of TNF-induced apoptosis causes numerous inflammatory and cancerous diseases. Thus, there is a clear need to identify cellular proteins that regulate cell fate in the presence of TNF. RNA interference technology provides an excellent tool to address that problem. It allows the rapid generation of transient protein depletion “mutants” in cell culture, whose behaviour in the context of TNF can be examined. I developed a quantitative high-throughput siRNA assay to identify modifiers of TNF-induced cell death in HeLa cells and screened a set of nine hundred eighty six proteins, which includes the entire set of human kinases and phosphatases and several of their binding partners or related proteins. Of all gene products tested, loss of hexokinase 1 (HK1) resulted in the greatest elevation in TNF-induced death. In secondary assays, I demonstrated that the presence of HK1 attenuates TNF-induced apoptosis. Specifically, HK1 attenuates the processing of key caspases and caspase substrates, and decrease of the mitochondrial membrane potential. The predominantly mitochondrial localization of HK1 prompted me to examine whether HK1 impacted TNF-induced apoptosis at the mitochondria. I found that HK1 constitutively stabilized the mitochondrial membrane potential at least in part through the inhibition of the pro-apoptotic Bcl-2 effector proteins Bax and Bak. In line with these findings, HK1 attenuated Bax translocation and oligomerization to and at the mitochondria in the absence and presence of an apoptotic stimulus. Finally, I found that attachment of hexokinases to the mitochondria is a prerequisite for mitochondrial integrity and essential for pro-survival functions of hexokinases in TNF-induced apoptosis.

These data are the first loss-of-function reports to examine the involvement of HK1 in the transduction of extrinsic apoptotic cues and identify HK1 as a potential target in deregulated TNF signaling.

ACKNOWLEDGEMENTS

Foremost, I want to thank my supervisor Dr. Edan Foley. Most of my skills as a scientist are the product of his mentorship. I am forever grateful for his tireless effort on that journey, his patience, and the trust that he had in me. I greatly appreciated the freedom he gave me in pursuing my own ideas and his input to realize them, his positive outlook, and infectious passion for science. I also want to express my gratitude for his support during my pregnancy with my son Menelik and the years as a mother of a young child.

I am grateful for the mentorship I experienced from my graduate committee members Drs. Michele Barry and Kevin Kane. I valued their insights into my project and their personal support over the years. I also want to thank Dr. Michele Barry for training me in various aspects of human tissue culture and for numerous reagents she generously provided.

I want to thank my external examiners Drs. Ing Swie Goping and Robert Screaton for their time and effort in the evaluation of my thesis. I am thankful for the advice and materials I kindly received from Dr. Ing Swie Goping to perform mitochondrial isolations.

My thanks also go to Dr. David Evans, who provided the siRNA libraries as the cornerstone of this project. Moreover, I greatly benefited from the excellent working environment in this department that is to a large extent the result of his engagement as the departmental chair. Thank you to the departmental support staff, especially Anne Giles and Tabitha Vasquez.

The time as a graduate student would not have been as joyful, were there not the marvellous crowd of colleagues and friends in the department with whom I have shared every aspect of the graduate student experience. I especially want to thank Silvia Guntermann, David Bond, Brendon Parsons, Tanja Lindahl, David Primrose, Derly Benitez, Chelsea Davidson, George Johnson, Brittany Fraser, and Kristina Petkau. I am also grateful for the experience, protocols, and materials that my colleagues in the entire department kindly shared in support of my work.

The work in this thesis would have been impossible without the human cell lines derived from individuals such as Henrietta Lacks.

Immeasurable thanks goes to my parents Rita and Hans-Albrecht, who fostered my curiosity and encouraged me to pursue a career path that aligns with my passion.

Finally, the strongest rocks along the road of my PhD were my husband Guy-Armel and my son Menelik. Without your loving support, I would not have been able to conduct the work presented in this thesis.

TABLE OF CONTENTS

CHAPTER 1. INTRODUCTION.....	1
1.1. Death receptor-induced apoptosis.....	2
1.1.1. Apoptosis.....	2
1.1.2. Apoptotic caspases.....	3
1.1.3. Death receptors.....	6
1.1.4. TNF receptor 1.....	8
1.1.4.1. The physiological role of TNF.....	8
1.1.4.2. TNF.....	9
1.1.4.3. The TNF receptor complex.....	9
1.1.4.4. TNF-induced NF- κ B signaling.....	12
1.1.4.5. TNF-induced MAPK signaling.....	13
1.1.4.6. TNF-induced apoptosis.....	15
1.1.5. Type I and type II death receptor-induced apoptosis.....	15
1.1.6. Type II mitochondrial apoptosis.....	20
1.1.6.1. The mitochondrial membranes.....	20
1.1.6.2. Bcl-2 proteins and the permeabilization of the mitochondrial outer membrane.....	22
1.1.6.3. Permeabilization of the mitochondrial inner membrane.....	24
1.2. Hexokinases.....	25
1.2.1. Hexokinase isozymes.....	25
1.2.2. Hexokinase function.....	29
1.2.2.1. Hexokinases and metabolism.....	29
1.2.2.2. Hexokinases and apoptosis.....	31
1.2.2.3. Hexokinases and cancer.....	35
1.3. RNA interference.....	36
1.4. Project objectives.....	39
CHAPTER 2. MATERIALS AND METHODS.....	41
2.1. Buffers and media.....	42
2.2. DNA cloning.....	46
2.2.1. Expression constructs.....	46
2.2.2. Preparation of bacterial culture plates with selective antibiotics.....	49
2.2.3. Preparation of fluid media for bacterial cultures.....	49
2.2.4. Generation of chemically competent bacteria.....	50
2.2.5. Set up of bacterial cultures on culture plates from a glycerol stock.....	50
2.2.6. Set up of bacterial mini cultures from bacterial colonies.....	50
2.2.7. Set up of bacterial midi cultures from mini cultures.....	50
2.2.8. Plasmid midi preparation.....	51
2.2.9. Measurement of DNA concentration and purity.....	52
2.2.10. Polymerase chain reaction (PCR) with Pfx polymerase.....	52
2.2.11. Agarose gel electrophoresis.....	52
2.2.12. Polymerase chain reaction (PCR) purification.....	53
2.2.13. Preparative restriction digest.....	53

2.2.14. Preparative agarose gel electrophoresis.....	54
2.2.15. DNA isolation from excised gel fragments.....	54
2.2.16. Ligation.....	55
2.2.17. Transformation of bacteria.....	55
2.2.18. Analytical polymerase chain reaction (PCR) from bacterial colonies.....	56
2.2.19. Plasmid mini preparations.....	56
2.2.20. Analytical restriction digest.....	57
2.2.21. Preparation of DNA samples for sequencing.....	57
2.2.22. Site directed mutagenesis of plasmid constructs.....	58
2.2.23. Preparation of glycerol stocks.....	59
2.3. Cell lines and cell culture.....	59
2.3.1. Cell lines.....	59
2.3.2. Passaging.....	60
2.3.3. Determination of the concentration of viable cells in a cell suspension.....	60
2.4. Cell treatments.....	61
2.5. siRNA and siRNA screening.....	61
2.5.1. siRNA transfections.....	61
2.5.2. GAPDH assay for the optimization of siRNA transfection efficiency.....	64
2.5.3. High-throughput siRNA screen for modifiers of TNF-induced death.....	65
2.5.4. Screen analysis.....	66
2.5.4.1. Plate normalization and data scoring.....	66
2.5.4.2. Visualization of 96-well plates.....	67
2.5.4.3. Kernel density estimates for behaviour of positive controls.....	67
2.5.4.4. Heat maps of viability values and death indices in the screen.....	67
2.6. DNA transfection.....	67
2.7. Microscopy.....	68
2.7.1. Light Microscopy.....	68
2.7.2. Confocal Immunofluorescence Microscopy.....	69
2.7.3. High-content fluorescence microscopy.....	70
2.8. Quantitative real-time PCR (qRT-PCR).....	71
2.8.1. RNA purification.....	71
2.8.2. Measurement of RNA concentration and purity.....	72
2.8.3. Synthesis of cDNA.....	72
2.8.4. qRT-PCR with the SYBR green method.....	73
2.8.5. qRT-PCR with the Taqman method.....	74
2.9. SDS-PAGE and Western blotting.....	75
2.9.1. Sample preparation.....	75
2.9.2. SDS-PAGE.....	76
2.9.3. Transfer.....	77
2.9.4. Western blotting.....	78
2.10. Cellular fractionation.....	80
2.11. 96-well Bradford assay.....	82
2.12. NF-κB reporter assay.....	83
2.13. Assays for the detection of cell viability and death.....	84
2.13.1. Resazurin viability assay.....	84

2.13.2. DNA staining with SYTO 60.....	84
2.13.3. Immunoprecipitation of complex II.....	84
2.13.4. Bax translocalization to the mitochondria and mitochondrial cytochrome c release.....	85
2.13.5. Bax oligomerization at the mitochondria.....	86
2.13.6. TMRE assay for the detection of the IMM potential.....	87
2.13.7. DEVDase assay for detection of caspase activity.....	88
2.13.8. Caspase and caspase substrate processing.....	89
CHAPTER 3. DEVELOPMENT OF A HIGH-THROUGHPUT siRNA ASSAY FOR MODIFIERS OF TNF-INDUCED DEATH.....	90
3.1. HeLa cells are a suitable system to examine TNF-induced death.....	91
3.2. HeLa cells are accessible to siRNA-mediated modification of TNF signals.....	96
3.3. A high-throughput siRNA assay for modifiers of TNF-induced death.....	103
CHAPTER 4. AN siRNA SCREEN FOR MODIFIERS OF TNF-INDUCED DEATH.....	113
4.1. An siRNA screen for modifiers of TNF-induced death.....	114
4.2. Analysis of the screen data.....	114
4.3. Quality of the screen data.....	115
4.4. Identification of high confidence modifiers of TNF-induced apoptosis and general cell viability.....	121
4.5. Evaluation of screen results for established TNF pathway components.....	127
4.6. HK1 is a negative regulator of TNF-induced death.....	130
CHAPTER 5. CHARACTERIZATION OF HK1 AS AN ANTI-APOPTOTIC PROTEIN.....	132
5.1. Background.....	133
5.2. Confirmation of HK1 as a negative regulator of TNF-induced death.....	134
5.3. Effects of HK1 depletion on the TNF signaling modules.....	137
5.3.1. HK1 depletion does not attenuate TNF-induced NF- κ B signaling.....	137
5.3.2. HK1 depletion accelerates TNF-induced apoptosis.....	139
5.4. HK1 localizes to the mitochondria.....	152
5.5. HK1 siRNA depletes mitochondrial HK1.....	154
5.6. HK1 siRNA decreases the IMM potential.....	154
5.7. Mitochondrial detachment of HKs decreases the IMM potential and mitochondrial integrity.....	157
5.8. Mitochondrial detachment of HKs accelerates TNF-induced apoptosis.....	159
5.9. Bcl-2 proteins modify the decrease of the IMM potential after HK1 depletion.....	161

5.9.1. Bcl-2 overexpression stabilizes the IMM potential after HK1 depletion.....	161
5.9.2. HK1 depletion decreases the IMM potential in a manner that requires Bak and Bax.....	162
5.9.3. HK1 depletion initiates and accelerates Bax activation.....	165
CHAPTER 6. DISCUSSION.....	168
6.1. A high-throughput siRNA assay for modifiers of TNF-induced death.....	169
6.2. An siRNA screen for modifiers of TNF-induced death.....	171
6.2.1. Analysis of the screen data.....	171
6.2.1.1. Data normalization.....	171
6.2.1.2. Data scoring.....	174
6.2.2. Quality of the screen.....	179
6.2. Characterization of HK1 as an anti-apoptotic protein.....	181
6.2.1. HK1 has an anti-apoptotic role in TNF signaling.....	182
6.2.2. HK1 is a general anti-apoptotic protein.....	183
6.2.3. HK1 attenuates TNF-induced apoptosis at the mitochondria....	184
6.2.4. Attachment of HK1 to the mitochondria attenuates TNF-induced apoptosis.....	185
6.2.5. A catalytically inactive HK1 attenuates TNF-induced death.....	186
6.2.6. Metabolic and anti-apoptotic functions of HK1 are distinct.....	186
6.2.7. HK1 stabilizes mitochondrial integrity and the IMM potential....	187
6.2.8. HK1 stabilizes the IMM potential against Bcl-2 effector proteins.....	188
6.2.9. Model.....	189
6.2.10. Future perspectives.....	189
6.3. Significance.....	191
CHAPTER 7. BIBLIOGRAPHY.....	192
APPENDIX 1. SEQUENCE ALIGNMENT OF HUMAN HKs.....	231
APPENDIX 2: SEQUENCE OF HK1 EXPRESSION CONSTRUCT.....	234
APPENDIX 3. HEAT MAP REPRESENTATION OF KINASE AND PHOSPHATASE PLATES IN THE siRNA SCREEN.....	237
APPENDIX 4. DATA TABLE OF THE VIABILITY VALUES AND DEATH INDICES FOR EACH siRNA IN THE SCREEN.....	246
APPENDIX 5. SUPPLEMENTARY DATA.....	273

LIST OF TABLES

Table 2.1.	List of primer sequences.....	48
Table 2.2.	List of siRNAs.....	63
Table 2.3.	List of primer sequences for qRT-PCR experiments.....	74
Table 2.4.	Components of resolving and stacking gels for SDS-PAGE..	77
Table 2.5.	List of primary antibodies used in Western blots.....	79
Table 2.6.	List of secondary antibodies used in Western blots.....	80
Table A4.1.	Viability values and death indices of each siRNA in the screen.....	247

LIST OF FIGURES

CHAPTER 1. INTRODUCTION.

Figure 1.1.	Domain structure of apoptotic caspases.....	4
Figure 1.2.	Mechanism of caspase activation.....	5
Figure 1.3.	Death receptor signaling.....	7
Figure 1.4.	The TNF receptor complex and NF- κ B activation.....	10
Figure 1.5.	TNF-induced MAPK signaling.....	14
Figure 1.6.	TNF-induced apoptosis.....	16
Figure 1.7.	Type I and type II apoptosis.....	17
Figure 1.8.	Release of pro-apoptotic factors from the mitochondria during apoptosis.....	19
Figure 1.9.	Mitochondrial structure and biochemical processes at the mitochondrial membranes.....	21
Figure 1.10.	Bcl-2 family proteins and their interactions.....	23
Figure 1.11.	Evolution of human hexokinases.....	26
Figure 1.12.	The metabolic function of hexokinases.....	30
Figure 1.13.	Mitochondrial HKs and their anti-apoptotic role in growth factor signaling.....	33
Figure 1.14.	The RNAi pathway and its technological application in vertebrate cells.....	37

CHAPTER 3. DEVELOPMENT OF A HIGH-THROUGHPUT siRNA ASSAY FOR MODIFIERS OF TNF-INDUCED DEATH.

Figure 3.1.	TNF activates NF- κ B and JNK modules in HeLa cells.....	92
Figure 3.2.	TNF combined with CHX induces apoptosis in HeLa cells.....	95
Figure 3.3.	siRNA-mediated depletion of caspase-8 blocks apoptosis in HeLa cells treated with TNF and CHX.....	98
Figure 3.4.	NEMO siRNA alters TNF-induced NF- κ B signaling.....	101

Figure 3.5.	Optimization of siRNA delivery for the high-throughput siRNA assay.....	105
Figure 3.6.	Optimization of the high-throughput viability assay.....	106
Figure 3.7.	A high-throughput siRNA assay for modifiers of TNF-induced cell death.....	108
Figure 3.8.	Depletion of caspase-8 or NEMO in the high-throughput siRNA assay modifies the rate of TNF-induced death.....	110
Figure 3.9.	The high-throughput siRNA assay identifies TNF signaling components as modifiers of TNF-induced death	111
CHAPTER 4.	AN siRNA SCREEN FOR MODIFIERS OF TNF-INDUCED DEATH.	
Figure 4.1.	Plate layout and flow chart of the assay employed in the siRNA screen for modifiers of TNF-induced death.....	115
Figure 4.2.	Normalization of screened plates.....	116
Figure 4.3.	Level of identity between replicate plates in the screen....	118
Figure 4.4.	Behaviour of positive plate controls over all screened plates.....	120
Figure 4.5.	Heat map representation of all viability values and death indices in the screen.....	122
Figure 4.6.	Distribution of the median viability values and death indices.....	123
Figure 4.7.	95% confidence pro-survival and pro-death proteins in the absence of TNF.....	124
Figure 4.8.	95% confidence pro-survival proteins in TNF-induced death.....	125
Figure 4.9.	95% confidence pro-death proteins in TNF-induced death	126
Figure 4.10.	Confirmation of NEMO as a modifier of TNF-induced death in the screen.....	128
Figure 4.11.	Heat map of the death indices of known TNF pathway components in the screen.....	129
Figure 4.12.	The siRNA screen revealed HK1 as a negative regulator of TNF-induced death.....	131

CHAPTER 5.	CHARACTERIZATION OF HK1 AS AN ANTI-APOPTOTIC PROTEIN.	
Figure 5.1.	HK1 regulates TNF-induced death.....	135
Figure 5.2.	Confirmation of siRNA-mediated HK1 depletion.....	136
Figure 5.3.	HK1 depletion does not attenuate NF- κ B signaling.....	138
Figure 5.4.	HK1 modifies TNF-signaling through the apoptotic cascade.....	140
Figure 5.5.	HK1 depletion accelerates TNF-induced caspase and caspase substrate processing.....	142
Figure 5.6.	HK1 depletion accelerates the TNF-induced decrease of the IMM potential.....	145
Figure 5.7.	HK1 depletion accelerates the formation of complex II.....	147
Figure 5.8.	HK1 depletion accelerates death receptor-induced cell death.....	150
Figure 5.9.	HK1 is predominately mitochondrial.....	153
Figure 5.10.	HK1 siRNA depletes mitochondrial HK1.....	155
Figure 5.11.	HK1 siRNA decreases the IMM potential.....	156
Figure 5.12.	Mitochondrial detachment of HKs decreases the IMM potential and disrupts mitochondrial integrity.....	158
Figure 5.13.	Mitochondrial detachment of HKs accelerates TNF-induced apoptosis.....	160
Figure 5.14.	Bcl-2 overexpression stabilizes the IMM potential after HK1 depletion.....	163
Figure 5.15.	The absence of Bak and Bax stabilizes the IMM potential after HK1 depletion.....	164
Figure 5.16.	HK1 depletion initiates and accelerates Bax activation.....	166
CHAPTER 6.	DISCUSSION.	
Figure 6.1.	Model of HK1 anti-apoptotic activity at the mitochondrion.	190

APPENDIX 1.	SEQUENCE ALIGNMENT OF HUMAN HKs.	
Figure A1.1.	Sequence alignment of human HKs.....	232
APPENDIX 2.	DNA SEQUENCE OF THE HK1 EXPRESSION CONSTRUCT.....	
Figure A2.1.	DNA sequence of the HK1 expression construct	235
APPENDIX 3.	HEAT MAP REPRESENTATION OF KINASE AND PHOSPHATASE PLATES IN THE siRNA SCREEN.	
Figure A3.1.	Heat map representation of all normalized phosphatase plates.....	238
Figure A3.2.	Heat map representation of all normalized kinase plates..	241
APPENDIX 5.	SUPPLEMENTARY DATA.	
Figure A5.1.	HK2 attenuates the TNF-induced decrease of the IMM potential.....	274
Figure A5.2.	Alternative attempts to induce or generate cytosolic HK1..	275

LIST OF ABBREVIATIONS AND SYMBOLS

A – Ampere

A₂₆₀ - absorption at a defined wavelength, here 260 nm

Ac-DEVD-AMC - N-acetyl-aspartyl-glutamyl-valyl-aspartyl-7-amido-4-methyl-coumarin

ADP – adenosine diphosphate

AIF – apoptosis-inducing factor

AIP – apoptosis-linked gene 2 interacting protein

Alg2 - apoptosis-linked gene 2

ANT - adenine nucleotide transporter

AP-1 - activator protein 1

Apaf-1 - apoptotic peptidase activating factor 1

APS – ammonium persulfate

ASK1 - apoptosis signal-regulating kinase 1

ASK2 - apoptosis signal-regulating kinase 2

ATF - activating transcription factor

ATP – adenosine triphosphate

Bak - Bcl-2 antagonist killer

Bax - Bcl-2 associated X protein

Bcl-2 - B-cell lymphoma-2

Bcl-x_L - Bcl-2 related gene, long isoform (extra long)

BH - Bcl-2 homology

Bid - BH3-interacting domain death agonist

BMH - bismaleimidohexane

Bok - Bcl-2 related ovarian killer

BSA – bovine serum albumin

CaCl₂ – calcium chloride

CARD - caspase recruitment domain

caspase - cysteine-dependent aspartate-directed protease

CD95 – cluster of differentiation 95, Fas

cDNA – complementary deoxyribonucleic acid

c-FLIP_L - cellular FLICE-like inhibitory protein, long

CHAPS – cholamidopropyldimethyl ammoniopropanesulfonate
CHX - cycloheximide
CI - confidence interval
c-IAP1 - cellular inhibitor of apoptosis 1
c-IAP2 – cellular inhibitor of apoptosis 2
CK – creatine kinase
CO₂ – carbon dioxide
ct – threshold cycle
CTZ - clotrimazole
CypD – cyclophilin D
D - Dalton
dATP – deoxyadenosine triphosphate
DD - death domain
DED - death effector domain
DH5α - *Escherichia coli* strain
DIABLO - direct inhibitor of apoptosis binding protein with low pI
DISC - death-inducing signaling complex
DKO - double knock-out
DMSO - dimethyl sulfoxide
DNA – deoxyribonucleic acid
DNase - deoxyribonuclease
dNTP – deoxyribonucleotide triphosphate
DR - death receptor
DR4 – death receptor 4, TRAIL-R1
DR5 – death receptor 5, TRAIL-R2
dsRNA - double-stranded ribonucleic acid
DTT - dithiothreitol
DUSP – dual specificity protein phosphatase
E2 - ubiquitin-conjugating enzyme
E3 - ubiquitin-ligating enzyme
EGTA – ethylene glycol tetraacetic acid
ERK - extracellular signal-regulated kinase, family of MAPKs
ERK1 – extracellular signal-regulated kinase 1, MAPK3
ESCRT - endosomal sorting complex required for transport

FAD - flavin adenine dinucleotide
FADD - Fas-associated death domain protein
FBS - fetal bovine serum
FDG - 2-^[18F]fluoro-2-deoxy-glucose
FMN - flavin mononucleotide
g – gram
g – gravitational constant
GAPDH - glyceraldehyde 3-phosphate dehydrogenase
GFP - green fluorescent protein
GKRP - glucokinase regulatory protein
Glut1 - glucose transporter 1
GSK3 β - glycogen synthase kinase 3 β
h – hour
H₂O - water
HEPES – hydroxyethyl piperazineethanesulfonic acid
HK – hexokinase
HK1 – hexokinase 1
HK2 – hexokinase 2
HK3 – hexokinase 3
HK4 – hexokinase 4, glucokinase
HtrA2 - high temperature requirement protein A2
IAP - inhibitor of apoptosis protein
ICS - intracristae space (ICS)
IgG – immunoglobulin G
IKK - inhibitor of nuclear factor kappa-B kinase
IKK- α – inhibitor of nuclear factor kappa-B kinase alpha
IKK- β – inhibitor of nuclear factor kappa-B kinase beta
IL – interleukin
IL1 – interleukin 1
IL-6 – interleukin 6
IMM - inner mitochondrial membrane
IMS - intermembrane space
I- κ B- α - inhibitor of nuclear factor kappa-B alpha
I- κ B- ϵ - inhibitor of nuclear factor kappa-B epsilon

JNK – c-Jun N-terminal kinase
JNK1 – c-Jun N-terminal kinase 1, MAPK8
JNK2 – c-Jun N-terminal kinase 2, MAPK9
k – kilo-
K48 – lysine 48 linkage between ubiquitin molecules
K63 – lysine 63 linkage between ubiquitin molecules
KCl – potassium chloride
KH₂PO₄ – potassium dihydrogen phosphate
l - liter
LB - Luria Bertani bacterial growth medium
lg - base two logarithm
LT - lymphotoxin or tumor necrosis factor beta
LUBAC – linear ubiquitin assembly complex
m - meter
m – milli-
M - molar
MAP2K - mitogen-activated protein kinase kinase
MAP2K4 – mitogen-activated protein kinase kinase 4, MKK4
MAP2K7 – mitogen-activated protein kinase kinase 7, MKK7
MAP3K - mitogen-activated protein kinase kinase kinase
MAP3K13 – mitogen-activated protein kinase 13
MAP4K – mitogen-activated protein kinase kinase kinase kinase
MAP4K1 – mitogen-activated protein kinase kinase kinase kinase 1, HPK1
MAPK - mitogen-activated protein kinase
MAPK11 – mitogen-activated protein kinase 11, p38β
MAPK12 – mitogen-activated protein kinase 12, p38γ
MAPK13 – mitogen-activated protein kinase 13, p38δ
MAPK8 – mitogen-activated protein kinase 8, JNK1
MAPK9 – mitogen-activated protein kinase 9, JNK2
MEF - mouse embryonic fibroblast
MEKK1 - MAPK/ERK kinase kinase 1, MAP3K1
MEKK2 - MAPK/ERK kinase kinase 2, MAP3K2
MEKK3 - MAPK/ERK kinase kinase 3, MAP3K3
MgCl₂ – magnesium chloride

min - minute

miRISC – micro RNA-induced silencing complex

miRNA - micro RNA

MKK3 - mitogen activated protein kinase kinase 3, MAP2K3

MKK4 – mitogen activated protein kinase kinase 4, MAP2K4

MKK6 - mitogen activated protein kinase kinase 6, MAP2K6

MKK7 – mitogen activated protein kinase kinase 7, MAP2K7

MLK – mixed lineage kinase, family of MAP3Ks

MOMP – mitochondrial outer membrane permeabilization

MOPS – morpholinopropane sulfonic acid

MPTP - mitochondrial permeability transition pore

mRNA – messenger RNA

n – nano-

Na₂HPO₄ - disodium hydrogen phosphate

Na₃VO₄ – sodium orthovanadate

NaCl – sodium chloride

NAD+ - nicotinamide adenine dinucleotide

NADPH - nicotinamide adenine dinucleotide phosphate

NaOH – sodium hydroxide

NCBI RefSeq number - National Center for Biotechnology Information reference sequence accession number

NDUFS1 - 75 kD complex I subunit NADH-ubiquinone oxidoreductase

NEMO - NF-κB essential modifier (NEMO)

NF-κB - nuclear factor of kappa light polypeptide gene enhancer in B-cells

OMM – outer mitochondrial membrane

ORF – open reading frame

OTE - off-target effect

p – mathematical probability

p – protein fragment

p10 - small caspase subunit of around 10 kD

p17 – cleavage product of caspase-3, large subunit

p18 – cleavage product of caspase-8, large subunit

p19 – cleavage product of caspase-3, large subunit

p20 – large caspase subunit of around 20 kD

p35 – cleavage product of caspase-9, prodomain and large subunit
p37 – cleavage product of caspase-9, prodomain and large subunit
p38 – family of MAPKs
p43/p41 – cleavage product of caspase-8, prodomain and large subunit
PARP - poly [ADP-ribose] polymerase
PARP1 - poly [ADP-ribose] polymerase 1
PBR - peripheral benzodiazepine receptor
PBS – phosphate-buffered saline
PBT - phosphate buffered saline with Triton X-100
PCR – polymerase chain reaction
PET - positron emission tomography
pH – potential of hydrogen ions
Pi - inorganic phosphate
PI3K - phosphatidylinoside 3-kinase
P-I- κ B- α - phosphorylated inhibitor of nuclear factor kappa-B alpha
P-JNK - phosphorylated c-Jun N-terminal kinase
PKB - protein kinase B, Akt
PLAD - pre-ligand assembly domain
PMSF - phenylmethylsulfonyl fluoride
pre-miRNA – precursor micro RNA
pri-miRNA – prietary micro RNA
qRT-PCR - quantitative real-time polymerase chain reaction
 R^2 - coefficient of determination
RHD – Rel homology domain
RIPK1 - receptor-interacting serine/threonine-protein kinase 1
RISC - RNA-induced silencing complex
RNA – ribonucleic acid
RNAi - RNA interference
RNase - ribonuclease
ROS - reactive oxygen species
rpm - revolutions per minute
RuCl₂ – rubidium chloride
s - second
S.E.M. - standard error from the mean

SDS – sodiumdodecyl sulphate
SDS-PAGE - sodium dodecyl sulphate-polyacrylamide gel electrophoresis
shRNA - short hairpin RNA
siRISC – short interfering RNA-induced silencing complex
siRNA - short interfering RNA
Smac - second mitochondria-derived activator of caspase
SODD - silencer of death domains
su - subunit
TAB2 – transforming growth factor beta-activated kinase 1-binding protein 2
TAB3 – transforming growth factor beta-activated kinase 1-binding protein 3
TACE - TNF-α converting enzyme
TAE – Tris base, acetic acid, EDTA
TAK1 - transforming growth factor beta-activated kinase 1
Taq – *T*hermus *a*quaticus
tBid - truncated Bid
TE – Tris base, EDTA
TEMED - tetramethylethylenediamine
TMRE - tetramethylrhodamine ethyl ester
TNF - tumor necrosis factor
TNF-R1 - tumor necrosis factor receptor 1
TNF-R2 - tumor necrosis factor receptor 2
TNFRSF - tumor necrosis factor receptor super family
TNF-α - tumor necrosis factor α
TNF-β - tumor necrosis factor β, lymphotoxin
TPL-2 - tumor progression locus 2
TRADD - tumor necrosis factor receptor type 1-associated death domain protein
TRAF – tumor necrosis factor receptor-associated factor
TRAF2 – tumor necrosis factor receptor-associated factor 2
TRAF5 – tumor necrosis factor receptor-associated factor 5
TRAIL-R1 - tumor necrosis factor-related apoptosis-inducing ligand receptor 1
TRAIL-R2 - tumor necrosis factor-related apoptosis-inducing ligand receptor 2
TRID - tumor necrosis factor receptor 1 internalization domain
UTR - untranslated region
V – volts

v – volume

v/v – volume per volume

VDAC - voltage-dependent anion channel

VDAC1 – voltage-dependent anion channel 1

VDAC2 – voltage-dependent anion channel 2

VDAC3 – voltage-dependent anion channel 3

w – weight

w/v – weight per volume

XIAP - X-linked inhibitor of apoptosis protein

z-score – standard score

z-VAD-fmk - carbobenzoxy-valyl-alanyl-aspartyl-[O-methyl]- fluoromethyl-
ketone

- number

[substance] - concentration of substance

°C - degree Celsius

μ - micro-

$\Delta\Psi_M$ – mitochondrial membrane potential

CHAPTER 1. INTRODUCTION.

1.1. Death receptor-induced apoptosis.

1.1.1. Apoptosis.

Apoptosis is a form of programmed cell death that allows the removal of cells without the release of cell content into the surrounding tissue [1-4]. One of the defining features of apoptosis is the maintenance of plasma membrane integrity while the cell retracts pseudopods, rounds up, reduces its volume (pyknosis) and blebs and sheds vesicles containing cytoplasm and cell organelles (apoptotic bodies) [1]. Apoptosis is accompanied by major structural changes to the nucleus and the mitochondria. Nuclear chromatin visibly condenses, and the nucleus disintegrates into fragments (karyorrhexis) [1, 5]. Fragmentation is also typical for mitochondria [5]. In addition, mitochondria lose the integrity of their membranes and increase in volume [5].

Morphological changes are initiated by the activity of intracellular nucleases and proteases. The primary biochemical markers for apoptosis are therefore oligonucleosomal DNA fragmentation [6], the presence of active cysteine-dependent aspartate-directed proteases (caspases) [7, 8] and cleavage products of their substrates [9]. The cues for the activation of intracellular nucleases and proteases may originate from the interior or the exterior of the cell. External cues initiate the extrinsic apoptotic pathway, whereas internal cues lead to intrinsic apoptosis [10]. Cytotoxic stresses and DNA damage are examples of intrinsic cues, whereas immune responses to an intracellular infection or tumorigenic quality are classical examples of extrinsic cues [10].

In vivo, apoptotic cells and apoptotic bodies are engulfed by neighboring cells or resident professional phagocytes [1]. As a result, apoptosis is a mostly non-immunogenic form of cell death that is essential for tissue homeostasis [1], morphological changes during development [1, 11], and for the selection of the immune repertoire and the removal of infected cells [12, 13]. Deregulation of apoptosis has very serious consequences for the organism, such as cancer [14, 15], neurodegenerative disorders [14, 16, 17], tissue damage during inflammation [18-20], and auto-immune diseases or immune deficiencies [14, 21].

1.1.2. Apoptotic caspases.

Caspases are the primary molecular initiator of apoptotic processes in the cell. Caspases employ a cysteine residue as their catalytic nucleophile and cleave their substrates after an aspartic acid residue [22, 23]. There are eleven human caspases [8]. Seven of those caspases, caspase-2, 3, and 6, 7, 8, 9, and 10, are classified as apoptotic caspases [8] (**figure 1.1.**).

Caspases are synthesized as inactive proenzymes [8]. Procaspases consist of an amino-terminal prodomain, followed by a large subunit of about 20 kD (p20) and a small subunit of about 10 kD (p10) [8]. Caspases transition to an active conformation through homo-dimerization and/or proteolytic cleavage at specific aspartates between the 3 subunits [24-27].

Apoptotic caspases activate each other in cascades that start with the initiator caspases caspase-2, -8, -9, or -10 [8] (**figure 1.2.**). Initiator caspases are characterized by long prodomains, which contain one of two homotypic interaction motifs: death effector domains (DEDs) [28] in the case of caspase-8 and 10, or caspase recruitment domains (CARDs) [28, 29] in the case of caspase-2 and 9 [8]. Apoptotic cues initiate formation of multimeric caspase activation complexes. DED and CARD domains are the basis for the recruitment of caspases to these complexes [8]. Dimerization of monomeric initiator caspases at the activation complexes fully activates initiator caspases [25, 27, 30, 31]. Subsequent auto-proteolytic processing of the caspase dimer stabilizes the active enzyme [25, 27, 30, 31].

Active initiator caspases target and activate effector caspases such as caspase-3, 6, and 7 [8]. Effector caspases have short prodomains and exist as dimers in the inactive state [8, 25-27]. However, the linker between the large and small subunit sterically blocks the active site [24, 26]. Therefore, effector caspase activation requires processing of the interdomain linker by initiator or other effector caspases [24, 26, 27]. Following cleavage at specific aspartates, the two large and small subunits of the caspase dimer reorganize to form a proteolytically active heterotetramer [24, 26, 27]. Active effector caspases process other effector caspases and induce apoptosis by proteolytic cleavage of several hundred intracellular proteins [9, 32].

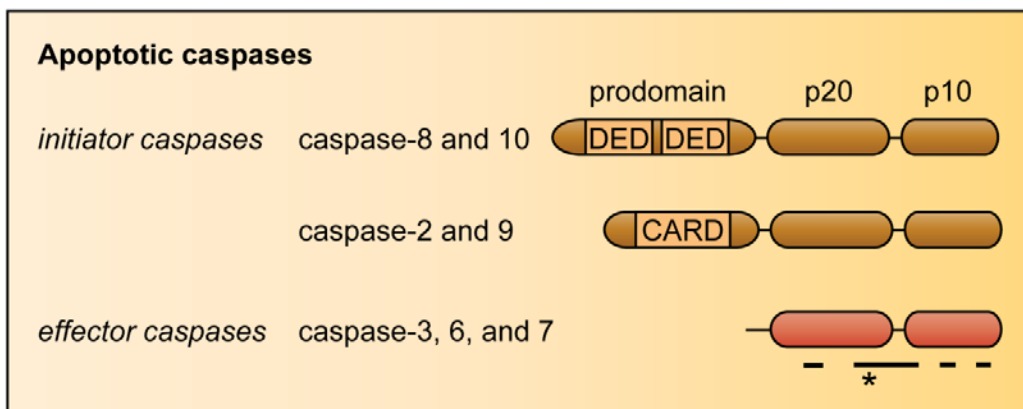


Figure 1.1. Domain structure of apoptotic caspases. All caspases consist of a large subunit p20 and a small subunit p10. Both subunits contribute loop structures to the substrate-binding groove (underlined) that harbours the active site of the caspase (*). Initiator caspases possess long prodomains with DED and CARD homotypic interaction motifs.

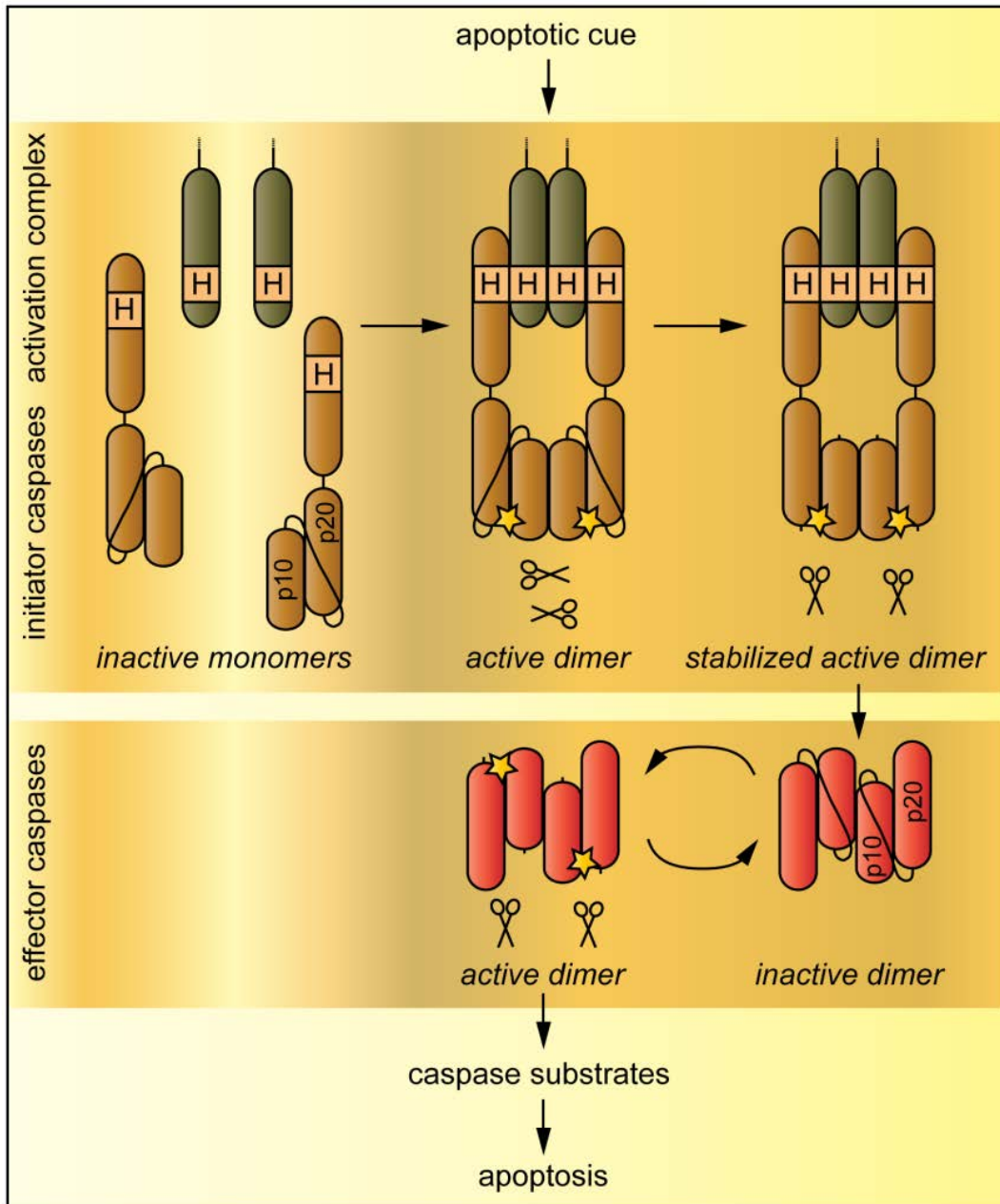


Figure 1.2. Mechanism of caspase activation. Initiator caspases exist as inactive monomers that are activated by dimerization at apoptotic activation complexes. Auto-proteolytic cleavage of the linker between the large (p20) and small subunit (p10) stabilizes the active dimer. Effector caspases exist as inactive dimers that are activated by initiator or effector caspases. Active effector caspases cleave intracellular substrates to initiate apoptosis. H: homotypic interaction motif, such as DED and CARD; yellow star: active center of the caspases.

1.1.3. Death receptors.

Death receptors [33] (**figure 1.3.**) are cell surface receptors that assemble multimeric caspase activation platforms to initiate the apoptotic caspase cascade in response to extrinsic death signals.

All eight human death receptors belong to the tumor necrosis factor receptor super family (TNFRSF) [34]. They are characterized by three to four extracellular cysteine-rich repeats that bind corresponding ligands [35]. In addition, death receptors contain an intracellular death domain (DD) [36, 37] that engages in homotypic interactions with other DD-containing adapter proteins [28].

Death receptors interact with defined sets of adapter proteins. Accordingly, death receptors are classified into tumor necrosis factor receptor type 1-associated death domain protein (TRADD) recruiting, and Fas-associated death domain protein (FADD) recruiting death receptors [38]. Tumor necrosis factor receptor 1 (TNF-R1) [39, 40] is a TRADD-recruiting death receptor [38]. CD95 or Fas, tumor necrosis factor-related apoptosis-inducing ligand receptor 1 (TRAIL-R1) or death receptor 4 (DR4), and TRAIL-R2 or DR5 belong the group of FADD recruiting receptors [38]. Tumor necrosis factor receptor 2 (TNF-R2) belongs to the TNFRSF, but does not contain DDs and is not considered a death receptor [34].

Death receptors recruit specific adapter molecules that determine downstream signaling events. FADD is a bipartite adapter molecule that contains two death folds, a DD and a DED [28, 41, 42]. The DD of FADD binds the death receptor, and the DED forms homotypic interactions with the DED of caspase-8 and 10 [41] to assemble 'death-inducing signaling complexes' (DISCs) directly at the cell membrane [43]. While both caspase-8 and caspase-10 are activated in DISCs, so far only caspase-8 DISCs have been shown to engage the pro-apoptotic caspase cascade and induce cell death [44, 45].

In contrast, TRADD-recruiting death receptors serve as a platform for the activation of pro-survival and pro-inflammatory nuclear factor kappa-B (NF- κ B) and mitogen-activated protein kinase (MAPK) modules [46, 47].

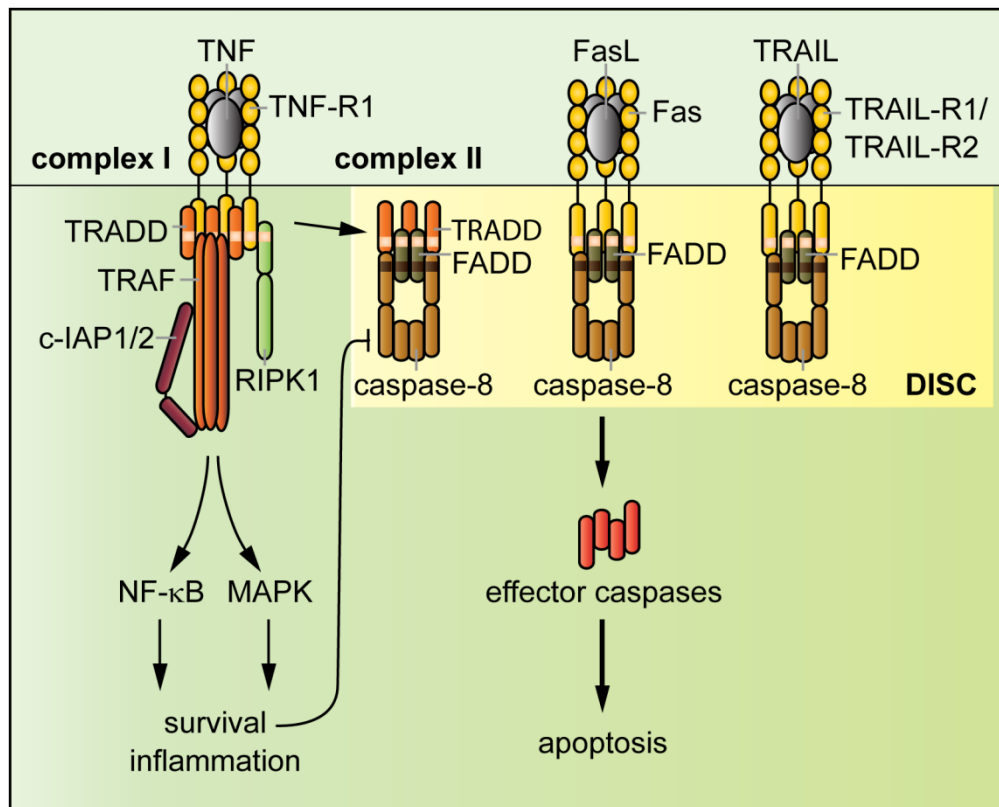


Figure 1.3. Death receptor signaling. Fas and TRAIL-R1 or TRAIL-R2 establish membrane-proximal death-inducing signaling complexes (DISCs) of FADD and caspase-8. TNF-R1 is a TRADD-recruiting death receptor that establishes a membrane-proximal complex I to initiate pro-survival NF-κB and MAPK signaling and a cytosolic complex II of TRADD, FADD and caspase-8. Complex II and Fas and TRAIL-R1/2 DISCs activate effector caspases that induce apoptosis. Death domains within the receptors, TRADD and FADD are shown in white, death effector domains in FADD and caspase-8 in dark brown. c-IAP1/2: cellular inhibitor of apoptosis 1 or 2, FADD: Fas-associated death domain protein, FasL: Fas ligand, RIPK1: receptor-interacting protein kinase 1, TNF: tumor necrosis factor, TNF-R1: tumor necrosis factor receptor 1, TRAF: TNF receptor-associated factor, TRAIL: TNF-related apoptosis-inducing ligand, TRAIL-R1/2: TNF-related apoptosis-inducing ligand receptor 1 or 2.

However, the DD of TRADD also connects with the FADD-caspase-8/10 axis in a second cytosolic complex (complex II) [46, 47]. Complex II induces apoptosis [48, 49] in the absence of anti-apoptotic NF- κ B signaling [50].

1.1.4. TNF receptor 1.

1.1.4.1. The physiological role of TNF.

TNF is the prototypical pro-inflammatory cytokine [51]. It is partially redundant with interleukin 1 (IL-1) and interleukin 6 (IL-6) [51], but surpasses the two in versatility [51]. Inflammation is an innate immune response to a local infection, antigen challenge or tissue injury with the goal to eliminate or at least to confine invaders and to promote tissue repair [51]. Resident tissue macrophages, dendritic cells, and mast cells recognize tissue infection or injury and initiate inflammation through synthesis and secretion of TNF and other second messengers [19, 51]. TNF promotes the recruitment of immunogenic components from the blood [19, 51] and activates resident and recruited immune cells to fight invading microorganisms [19, 51]. Systemic TNF triggers fever, the secretion of acute-phase protein by the liver, activation of the coagulation cascade, myocardial suppression and systemic vasodilation [51]. In the resolution phase of inflammation, TNF contributes to the elimination of infiltrated immune cells and promotes tissue repair [51]. On a cellular level, TNF is therefore a pleiotropic cytokine that mediates processes as diverse as cell activation and survival, differentiation, proliferation, cytokine release, and cell death [52, 53].

Inflammation and its mediator TNF cause serious medical problems during severe acute inflammation and chronic inflammation associated with persistent infections, or auto-immune diseases such as rheumatoid arthritis, inflammatory bowel diseases, and multiple sclerosis [19, 20, 54]. Severe acute inflammation causes septic shock and death, and chronic inflammation tissue injury and organ dysfunction [19, 20]. In addition, prolonged exposure to low concentrations of TNF can lead to exhaustion of the organism and a condition described as wasting syndrome or cachexia [55].

The clinical impact of diseases with deregulated inflammation and the importance of TNF are reflected in the common use of TNF and anti-TNF therapies. Some cancers are treated with regional TNF perfusion [56, 57], while the tissue-damaging side effects of chronic inflammation are minimized with anti-TNF antibodies or artificial TNF receptor decoys [58, 59].

1.1.4.2. TNF.

Tumor necrosis factor alpha (TNF- α , commonly abbreviated as TNF) [60-62] is a cytokine of the TNF super family (TNFSF) and the ligand of death receptor TNF-R1 and the non-death receptor TNF-R2 [34, 63]. TNF exists in a membrane-bound and a soluble form. The membrane-bound version consists of three type II transmembrane proteins that form a stable homotrimer [64, 65]. TNF- α converting enzyme (TACE) processes all three TNF molecules at extracellular sites to generate trimeric soluble TNF [66, 67]. TNF is closely related to lymphotoxin alpha (LT- α , or TNF- β), which only exists in soluble form [68]. Whereas LT- α is mostly generated by T-lymphocytes [68], TNF is mainly produced by macrophages, and a broad variety of other cell types, including lymphoid cells, dendritic cells, mast cells, endothelial cells, cardiac myocytes, adipose tissue, fibroblasts, and neuronal tissue [52].

1.1.4.3. The TNF receptor complex.

TNF binds the death receptor TNF-R1 and the non-death receptor TNF-R2 [52]. Soluble and membrane-bound TNF as well as soluble LT- α activate TNF-R1 [69], which is expressed on most tissues [52]. In contrast, only membrane-bound TNF efficiently activates TNF-R2 on lymphocytes, endothelial cells and other immune-related cells [70]. TNF receptors are type I transmembrane proteins with 4 extracellular cysteine-rich repeats [35] and an intracellular DD [36]. Like TNF, TNF receptors exist as spontaneously pre-assembled trimeric complexes at the cell membrane (**figure 1.4.**). The pre-ligand assembly domain (PLAD) in cysteine repeat 1 stabilizes that configuration [71]. Ligand binding [72] triggers conformational changes that lead to the dissociation of the intracellular DD protein silencer of death domains (SODD) from the receptor DDs [73]. Release of SODD allows the assembly of a TNF receptor complex (complex I) at the plasma membrane.

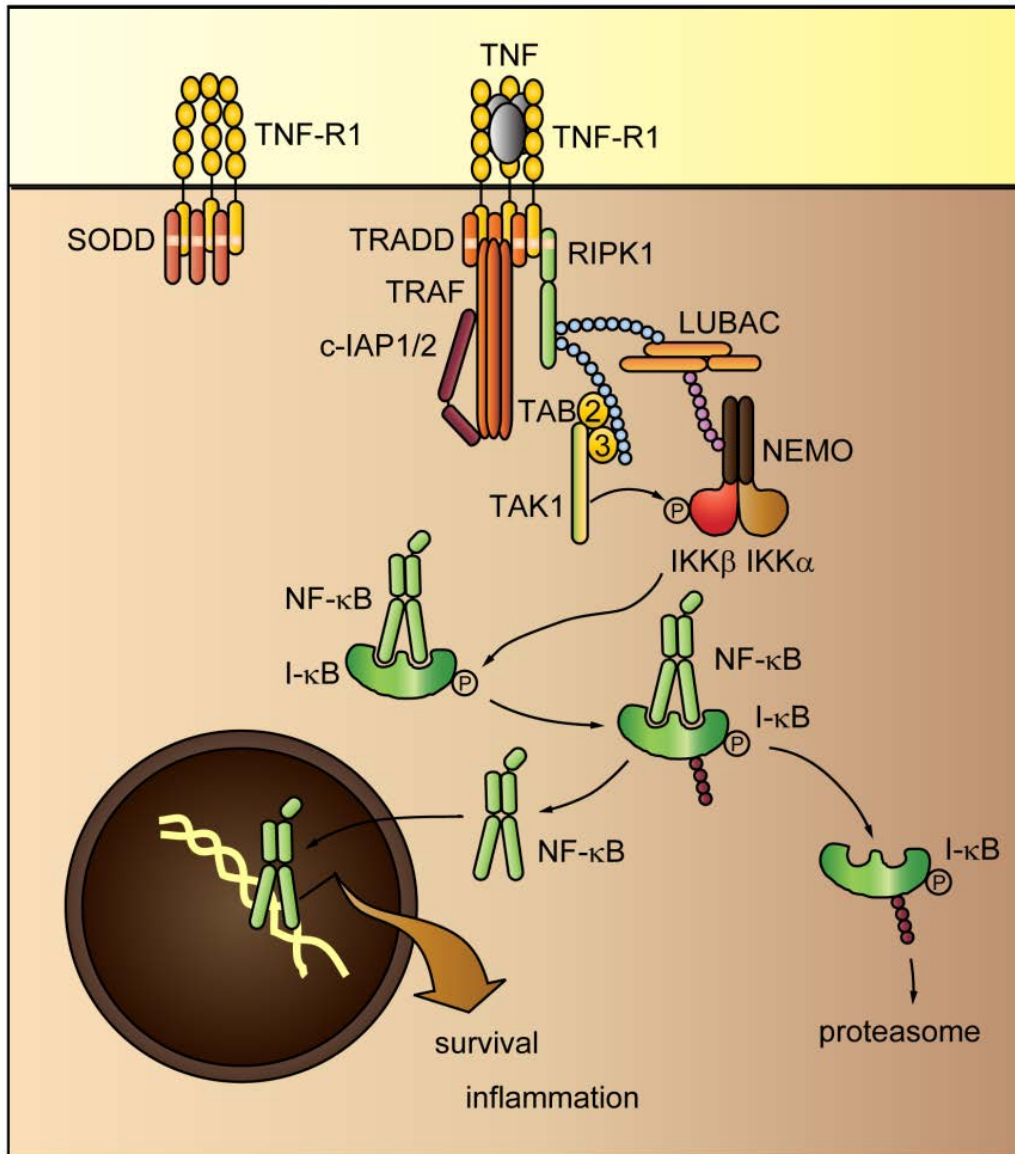


Figure 1.4. The TNF receptor complex and NF- κ B activation. Binding of TNF to the pre-assembled TNF-receptor leads to the assembly of a TRADD-based TNF receptor complex (complex I). Predominantly c-IAPs attach K63 and K11 poly-ubiquitin chains (light blue) to components of complex I. The linear ubiquitin assembly complex (LUBAC) attaches linear ubiquitin chains (pink). For simplicity, only ubiquitin chains on RIPK1 and LUBAC are depicted. Ubiquitin chains act as a platform for the recruitment of the TAK1 and IKK complexes. Phosphorylation-dependent proteasomal degradation of I- κ B frees NF- κ B to initiate transcription of pro-survival and pro-inflammatory gene products. Death domains in the TNF-R1, SODD, TRADD and RIPK1 are depicted in white.

TNF-R1 is a TRADD-recruiting death receptor that predominantly induces pro-survival and pro-inflammatory responses through NF- κ B and MAPK signaling modules [46]. In addition to TRADD [74], common elements of complex I are receptor-interacting serine/threonine-protein kinase 1 (RIPK1) [75], TNF receptor-associated factor 2 or 5 (TRAF2/5) [76], and cellular inhibitor of apoptosis 1 or 2 (c-IAP1/2) [77] (**figure 1.4.**). However, some of those components seem to be absent and dispensable in some TNF receptor complexes [78]. In the traditional model, TRADD uses its DDs to recruit DD protein RIPK1 [74, 75]. However, RIPK1 may also engage in a direct homotypic interaction with the receptor [78]. TRADD also recruits TRAF2 or TRAF5 [46, 78, 79] that in turn recruit c-IAP1 or 2 [80, 81]. A crystal structure revealed that one c-IAP2 molecule binds a trimer of TRAF molecules [82].

Recently, we began to understand the importance of poly-ubiquitin chains for the recruitment of NF- κ B and MAPK modules through complex I [78, 83, 84]. Complex I serves as a platform for E2 ubiquitin-conjugating and E3 ubiquitin-ligating enzymes and as an acceptor for ubiquitin chains [78]. E3 ubiquitin ligase activity in complex I mostly derives from c-IAPs [77, 85, 86]. cIAPs add K63 and K11-linked poly-ubiquitin chains to many components of complex I, including RIPK1 [77, 85-88], themselves, and possibly TRAF2, TRADD, and the TNF-R [83]. The linear ubiquitin assembly complex (LUBAC) binds to these poly-ubiquitin chains and creates K1-linked linear polyubiquitin chains on itself as well as complex I components. The variety of poly-ubiquitin chains on complex I recruit 2 essential complexes for NF- κ B and MAPK activation. The trimeric inhibitor of nuclear factor kappa-B kinase (IKK) complex consists of IKK- α , IKK- β [89], and NF- κ B essential modifier (NEMO) [90, 91], and the trimeric transforming growth factor-beta-activated kinase 1 (TAK1) complex [92] consists of TAK1, and TAK1-binding proteins 2 and 3 (TAB2 and 3). NEMO in the IKK complex and TAB2 and TAB3 in the TAK1 complex bind ubiquitin chains in complex I [93-96]. Upon recruitment, the proximity of IKK and TAK1 complex, allows TAK1 to phosphorylate and activate IKKs [92]. The IKK complex promotes NF- κ B signaling, while TAK1 also promotes signal transduction through the MAPK cascade [92].

1.1.4.4. TNF-induced NF- κ B signaling.

Membrane-associated complex I activates NF- κ B signaling within minutes of TNF binding. NF- κ B signaling leads to the activation of NF- κ B transcription factors, which elicit immune and survival responses through the regulation of cellular gene transcription (**figure 1.4.**). NF- κ B transcription factors consist of homo- or heterodimers of Rel family proteins [97, 98]. Rel proteins are characterized by a Rel homology domain (RHD), which mediates dimerization, nuclear localization and DNA binding [97, 98]. In the absence of an activating stimulus like TNF, proteins of the inhibitor of nuclear factor kappa-B (I- κ B) family sequester NF- κ B in the cytoplasm by masking its nuclear localization signals [98]. TNF activates TAK1 that phosphorylates two serine residues in the activation loop of IKK- β [92, 99, 100]. TNF also activates MAPK/ERK kinase kinase 3 (MEKK3) and MAPK/ERK kinase kinase 2 (MEKK2) that can functionally replace TAK1 under specific circumstances [101-103]. However, the exact molecular activation mechanisms for MEKK2 and MEKK3 by TNF are unknown. Active IKK- β phosphorylates I- κ B proteins on conserved serine residues [98]. Upon phosphorylation, I- κ B proteins are poly-ubiquitylated and destroyed by the proteasome [98]. The liberated NF- κ B dimers translocate to the nucleus, bind conserved promoter sequences and initiate gene transcription [98].

NF- κ B controls the expression of several hundred gene products, including cell survival/anti-apoptotic, cell proliferatory, inflammatory, and auto-regulatory genes [104]. For example, I- κ B- α and A20 are auto-regulatory gene products that act in a negative feedback-loop to terminate NF- κ B activity [104]. A20 is part of a ubiquitin-editing complex that targets RIPK1 for proteasomal degradation [105-107].

NF- κ B-induced anti-apoptotic gene products, such as cellular FLICE-like inhibitory protein long (c-FLIP_L) [108-111], secure cell survival after TNF. Loss of c-FLIP_L sensitizes cells to apoptosis, even if NF- κ B signaling is fully activated [112]. c-FLIP_L is highly similar to caspase-8 (21% amino acid identity, 61% similarity), but lacks an active proteolytic site. c-FLIP_L homodimerizes or heterodimerizes with caspase-8 in complex II through homotypic DED interactions and blocks caspase-8 activation in a dominant negative fashion [47, 113].

In the spectrum of NF- κ B induced anti-apoptotic proteins, Bcl-2 proteins [114-116] control mitochondrial apoptotic signaling, and inhibitor of apoptosis proteins (IAPs) [117] block the activity of caspases 3, 7, and 9 [118, 119].

1.1.4.5. TNF-induced MAPK signaling.

Complex I also induces MAPK signaling [47] (**figure 1.5.**). MAPK pathways are characterized by a tripartite core signaling module, which consists of a linear phosphorylation and activation cascade of an upstream mitogen-activated protein kinase kinase kinase (MAP3K), an interjacent mitogen-activated protein kinase kinase (MAP2K) and a downstream MAPK [120]. MAP2Ks are threonine and tyrosine protein kinases that dually phosphorylate the conserved Thr-X-Tyr motif in the MAPK activation loop [120]. TNF activates three major human MAPK groups; c-Jun N-terminal kinases (JNK), p38 kinases, and extracellular signal-regulated kinases (ERK) [120]. However, it is poorly understood how the TNF receptor complex connects to these MAPK cascades. The MAP3Ks involved in the TNF-induced activation of MAPKs are TAK1 [92, 121], MEKK3 [102, 120], MEKK1 [120, 122, 123] apoptosis signal-regulating kinase 1 and 2 (ASK1/2) [120, 124] and tumor progression locus 2 (TPL-2) [125-127]. The MAP2Ks leading to JNK, p38 MAPK, or ERK signaling are conserved [120]. MKK4 and MKK7 activate three JNK isoforms [128-133], MKK3 and MKK6 activate four p38 isoforms [129, 134-136], and MEK1 and MEK2 activate two ERK isoforms [137] (**figure 1.5.**).

Active MAPKs phosphorylate a number of transcription factors and transcriptional activators. The transcription factors are primarily components of the homo- or heterodimeric activator protein 1 (AP-1) [120, 138] such as Jun, fos, or activating transcription factor (ATF) family proteins. AP-1 activates inflammation and stress-related genes [138-140].

Prolonged JNK signaling can favour TNF-induced death [140-142] through activation of complex II [143] and mitochondrial apoptotic signaling [142, 144, 145]. However, NF- κ B dependent gene products counter prolonged JNK signaling [146-148].

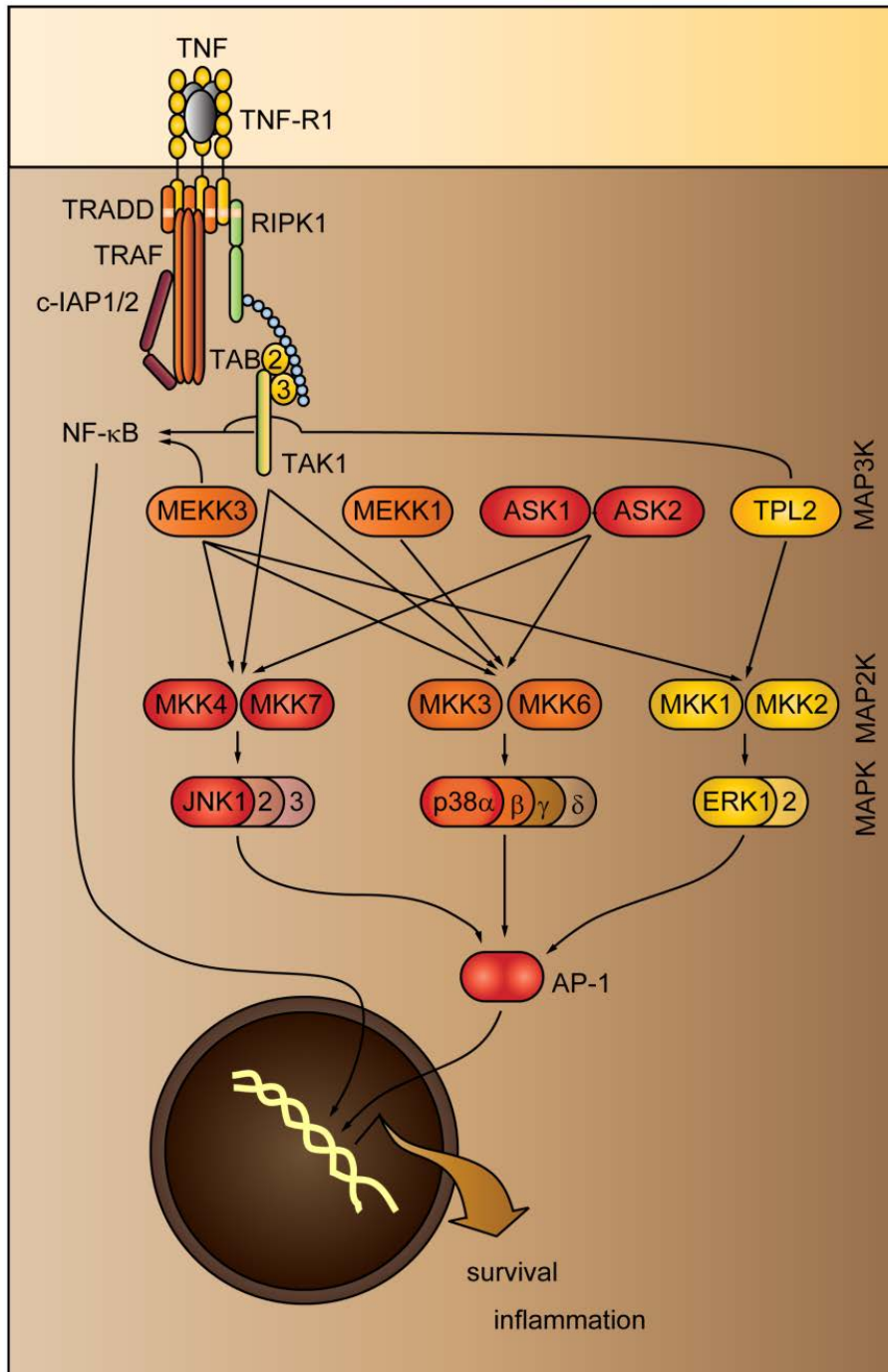


Figure 1.5. TNF-induced MAPK signaling. The TNF-receptor complex activates tripartite MAPK cascades such as JNK, p38, and ERK modules. MAP3Ks and MAP2Ks for the respective modules are indicated. JNK, p38, and ERK isoforms predominantly activate versions of the bipartite transcription factor AP-1, which transcribes pro-survival and pro-inflammatory genes.

1.1.4.6. TNF-induced apoptosis.

TNF also activates a pro-apoptotic caspase signaling module [52]. The mechanism and temporal pattern of caspase activation is different to the mechanics of NF- κ B and MAPK activation. Activation of the caspase module occurs after NF- κ B and MAPK activation and requires the formation of a second molecular complex (complex II) [47].

It is believed that complex II derives directly from molecular reorganization of complex I [47]. Molecular reorganization of complex I is accompanied and possibly triggered by endocytosis of TNF-R1 [149, 150] (**figure 1.6.**). TNF-R1 endocytosis is mediated by clathrins [149, 151-154] and based on the interaction of the cytosolic tumor necrosis factor receptor 1 internalization domain (TRID) with the clathrin recruitment machinery [149].

In a process that involves apoptosis-linked gene 2 (Alg2), Alg2 interacting protein (AIP) and the endosomal sorting complex required for transport (ESCRT), caspase-8 is recruited to the TNF receptor complex at the endosome membrane [155]. Caspase-8 binds TRADD via the adapter molecule FADD [46, 47, 149, 156]. Caspase-8 dimerization at the TNF receptosome allows caspase-8 activation [31, 47]. Active caspase-8 processes RIPK1 in complex II [157, 158] and contributes to RIPK1 degradation in combination with a number of E3 ubiquitin ligases [83, 159-161] that attach poly-ubiquitin chains. Ubiquitination targets RIPK1 for proteasomal degradation and terminates NF- κ B signaling in the TNF receptosome. Active caspase-8 then activates the pro-apoptotic cascade.

1.1.5. Type I and type II death receptor-induced apoptosis.

Caspase-8 activates effector caspases through two different pathways [162-164] (**figure 1.7.**). Pathway selection depends on the relative magnitude of caspase-8 activation at the receptor complex [162] and the levels of the X-linked inhibitor of apoptosis protein (XIAP) [165]. In so-called 'type I' cells, which include thymocytes and mature T-cells, death receptor signaling induces high levels of caspase-8 activity at the receptor complex [162] and rapid degradation of XIAP [165].

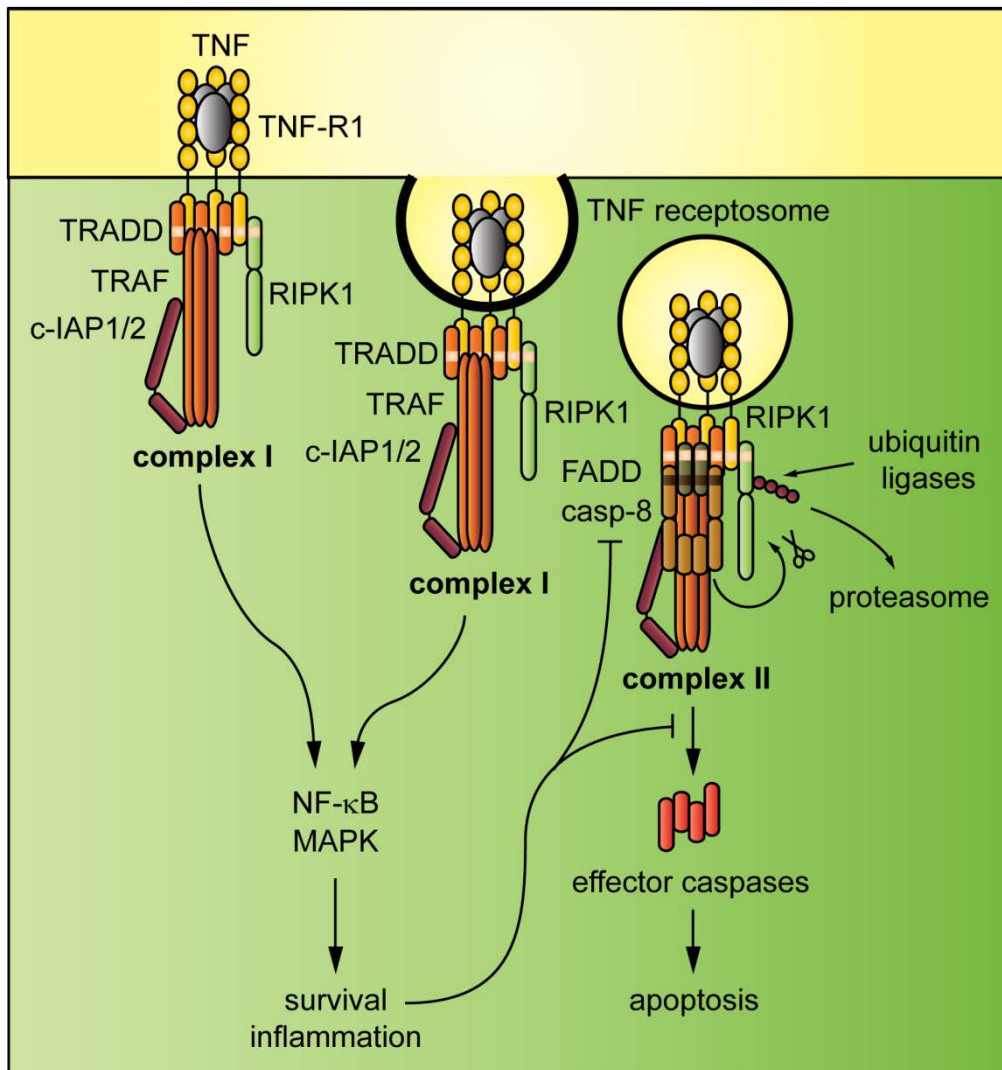


Figure 1.6. TNF-induced apoptosis. Endocytosis of the TNF receptor complex initiates the recruitment of pro-apoptotic FADD and caspase-8 (casp-8) and the 2-fold proteolytic destruction of RIPK1 through caspase-8 and the proteasome. RIPK1 destruction terminates TNF-induced pro-survival NF-κB and MAPK signaling. Caspase-8 activates effector caspases and induces apoptosis. Death domains in TNF-R1, TRADD, and RIPK1 are depicted in white, death effector domains in FADD and caspase-8 in dark brown.

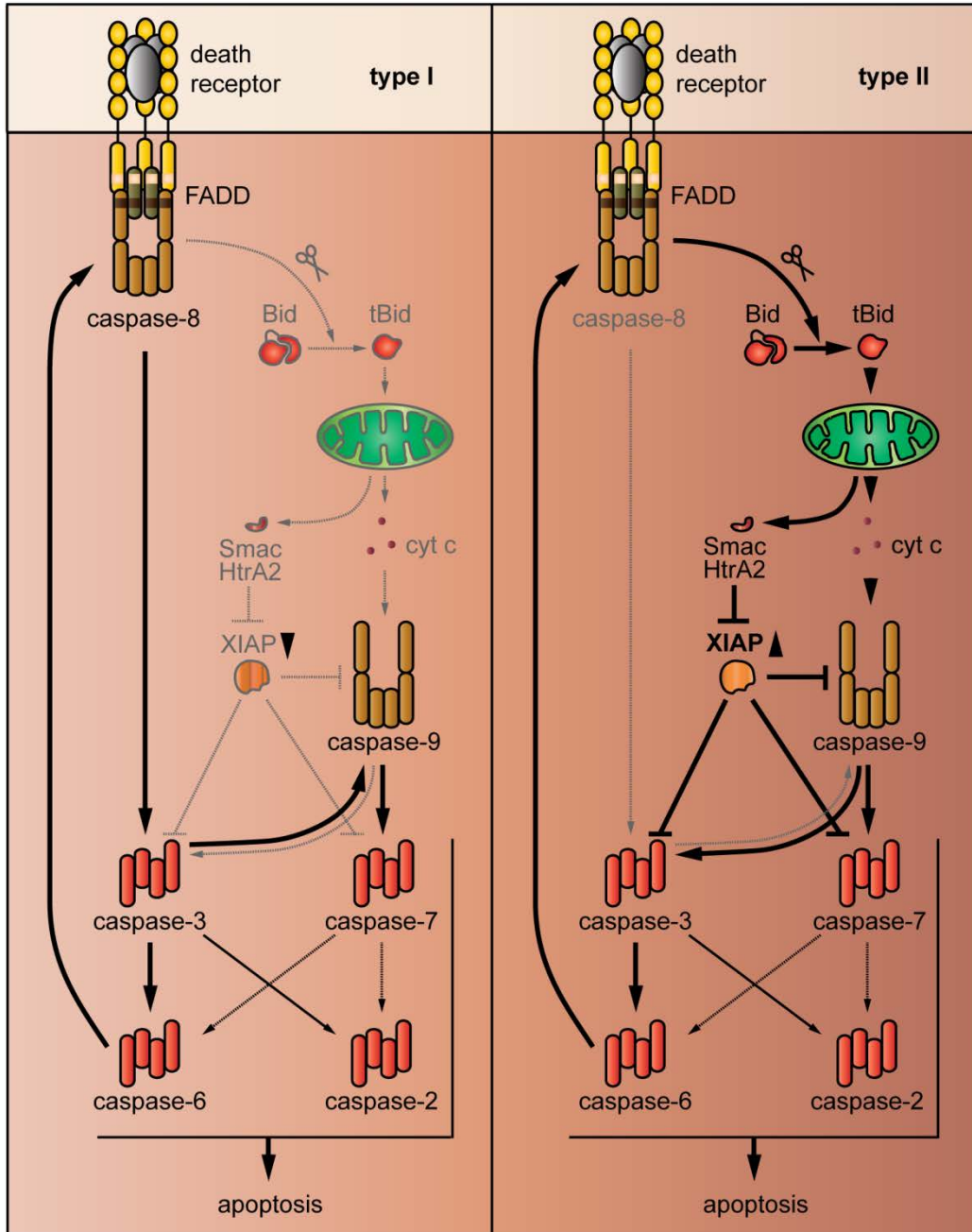


Figure 1.7. Type I and type II apoptosis. In type I cells (left panel), pronounced caspase-8 activity at the death receptor complex and decreased XIAP levels allow the direct activation of effector caspases. In type II cells (right panel), low caspase-8 activation and increased levels of XIAP prohibit the direct activation of effector caspases. The activation of the mitochondrial apoptotic pathway amplifies the apoptotic signal from caspase-8 to caspase-9 and effector caspases. Effector caspase-6 establishes feedback signaling to caspase-8.

Degradation of XIAP unlocks caspase-8 mediated activation of caspase-3, 7 [119], and 9 [118]. Type II cells, such as hepatocytes or pancreatic β -cells, are characterized by low caspase-8 activity at the death receptor complex [162], increased XIAP levels [165] and minimal direct activation of effector caspases [162]. In type II cells, caspase-8 induces the release of pro-apoptotic factors from the mitochondria to amplify the apoptotic signal for the activation of caspase-9 and effector caspases [162].

Specifically, caspase-8 cleaves the pro-apoptotic Bcl-2 family member BH3-interacting domain death agonist (Bid) [166] into truncated Bid (tBid), which permeabilizes the mitochondrial membranes [167-169] (**figure 1.8.**). tBid and mitochondrial membrane permeabilization are also induced in type I cells, but they are dispensable for the activation of effector caspases [162]. Mitochondrial membrane permeabilization leads to the release of mitochondrial pro-apoptotic factors [170-172] (**figure 1.8.**). These include the two endonucleases endoG and apoptosis-inducing factor (AIF) [173-176], cytochrome c, second mitochondria-derived activator of caspase (Smac), also called direct inhibitor of apoptosis binding protein with low pI (DIABLO) [177], and the serine protease Omi, also called high temperature requirement protein A2 (HtrA2) [178, 179].

Cytochrome c promotes the assembly of a multi-protein complex called the 'apoptosome' [180-182]. Cytochrome c introduces dATP or ATP-dependent conformational changes in the cytosolic adapter molecule apoptotic peptidase activating factor 1 (Apaf-1) [183]. These conformational changes result in the formation of wheel-like Apaf-1/cytochrome c heptamers [184-188]. The Apaf-1 CARD domain mediates the oligomerization process and recruits pro-caspase-9 [189] to form an active apoptosome [30, 190-193]. Active caspase-9 cleaves and activates effector caspases such as caspase-3 and 7 [189, 194]. Effector caspases enhance caspase-8 activation and apoptotic signaling in a feedback loop. In this feedback loop, caspase-3 and 7 process caspase-6, which activates caspase-8 [194-196].

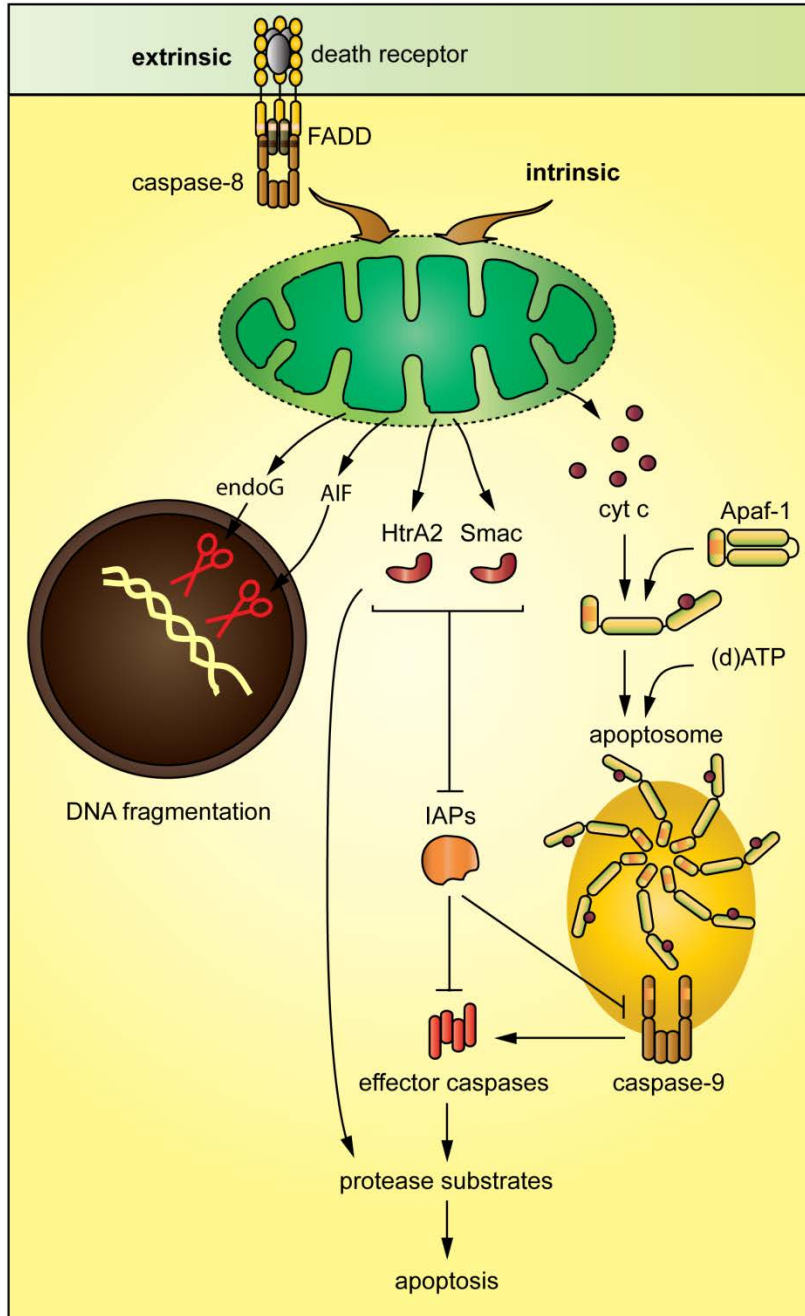


Figure 1.8. Release of pro-apoptotic factors from the mitochondria during apoptosis. Intrinsic and extrinsic apoptotic cues lead to the permeabilization of the mitochondrial membranes and the release of pro-apoptotic factors. EndoG and AIF initiate large-scale DNA fragmentation. HtrA2 and Smac neutralize IAPs. Cytochrome c (cyt c) is the initiating factor for the assembly of the caspase-9 activating apoptosome protein complex (yellow oval). The active apoptosome activates effector caspases. The combined proteolytic activity of effector caspases and HtrA2 induces apoptosis. Death domains in the death receptor and FADD are depicted in white, death effector domains in FADD and caspase-8 in dark brown, and CARD domains in Apaf-1 and caspase-9 in orange.

Mitochondrial Smac and HtrA2 block inhibitor of apoptosis proteins (IAPs) such as XIAP [197-199]. Specifically, Smac and HtrA2 relieve IAP-mediated inhibition of caspase-9 dimerization and caspase-3 and -7 processing [197-199]. In addition, the serine protease activity of HtrA2 expands the proteolytic capacity of effector caspases, and processes an array of cellular substrates such as cytoskeletal proteins and IAPs [200, 201].

1.1.6. Type II mitochondrial apoptosis.

1.1.6.1. The mitochondrial membranes.

Mitochondria (**figure 1.9.A**) are surrounded by two lipid membrane bilayers [202] that lose their integrity during apoptosis [170-172]. The inner mitochondrial membrane (IMM) has numerous involutions, which form the typical cristae structures [202]. Cristae are dynamic structures regulated by cristae junctions [202]. The IMM borders the mitochondrial matrix in the lumen of the mitochondria [202]. The space between OMM and IMM is called the intermembrane space (IMS), while the cristae lumen separated by cristae junctions is referred to as the intracristae space (ICS) [202]. OMM and IMM approximate in so-called 'contact sites' [203].

In the absence of an apoptotic stimulus, the OMM is permeable to molecules lighter than 5 kD due to integral voltage-dependent anion channels (VDAC) [204] (**figure 1.9.B**). VDACs form β -barrel structures composed of nineteen β -strands [205, 206]. Molecules of a molecular weight above 5 kD, such as the pro-apoptotic molecules cytochrome c and Smac, have to be actively transported through the OMM into the IMS.

The IMM is impermeable to ions and highly polarized. The IMM potential is a result of the metabolic activity of the mitochondria [207, 208]. Catabolic processes, like glycolysis and the tricarboxylic acid cycle, reduce electron carriers that ultimately accumulate in the mitochondrial matrix. In the process of oxidative phosphorylation, four major protein complexes together with the mobile electron carriers ubiquinone and cytochrome c transfer those electrons to oxygen and simultaneously transport protons from the matrix to the mitochondrial IMS [207-210].

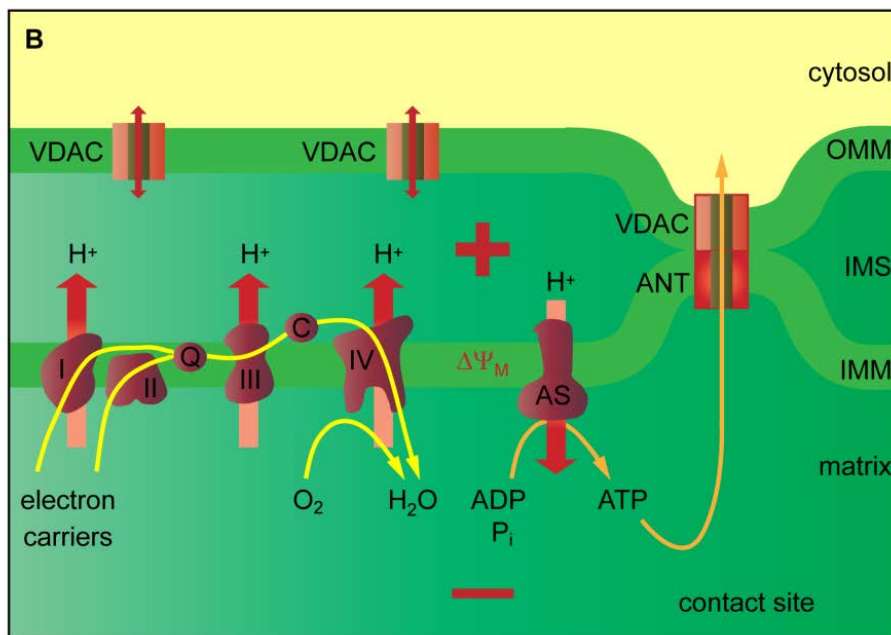
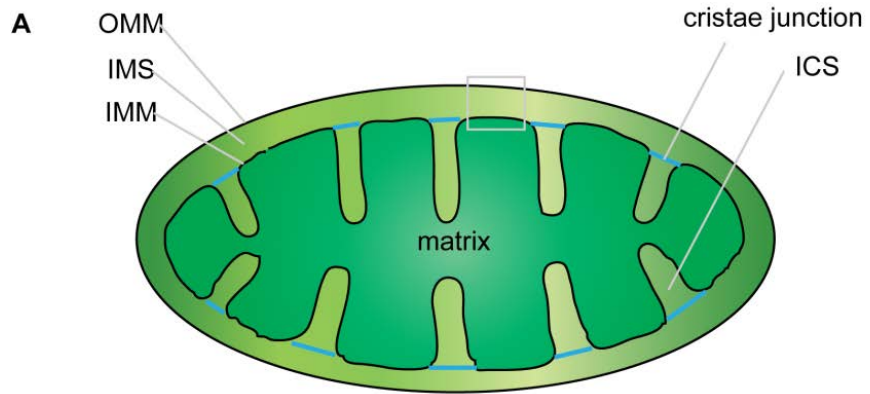


Figure 1.9. Mitochondrial structure and biochemical processes at the mitochondrial membranes. **A:** Structure of the mitochondrion. OMM: outer mitochondrial membrane (OMM), intermembrane space (IMS), inner mitochondrial membrane (IMM), intracristae space (ICS). The framed area is enlarged in B. **B:** Close-up into the OMM and IMM. VDAC channels allow ion exchange through the OMM. The IMM is impermeable and highly polarized due to oxidative phosphorylation. Reduced electron carriers pass their electrons to an electron transport chain that consists of four major transport complexes (I-IV) and the mobile electron carriers ubiquinone (Q) and cytochrome c (C) to reduce molecular oxygen. Electron transport drives the transport of protons from the mitochondrial matrix into the IMS, which builds a membrane potential across the IMM ($\Delta\Psi_M$). The IMM potential is the motor for ATP synthesis through the ATP-Synthase complex (AS). ATP leaves the mitochondria through the joint channels of ANT and VDAC in the mitochondrial contact sites.

As a consequence, the mitochondrial matrix is negatively charged and basic in comparison to the IMS [207, 208]. The proton gradient serves the generation of ATP through the ATP synthase complex in the IMM membrane [207, 208]. ATP leaves the mitochondrial matrix through the adenine nucleotide transporter (ANT) in the IMM and VDAC in the OMM [211, 212]. ADP re-enters the mitochondria in the opposite direction [213].

1.1.6.2. Bcl-2 proteins and the permeabilization of the mitochondrial outer membrane.

The integrity of the OMM is controlled by proteins of the B-cell lymphoma-2 (Bcl-2) family that are characterized by one to four Bcl-2 homology (BH) domains [214, 215]. The Bcl-2 family consists of three subgroups with pro- or anti-apoptotic activity [214, 215] (**figure 1.10.**).

The pro-apoptotic BH3-only family is a divergent family with a single conserved BH3 domain [214, 215]. Apoptotic cues result in post-translational modifications, including phosphorylation, ubiquitination, and proteolytic cleavage of BH3-only proteins. For example, caspase-8 processes the cytosolic BH3-only protein Bid [166] to generate tBid [167, 168].

Activated BH3-only proteins directly and/or indirectly promote the permeabilization of the OMM through a group of Bcl-2 effector proteins [214-216]. Bcl-2 effector proteins contain a transmembrane domain and four BH domains [214, 217]. There are three Bcl-2 effector proteins, Bcl-2 associated X protein (Bax) [218], Bcl-2 antagonist killer (Bak) [219-221], and Bcl-2 related ovarian killer (Bok) [222]. While Bok has a restricted expression pattern and no reported function in apoptosis [223], the presence of at least Bak or Bax is essential for pro-apoptotic permeabilization of the mitochondrial outer membrane (MOMP) [216]. In non-apoptotic cells, Bax locates to the cytoplasm or associates with the periphery of the OMM [224-226]. During apoptosis, specific BH3-only proteins dubbed 'activator' BH3-only proteins, like tBid [227-230], induce Bax conformational changes [231] that induce its translocation to the mitochondria [224, 225] and insertion into the OMM [226]. Bak constitutively resides at the mitochondria [232] stabilized by VDAC2 [233, 234] and anti-apoptotic Bcl-2 proteins [235]. Active Bak and Bax oligomerize in the mitochondrial OMM.

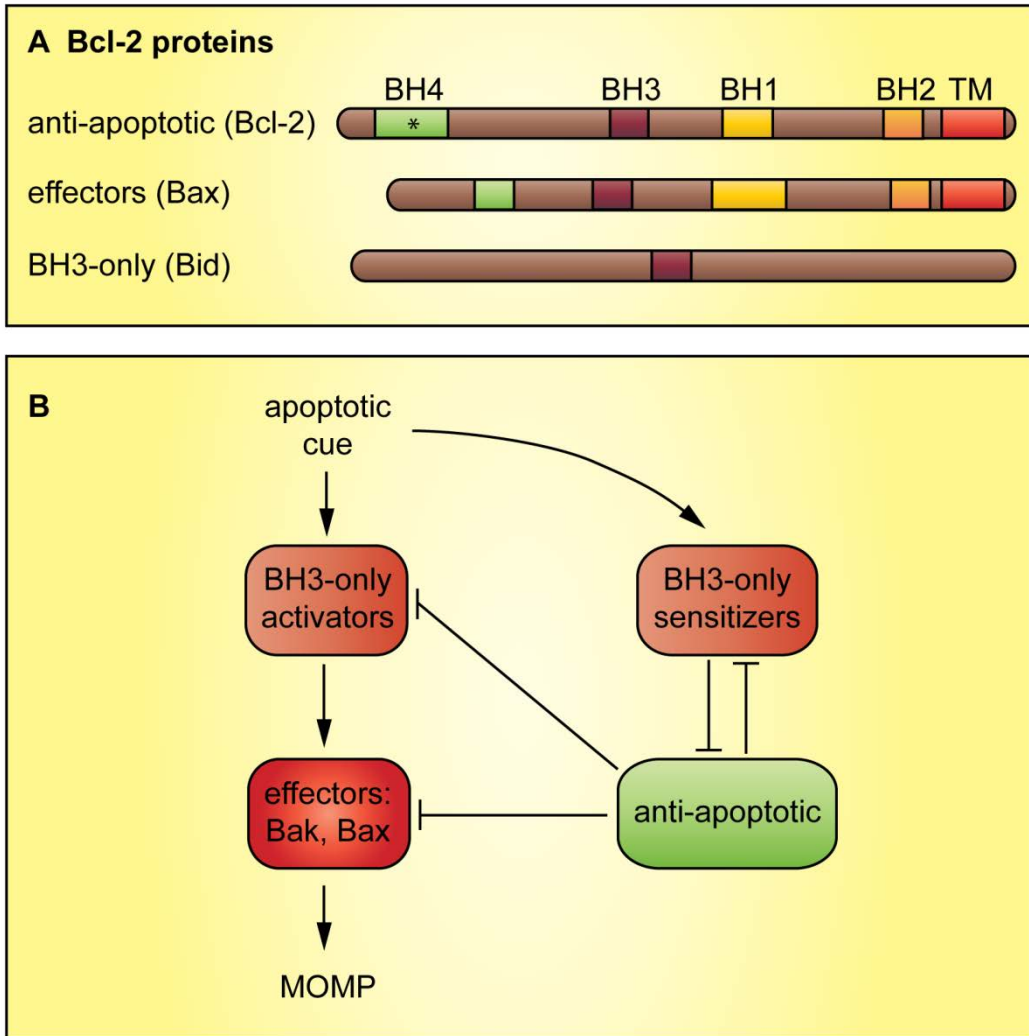


Figure 1.10. Bcl-2 family proteins and their interactions. **A:** Domain structure of representative members of the 3 classes of Bcl-2 proteins. BH: Bcl-2 homology domain. TM: transmembrane domain. *: optional domain for this class.(Adapted from [214].) **B:** Diagram of the interactions between Bcl-2 proteins. An apoptotic cue activates BH3-only proteins. Activating BH3-only proteins activate the effector Bcl-2 proteins Bak and Bax to induce mitochondrial outer membrane permeabilization (MOMP). Anti-apoptotic Bcl-2 proteins sequester BH3-only and Bcl-2 effector proteins to inhibit their pro-apoptotic activity. Sensitizer BH3-only proteins antagonize the activity of anti-apoptotic Bcl-2 proteins.

In the initial step of oligomerization, both Bak and Bax homo-dimerize [236, 237]. Subsequently, Bak and Bax dimers form higher order oligomers through dimer-dimer interactions [238-240]. Oligomerized Bak and Bax form toroidal pores [241] in the OMM that release pro-apoptotic factors, such as cytochrome c, from the mitochondria [242-244].

Anti-apoptotic Bcl-2 proteins control and antagonize the pro-apoptotic activity of BH3-only and Bcl-2 effector proteins [214, 215, 245]. Anti-apoptotic Bcl-2 proteins contain three to four BH domains and a transmembrane domain that anchors them in the OMM, the endoplasmic reticulum, or the nuclear envelope [246-252]. In addition, anti-apoptotic Bcl-2 proteins may reside in the cytoplasm [215]. Typical group members are Bcl-2 [253-257], and Bcl-2 related gene, long isoform (Bcl-x_L) [214, 215]. Anti-apoptotic Bcl-2 proteins antagonize activated pro-apoptotic Bcl-2 proteins by sequestration [218, 235, 258-262]. Active 'derepressor/sensitizer' BH3-only proteins relieve or prevent the sequestration of pro-apoptotic Bcl-2 proteins by anti-apoptotic Bcl-2 proteins [227-229, 259, 260, 263].

1.1.6.3. Permeabilization of the mitochondrial inner membrane.

Even though MOMP is sufficient to induce caspase activation and apoptosis, it also affects the integrity of the IMM [171]. Most importantly, MOMP progressively blocks electron transport through the respiratory chain with deadly consequences for the cell [171]. Part of the decline of the mitochondrial electron transport may be due to the loss of the essential soluble electron carrier cytochrome c from IMS and ICS to the cytoplasm [171]. Furthermore, the loss of OMM integrity allows the flux of cytosolic effector caspases into the IMS, which process components of the respiratory chain complexes [171]. For example, effector caspases process the essential 75 kD complex I subunit NADH-ubiquinone oxidoreductase (NDUFS1) [264]. Complex II activity is also reduced in a caspase-dependent manner, however, the structural basis for that observation is not resolved [264, 265]. As a result, electron transport declines and the IMM transmembrane potential dissipates. All processes that depend on the IMM potential, such as ATP synthesis, come to a halt. The destruction of specific subunits of respiratory chain complexes and release of cytochrome c also uncouples electron transport and leads to the overproduction of reactive oxygen species (ROS) [264, 266].

ROS damage the mitochondrial membranes [267, 268], proteins, and DNA, and modulate cellular signaling pathways to amplify the apoptotic signal.

MOMP also leads to a phenomenon called 'mitochondrial permeability transition' [269]. Mitochondrial permeability transition is caused by the opening of a pore that originates in the IMM, which allows unselective ion flux through the IMM. Permeability transition leads to a massive influx of water into the mitochondrial matrix, which results in matrix swelling, remodeling of the cristae, local rupture of the OMM due to its smaller surface [270] and additional spill of pro-apoptotic molecules from the IMS [271].

The molecular composition of the so-called 'mitochondrial permeability transition pore' (MPTP) is unknown [172]. The MPTP is proposed to be a multi-protein complex of roughly 600 kD [212, 272] that resides at contact sites between the OMM and IMM [269, 273-278]. While the exact composition of the MPTP is unknown, a number of proteins are implicated in MPTP activity. These proteins include VDAC in the OMM, ANT in the IMM, the peripheral benzodiazepine receptor (PBR) and hexokinase on the cytosolic site of the OMM, creatine kinase (CK) in the IMS, and cyclophilin D (CypD) on the IMM facing the mitochondrial matrix [212, 279]. However, all studies to date have failed to identify a single essential component of the MPTP complex [280-285].

1.2. Hexokinases.

1.2.1. Hexokinase isozymes.

There are four distinct human isozymes of hexokinase; HK1 [286], HK2 [287], HK3 [288], and HK4 (also called glucokinase) [289-292] with different enzyme kinetics, regulatory properties, intracellular distribution, and expression patterns [293-296]. Human HKs originate from a 50 kD ancestral hexokinase (**figure 1.11.**). 50 kD HK4 is most closely related to the ancestor hexokinase. 100 kD HK1 to 3 developed through gene duplication and fusion events and therefore contain highly similar amino- and carboxyl-terminal domains [297-300]. Both domains are catalytically active in HK2.

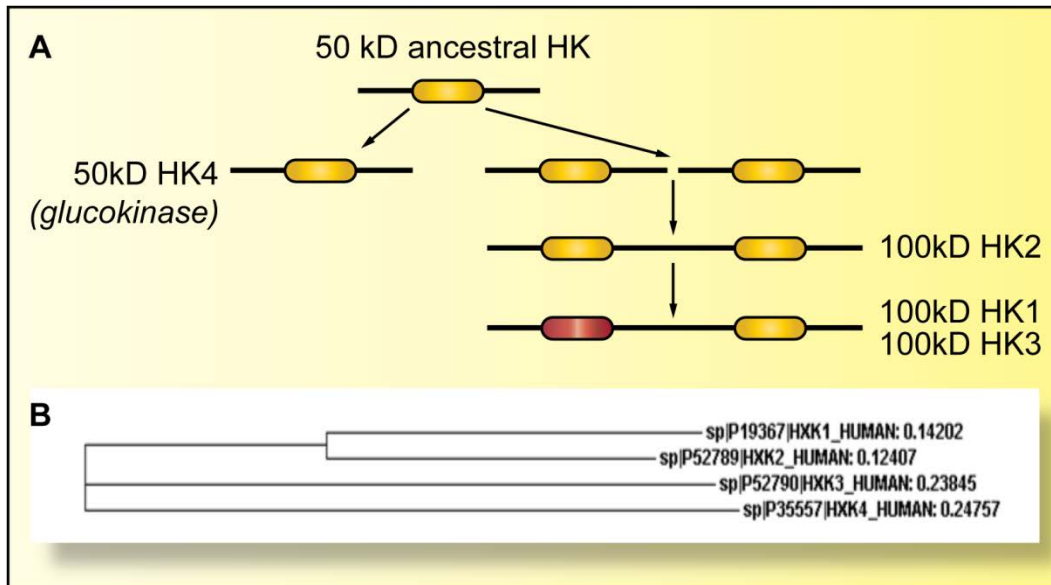


Figure 1.11. Evolution of human hexokinases. **A:** Human HKs likely derived from a 50 kD ancestral HK with relation to the 50 kD human HK4. Duplication and fusion of the gene encoding the ancestral HK created the 100 kD HK2 with two highly similar and catalytically active hemidomains. The amino-terminal hemidomain in HK1 and HK3 evolved into a regulatory domain without catalytic activity. (Adapted from [301].) **B:** Phylogram of human HKs. Sequence alignment of the four human HKs reveals that human HK1 and HK2 are most closely related to each other.

Only the carboxyl-terminal domains are catalytically active in HK1 and HK3, and the amino-terminal domains adopted regulatory functions [299]. A full sequence alignment of all four human HKs is shown in **appendix 1**. The fact that most mammalian tissues express a specific combination of multiple isozymes [302, 303] suggests a diversification of the roles of HKs in different tissues and perhaps locations within the cell.

HK1 is ubiquitously expressed with enhanced expression in brain and kidney [293, 302]. In 1953, Crane and Sols found 80% to 90% of cellular HK activity from brain homogenates (which refers to HK1 activity) in the 'particulate fraction' [304]. They proposed that the 'particulate fraction' constitutes the mitochondria, which was corroborated a few years later [305, 306] and extended subsequently to many primary tissues and cancerous cell lines. The mitochondrial HK1 pool stands in dynamic and regulated exchange with a smaller cytosolic HK1 pool [307].

Mitochondrial HK1 associates with the OMM [306, 308], but lacks a distinct transmembrane domain. Chymotryptic digestion of HK1 abolished its association with the mitochondria [306, 309] and with a hydrophobic matrix [309]. These findings demonstrated that the hydrophobic amino-terminus of HK1, selectively removed by chymotrypsin, mediates the interaction with the mitochondrion [310-312]. Subsequent studies showed that the amino-terminus of HK1 inserts into the hydrophobic core of the OMM [313] and that the fifteen amino-terminal amino acids were necessary and sufficient to target HK1 to the mitochondria [311]. However, the binding is most likely supported by hydrophobic and electrostatic interactions with other regions of HK1 [306, 314, 315].

HK1 interacts with VDAC in the OMM [316-318]. Interestingly, HK1 preferentially binds to VDAC in contact sites of the OMM with the IMM [319-321]. Humans express three isoforms of VDAC, VDAC1, VDAC2, and VDAC3 [322-324], and several studies demonstrated interactions between HK1 and VDAC1 [325, 326]. HK1 exhibited a higher affinity for VDAC1 in isolated yeast mitochondria that expressed human VDAC1 or VDAC2 [322, 327]. However, studies with super resolution microscopes showed that all 3 VDAC isoforms colocalize to varying degrees with HK1. The highest level of colocalization was

observed with VDAC3, and lower degrees of colocalization existed between HK1 and VDAC1 or VDAC2 [328]. The interaction of VDAC1 with HK1 requires the VDAC1 carboxyl-terminal extramitochondrial domains [315, 327] as well as the conserved membrane-facing glutamate residue seventy three of the VDAC1 β -barrel [329, 330]. Recently, a computational model based on the crystal structures of VDAC1 and HK1 with a modeled amino-terminus suggested that the fifteen amino-terminal amino acids of HK1 insert into the VDAC1 pore [331].

HK2 is the principal regulated isozyme in many cell types [332-335], and is highly expressed in insulin-sensitive tissues, such as skeletal muscle and adipose tissue. In addition, HK2 is highly expressed in many cancers [301, 302, 336]. Like HK1, HK2 is mitochondrial in various mammalian tissues and cancerous cell lines [301, 337-339], and the hydrophobic amino-terminus of HK2 is the basis for this mitochondrial interaction [312, 339]. A cell-permeable peptide, which mimics the amino-terminus of HK2 displaces HK2 from the mitochondria [340-342], but the effect of the same peptide on HK1 has not been examined. However, HK1 and HK2 compete with each other in mitochondrial re-binding experiments, which suggest identical binding mechanisms [339]. Interactions between HK2 and mitochondria are dynamic and regulated, and balanced with a cytosolic HK2 pool [293].

HK3 is characterized by a broad expression pattern with enriched expression in lung and spleen [293, 295]. HK3 lacks an amino-terminal hydrophobic sequence and localizes to the cytoplasm [293].

HK4 expression is regulated by the hormones that control glucose homeostasis [343] and predominantly found in the liver and the β -cells of the pancreas [344-346]. HK4 localizes to the cytoplasm or is sequestered by glucokinase regulatory protein (GKRP) and transported to the nucleus to downregulate cytosolic HK4 levels [347, 348]. Although HK4 lacks the amino-terminal hydrophobic sequence that mediates mitochondrial localization [310, 312], there are indications that it establishes an indirect association with mitochondria [349, 350].

1.2.2. Hexokinase function.

1.2.2.1. Hexokinases and metabolism.

HKs are best known for their role in cell metabolism. They catalyze the transfer of a phosphoryl group from ATP to the 6-hydroxyl of a hexose to yield the 6-phosphoester [293]. Most commonly, HKs convert glucose into glucose-6-phosphate. This is the initial reaction in glycolysis, the pentose phosphate pathway and gluconeogenesis [293] (**figure 1.12.**). Glycolysis, the tricarboxylic acid cycle, and phosphorylative oxidation in the mitochondria are the main pathways for the production of energy equivalents (ATP) in the cell. Some glycolytic intermediates, such as glyceraldehyde 3-phosphate and pyruvate, are also used as building blocks in anabolic processes [293]. In contrast, the pentose phosphate pathway has an exclusively anabolic role. It delivers glucose-derived intermediates for the synthesis of nucleotides and aromatic amino acids and the reducing equivalent NADPH for reductive synthetic reactions [293]. Glucose-6-phosphate is also the precursor for the polymeric glycogen, which is the non-osmotic storage product of glucose. Glycogen storage allows the quick release of glucose in case of a sudden energy demand [293]. The relative importance of those pathways depends on the specific situation and tissue. Therefore it was proposed that the selective expression of individual HK isozymes with different affinities for glucose, ATP and inhibitors, is an adaptation to the specific metabolic needs of those tissues [293].

HK1 likely has the strongest ties to cellular energy metabolism and channels glucose into the glycolytic pathway [293]. HK1 is ubiquitously expressed, and its expression levels are especially high in the brain, a tissue known for high energy demand and strong reliance on glycolysis to meet that demand [351]. Like HK2 and HK3, HK1 is inhibited by its product glucose-6-phosphate [293]. However, in contrast to the other HKs, the presence of inorganic phosphate (Pi) attenuates the feedback-inhibition [293]. Pi is generated in situations of high energy demand due to the hydrolysis of high energy phosphate compounds, like ATP. Thus, the derepression of HK1 through Pi points to a glycolytic, ATP-generating role for HK1 [293].

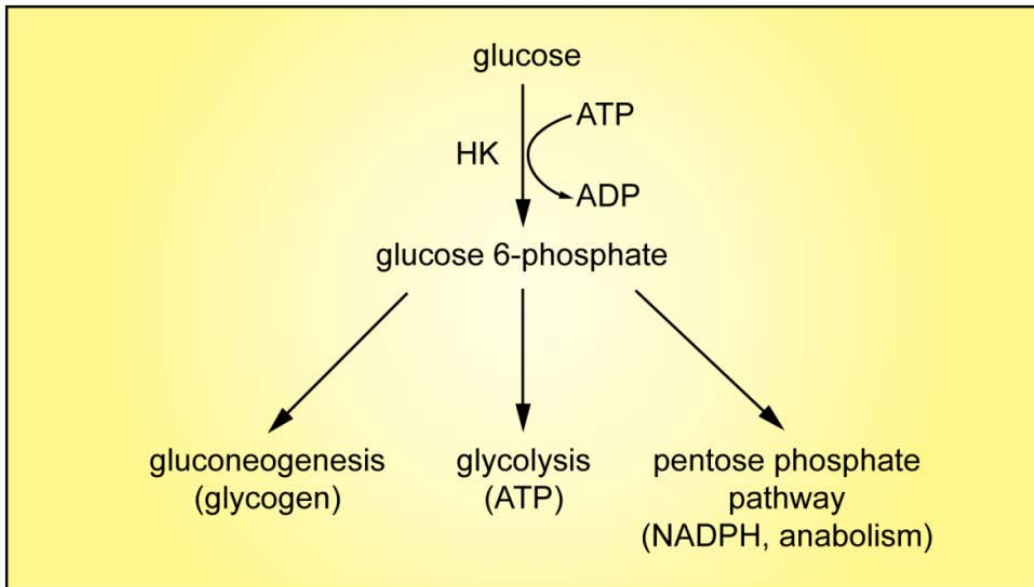


Figure 1.12. The metabolic function of hexokinases. HKs convert glucose into glucose 6-phosphate. Glucose 6-phosphate is the base product for gluconeogenesis to build a glucose store, for glycolysis to generate energy equivalents, and for the pentose phosphate pathway to synthesize building blocks and reduction equivalent NADPH for anabolic reactions. (Adapted from [293].)

Furthermore, mitochondrial HK1 exclusively uses intramitochondrial ATP as a substrate [352-356], which leaves the mitochondria through ANT in the IMM and VDAC in the OMM [211, 212]. The resultant ADP re-enters the mitochondria through same channels [213]. Therefore, mitochondrial HK1 couples the rates of intramitochondrial oxidative phosphorylation and ATP production with the rates of cytosolic glycolysis. In addition, the mitochondrial localization of HK1 dampens the inhibitory effect of glucose-6-phosphate on the rate of glycolysis, and increases HK1 activity [301]. An additional factor in the regulation of glycolytic activity is therefore the localization of HK1 either to the mitochondria or to the cytosol. Growth factors promote the interaction of HK1 with the mitochondria [357], and glucose-6-phosphate has a dissociating effect [358, 359]. Pi, ATP, glucose and the pH are additional regulators of the subcellular localization of HK1 [306, 307, 360-362].

The inhibitory influence of Pi on HK2 and HK3 activity may suggest that both play an anabolic role and channel glucose into the pentose phosphate pathway or gluconeogenesis [293]. In addition, HK2 has an anabolic role during lipid synthesis in the liver [363] and in the lactating mammary gland [364]. In hepatoma cells, mitochondrial HK2 also preferably uses intramitochondrial ATP [365]. However, the existence of such a coupling mechanism has not been demonstrated for unmodified cells to date [293].

HK4 is not regulated by glucose-6-phosphate or by Pi [366]. In comparison to the other HKs, HK4 has a very low affinity for glucose [366], probably due to structural differences in its active center caused by the absence of the second hemidomain. However, this seems the ideal adaptation for its role as part of a glucose sensing mechanism to regulate insulin release from the pancreatic β -cells and to regulate glucose uptake and utilization in the glucose-rich liver [366].

1.2.2.2. Hexokinases and apoptosis.

In recent years, there is accumulating evidence that HKs also exhibit anti-apoptotic functions. Specifically, HKs contribute to the anti-apoptotic effects of growth factor signaling. Growth factors signal through phosphatidylinositol 3-kinases (PI3Ks) and Akt/protein kinase B (PKB) to stimulate metabolism and to inhibit apoptosis upstream of cytochrome c release [367]. The anti-apoptotic roles

of growth factors require glucose and HK activity, and involve an increase of mitochondrial, but not general HK activity [357, 368]. The anti-apoptotic role of growth factors is mimicked by induced expression of HK1 [357, 368, 369] or HK2 [340, 370] and disturbed by peptides or chemicals that displace HKs from the mitochondria [340-342]. These findings suggest that growth factor signaling prevents pro-apoptotic cytochrome c release from the mitochondria by promoting HK-mediated glucose metabolism at the mitochondria (**figure 1.13.**).

There are several theories about the molecular consequences of HK association with mitochondria and the inhibition of mitochondrial apoptosis [295]. The first theory suggests that mitochondrial HKs impact the conductance of the VDAC channels with effects on the permeability of the mitochondrial membranes [295]. One model proposes that mitochondrial HKs maintain VDAC channels in the open state [371] and is in line with the fact that mitochondrial HKs exclusively use mitochondrial ATP [293]. The model is supported by the observation that the decrease of mitochondrial HKs during growth factor deprivation correlates with the accumulation of phospho-creatin in the IMS and the acidification of the cytoplasm [357, 372]. Both effects are signs of VDAC closure and blockade of the ATP/ADP and pyruvate/metabolite transport through the OMM [357, 372]. Growth factor deprivation also leads to a decrease of the IMM potential, mitochondrial matrix condensation and cristae unraveling that facilitates the release of cytochrome c [373]. Therefore, the presence of HKs at the mitochondria and the execution of its metabolic function would promote cell survival.

An alternative model suggests that mitochondrial HKs lead to VDAC channel closure. This model is based on the ability of purified HK1 to decrease the *in vitro* conductivity of purified VDAC reconstituted into planar lipid bilayers by approximately 70% [374]. The model is also based on the assumption that during apoptosis cytochrome c is released via VDAC and argues that HK-induced VDAC closure prevents MPTP formation [329, 374]

A second hypothesis proposes that the anti-apoptotic activity of HK results from its competition with Bcl-2 proteins for the binding to VDAC [295]. VDAC, HK and Bcl-2 proteins may all meet and interact at mitochondrial contact sites.

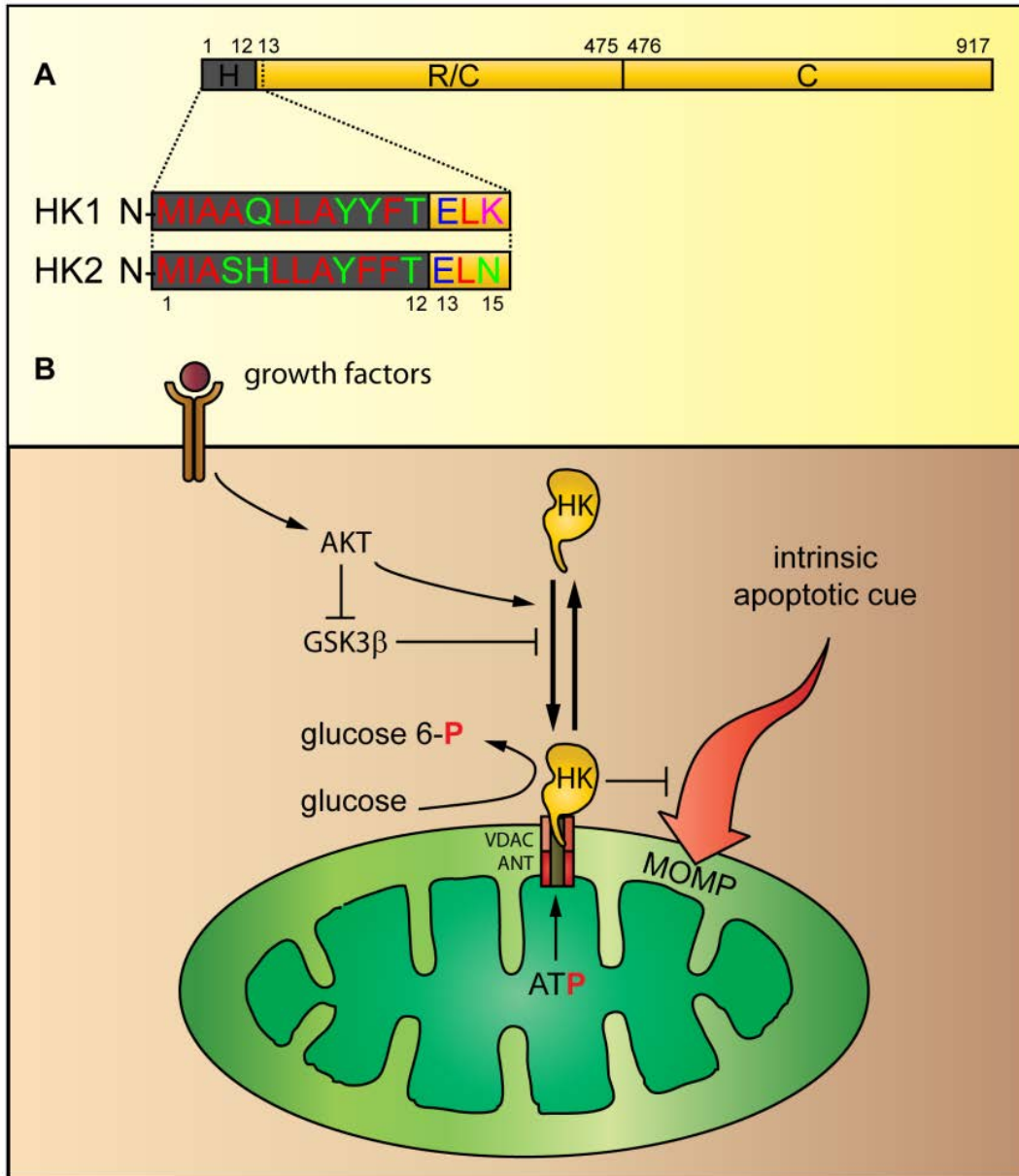


Figure 1.13. Mitochondrial HKs and their anti-apoptotic role in growth factor signaling. **A:** Domain structure and N-terminal sequence of human HK1 and HK2. Both HKs consist of two highly similar hemidomains that are catalytically active in HK2 (C), or have evolved into a regulatory (R) and a catalytic domain (C) in HK1. The sequences of the first fifteen amino-terminal amino acids of HK1 and HK2 are shown. Red amino acids are hydrophobic, green amino acids are polar, blue amino acids are charged and acidic, and pink amino acids are charged and basic. **B:** The anti-apoptotic role of mitochondrial HKs in growth factor signaling. Growth factor signaling promotes the interaction of HK1 and HK2 with the mitochondria through activation of AKT and inhibition of GSK3 β . Mitochondrial HKs attenuate intrinsic apoptosis.

Contact sites are rich in HK and the charged phospholipid cardiolipin [375]. Cardiolipin is also the reported requirement for mitochondrial tBid localization and Bak and Bax-mediated cytochrome c release [376-380]. Furthermore, purified VDAC reconstituted in detergent lipid micelles interacted with anti-apoptotic Bcl-x_L and pro-apoptotic Bak and Bax [381, 382]. The large HK tetramer [211, 383-385] might thus sterically hinder the mitochondrial binding of anti-apoptotic Bcl-2 proteins, or the binding and oligomerization of pro-apoptotic Bak and Bax. In support of this hypothesis, Pastorino *et al.* [340] demonstrated that displacement of HK2 from mitochondria with chemicals or a specific HK2 peptide allowed Bax binding, cytochrome c release and apoptosis. Ectopic expression of HK2 had the opposite effect. In other studies, the ectopic expression of HK1 or the amino-terminal hemidomain of HK2 attenuated the exposure of the Bax amino-terminus, while the decrease of mitochondrial HK activity after glucose deprivation led to increased Bax oligomerization at the mitochondria [368, 370]. However, it was also observed that the prolonged displacement of mitochondrial HKs or growth factor withdrawal led to cytochrome c release and apoptosis in the absence of Bak and Bax, albeit with much slower kinetics [341]. This suggests that the hindrance of Bak and Bax activation at the mitochondria may be only one of the anti-apoptotic mechanisms of mitochondrial HKs.

The mechanism, by which growth factors mediate the interaction of HK1 and HK2 with the mitochondria, is unknown. As growth factor signaling impacts metabolism at various points, a network of indirect factors are conceivable. However, one of two direct effects of growth factor signaling on the interaction of HKs with VDAC, is the phosphorylation of VDAC1 on the conserved threonine fifty one [386]. Threonine fifty one is on the cytosolic side of VDAC1, and the mutation of threonine fifty one prevents the binding of HK2 to VDAC1 [386]. Interestingly, threonine fifty one positions close to glutamate seventy three of VDAC1, which was shown to be critical for HK1 binding to VDAC1 [329, 330]. Glycogen synthase kinase 3 β (GSK3 β) phosphorylates VDAC1 on threonine fifty one [386]. In the presence of growth factors, Akt constitutively inhibits GSK3 β [387]. Therefore, growth factor deprivation derepresses GSK3 β and VDAC1 phosphorylation and detaches mitochondrial HK2 [386].

There are also Akt phosphorylation motifs on HK2, and phosphorylation of one of those motifs on threonine four hundred seventy three increases HK2 interaction with the mitochondria [388].

1.2.2.3. Hexokinases and cancer.

Many tumors exhibit a marked increase in the expression of HKs, and particularly in the expression of mitochondrial HKs [389-395]. The upregulation of mitochondrial HKs contributes, at least in part, to a classic biochemical phenotype associated with cancer. The 'Warburg effect', named after its discoverer Heinrich Otto Warburg, describes the shift of cancer cells to a glycolytic energy metabolism irrespective of the availability of oxygen [396]. Normally, the presence of oxygen slows glycolysis and employs oxidative phosphorylation as a more efficient way to produce ATP (Pasteur effect). To cover the immense demand for energy in rapidly growing cancer cells exclusively by glycolysis, the rates of glucose uptake and glycolysis increase dramatically. In addition, the accumulation of the reducing equivalent NADH in the absence of oxidative phosphorylation results in the conversion of pyruvate into lactate.

The reasons for the glycolytic phenotype of cancer cells are insufficiently explained. Vander Heiden *et al.* [397] proposed that the increased need for building blocks and the reducing equivalent NADPH for anabolic processes in proliferating cancer cells trumps the need for ATP. The fact that most of those building blocks are intermediates of glycolysis or the first steps of the tricarboxylic acid cycle provides a reasonable explanation for why glucose is not degraded to the final product CO₂ to maximize energy gain. For example, the production of NADPH requires the introduction of glucose into the pentose phosphate pathway as opposed to entry into glycolysis [397]. The hypoxic conditions in the early stages of cancer development are likely a supporting factor in the shift of metabolic balance away from oxidative phosphorylation [398]. Hypoxia activates hypoxia inducible factor (HIF) transcription factor, which upregulates the glucose transporter Glut1 as well as HK2 and HK3 [333, 399, 400]. Together with common oncogenic mutations that affect proliferation and metabolism [397] these factors likely lead to the Warburg effect. Another intriguing possibility is that cancer cells gain a powerful advantage through the anti-apoptotic effect of a high glycolytic rate coupled with mitochondrial association of HKs.

The signature appearance of the 'Warburg effect' in cancer cells also led to the development of the major cancer detection system worldwide. In positron emission tomography (PET), the radio labelled glucose analog 2-[¹⁸F]fluoro-2-deoxy-glucose (FDG) is administered and taken up into cells through regular glucose transporters. Intracellular HKs generate FDG-6-phosphate, which is not further metabolized [401]. Based on the levels of accumulated FDG-6-phosphate, PET draws a three-dimensional image of the levels of glucose transport and glycolytic activity in the human body and is an excellent tool to diagnose and stage cancer.

1.3. RNA interference.

RNA interference (RNAi) is a highly efficient post-transcriptional gene silencing mechanism that is induced by double-stranded RNA (dsRNA) molecules [402, 403]. RNAi is an evolutionarily ancient regulatory mechanism that controls gene expression, safeguards genomes against transposable elements, and protects host cells against viral invaders [402, 403]. Functional RNAi machinery has been characterized in representatives of the plant, animal and fungal kingdoms [402, 403].

There are at least two converging RNAi pathways in cells of these organisms (**figure 1.14.**). The micro RNA (miRNA) pathway regulates cellular translation [402, 403]. Bioinformatics studies suggested that the expression of more than 60% of all human genes are regulated through RNAi-dependent mechanisms [404]. The miRNA pathway begins with the transcription of a miRNA-coding gene in the nucleus [405, 406]. The resultant primary transcript (pri-miRNA) undergoes extensive post-translational modification [405, 406]. The RNase activity of the RNase III Drosha creates a sixty five to seventy five base pair stem-loop structure with incomplete double-stranded character [406-408]. The so-called pre-miRNA is exported to the cytoplasm [409, 410], where the double-stranded portion binds to the cytosolic RNase III Dicer [406, 411]. Dicer RNase activity generates the mature double-stranded miRNA of around twenty one to twenty three base pairs with a two nucleotide overhang on both 3' ends [406, 411].

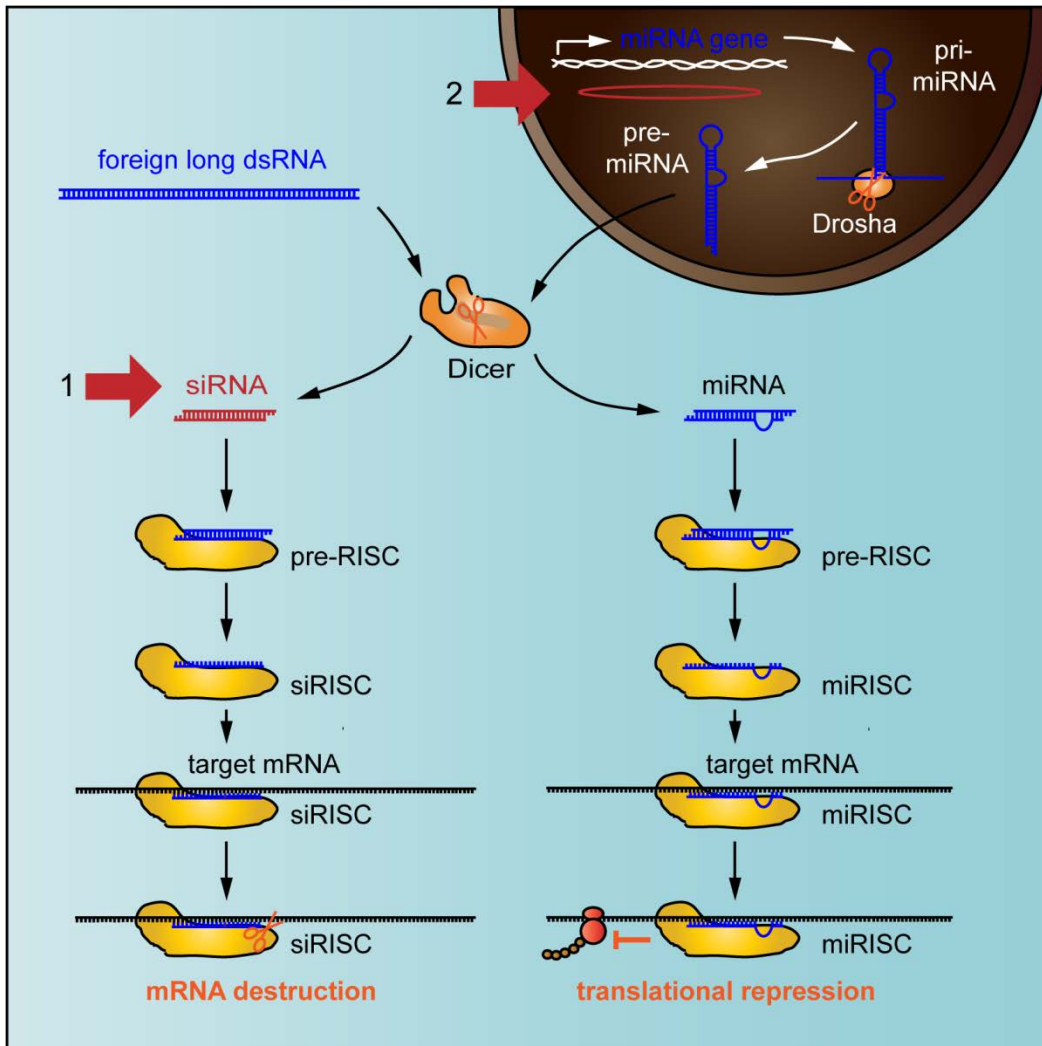


Figure 1.14. The RNAi pathway and its technological application in vertebrate cells. Dicer processes foreign long dsRNAs and precursors of miRNA-encoding genes into siRNAs and miRNAs, respectively. siRNAs and miRNA guide strands are incorporated into RISC and lead to destruction and translational repression of target mRNAs, respectively. Vertebrate cells are transfected or transduced with synthetic siRNAs (1) or plasmids encoding miRNA precursors (2) to inhibit translation of specific target proteins.

Invertebrate, plant, and fungal orthologs of Dicer process long dsRNA molecules of viral origin into a series of short interfering RNA (siRNA) duplexes [412-414]. siRNA duplexes are roughly twenty one to twenty three nucleotides long with two nucleotide overhangs at the 3' end [412-414].

Cytosolic RNA-induced silencing complexes (RISCs) separate miRNA and siRNA duplexes into two RNA single strands [414, 415]. RNA-binding argonaute proteins integrate one of the strands, the so-called the guide strand, into the RISC complex [414-420]. The complementary passenger strand is cleaved, released and destroyed by exonucleases [414, 421]. siRISCs usually target viral transcripts and single-stranded RNA genomes with perfect sequence complementarity [402, 403, 414]. miRISCs require a sequence match between nucleotides two to eight of the 5' end of the guide strand (seed region) and the mRNA and allow for a degree of mismatch between the remaining nucleotides [422-428].

Activated RISCs silence mRNAs through several mechanisms. siRISCs usually instruct argonaute-dependent endonucleolytic destruction of foreign RNA transcripts and genomes [429-431]. The RNA cleavage products are degraded. miRISCs more frequently repress translation of the target mRNAs through interference with the translation machinery [402, 403, 432].

Given that the RNAi pathway efficiently silences translation of specific target transcripts, the mechanism was soon exploited to artificially deplete gene products of choice. Invertebrate cells readily take up and tolerate five hundred to seven hundred base pair dsRNAs that they channel into the RNAi pathway to deplete target mRNAs with matching sequence [433-435]. Long dsRNAs are not taken up by vertebrate cells and cause potent innate immune responses if introduced by other means [433, 436]. Therefore, vertebrate cell lines are transfected with non-immunogenic siRNAs of around twenty one base pairs [437] and plasmid-based miRNA precursors (short hairpin RNAs, shRNAs) [438] or transduced with shRNAs packaged into viral vectors [439] (**figure 1.14.**). Sequence-specific siRNAs form siRISCs that destroy complementary mRNAs [440].

RNAi technology reached one of its high points with the construction of RNAi libraries that cover entire genomes of mammals (for example, human and mouse genomes [441-448]) and invertebrates (for example, *Drosophila melanogaster* [449, 450] and *Caenorhabditis elegans* [451-453]). These libraries allow the systematic depletion of cellular gene products to identify regulators of biomedically relevant cellular processes.

1.4. Project objectives.

In the present study, I examined the regulation of cell fate in the presence of the cytokine TNF. TNF signals through NF- κ B, JNK, and caspase modules to drive physiological responses that range from inflammation to cell death. The balance between the individual modules determines the nature of the response, and deregulated TNF signaling has been implicated in numerous pathological conditions. Therefore, it is essential to understand the activation of the TNF-dependent modules and the integration of signals from each module. I sought to address these questions with an siRNA screen for regulators of TNF-dependent cell death. I reasoned that siRNA-mediated protein depletion will help me to identify critical, non-redundant players in the pathway. Such gene products could be important candidates for the treatment of inflammatory diseases, and diseases with a disturbed balance of survival or death signaling, such as cancer.

This question is addressed in two sections of this thesis:

1. Development of a high-throughput siRNA assay for modifiers of TNF-induced death (chapter 3).

In this section I established a cell culture system, siRNA transfection, and a viability assay for an siRNA screen for modifiers of TNF-induced apoptosis. The results of the screen are presented in chapter four:

2. An siRNA screen for modifiers of TNF-induced apoptosis (chapter 4).

In the siRNA screen for modulators of TNF-induced death, I identified HK1 as a negative regulator of TNF-induced death in cell culture assays. In the light of the reports of the anti-apoptotic role of mitochondrial HKs in growth factor signaling [340-342, 357, 368-370], I hypothesized that:

(1) HK1 is a negative regulator of extrinsic death receptor-induced apoptosis.

(2) HK1 acts at the mitochondria to block TNF-dependent cell death.

These hypotheses are examined in chapter five of the thesis:

3. Characterization of HK1 as an anti-apoptotic protein (chapter 5).

CHAPTER 2. MATERIALS AND METHODS.

2.1. Buffers and media

All buffers are listed in alphabetical order and were prepared in Milli-Q ultrapure water unless indicated otherwise.

v/v: volume per volume, w/v: weight per volume

DNA gel loading buffer (6X)

30 mM Tris, pH=7.5
36% glycerol (v/v)
0.15% bromophenol blue (w/v)
0.15% xylene cyanol (w/v)

DNA resuspension buffer for plasmid mini preparations

1 μ l 10 mg/ml RNase A (Sigma)
200 μ l TE

EB elution buffer for QIAquick spin columns for PCR purification and gel extraction (Qiagen)

10 mM Tris, pH = 8.5

Fractionation buffer for cellular fractionation

200 mM mannitol
70 mM sucrose
10 mM HEPES, pH=7.5
1 mM EGTA, pH=8.0

LB (Luria Bertani) bacterial growth medium (500 ml)

5 g tryptone (BD)
2.5 g yeast extract (BD)
5 g NaCl
7.5 g Agar (Sigma) (*for culture plates*)
autoclaved

Lysis buffer 1, general lysis buffer for Western blotting

20 mM Tris, pH=7.5
25 mM glycerol-2-phosphate
150 mM NaCl
1% Triton X-100 (v/v)
2 mM Na_3VO_4
1 mM PMSF
0.04% 1 protease inhibitor cocktail tablet/2 ml (Roche, 11873580001)(v/v)

Lysis buffer 2 for immunoprecipitation of complex II

20 mM HEPES, pH=7.5
150 mM NaCl
1% Triton X-100 (v/v)
10% glycerol (v/v)
1 mM PMSF
0.04% 1 protease inhibitor cocktail tablet/2 ml (Roche, 11873580001)(v/v)

Lysis buffer 3 for lysis of the heavy membrane/mitochondrial fraction

150 mM NaCl
50 mM Tris, pH=7.5
5 mM EGTA, pH= 8.0
2% CHAPS (w/v)

Lysis buffer 4 for the caspase activity assay

20 mM HEPES, pH=7.5
150 mM NaCl
10% glycerol (v/v)
2% CHAPS (w/v)

P1 bacterial resuspension buffer for plasmid mini preparations/TE

10 mM Tris, pH=7.5
1 mM EDTA, pH=8.0

P1 bacterial resuspension buffer for plasmid midi preparations (Qiagen)

50 mM Tris, pH=8.0
10 mM EDTA, pH=8.0
100 µg/ml RNase A

P2 bacterial lysis buffer for plasmid mini preparations

200 mM NaOH
1% SDS (w/v)

P2 bacterial lysis buffer for plasmid midi preparations (Qiagen)

200 mM NaOH
1% SDS (w/v)

P3 neutralization buffer for plasmid mini preparations

3M potassium acetate, pH=5.5

P3 neutralization buffer for plasmid midi preparations (Qiagen)

1M potassium acetate, pH=5.5

PB DNA resuspension buffer for PCR purification (Qiagen)

5 M guanidine hydrochloride
30% isopropanol (v/v)
pH = 5.0

PBS buffer (10X)

1.4 M NaCl
27 mM KCl
100 mM Na₂HPO₄ · 7H₂O
14 mM KH₂PO₄

PBT buffer

0.1% Tween-20 (v/v)
in PBS

PE wash buffer for QIAquick spin columns for PCR purification and gel extraction (Qiagen)

10 mM Tris, pH = 7.5
80% ethanol (v/v)

QC wash buffer for QIAGEN-tips for plasmid midi preparations (Qiagen)

1 M NaCl
50 mM MOPS, pH=7.0
15% isopropanol (v/v)

QBT equilibration buffer for QIAGEN-tips for plasmid midi preparations (Qiagen)

750 mM NaCl
50 mM MOPS, pH=7.0
15% isopropanol (v/v)
0.15% Triton X-100 (v/v)

QF elution buffer for QIAGEN-tips for plasmid midi preparations (Qiagen)

1.25 M NaCl
50 mM Tris, pH=8.5
15% isopropanol (v/v)

QG agarose gel dissolution buffer for gel extraction (Qiagen)

5.5 M guanidine thiocyanate
20 mM Tris, pH = 6.6

Saponin buffer

0.2% saponin (w/v)

0.1% BSA (w/v)

in PBS

Sample buffer (2X)

62.5 mM Tris, pH=6.8

10% glycerol (v/v)

2% SDS (w/v)

50mM β -mercaptoethanol (BioShop)

0.00125% bromophenol blue (w/v)

Sample buffer (2X) with urea for PARP1 Western blots

62.5 mM Tris, pH=6.8

10% glycerol (v/v)

2% SDS (w/v)

50mM β -mercaptoethanol (BioShop)

0.00125% bromophenol blue (w/v)

8 M urea

Sample buffer (2X) with 2X β -mercaptoethanol for cross-linking experiments

62.5 mM Tris, pH=6.8

10% glycerol (v/v)

2% SDS (w/v)

100 mM β -mercaptoethanol (BioShop)

0.00125% bromophenol blue (w/v)

Sample buffer (6X)

187.5 mM Tris, pH=6.8

30% glycerol (v/v)

6% SDS (w/v)

150 mM β -mercaptoethanol (BioShop)

0.00375% bromophenol blue (w/v)

SDS-PAGE resolving gel

380 mM Tris, pH=8.8

8-13.5% 29:1 acrylamide:bisacrylamide solution (Bio-Rad)

0.1% SDS (w/v)

0.1% APS (w/v)

0.1% TEMED (v/v)(Sigma)

SDS-PAGE stacking gel

125 mM Tris, pH=6.8
5% 29:1 acrylamide:bisacrylamide solution(Bio-Rad)
0.1% SDS (w/v)
0.1% APS (w/v)
0.1% TEMED (v/v) (Sigma)

SDS-PAGE running buffer (10X)

250 mM Tris
2 M glycine
1% SDS (w/v)

TAE buffer (50X)

2 M Tris
500 mM EDTA, pH = 8.0
5.71% glacial acetic acid (v/v)

TE buffer

10 mM Tris, pH=7.4
1 mM EDTA, pH=8.0

Transformation solution 1 (2X) for the generation of competent cells

200 mM CaCl₂
20 mM MgCl₂
10 mM RuCl₂
filter sterilized

Transformation solution 2 for the generation of competent cells

100 mM CaCl₂
10 mM MgCl₂
5 mM RuCl₂
10% glycerol (v/v)
filter sterilized

Western blot transfer buffer

25 mM Tris
192 mM glycine
0.37% SDS (m/v)
20% methanol (v/v)

Reaction buffer for the caspase activity assay

10 mM HEPES, pH=7.5
50 mM NaCl
0.5 mM EDTA
10% glycerol (v/v)
0.1% CHAPS (w/v)
10 mM DTT

2.2. DNA cloning

2.2.1. Expression constructs

The NF- κ B reporter construct pNF- κ Bluc was received from Dr. Michele Barry (University of Alberta, Edmonton, AB). The control reporter plasmid pRL-TK was purchased from Promega.

The pEGFP-N1 vector (Invitrogen) was received from Dr. Michele Barry. A glycerol stock of *Escherichia coli* transformed with the cDNA for HK1 (variant 1) in plasmid pOTB7 was purchased from Open Biosystems. A single colony of the glycerol stock was used (**chapter 2.2.4.**) to set up a midi culture (**chapter 2.2.5.** and **2.2.6.**) for plasmid isolation (**chapter 2.2.7** and **2.2.8.**). To generate a carboxyl-terminally tagged full-length HK1-GFP and a HK1-GFP construct lacking the twenty one amino-terminal amino acids (HK1 Δ 21-GFP), HK1 cDNA was amplified with a forward primer that contained a SacI restriction site and a reverse primer that contained a PstI restriction site and eliminated the carboxyl-terminal stop codon (**table 2.1.** and **chapter 2.2.9.**). The forward primer for HK1 Δ 21-GFP replaced amino acid twenty one of HK1 with methionine and annealed at the codon for amino acid twenty two to create a deletion of the twenty one HK1 amino-terminal amino acids (**table 2.1.**). The PCR products were analysed by agarose gel electrophoresis (**chapter 2.2.10.**), purified (**chapter 2.2.11.**) and subcloned into the vector pEGFP-N1 (Invitrogen)(**chapter 2.2.12.** to **chapter 2.2.17.**). Mini (**chapter 2.2.18.**) and midi cultures (**chapter 2.2.6**) were set up to amplify the corresponding constructs and verified by analytical restriction digests (**chapter 2.2.19.**). The HK1-GFP construct was used as the template to generate the expression construct for catalytically inactive HK1S603A-GFP (**chapter**

2.2.21.) Primer sequences are listed in **table 2.1**. The complete HK1-GFP construct in pEGFP-N1 is depicted in **appendix 2**.

The pcDNA3 vector (Invitrogen) was received from Dr. Michele Barry (University of Alberta, Edmonton, Alberta). The expression vector for human Bcl-2 was received from Dr. Ing Swie Goping (University of Alberta, Edmonton, Alberta) and had been generated by ligating the Bcl-2 mRNA that contained the Bcl-2 open reading frame (ORF) and flanking untranslated regions into the EcoRI site of the pcDNA3 vector.

All constructs were sequenced (**chapter 2.2.20.**) using sequencing primers listed in **table 2.1**.

Table 2.1. List of primer sequences. Restriction sites are underlined. Fragments of the HK1 ORF are printed in italics. The codon containing the S603A substitution in HK1 is printed in bold.

construct	primer
HK1-GFP	F(SacI, HK1 amino terminus): 5'-AATT <u>GAGCTCATGATCGCCGCGCAGCTCCTG</u> -3' R(PstI, HK1 carboxyl terminus): 5'-AATT <u>CTGCAGGCTGCTTGCCTCTGTGCGTAAC</u> -3'
HK1S603A -GFP	F: 5'-ATGCCTCTGGGCTTCACGTT CGC TTTCCCTGCCAG CAGACGAGT -3' R: 5'-ACTCGTCTGCTGGCAGGGAA AGG CGAACGTGAAGC CCAGAGGCAT -3'
HK1Δ21 -GFP	F(SacI, HK1 amino terminus lacking first twenty one amino acids): 5'-AATT <u>GAGCTCATGATTGACAAGTATCTCTATGCC</u> -3' R(PstI, HK1 carboxyl terminus): 5'-AATT <u>CTGCAGGCTGCTTGCCTCTGTGCGTAAC</u> -3'
HK1 sequencing 1	F: 5'-AAATGGGCGGTAGGCGTGTACGG-3'
HK1 sequencing 2	F: 5'-TGGGAGATTTTCATGGAGAAAAGGAAGATCA-3'

HK1 sequencing 3	F: 5'-TACTTGGGAGAGCTGGTTCGACTGAT-3'
HK1 sequencing 4	F: 5'-CCGGCAGATAGAGGAGACCCTG-3'
HK1 sequencing 5	F: 5'-TCACCTTACTAAGGGATGCGATAAAAAGGA-3'
HK1 sequencing 6	F: 5'-CGGGCTATCCTCCAGCAGCTAG-3'
Bcl-2 sequencing 1	F: 5'-CTGTGGCTAACTAGAGAACC-3'
Bcl-2 sequencing 2	R: 5'-CGCGGCGCCCACATCT-3'
Bcl-2 sequencing 3	F: 5'-ATGGCGCACGCTGGGA-3'
Bcl-2 sequencing 4	F: 5'-TCGCCAGGACCTCGCC-3'

2.2.2. Preparation of bacterial culture plates with selective antibiotics.

500 ml LB (Luria Bertani) bacterial growth medium with agar (**chapter 2.1.**) were prepared and autoclaved. When the medium cooled to about 50°C, 25 µg/ml chloramphenicol (Sigma) or 30 µg/ml kanamycin (Sigma) were added, respectively, under semi-sterile conditions. The medium was carefully mixed by swirling. Around 25 ml of medium were poured into each of around twenty culture plates. After solidification of the medium, plates were inverted and stored at 4°C.

2.2.3. Preparation of fluid media for bacterial cultures.

Bacterial mini cultures were set up in 2 ml LB bacterial growth medium without agar (**chapter 2.1.**) with 25 µg/ml chloramphenicol (Sigma) or 30 µg/ml kanamycin (Sigma) as the selective antibiotic in glass test tubes. Bacterial midi cultures were set up in 200 ml LB bacterial growth medium with 25 µg/ml chloramphenicol (Sigma) or 30 µg/ml kanamycin (Sigma) as the selective antibiotic in glass Erlenmeyer flasks with baffles.

2.2.4. Generation of chemically competent bacteria.

Chemically competent bacteria were generated with a modified calcium chloride method. 2 ml LB bacterial growth medium (**chapter 2.1.**) were inoculated with *Escherichia coli* DH5 α under semi-sterile conditions and grown overnight in a horizontal shaker at 250 rpm and 37°C. 300 μ l of that culture were used to inoculate 30 ml LB bacterial growth medium in a glass Erlenmeyer flask with baffles. The culture was grown for around 2 to 3 h until it was visibly turbid. The culture was placed on ice for 10 min and then spun in a multi-purpose bench top centrifuge (Eppendorf, 5810R) for 5 min at 3000 x g and 4°C. The bacterial pellet was gently resuspended in 15 ml transformation solution 1 (**chapter 2.1.**) in a sterile 50 ml centrifuge tube and incubated on ice for 1 h. The culture was spun in a multi-purpose bench top centrifuge for 5 min at 3000 x g and 4°C. The bacterial pellet was gently resuspended in 2 ml of transformation solution 2 (**chapter 2.1.**) and incubated on ice overnight. 50 μ l aliquots were prepared in microfuge tubes and rapidly transferred to -80°C for storage.

2.2.5. Set up of bacterial cultures on culture plates from a glycerol stock.

The bacterial glycerol stock was thawed on ice. A sterile pipette tip was dipped into the glycerol stock once and used to streak bacteria onto a bacterial culture plate with the appropriate selection antibiotic under semi-sterile conditions. The culture plate was inverted and incubated at 37°C overnight.

2.2.6. Set up of bacterial mini cultures from bacterial colonies.

A sterile pipette tip was used to sample a single bacterial colony and to inoculate 2 ml LB bacterial growth medium (**chapter 2.1.**) with the appropriate selection antibiotic (**chapter 2.2.3.**) in a glass test tube under semi-sterile conditions. The test tube was covered and incubated overnight in a horizontal shaker at 250 rpm and 37°C.

2.2.7. Set up of bacterial midi cultures from mini cultures.

2 ml bacterial mini culture in a glass test tube were used to inoculate 200 ml LB culture medium (**chapter 2.1.**) with appropriate selection antibiotic (**chapter 2.2.3.**) in a glass Erlenmeyer flask with baffles under semi-sterile conditions.

The flask was covered and incubated overnight in a horizontal shaker at 250 rpm and 37°C.

2.2.8. Plasmid midi preparation.

Plasmid midi preparations were performed with the Qiagen Plasmid Midi Kit (Qiagen) according to the manufacturer's instructions. 200 ml bacterial culture were transferred into a 250 ml screw cap centrifuge bottle and spun for 15 min at 5,000 rpm and 4°C in a high performance centrifuge (Sorvall, RC5C with GSA rotor). The bacterial pellet was resuspended in 5 ml ice-cold resuspension buffer (P1; **chapter 2.1.**) and transferred into 50 ml screw cap centrifuge tubes. 5 ml lysis buffer (P2; **chapter 2.1.**) were added and mixed by inversion of the centrifuge tube. The mixture was incubated for 5 min at room temperature. 5 ml ice-cold neutralization buffer (P3; **chapter 2.1.**) were added and mixed by inversion of the centrifuge tube. The centrifuge tube was incubated on ice for 15 min. Subsequently, the tube was centrifuged in a high performance centrifuge (Sorvall, RC5C with SS-34 rotor) for 30 min at 20,000 x g and 4°C. The supernatant was transferred into another centrifuge tube and respun for 15 min at 20,000 x g and 4°C. The supernatant was loaded into a QIAGEN-tip 100 DNA-binding column (Qiagen) that had previously been equilibrated with equilibration buffer (QBT; **chapter 2.1.**). The column was washed twice with 10 ml wash buffer (QC), and eluted with 5 ml elution buffer (QF; **chapter 2.1.**). The eluate was mixed with 3.5 ml room temperature isopropanol and divided equally between 6 microfuge tubes. The microfuge tubes were spun in a benchtop centrifuge (Eppendorf, 5415R) for 30 min at maximum speed and 4°C. The supernatant was discarded. 200 µl 70% ethanol were added to the pellet. The microfuge tubes were spun in a benchtop centrifuge for 10 min at maximum speed and 4°C. The supernatant was discarded. The pellet was air dried for about 10 min until the colour of the pellet changed from white to transparent. The pellet was resuspended in 120 µl nuclease-free water (HyClone).

2.2.9. Measurement of DNA concentration and purity.

A DNA solution of unknown concentration was diluted 1:100 in water. The absorbance at 260 nm (A_{260}) and 280 nm (A_{280}) was measured in a spectrophotometer (Jenway, Genova) with water as a reference. The concentration of the DNA was calculated according to the following formula:

$$[\text{DNA}] (\mu\text{g/ml}) = A_{260} \times \text{dilution factor (here: 100)} \times 50 \mu\text{g/ml}$$

The purity of the DNA (p_{DNA}) was calculated as:

$$p_{\text{DNA}} = A_{260} / A_{280}$$

2.2.10. Polymerase chain reaction (PCR) with Pfx polymerase.

DNA templates were amplified according to the following protocol:

- 5.0 μl 10X Pfx amplification buffer (Invitrogen)
- 1.0 μl 50 mM MgSO_4 (Invitrogen)
- 1.5 μl 10 mM dNTP mixture (Invitrogen)
- 1.0 μl 200 ng DNA template
- 1.5 μl 10 mM forward primer (IDT; **table 2.1.**)
- 1.5 μl 10 mM reverse primer (IDT; **table 2.1.**)
- 0.5 μl Platinum Pfx DNA polymerase (Invitrogen)
- 38.0 μl nuclease-free water (HyClone)

The PCR was run in a thermocycler (Eppendorf, Mastercycler ep gradient S) under the following conditions: one cycle of 95°C for 2 min; fourty cycles of 95°C for 1 min, 55°C for 1 min and 68°C for 1 min per kb of DNA template; one cycle of 68°C for 10 min; hold at 4°C.

2.2.11. Agarose gel electrophoresis.

1% w/v agarose (Invitrogen) was added to TAE buffer (**chapter 2.1.**) and boiled until it was completely dissolved. 0.5 $\mu\text{g/ml}$ ethidium bromide (Sigma) were added and uniformly mixed. The solution was poured into a gel caster, and a comb for the appropriate size of loading pockets was inserted. After polymerization, the gel was submerged in TAE buffer (**chapter 2.1.**). The DNA samples were mixed with 6X DNA gel loading buffer (**chapter 2.1.**) and loaded into the loading pockets. A 1 kb (New England Biolabs) or 100 bp (Invitrogen) DNA size marker was loaded into a separate pocket.

The gel chamber was closed and a voltage of 100 V was applied. Samples were run through the gel matrix until the bromophenol blue band originating from the loading buffer covered around 75% of the total gel length. The gel was visualized with an ImageQuant300 UV light box with a digital camera (GE).

2.2.12. Polymerase chain reaction (PCR) purification.

DNA fragments were purified with the QIAquick PCR Purification Kit (Qiagen) according to the manufacturer's instructions. 250 μ l DNA resuspension buffer (PB; **chapter 2.1.**) were added to 50 μ l PCR product and mixed. The mixture was loaded into a DNA binding QIAquick spin column (Qiagen) that was placed into a 2 ml collection tube (Qiagen). The column was spun in a bench top centrifuge (Eppendorf, 5415R) for 1 min at maximum speed. The flow-through was discarded and the QIAquick spin column was placed back into the collection tube. The column was washed twice with 750 μ l wash buffer (PE; **chapter 2.1.**). At each wash step the column was spun in a bench top centrifuge for 1 min at maximum speed, and the flow-through discarded. The QIAquick spin column was then placed into a new microfuge tube. The column was incubated with 32 μ l of elution buffer (EB; **chapter 2.1.**) for 1 min and then spun in a benchtop centrifuge for 1 min at maximum speed.

2.2.13. Preparative restriction digest.

To prepare DNA fragments for ligation reactions, purified PCR products that constituted the insert were digested according to the following protocol:

- 14 μ l insert DNA
- 2 μ l 10X NEBuffer (New England Biolabs)
- 1 μ l restriction enzyme 1 (New England Biolabs)
- 1 μ l restriction enzyme 2 (New England Biolabs)
- 2 μ l nuclease-free water (HyClone)

The target vector was digested according to the following protocol:

- 8 μ l vector DNA
- 2 μ l 10X NEBuffer (New England Biolabs)
- 1 μ l restriction enzyme 1 (New England Biolabs)
- 1 μ l restriction enzyme 2 (New England Biolabs)
- 8 μ l nuclease-free water (HyClone)

If both restriction enzymes exhibited maximal performance in the presence of BSA, 2 µl of water were replaced with 2 µl of a 1:10 dilution of a 10 mg/ml BSA solution (New England Biolabs). The reactions were incubated for a minimum of 2 h or overnight at 37°C. The vector was digested a second time by adding an additional 1 µl of each enzyme and incubated at 37°C for a minimum of two additional hours.

2.2.14. Preparative agarose gel electrophoresis.

An agarose gel with larger loading pockets was prepared for preparative gel electrophoresis and run in fresh TAE buffer (**chapter 2.1.**) under the conditions described in **chapter 2.2.11.** The gel was visualized on a UV light box (UVP) and the respective band was excised with a clean scalpel or razor blade and transferred to a microfuge tube.

2.2.15. DNA isolation from excised gel fragments.

DNA fragments were purified from agarose gel fragments with the QIAquick gel extraction Kit (Qiagen) according to the manufacturer's instructions. The gel fragments in microfuge tubes were submerged in 600 µl of agarose gel dissolution buffer (QG; **chapter 2.1.**) and placed in a 50°C water bath until they were completely dissolved. During incubation, the microfuge tubes were vortexed every 2 to 3 min. If the buffer had a pH>7.5 after dissolution of the gel slice, indicated by orange to violet colour, 10 µl 3 M sodium acetate, pH=5.0, were added. If the DNA fragments in solution were larger than 4 kb or smaller than 500 bp in size, an additional 200 µl isopropanol were added to the mixture. Finally, 750 µl of the mixture were loaded into a DNA binding QIAquick spin column (Qiagen) that was placed into a 2 ml collection tube (Qiagen). The column was spun in a bench top centrifuge (Eppendorf, 5415R) for 1 min at maximum speed. The flow-through was discarded and the QIAquick spin column was placed back into the collection tube. The second part of the DNA mixture was loaded in the same manner. Then the column was washed once with 500 µl agarose gel dissolution buffer (QG) and twice with 750 µl wash buffer (PE; **chapter 2.1.**). At each wash step the column was spun in a bench top centrifuge for 1 min at maximum speed, and the flow-through discarded. The QIAquick spin column was then placed into a new microfuge tube.

To elute the DNA, the column was incubated in 34 μl of elution buffer (EB; **chapter 2.1.**) for 1 min and then spun in a benchtop centrifuge for 1 min at maximum speed. The DNA in the flow-through was collected in the microfuge tube.

2.2.16. Ligation.

Reactions for the ligation of digested and purified DNA fragments were set up according to the following protocol:

- 17 μl 3:1 molar ratio of insert to vector DNA
- 2 μl 10X T4 DNA ligase buffer (New England Biolabs)
- 1 μl T4 DNA ligase (New England Biolabs)

The molar ratio of insert to vector DNA was estimated from fragment size and band intensity on an agarose gel. An additional reaction mixture, in which the insert DNA solution was replaced with water, was set up to control re-ligation of the empty vector. The reactions were incubated for 10 min at room temperature. 10 μl of the reaction were transformed into 100 μl competent *Escherichia coli* DH5 α and then plated on bacterial culture plates with appropriate selection antibiotic (**chapter 2.2.2.**).

2.2.17. Transformation of bacteria.

Escherichia coli DH5 α competent bacteria (**chapter 2.2.3.**) were thawed on ice. 10 μl of ligation reaction were mixed with 100 μl competent bacteria under semi-sterile conditions. 5 μl plasmid generated in PCR reactions were mixed with 100 μl bacteria, and 2 μl of plasmid mini or midi preparations were mixed with 50 μl bacteria. The bacteria plasmid mixture was incubated for 5 min on ice, heat-shocked for 1 min at 42°C in a water bath and then incubated on ice for another 3 min. Bacteria were transferred to 1 ml LB bacterial growth medium (**chapter 2.1.**) in a microfuge tube and incubated in a horizontal shaker at 250 rpm and 37°C for 1 h. Starter cultures that were intended to grow on culture plates were spun in a benchtop centrifuge (Eppendorf 5415R) for 1 min at maximum speed. The supernatant was removed, and the bacterial pellet was resuspended in 100 μl of culture medium and transferred to a bacterial culture plate with the appropriate selection antibiotic (**chapter 2.2.2.**). Bacteria were spread with a sterile Drigalski spatula (Fisher).

Bacterial culture plates were inverted and incubated overnight in a 37°C incubator. To set up plasmid mini preparations, the starter culture of transformed bacteria was transferred to 1 ml of LB bacterial growth medium with the appropriate selection antibiotic (**chapter 2.2.3.**) in a glass test tube. The tube was covered and incubated overnight in a horizontal shaker (Barnstead Labline MaxQ4000) at 250 rpm and 37°C. To set up plasmid midi preparations, the bacteria were transferred to 200 ml LB bacterial growth medium with the appropriate selection antibiotic in a glass Erlenmeyer flask with baffles. The flask was covered and incubated overnight in a horizontal shaker at 250 rpm and 37°C.

2.2.18. Analytical polymerase chain reaction (PCR) from bacterial colonies.

Analytical PCRs from bacterial colonies were set up according to the following protocol:

- 2.5 µl 10X ThermoPol reaction buffer (New England Biolabs)
- 0.5 µl 10 mM dNTP mixture (Invitrogen)
- 0.5 µl 10 mM forward primer (IDT; **table 2.1.**)
- 0.5 µl 10 mM reverse primer (IDT; **table 2.1.**)
- 0.125 µl *Taq* DNA polymerase
- 20.875 µl nuclease-free water (HyClone)

One bacterial colony from a culture plate was sampled with a sterile tip and dipped into the PCR mixture to provide the plasmid DNA template for the PCR reaction. Finally, the infected tip was used to inoculate 2 ml sterile LB culture medium with the appropriate selection antibiotic in a glass test tube to set up a plasmid mini preparation. The PCR was run in a thermocycler (Eppendorf, Mastercycler ep gradient S) under the following conditions: one cycle of 95°C for 30 s; forty cycles of 95°C for 30 s, 55°C for 1 min and 72°C for 1 min per kb of DNA template; one cycle of 72°C for 10 min; hold at 4°C.

2.2.19. Plasmid mini preparations.

2 ml overnight culture were transferred to a microfuge tube and spun in a benchtop centrifuge (Eppendorf 5415R) for 1 min at maximum speed. The supernatant was removed. The bacterial pellet was resuspended in 100 µl resuspension buffer (P1; **chapter 2.1.**). 100 µl lysis buffer (P2; **chapter 2.1.**) were added and mixed by inversion of the microfuge tube.

The mixture was incubated for 5 min at room temperature. 100 µl neutralization buffer (P3; **chapter 2.1.**) were added and mixed by inversion of the microfuge tube. The microfuge tube was centrifuged in a bench top centrifuge for 1 min at maximum speed. The supernatant was transferred to another microfuge tube. 250 µl Tris-buffered phenol (Invitrogen) were added and mixed. The microfuge tubes were spun in a bench top centrifuge (Eppendorf, 5415R) for 1 min at maximum speed. The upper aqueous phase was transferred into another microfuge tube. 500 µl 100% ethanol were added and mixed. Microfuge tubes were spun in a bench top centrifuge for 10 min at maximum speed and 4°C. The supernatant was discarded. 70% ethanol was added to the pellet. The microfuge tube was spun in a benchtop centrifuge for 1 min at maximum speed and 4°C. The supernatant was removed. The pellet was air dried for about 10 min until the colour of the pellet changed from white to transparent. The pellet was resuspended in 20 µl of resuspension buffer (**chapter 2.1.**).

2.2.20. Analytical restriction digest.

Analytical restriction digests of plasmids isolated through plasmid mini preparations were set up according to the following protocol:

- 1.0 µl 10X NEBuffer (New England Biolabs)
- 2.0 µl plasmid DNA
- 0.3 µl restriction enzyme 1 (New England Biolabs)
- 0.3 µl restriction enzyme 2 (New England Biolabs)
- 7.4 µl nuclease-free water (HyClone)

For an analytical restriction digest of plasmids isolated through plasmid midi preparations 1 µl plasmid DNA and 8.4 µl of water were used instead. If both restriction enzymes exhibited maximal performance in the presence of BSA, 1 µl of water was replaced by 1 µl of a 1:10 dilution of a 10 µg/ml BSA (New England Biolabs) solution. The mixture was incubated at 37°C for 1 h.

2.2.21. Preparation of DNA samples for sequencing.

Sequencing primers were designed for approximately every 500 bp fragment of the region of interest. The first primer annealed 100 bp upstream of the region of interest (**table 2.1.**)

The primers were used to run the chain termination reaction with DYEnamic ET Terminator Cycle Sequencing Kit (Amersham Biosciences) according to the manufacturer's instructions. The reaction mixture consisted of:

- 12 μ l 500 ng plasmid DNA in nuclease-free water (HyClone)
- 1 μ l 5 μ M sequencing primer (**table 2.1.**)
- 8 μ l DYEnamic ET reagent mix (Amersham Biosciences)

The reaction was incubated in a thermocycler (Eppendorf, Mastercycler ep gradient S) for 30 cycles of the following conditions: 95°C for 20 s, 50°C for 15 s, and 60°C for 1 min, followed by a hold at 4°C. The reaction was transferred to a microfuge tube. 2 μ l 7.5 M ammonium acetate and then 55 μ l of 100% ethanol were admixed to the reaction. The microfuge tubes were spun in a bench top centrifuge (Eppendorf, 5415R) for 15 min at 12,000 rpm and 4°C. The supernatant was aspirated. The pellet was washed with 100 μ l 70% ethanol and spun for 5 min at 12,000 rpm and 4°C. The supernatant was aspirated. The pellets were air-dried for approximately 10 min and then stored at -20°C in the dark until sequencing was performed. Samples were run on a Sanger DNA sequencer (Applied Biosystems, 3730) by the Sequencing Service of the Molecular Biology Service Unit at the University of Alberta.

2.2.22. Site directed mutagenesis of plasmid constructs.

The HK1-GFP construct was used as the template to generate the expression construct for inactive HK1S603A-GFP according to the Stratagene protocol for site directed mutagenesis. The entire plasmid that contained the open reading frame of HK1-GFP was amplified with a pair of complementary primers that contained the S603A mutation and 21 bp upstream and downstream flanking regions (**table 2.1.**). The following reaction mixture was prepared:

- 5.0 μ l 10X Pfx amplification buffer (Invitrogen)
- 1.0 μ l 50 mM MgSO₄ (Invitrogen)
- 2.0 μ l 10 mM dNTP mixture (Invitrogen)
- 1.0 μ l 20 ng DNA template
- 1.25 μ l of 10 mM forward primer (IDT; **table 2.1.**)
- 1.25 μ l of 10 mM reverse primer (IDT; **table 2.1.**)
- 1.0 μ l Platinum Pfx DNA polymerase (Invitrogen)
- 37.5 μ l nuclease-free water (HyClone)

The reaction was run in a thermocycler (Eppendorf, Mastercycler ep gradient S) under the following conditions: one cycle of 95°C for 40 s; eighteen cycles of 95°C for 40 s, 63°C for 1 min and 68°C for 1 min per kb of DNA template; one cycle of 68°C for 10 min; hold at 4°C. The parental, non-mutated and methylated plasmid DNA was digested twice through the addition of 1 µl DpnI (Invitrogen) and incubation at 37°C for 30 min, while the mutated and non-methylated daughter DNA remained intact. 5 µl of the digest were transformed (**chapter 2.2.16.**) into 100 µl competent *Escherichia coli* DH5α (**chapter 2.2.2.**) and plated on bacterial culture plates with the appropriate selection antibiotic (**chapter 2.2.3.**).

2.2.23. Preparation of glycerol stocks.

For long term storage of all constructs, bacterial glycerol stocks were prepared by mixing 500 µl of a dense bacterial culture in LB medium with 500µl of a sterile 80% glycerol solution in water. The glycerol stocks were stored at -80°C.

2.3. Cell lines and cell culture.

2.3.1. Cell lines.

HeLa cells and U2OS cells were received from Dr. James Smiley, A549 cells from Dr. Michael Weinfeld, HEK293T cells from Dr. Deborah Burshtyn, and MEF and Bak^{-/-}, Bax^{-/-} DKO MEF cells from Dr. Michele Barry (University of Alberta, Edmonton, Alberta). All cells were cultured in 75 cm² canted neck culture flasks with vent cap (Corning) at 37°C and 5% CO₂ in a water jacketed CO₂ incubator (Thermo Electron Corporation, Forma Series II) in Dulbecco's Modified Eagle Medium with 4.5 g/l D-glucose and L-glutamine and sodium bicarbonate (Sigma, D5796) supplemented with 10% (v/v) fetal bovine serum (GIBCO), 50 U/ml penicillin and 50 µg/ml streptomycin (GIBCO). In addition, MEF and Bak^{-/-}, Bax^{-/-} DKO MEF cells were supplemented with 2 mM L-glutamine (GIBCO) and 1% (v/v) MEM non-essential amino acids (GIBCO).

2.3.2. Passaging.

The above listed adherent cell lines were passaged according to the following protocol in the sterile environment of a laminar flow hood. All media were warmed to 37°C in a water bath (Fisher, Isotemp 200).

Health and density of the cells was inspected with a light microscope (Zeiss, Axiovert 40C). The culture medium was aspirated, and the cells were washed with 10 ml sterile PBS by gently panning the culture flask. The PBS was aspirated and 3 ml 0.25% Trypsin-EDTA (GIBCO) were added and incubated with the cells for 5 to 10 min at 37°C in the incubator. Successful cell detachment was confirmed under the light microscope. 5 ml culture medium were added to the cells, and the surfaces of the flask were washed clean of cells. The cell suspension was transferred into a 15 ml centrifuge tube (Corning). The cells were spun in a multi-purpose bench top centrifuge (Eppendorf, 5810R) for 2 min at 1,000 x g and room temperature, and the culture medium was aspirated. The cell pellet was vigorously resuspended in 5 ml culture medium. 1 ml of cell suspension were retransferred into the original culture flask and supplemented with 14 ml fresh culture medium. Cells were split every three to four days. Culture flasks were regularly replaced and never used beyond ten passages.

2.3.3. Determination of the concentration of viable cells in a cell suspension.

Adherent cells were detached with Trypsin-EDTA prior to counting (**chapter 2.3.2.**). 10 µl of the cell suspension were mixed with 90 µl Trypan Blue (GIBCO). An improved Neubauer hemacytometer and coverslip (Hausser Scientific, Bright Line) were cleaned with water and 70% ethanol. The coverslip was firmly placed over the chamber of the hemacytometer until Newton's rings appeared. 10 µl of the cell suspension in Trypan Blue were loaded into each of the two chambers of the hemacytometer. The sum (s) of all cells that excluded Trypan blue from their cytoplasm and within the four corner squares of the nine square grid was determined under the light microscope (Zeiss, Axiovert 40C) for both chambers of the hemacytometer. The concentration of cells (c_{cells}) in the original cell suspension was calculated as

$$c_{\text{cells}} \text{ (cells/ml)} = (s_1 + s_2)/2 \times \text{dilution factor (here: } 10) \times 10^4/\text{ml}$$

2.4. Cell treatments.

Cells were treated with 20 ng/ml tumor necrosis factor alpha (TNF-α) (Roche) to induce NF-κB signaling or 20 ng/ml TNF-α and 5 µg/ml cycloheximide (CHX) (Sigma) to induce apoptosis. Control cells were treated with 5 µg/ml CHX.

For immunoprecipitations of the apoptotic complex II, cells were treated with 20 ng/ml TNF- α and 10 μ g/ml CHX (Sigma). 200 ng/ml anti-Fas human activating antibody (Millipore, mouse monoclonal antibody, clone CH11, #05-201), or 50 ng/ml recombinant soluble TNF-related apoptosis-inducing ligand (TRAIL) (Peptidech) were used to induce death receptor-mediated apoptosis.

The general caspase inhibitor z-VAD-fmk (R&D Systems) was dissolved in DMSO (Sigma) and added at a concentration of 25 μ M 2 h prior to treatment with TNF and CHX. Control cells were incubated with an equal volume of DMSO.

20 μ M or indicated concentration of CTZ (Sigma) in DMSO were added in serum-free culture medium to cells that were previously washed twice with serum-free culture medium. Control cells received an equal volume of DMSO in serum-free medium.

5 to 40 μ M HK1 amino-terminal peptide acetyl-MIAAQLLAYFTELKdA-GYGRKKRRQRRRG-amide (CanPeptide) or control peptide acetyl-GYGRKKRRQRRRG-dAEEEEAKNAAKLAVEILNKEKK-amide (Canpeptide) were added in serum-free culture medium to cells that were previously washed twice with serum-free culture medium.

In general, stimulations in twelve-well plates were performed in 500 μ l medium, and stimulations in six-well plates in 1 ml medium.

2.5. siRNA and siRNA screening.

2.5.1. siRNA transfections.

For transfections in ninety six-well format, 10 μ l of a 200 nM siRNA predilution in sterile nuclease-free water (HyClone) were spotted into each well. 15 μ l transfection mixture containing 0.2 μ l Dharmafect 1 transfection reagent (Dharmacon) and 14.8 μ l OptiMEM (GIBCO) per well were prepared and incubated for 5 min at room temperature. The transfection mixture was added to the siRNA in the ninety six-well plate. Both components were mixed by gently tapping the plate and incubated for 30 min at room temperature. Six thousand five hundred HeLa cells in 75 μ l antibiotic-free culture medium were added. The final siRNA concentration was 20 nM. Controls cells were not treated with siRNA or transfection reagent.

If the plate was not completely filled, surrounding wells were filled with 100 μ l sterile water to minimize edge effects. Cells were incubated for seventy two hours. For the parallel transfection of 2 siRNAs, 10 μ l of a predilution of 100 nM siRNA 1 and 100 nM siRNA 2 in water were spotted into each well. To transfect U2OS cells, water and OptiMEM were replaced by DMEM (Sigma, D5796). 0.375 μ l HiPerfect (Qiagen) were used as a transfection reagent, and three thousand cells were seeded into each well.

For siRNA transfections in twelve or six-well format, all volumes were scaled up by a factor of ten or twenty, respectively. However, all components were mixed in a microfuge tube, not directly in the well. 1×10^5 HeLa cells, four thousand eight hundred seventy five U2OS cells, or four thousand eight hundred seventy five A549 cells were seeded into twelve-well plates, and 2.25×10^5 HeLa cells into six-well plates. siRNA transfections in MEF were performed as described for HeLa cells with the exception that 7.5×10^4 cells were used per well of a twelve-well plate and 1.77×10^5 were used per well of a six-well plate.

For siRNA transfections that were followed by DNA transfections two days later, 1.125×10^5 HeLa cells were seeded into twelve-well plates and nine thousand HeLa cells were seeded into ninety six-well plates.

siRNA transfections for the NF- κ B reporter assay were done in three hundred eighty four-well format. Per well, 5 μ l of a 160 nM siRNA solution in OptiMEM were mixed and incubated with 5 μ l OptiMEM containing 0.0875 μ l Dharmafect 1 transfection reagent for 20 min at room temperature. The mix was spotted into a well of the three hundred eighty four-well plate. Three thousand five hundred HEK293T cells were added in 30 μ l antibiotic-free culture medium and incubated for forty eight hours, prior to the second transfection with reporter plasmids. The final siRNA concentration was 20 nM.

Table 2.2. List of siRNAs. (h): siRNA against human gene product, (m): siRNA against mouse gene product. HK1#1-3, HK2#1-3, and HK3#1-3 are part of the human kinase siRNA library V3. cm: chemical modification to preclude incorporation of the siRNA passenger strand into the RISC, suppl: supplier, Q: Qiagen, AB: Applied Biosystems.

target gene product	siRNA ID#	target sequence	cm	suppl
non-silencing (h/m)	AllStars negative control	proprietary	no	Q
non-silencing (h/m)	negative control #1 siRNA	proprietary	yes	AB
caspase-8 (h)	Hs_ CASP8_11_HP	AAGAGTCTGTGCCCAAATCAA	no	Q
NEMO (h)	139260	CACCTTACGCTTCAGCTGTTG	no	AB
HK1#1 (h)	1689	AAGGTATGAGAAGATGATCAG	no	AB
HK1#2 (h)	1506	CAGGAAGGAGATGAAGAATGG	no	AB
HK1#3 (h)	1599	AAGGAGATGAAGAATGGCCTC	no	AB
HK1#4 (h)	Hs_HK1_9	CACGATGTAGTCACCTTACTA	no	Q
HK1#5 (h)	Hs_HK1_10	CCGTGTCGTATGACCTAGTAA	no	Q
HK1#6 (h)	Hs_HK1_1	AACGGTGGAAATGCACAACAA	no	Q
HK1#7 (h)	Hs_HK1_11	TTGGTGGGTCTTCCTTTTCGAA	no	Q
HK2#1 (h)	1528	AAGGAGATGGAGAAAGGGCTT	no	AB
HK2#2 (h)	1433	AAGGTTGACCAGTATCTCTAC	no	AB
HK2#3 (h)	1618	AAGGATTTGTTACATGCATC	no	AB

HK3#1 (h)	210	GAGGTTTGAAAAGATGATCAG	no	AB
HK3#2 (h)	208	AAGGTGACAAGGGCACAGCTA	no	AB
HK3#3 (h)	144906	CACCCGCTTTGATGCAAGTGT	no	AB
HK4#1 (h)	1600	CAGCGTGAGCTAAGCACCAAA	no	AB
HK4#2 (h)	1507	GAGGACCTGAAGAAGGTGATG	no	AB
HK4#3 (h)	1690	CAGGACTTTGATGCATTTCCA	no	AB
TAB2 (h)	136741	proprietary	no	AB
TNF-R1 (h)	Hs_ TNFRSF1A_5	proprietary	no	Q
c-FLIP (h)	4822	CAGGGACCTTCTGGATATTTT	no	AB
GAPDH (h,m)	Hs_GAPD_5	CCGAGCCACATCGCTCAGACA	no	AB
HK1 (m)	s67555	TTGGATCTCGGAGGAACGAAT	yes	AB

2.5.2. GAPDH assay for the optimization of siRNA transfection efficiency.

Six thousand five hundred HeLa cells were plated into each well of a ninety six-well plate and transfected with GAPDH (Hs_GAPD_5; Qiagen) or non-silencing AllStars negative control siRNA (Qiagen) (**table 6.2**) as described (**chapter 2.5.1.**) with varying amounts of Dharmafect 1 transfection reagent. Each experimental condition was set up in duplicate. Three days after the transfection, the GAPDH assay was performed with the KDAlert GAPDH Assay Kit (Applied Biosystems) according to the manufacturer's instructions. Briefly, the culture medium was removed from the ninety six-well plate, and the cells were washed once with PBS. Then 200 μ l ice-cold KDAlert lysis buffer (Applied Biosystems) were added to each sample well, and the culture plate was incubated for 20 min at 4°C. The cell lysate was homogenized with five pipette strokes.

10 μ l of the homogenous lysate were transferred to a separate ninety six-well plate, mixed with 90 μ l KAlert Master Mix (88.8 μ l solution A, 0.68 μ l solution B, and 0.47 μ l solution C; Applied Biosystems) and the fluorescence resulting from GAPDH enzymatic activity in the lysates was immediately measured in a kinetic assay every min for 10 min in an EnVision plate reader (PerkinElmer) using a 544 nm excitation filter and a 590 nm emission filter. The fluorescence of each sample was graphed as a function of the time. The GAPDH activity in each sample was defined as the fluorescence increase over 4 min in the area of linear fluorescence increase.

$$\text{GAPDH activity} = \text{fluorescence}_{4 \text{ min}} - \text{fluorescence}_{0 \text{ min}}$$

The relative GAPDH activity (or GAPDH depletion through GAPDH siRNA) was calculated as the ratio of the GAPDH activity in samples that were treated with GAPDH siRNA and the GAPDH activity in samples that were treated with control siRNA.

$$\text{relative GAPDH activity} = \text{GAPDH activity}_{\text{GAPDH siRNA}} / \text{GAPDH activity}_{\text{control siRNA}}$$

The optimal balance factor (OBF) determined the transfection condition that yielded maximal GAPDH depletion and minimal transfection-related toxicity. The transfection-related toxicity is represented by the GAPDH activity in the cells transfected with control siRNA.

$$\text{OBF} = (1 - \text{relative GAPDH activity}) * \text{GAPDH activity}_{\text{control siRNA}}$$

2.5.3. High-throughput siRNA screen for modifiers of TNF-induced death.

The screen employed the human kinase siRNA library V3 and human phosphatase siRNA library V3 (Applied Biosystems) with three distinct siRNAs per gene target. Each library plate was complemented with control siRNAs as outlined in **figure 2.1.A**. Each source plate with controls was transfected in quadruplicate. With a multi-channel pipette 10 μ l of a 200 nM siRNA predilution in sterile nuclease-free water (HyClone) were spotted into each well. 15 μ l transfection mix containing 0.2 μ l Dharmafect 1 transfection reagent (Dharmacon) and 14.8 μ l OptiMEM (GIBCO) were prepared per well and incubated for 5 min at room temperature.

The transfection mixture was added to the siRNA in the ninety six-well plate with a multi-channel pipette. Both components were mixed by gently tapping the plate. The plates were incubated in a moist environment for 30 min at room temperature. Finally, Six thousand five hundred HeLa cells in 75 μ l antibiotic-free culture medium were added. The final siRNA concentration was 20 nM. Control cells were not treated with siRNA or transfection reagent. The cells were incubated for 72 h. Then two plates of the quadruplicate plate sets were treated with 20 ng/ml TNF and 5 μ g/ml CHX; two received fresh antibiotic-free culture medium only. Each well was incubated with a total of 100 μ l culture medium with TNF and CHX or without TNF or CHX for 13.5 h. 11 μ l of a 440 μ M resazurin sodium salt (Sigma) solution were added, mixed and incubated with the cells for an additional 1.5 h. Reduction of non-fluorescent resazurin into fluorescent resorufin by living cells was measured with an EnVision plate reader (PerkinElmer) using a 540 nm excitation filter and a 590 nm emission filter.

2.5.4. Screen analysis.

2.5.4.1. Plate normalization and data scoring.

Each raw fluorescence/viability value was normalized to the mean viability of the non-silencing siRNA controls of the same plate. Normalized viability values were then averaged for replicate plates. The death index was defined as the ratio of the mean viability without TNF or CHX to the mean viability with TNF and CHX. These steps assigned the non-silencing siRNA controls a death index of one. All genes were then sorted according to (1) their median viability in the absence of TNF or CHX, (2) their median viability in the presence of TNF and CHX, and (3) their median death index. Due to the skewedness of all three distributions, confidence intervals (CIs) were determined independently for genes with a greater or lower viability/death index than the non-silencing siRNA control, respectively. To this end, the standard deviation (stdev) of the median viabilities/death indices from the non-silencing siRNA control was determined for both groups. Confidence thresholds were set at a distance (d) from the non-silencing control that was calculated with the help of the tabulated x-values (x) of the Gaussian density function according to the desired level of confidence:

$$d = x * \text{stdev}$$

For example, genes with a median siRNA viability/death index greater than 2.48 standard deviations from the non-silencing control belonged in the 99% confidence interval group. Genes with a median siRNA viability/death index greater than 1.96 standard deviations from the non-silencing control belonged in the 95% confidence interval group.

2.5.4.2. Visualization of ninety six-well plates.

A combination of heat map and bubble chart was created with the Microsoft Office 2010 Excel software according to the instructions in the company Blog of XLCubed Ltd. [454].

2.5.4.3. Kernel density estimates for behaviour of positive controls.

Kernel density estimates for the histograms of all viability values and death indices of the positive controls caspase-8 and NEMO in the screen were generated with the web application [455, 456]. The optimized density estimation was visualized as a scatter chart with smooth lines using the Microsoft Office 2010 Excel software.

2.5.4.4. Heat maps of viability values and death indices in the screen.

All kinases and phosphatases were sorted according to the median death index in descending order. Viability values in presence and absence of TNF or CHX and death indices for all three siRNAs per gene were base two log-transformed and organized into one cluster in Cluster 3.0 software. All data were then visualized as a heat map with Java TreeView 1.1.6r2 software.

2.6. DNA transfection.

HeLa cells were detached with 0.25% Trypsin-EDTA (GIBCO) and counted. 1 ml HeLa cells were plated into the wells of a twelve-well plate at a concentration of 2×10^5 cells/ml. 2 ml of HeLa cells were plated into the wells of a six-well plate at a concentration of 2.5×10^5 cells/ml. The next day, transfection reagents were prepared in 2 microfuge tubes. For each well of a twelve-well plate, 125 μ l OptiMEM (GIBCO) and 1 μ g DNA were mixed in one tube. 125 μ l OptiMEM and 2 μ l Lipofectamine 2000 (Invitrogen) were mixed in a separate tube. For each well of a six-well plate, 250 μ l OptiMEM and 2 μ g DNA were mixed in one tube. 250 μ l OptiMEM and 4 μ l Lipofectamine 2000 were mixed in a separate tube.

Both microfuge tubes were incubated for 5 min at room temperature. The contents of both tubes were then mixed and incubated for an additional 20 min. The cells in twelve-well plates were washed with 500 μ l sterile PBS and incubated with 250 μ l OptiMEM until transfection. The cells in six-well plates were washed with 1 ml sterile PBS, and incubated with 500 μ l OptiMEM. Finally, 250 μ l or 500 μ l transfection mixture were added dropwise to the cells in a twelve-well plate or six-well plate, respectively, and gently mixed. The cells were incubated in the transfection mixture for a minimum of two hours and a maximum of five hours. Then 500 μ l or 1 ml antibiotic-free culture medium with 20% FBS were added to the cells in a twelve-well or six-well plate, respectively, and gently mixed. The cells were incubated overnight.

HeLa cells in twelve-well plates that had been transfected with siRNA for two days were transfected with 2 μ g DNA in 125 μ l OptiMEM and 3 μ l Duo Transfection Reagent (Dharmacon). Cells were incubated for five hours before 500 μ l antibiotic-free culture medium with 20% FBS were added. For sequential siRNA and DNA transfections in ninety six-well format all volumes were scaled by a factor of 0.1. To transfect the NF- κ B reporter plasmid pNF- κ Bluc and control reporter pRL-TK into HEK293T cells in three hundred eighty four-well plates, 25 μ l of the siRNA transfection mix were aspirated and the remaining 15 μ l were supplemented with 10 μ l of a reporter transfection mix. The reporter transfection mix consisted of 1 μ g NF- κ B reporter pNF- κ Bluc and 0.1 μ g control reporter pRL-TK in 5 μ l OptiMEM and 0.075 μ l Lipofectamine 2000 in 5 μ l OptiMEM, mixed and incubated for 20 min. After six hours, cells were recovered with 10 μ l culture medium with 20% fetal bovine serum (Sigma).

2.7. Microscopy.

2.7.1. Light Microscopy.

1 ml of a HeLa cell suspension at a concentration of 4×10^5 cells/ml were plated into a twelve-well plate to visualize apoptosis. The following day, the cells were pre-treated with 25 μ M z-VAD-fmk or an equal amount of DMSO for two hours in complete culture medium. Cells were then treated with combinations of 20 ng/ml TNF and 5 μ g/ml CHX in complete culture medium in addition to z-VAD-fmk or DMSO for ten hours.

HeLa cells that were treated with siRNAs before the visualization of their apoptotic state were plated as 1×10^5 cells per well and transfected with siRNAs as described (**chapter 2.5.1.**). After seventy two hours cells were treated with 20 ng/ml TNF and 5 μ g/ml CHX for 5 h in culture medium without antibiotics or with fresh culture medium without antibiotics only.

Cell morphology was visualized with an inverted transmitted light microscope (Zeiss, Axiovert 40C). Images were recorded with a digital camera (Canon, PowerShot S2 1S) that was connected through a conversion lens adapter (Canon, LA-DC58E) and the ZoomBrowser EX 6.6 software (Canon).

2.7.2. Confocal Immunofluorescence Microscopy.

1 ml HeLa cells were plated onto round sterile coverslips (22 mm diameter, 0.16-0.19 mm thickness, Electron Microscopy Sciences, 72224-01) in the wells of a twelve-well plate at a concentration of 3.5×10^5 cells/ml. The following day, the cells were treated with 5 μ M to 40 μ M HK1 peptide or control peptide in serum-free culture medium for one hours after two washes in serum-free culture medium, if needed. The culture medium was aspirated and replaced with culture medium that contained 2 nM MitoTracker Red to visualize mitochondria (Molecular Probes) and incubated for 30 min. The cells were washed twice in 1 ml 37°C PBS and subsequently fixed with 1 ml 2% formaldehyde (Sigma) in PBS for 15 min at room temperature. The cells were washed three times in 1 ml PBS for 5 min each. The cells were then permeabilized and blocked with 500 μ l saponin buffer (**chapter 2.1.**) three times for 5 min each. A 100 μ l drop of a 1:100 dilution of the rabbit anti-HK1 primary antibody (Cell Signaling, rabbit monoclonal, clone C35C4, #2024) in saponin buffer (**chapter 2.1.**) was placed onto parafilm in a moist chamber. The coverslip was then carefully removed from the twelve-well plate using high precision tweezers. Excess moisture from the coverslip was removed by touching the edge of the coverslip to a kimwipe (Kimtech Science). Finally, the coverslip was placed upside down onto the drop of primary antibody in the moist chamber and incubated for one hour at room temperature. The coverslip was then carefully retransferred into the twelve-well plate with the fixed cells facing up. The cells were then washed twice in 500 μ l saponin buffer (**chapter 2.1.**) for 5 min each.

A 100 μ l drop of a 1:1000 dilution of goat anti-rabbit secondary antibody (Molecular Probes, goat polyclonal conjugated to Alexa Fluor 488) and a 1:1000 dilution of the nucleic acid stain Hoechst 33258 (Molecular Probes) in saponin buffer (**chapter 2.1**) was placed on a second parafilm in a moist chamber. As described above, the coverslip was carefully positioned on the drop and incubated for 30 min in the dark at room temperature. The coverslip was carefully retransferred into the twelve-well plate with the fixed cells facing up and washed twice with 500 μ l saponin buffer for 5 min each. The stained cells were fixed with 2% formaldehyde in PBS for 15 min at room temperature and subsequently washed twice in 1 ml PBS for 5 min each. A microscope slide (Fisher) was cleaned with 70% ethanol. A drop of 12 μ l Fluoromount (Sigma) was placed in the center of the microscope slide. The coverslip was carefully removed from the twelve-well plate. Excess PBS was removed with a kimwipe. The coverslip was placed upside down onto the drop of Fluoromount while avoiding the formation of air inclusions. The slides were stored at 4°C and in the dark until visualization.

The slides were visualized in the Faculty of Medicine and Dentistry Core Imaging Facility, at the University of Alberta. Images were acquired with a spinning disc confocal fluorescence microscope integrated by Quorum Technologies based on an IX-81 microscope stand (Olympus), laser excitation from a Laser Merge Module (LMM5, Spectral Applied Research), and a CSU-X1 spinning disk confocal scan head (Yokogawa Electric Corporation). All images were taken at 60X magnification and recorded on an EMCCD (C9100-13, Hamamatsu Photonics), using Quorum WaveFX imaging software (Quorum Technologies Inc). The images were analyzed with Imaris software (Bitplane).

2.7.3. High-content fluorescence microscopy.

HeLa cells were plated into glass-bottom ninety six-well plates (PerkinElmer) at nine thousand cells per well, and duplicate samples were reverse transfected with siRNAs as described (**chapter 2.5.1.**). Two days after the siRNA transfection some of the cells were transfected with the pEGFP-N1 GFP expression construct as described (**chapter 2.6.**) On the following day, cells were fixed and stained. The culture medium was removed by inversion of the plate, and the cells were washed twice with 100 μ l 37°C PBS. The cells were fixed with 100 μ l 2% formaldehyde (Sigma) in PBS.

Cells were then washed three times in 100 μ l PBS for 5 min each. Cells were permeabilized and blocked with 100 μ l saponin buffer (**chapter 2.1.**) three times for 5 min each. 50 μ l of a 1:100 dilution of the rabbit anti-HK1 primary antibody (Cell Signaling, rabbit monoclonal, clone C35C4, #2024) in saponin buffer were added to each well. The plate was incubated for one hour at room temperature. The cells were then washed twice in 100 μ l saponin buffer for 5 min each. 50 μ l of a 1:1000 dilution of goat anti-rabbit secondary antibody (Molecular Probes, goat polyclonal conjugated to Alexa Fluor 488) and 1:1000 dilution of the nuclear stain Hoechst 33258 (Molecular Probes) in saponin buffer were added to the cells. Cells were incubated in the dark for 30 min. Cells were washed twice with 100 μ l saponin buffer for 5 min each. The stained cells were fixed with 100 μ l 2% formaldehyde in PBS for 15 min at room temperature and subsequently washed twice in 100 μ l PBS for 5 min each. Cells were stored in the dark at 4°C until visualization.

The plate surface was cleaned with 70% ethanol and visualized with the Operetta High Content Imaging System (PerkinElmer) and the Harmony high content imaging and analysis software (PerkinElmer).

2.8. Quantitative real-time PCR (qRT-PCR).

2.8.1. RNA purification.

2 ml HeLa cells were plated into six-well plates at a concentration of 4.75×10^5 cells/ml if the RNA extraction was planned for the subsequent day. To extract RNA from cells treated with siRNAs, 2.25×10^5 cells were plated into each well, transfected with siRNAs as described (**chapter 2.5.1.**) and incubated for 72 h. Two wells were set up per experimental condition. The cells were treated with 20 ng/ml TNF, if needed. The cells were washed once with 1 ml 37°C PBS, and 500 μ l TRIzol reagent (Invitrogen) were added directly into the well. The cells were incubated for 5 min at room temperature and the cell lysates were scraped off with a cell scraper (Fisher) and transferred into a microfuge tube. The lysates were spun in a bench top centrifuge (Eppendorf, 5415R) for 10 min at 12,000 x g and 4°C and the supernatant was transferred to another microfuge tube. 100 μ l chloroform (Fisher Scientific) were added, and the samples were shaken vigorously for 15 s.

The samples were incubated for 3 min at room temperature and then spun in a bench top centrifuge for 15 min at 12,000 x g and 4°C. The upper aqueous phase was carefully extracted using gel loading tips and transferred into a new microfuge tube. 250 µl isopropanol were added. The samples were incubated for 10 min at room temperature (or overnight at -20°C to maximize RNA yield) and then spun in a bench top centrifuge for 10 min at 12,000 x g and 4°C. The supernatant was discarded and the pellet was washed once with 75% ethanol and spun in a bench top centrifuge for 5 min at 7,500 x g and 4°C. The pellet was dissolved in 20 µl nuclease-free water (HyClone). 1 µl DNase 1 (Invitrogen) was added and mixed. The samples were incubated at 37°C for one hour to degrade residual DNA and stored at -20°C.

2.8.2. Measurement of RNA concentration and purity.

The absorbances at 260 nm (A_{260}) and 280 nm (A_{280}) of a 1:50 dilution of RNA in water were measured in a spectrophotometer (Jenway, Genova) with water as a reference. The concentration of the DNA (C_{RNA}) was calculated according to the following formula:

$$C_{RNA} (\mu\text{g/ml}) = A_{260} \times \text{dilution factor (here: 50)} \times 40 \mu\text{g/ml}$$

The purity of the DNA (p_{RNA}) was calculated as:

$$p_{RNA} = A_{260} / A_{280}$$

2.8.3. Synthesis of cDNA.

cDNA was generated from 5 µg template RNA with the qScript cDNA SuperMix (Quanta Biosciences) according to the following protocol:

- 16 µl 5 µg template RNA in nuclease-free water (HyClone)
- 4 µl 5X qScript cDNA SuperMix (Quanta Biosciences)

The mixture was incubated in a Mastercycler ep gradient S thermocycler (Eppendorf) under the following conditions: 25°C for 5 min, 42°C for 30 min, and 85°C for 5 min, followed by a hold at 4°C. The cDNA was diluted 1:4, 1:16, or 1:64 in nuclease-free water and stored at -20°C.

2.8.4. qRT-PCR with the SYBR green method.

For quantitative real-time PCR with the SYBR green method, the following reaction was set up in each well of a full-skirted 96-well PCR plate (twin.tec 0030132521; Eppendorf):

2.5 µl diluted cDNA

2.5 µl 1.6 µM of forward and reverse primer (IDT; **table 2.3.**)

5.0 µl 2X PerfeCTa SYBR Green FastMix (Quanta Biosciences)

Each sample was measured in technical triplicates for the gene of interest and the housekeeping gene actin. Transcript amplification was conducted and monitored with a realplex² PCR machine (Eppendorf) and realplex 2.2 software (Eppendorf) according to the following two-step PCR program: one cycle 95°C for 2 min; forty cycles of 95°C for 15 s and 60°C for 1 min. SYBR green fluorescence, which indicated the level of dsDNA, was measured at the end of each 60°C cycle. The fluorescence in all wells was graphed as a function of the cycle number, and a fluorescence threshold t was identified for the linear stages of DNA amplification. The corresponding cycle number was defined as the ct value of the respective well. The melting temperature was determined for each PCR product by increasing the temperature step-wise from 60°C to 95°C. Melting of the double-stranded PCR product was indicated by a sudden decrease of SYBR green fluorescence. The presence of a single fluorescence decrease across all temperatures confirmed the synthesis of only one specific PCR product.

The $\Delta\Delta ct$ method was used to calculate the expression levels of the gene of interest in each sample relative to the expression of the experimental control.

To calculate $\Delta\Delta ct$ values, the mean of the triplicate ct values for each target gene was determined. If one of the triplicate values differed from the other two values by more than a cycle, it was excluded from analysis, and the mean of the remaining two values was determined.

$$\text{Mean } ct = (ct_1 + ct_2 + ct_3)/3$$

Then the mean ct values for each gene of interest were normalized to the ct value of the house-keeping gene actin in the same sample.

$$\Delta ct_{\text{sample}} = \text{mean } ct_{\text{gene of interest sample}} - \text{mean } ct_{\text{actin sample}}$$

$$\Delta ct_{\text{control}} = \text{mean } ct_{\text{gene of interest control}} - \text{mean } ct_{\text{actin control}}$$

The Δct values of each gene of interest were then normalized to the experimental control.

$$\Delta\Delta ct = \Delta ct_{\text{sample}} - \Delta ct_{\text{control}}$$

Finally, the relative expression level of the gene of interest was calculated as:

$$\text{relative expression level}_{\text{gene of interest}} = 2^{-\Delta\Delta ct}$$

Table 2.3. List of primer sequences for qRT-PCR experiments.

Gene	Primer
<i>A20</i>	F: 5'-CTGCCCAGGAATGCTACAGATAC-3' R: 5'-GTGGAACAGCTCGGATTTTCAG-3'
<i>IKBA</i>	F: 5'-GATCCGCCAGGTGAAGGG-3' R: 5'-GCAATTTCTGGCTGGTTGG-3'
<i>HK1</i>	F: 5'-GGA CTGGACCGTCTGAATGT-3' R: 5'-ACAGTTCCTTCACCGTCTGG-3'
<i>HK2</i>	F: 5'-CCCCGGCAAGCAGAGGTTTCGAGAAA-3' R: 5'-CAGCAGGGCCAGGCAGTCACTCTCAA-3'
<i>actin</i>	F: 5'-AAGACCTGTACGCCAACAC-3' R: 5'-TCCACACGGAGTACTTGC-3'

2.8.5. qRT-PCR with the Taqman method.

For quantitative real-time PCR with the Taqman method, the following reaction was set up in each well of a full-skirted ninety six-well PCR plate (twin.tec, 0030132521; Eppendorf):

9 μ l diluted cDNA
10 μ l 2X Taqman Gene expression Master Mix (Applied Biosystems)
1 μ l 20X Taqman Gene Expression Assay (Applied Biosystems)

The Taqman Gene Expression Assay contained specific primers and Taqman probes for caspase-8 (Hs01018151_m1; Applied Biosystems) or GAPDH (Hs02758991_g1; Applied Biosystems). Sample and experimental control were set up as a triplicate measurement of the cDNA levels of caspase-8 and a triplicate measurement of the cDNA levels of the house-keeping gene GAPDH. Transcript amplification was conducted and monitored with a realplex² PCR machine (Eppendorf) and realplex 2.2 software (Eppendorf) according to the following 2-step PCR program: one cycle 50°C for 2 min; one cycle 95°C for 10 min; forty cycles of 95°C for 15 s and 60°C for 1 min. Taqman probe fluorescence, which indicated the level of specific PCR product, was monitored at the end of each 60°C cycle. The fluorescence in all wells was graphed as a function of the cycle number, and a fluorescence threshold t was identified for the linear stages of DNA amplification. The corresponding cycle number was defined as the ct value of the respective well.

The $\Delta\Delta ct$ method was used to calculate the expression levels of caspase-8 relative to GAPDH relative to the one of the samples with treated with non-silencing control siRNA as described (**chapter 2.8.4.**)

2.9. SDS-PAGE and Western blotting.

2.9.1. Sample preparation.

In general, Western blot samples were prepared from the lysates of a confluent cell population in one well of a twelve-well plate. To this end, 1 ml cells was plated at a concentration of 4×10^5 cells/ml if sample preparation was planned for the subsequent day. siRNA transfection or siRNA and DNA double transfection experiments cells were plated and transfected as described (**chapter 2.5.1.**)

Samples of cellular fractionation, complex II immunoprecipitation, and Bax cross-linking experiments were prepared as described (**chapter 2.10., 2.13.3., chapter 2.13.5.**)

If the cells were not apoptotic and did not detach, they were harvested according to the following protocol: The culture medium was aspirated, and the cells were washed once in 1 ml PBS. The plate was positioned on an ice bath, and 50 μ l lysis buffer 1 (**chapter 2.1.**) were added. The cells were incubated for 10 min and scraped from the well bottom with a cell scraper (Fisher) and transferred to a microfuge tube.

If the cells were apoptotic and began to detach, they were harvested according to the following protocol: The culture medium was collected into a microfuge tube. The cells were washed once in 500 μ l 37°C PBS, which was also collected in the microfuge tube. 250 μ l 37°C 0.25% Trypsin-EDTA (GIBCO) were added to the cells. The cells were incubated at 37°C in the incubator for 5 to 10 min. The detachment of cells was confirmed with a light microscope (Zeiss, Axiovert 40C). The mixture of detached cells, culture medium and PBS in the microfuge tube was spun in a bench top centrifuge (Eppendorf, 5415R) for 2 min at 1,000 x g and room temperature. The supernatant was aspirated until around 250 μ l supernatant remained in the microfuge tube. The 250 μ l of supernatant in the microfuge tube were used to wash the well and to transfer all cells into the microfuge tube. The microfuge tubes were then spun in a bench top centrifuge for 2 min at 1,000 x g and room temperature. The supernatant was carefully removed with a micropipette. The pellet was resuspended in 50 μ l lysis buffer 1 (**chapter 2.1.**). The cells were incubated for 10 min on ice.

The lysates were spun in a bench top centrifuge (Eppendorf, 5415R) for 5 min at maximum speed and 4°C. The soluble fraction of the lysates was transferred into a new microfuge tube with 80 μ l 2X sample buffer (**chapter 2.1.**) and boiled for 5 min. Samples that were intended to be probed with PARP1 antibody were boiled with a modified sample buffer that contained 8M urea (**chapter 2.1.**). Samples were stored at -20°C.

2.9.2. SDS-PAGE.

Proteins were separated by sodium dodecyl sulphate-polyacrylamide gel electrophoresis (SDS-PAGE) using the Mini-PROTEAN 3 system (Bio-Rad). All gels were prepared as 1.00 mm gels with the exception of the gels for Bax cross-linking experiments that required 0.75 mm gels.

The mixtures for resolving and stacking gel were prepared as listed in **table 2.4**. In general, 15-well gels were loaded with 15 μ l sample, and 10-well gels with 20 μ l sample. The gels were run with a constant current of 25 mA per gel. The gels were run until the visible bromophenol blue front reached the lower end of the glass plates.

Table 2.4. Components of resolving and stacking gels for SDS-PAGE.

component	resolving gel				stacking gel
	8%	10%	12%	13.5%	4%
water	1.7 ml	1.3 ml	1.0 ml	0.83 ml	2.0 ml
30% acrylamide: bisacrylamide (Bio-Rad)	1.3 ml	1.7 ml	2.0 ml	2.17 ml	496 μ l
1M Tris	pH=8.8 1.9 ml				pH=6.8 376 μ l
10% SDS	50 μ l				30 μ l
10% APS	50 μ l				30 μ l
TEMED (Sigma)	2 μ l				4 μ l

2.9.3. Transfer.

Proteins separated by SDS-PAGE were transferred to a nitrocellulose membrane by semi-dry transfer in a Trans-Blot SD Semi-Dry Transfer Cell (Bio-Rad). The stacking gel was removed before the transfer. The resolving gel, six equally sized sheets of chromatography paper (Fisher), and one nitrocellulose membrane, previously soaked in water, were placed into transfer buffer. The gel was carefully placed onto the nitrocellulose membrane on top of three sheets of chromatography paper on the cathode side of the transfer apparatus, and all bubbles were removed. The gel was covered with three sheets of chromatography paper. The transfer cell was closed by placing the anode plate over the gel sandwich. A constant voltage of 20 V was applied.

The current was set to 0.4 mA per gel. The time period of the transfer varied with the size of the proteins to transfer. Proteins smaller than 25 kD that were run on 13.5% gels were transferred for 15 min. Proteins larger than 80 kD that were separated on 8% gels were transferred for 30 min. Intermediate size proteins that were resolved on 10% or 12% gels were transferred for 20 min.

Polyacrylamid gels of Bax cross-linking experiments were transferred via wet-transfer in a Mini Transblot Cell (Bio-Rad). In contrast to the semi-dry transfer, the sandwich of chromatography paper, gel, nitrocellulose membrane, and chromatography paper was placed between two fiber pads of a gel holder cassette and inserted into the electrode module in the buffer tank. Thereby, the nitrocellulose membrane was positioned between gel and cathode (red). A constant voltage of 100 V was applied for 1 h.

2.9.4. Western blotting.

Nitrocellulose membranes were placed into a light-proof Western blot incubation box (LI-COR Biosciences) with PBS. The PBS was replaced by 4 ml blocking buffer (1:1 mixture of LI-COR blocking buffer (LI-COR Biosciences) and PBS). The membrane was incubated in blocking buffer for one hour at room temperature on an orbital shaker under gentle agitation. Subsequently, the blocking buffer was removed and mixed with 0.1% Tween-20 and primary antibodies according to the concentrations listed in **table 2.5**. The primary antibody solution was poured into the Western blot incubation box and incubated with the membrane for at least three hours at room temperature or overnight at 4°C on an orbital shaker. The primary antibody solution was removed and stored at 4°C for subsequent uses. The membrane was washed four times in PBT (**chapter 2.1.**) for 5 min each at room temperature and on an orbital shaker. The secondary antibody solution was prepared in PBT according to the concentrations listed in **table 2.5**. and incubated with the membrane for 30 min at room temperature on an orbital shaker. The membrane was washed 4 times in PBT for 5 min each on an orbital shaker. Finally, the membrane was rinsed once in PBS and incubated with PBS on an orbital shaker until visualization.

Visualization was conducted with the Aerius automated imaging system (LI-COR Biosciences) and Aerius 1.0 software (LI-COR Biosciences).

The stained membranes were scanned at 700 nm for Alexa Fluor 680 conjugated secondary antibodies and at 800 nm for Alexa Fluor 750 conjugated secondary antibodies. The resolution was set to 200 μ m, and the focus offset was 3.0 mm. The sensitivity of the detectors for the fluorescence emission was set to 7.5 initially and then modified according to the requirements of the individual blots.

Table 2.5. List of primary antibodies used in Western blots. M: mouse, R: rabbit, MC: monoclonal, PC: polyclonal.

antibody	type	source	dilution
P-I- κ B- α , S32/S36, 5A5	M, MC	Cell Signaling, #9246	1:2,000
P-JNK, pTPpY	R, PC	Promega, V7932	1:2,000
FADD, H-181	R, PC	Santa Cruz, sc- 5559	1:1,000
Bax, YTH-2D2	M, MC	Trevigen, 2282- MC-100	1:1,000
cytochrome c	M, MC	Millipore, MAB1800	1:1,000
caspase-8, 1C12	M, MC	Cell Signaling, #9746	1:1,000
caspase-9	R, PC	Cell Signaling, #9502	1:1,000
cleaved caspase-3, A175	R, PC	Cell Signaling, #9661	1:1,000
PARP1, C2-10*	M, MC	Trevigen, #4338- MC-50	1:2,000
HK1, C35C4	R, MC	Cell Signaling, #2024	1:1,000
HK2, C64G5	R, MC	Cell Signaling, #2867	1:1,000

VDAC1, 20B12	M, MC	Santa Cruz, sc-58649	1:1,000
actin, AC-40	M, MC	Sigma, A3853	1:5,000
pan-actin	R, PC	Cell Signaling, #4968	1:1,000
Tubulin, E7	M, PC	DSHB	1:1,000

*8M urea in sample buffer

Table 2.6. List of secondary antibodies used in Western blots. G: goat, WB: Western blot, IF: immunofluorescence.

antibody	fluorochrome	type	source	dilution
mouse IgG	Alexa Fluor 680	G	Molecular Probes, A21057	1:10,000
mouse IgG	Alexa Fluor 750	G	Molecular Probes, A21037	1:10,000
rabbit IgG	Alexa Fluor 680	G	Molecular Probes, A21076	1:10,000
rabbit IgG	Alexa Fluor 750	G	Molecular Probes, A21039	1:10,000

2.10. Cellular fractionation.

2 ml HeLa or A549 cells were plated into a six-well plate at a concentration of 4.75×10^5 cells/ml or 3×10^5 cells/ml, respectively, if the cellular fractionation was planned for the subsequent day. For experiments with siRNAs, 2.25×10^5 HeLa or 1.77×10^5 MEF cells were plated into each well of a six-well plate, transfected with siRNA as described (**chapter 2.5.1.**) and incubated for seventy two hours. An entire six-well plate was set up for each experimental condition. If required, cells were treated with 20 ng/ml TNF and 5 μ g/ml CHX, 20 μ M CTZ or the CTZ solvent DMSO in serum-free culture medium for one hour after two washes in serum-free culture medium, or 5 μ M to 40 μ M HK1 peptide or control peptide in serum-free culture medium for one hour after two washes with serum-free culture medium.

The cells were washed once in 37°C PBS and incubated with 37°C 0.25% Trypsin-EDTA (GIBCO) for 5 to 10 min at 37°C in the incubator. Cell detachment was confirmed with a light microscope (Zeiss, Axiovert 40C). All supernatants and cells were collected in a 50 ml centrifuge tube (Corning) and then spun in a bench top multi-purpose centrifuge (Eppendorf, 5810R) for 3 min at 1,000 x g and room temperature. The pellet was washed twice in 37°C PBS, resuspended and centrifuged for 2 min at 1,000 x g and room temperature. The cell pellet was resuspended in 1 ml hypotonic fractionation buffer (**chapter 2.1.**) and incubated on ice for 10 min. The cell suspension was then transferred to a pre-cooled 5 ml glass Potter-Elvehjem type tissue grinder with teflon pestle (Wheaton). The pestle was connected to a drill press (Caframo Wiarton, RZR1) rotating on level six for 30 s. The cells in suspension were lysed mechanically through the movement of the pestle against the tissue grinder. The lysis was supported by up and down strokes of the tissue grinder. Lysis was confirmed by inspection of 10 µl lysate with a light microscope (Zeiss, Axiovert 40C). The lysate was transferred into a pre-cooled microfuge tube, and unbroken cells and nuclei were precipitated through a 5 min spin in a bench top centrifuge (Eppendorf, 5415R) at 700 x g and 4°C. The supernatant was removed without touching the pellet and transferred to a new microfuge tube. The microfuge tube was respun in a bench top centrifuge for 5 min at 700 x g and 4°C. The supernatant was removed and transferred to a new microfuge tube. 50 µl supernatant were transferred to a separate microfuge tube and stored on ice as a control for the total lysed fraction without nuclei. The heavy membrane fraction containing the mitochondria was precipitated from the remaining supernatant with a 15 min spin in a bench top centrifuge at 7,000 x g and 4°C. The supernatant consisting of cytosol and the light membrane fraction/microsomes was removed without touching the pellet and transferred to another microfuge tube. To remove the majority of the light membrane fraction/microsomes the supernatant was spun in a bench top centrifuge for 30 min at maximum speed and 4°C. The supernatant was considered the cytosolic fraction and transferred to a new microfuge tube.

As an alternative to centrifugation in the bench top centrifuge, the samples were transferred to ultracentrifuge tubes (Beckman Coulter, 0.5 ml thickwall polyallomer open-top tube, 343777) and spun for one hour at 100,000 x g and 4°C in an ultracentrifuge (Beckman Coulter, Optima TLX Preparative Ultracentrifuge, 120K with TLA 120.1 rotor) to completely clear the cytosolic fraction of the light membrane fraction/microsomes. The cytosolic supernatant was transferred to a new microfuge tube. 100 µl of the pure or lightly contaminated cytosolic fraction were transferred to a new microfuge and stored on ice.

The heavy membrane/mitochondrial fraction was washed twice with 500 µl fractionation buffer (**chapter 2.1.**) and pelleted with a 10 min spin at 7,000 x g and 4°C. Finally, the fraction was resuspended in 50 µl fractionation buffer and stored on ice.

The protein content of all samples and fractions was measured with a ninety six-well Bradford assay (**chapter 2.11.**) and adjusted to the sample with the lowest concentration using fractionation buffer (**chapter 2.1.**). 6X sample buffer (**chapter 2.1.**) was added to all samples. The samples were boiled for 5 min and probed for the proteins of interest by Western blot analysis. VDAC1 served as a control for the heavy membrane/mitochondrial fraction and tubulin as a control for the cytosolic fraction.

2.11. 96-well Bradford assay.

The Bradford assay was performed in ninety six-well plates to determine the protein concentration of cell lysates. Each sample was measured in duplicate. Each sample well received 9 µl water and 1 µl homogenous cell lysate. Protein standards were prepared in three duplicate wells that received 1) 10 µl water, 2) 1 µl of a 1:10 dilution of 10 mg/ml BSA (New England Biolabs, equals 1 µg BSA), 3) 8 µl water and 2 µl of a 1:10 dilution of 10 mg/ml BSA (equals 2 µg BSA). 90 µl of a 1:4.75 dilution of Protein Assay Dye (Bio-Rad) were added to each well and carefully mixed with the protein solution by gently tapping the plate. The plate was incubated for 10 min at room temperature and measured with an Envision fluorescence plate reader (PerkinElmer) with a 590 nm monochromatic filter in absorbance mode.

The standard curve was generated in Microsoft Office 2010 Excel as a trend line of the absorbance (A_{590}) as a function of the amount of BSA (x) with a and b as factors that describe the slope and the y-intercept of the trend line, respectively.

$$A_{590} = ax + b$$

The protein concentration of experimental samples (C_{sample}) was calculated as:

$$C_{\text{sample}} (\mu\text{g}/\mu\text{l}) = (A_{590} - b)/a$$

2.12. NF- κ B reporter assay.

Three thousand five hundred HEK293T cells per well of a three hundred eighty four-well plate were transfected with siRNAs as described (**chapter 2.5.1.**). Each sample was set up in triplicate. 24 h after transfection of the cells with reporter plasmids (**chapter 2.6.**), 5 μl antibiotic-free culture medium with 160 ng/ml TNF were added to 35 μl culture medium in the wells. The cells were incubated with a final concentration of 20 ng/ml TNF for nine hours. Subsequently, 25 μl culture medium were aspirated from each well, and a Dual Glo luminescence assay (Promega) was performed with the exception of the use of half the recommended amount of STOP and Glo reagent. Briefly, the plate was incubated at room temperature for 5 min. Then 10 μl Dual Glo Luciferase Assay Reagent (Promega) were added. Plates were placed on an orbital shaker for 10 min. The luminescence derived from the NF- κ B-induced expression of Firefly luciferase (pNF- κ Bluc vector) was measured with an EnVision plate reader (PerkinElmer) using the settings for ultrasensitive luminescence. A 1:125 dilution of the Dual Glo Stop and Glo Reagent (Promega) in Dual Glo Stop and Glo Buffer (Promega) was prepared. 10 μl of the mixture were added to each well of the three hundred eighty four-well plate. The plate was incubated for 10 min and the luminescence from the constitutive expression of a thymidine kinase promoter-dependent Renilla luciferase (pRL-TK vector) was measured with an EnVision plate reader (PerkinElmer) using the settings for ultrasensitive luminescence. Induced NF- κ B activity was calculated as the difference of the ratio of the Firefly luminescence to Renilla luminescence between TNF-stimulated and unstimulated samples.

2.13. Assays for the detection of cell viability and death.

2.13.1. Resazurin viability assay.

The resazurin viability assay was performed as described (**chapter 2.5.4.**).

2.13.2. DNA staining with SYTO 60.

Cells in a ninety six-well plate that had been examined in a resazurin viability assay (**chapter 2.13.1.**) were washed once with 100 μ l PBS and then fixed with 100 μ l 2% formaldehyde (Sigma) in PBS for 15 min at room temperature. The cells were washed three times with 100 μ l PBS for 5 min each. All media were removed by inversion of the plate. The cells were stained with 100 μ l 250 nM SYTO 60 (SYTO Nucleic Acid Stain Sampler kit, Molecular Probes) in 50 mM Tris, pH=7.5 for 60 min at room temperature. The samples were washed two times with 100 μ l PBS for 5 min each. The SYTO 60 fluorescence was visualized with an Aerius automated imaging system (LI-COR Biosciences) and Aerius 1.0 software (LI-COR Biosciences) at 700 nm. The resolution was set to 200 μ m, and the focus offset was 3.0 mm. The sensitivity of the detectors for the fluorescence emission was set to 7.5 initially and then modified according to the requirements of the plate.

2.13.3. Immunoprecipitation of complex II.

1.125×10^5 HeLa cells were plated into the wells of a twelve-well plate and transfected with siRNAs as described (**chapter 2.5.1.**). A twelve-well plate of cells was set up for each experimental condition. Seventy two hours after transfection, the cells were treated with 20 ng/ml TNF and 10 μ g/ml CHX to induce complex II formation. The supernatant of one culture plate was transferred into a 50 ml centrifuge tube (Corning). All wells of the plate were washed with 1 ml 37°C PBS. The PBS was removed and added to the cell culture supernatant. 500 μ l 37°C 0.25% Trypsin-EDTA (GIBCO) were added to each well. The cells were incubated in Trypsin-EDTA for 5 to 10 min at 37°C in the incubator. Detachment of the cells was confirmed by visual inspection with a light microscope (Zeiss, Axiovert 40C). 500 μ l antibiotic-free culture medium were added to each well and used to transfer the detached cells to the 50 ml centrifuge tube that contained the original supernatant. The centrifuge tube was spun in a multi-purpose centrifuge (Eppendorf, 5810R) for 3 min at 1,000 x g and room temperature.

The cell pellet was resuspended in 5 ml 37°C PBS and respun under the same conditions. The cell pellet was resuspended in 1 ml ice-cold lysis buffer 2 (**chapter 2.1.**) and transferred to a microfuge tube. Microfuge tubes were incubated for 10 min on ice and spun in a bench top centrifuge (Eppendorf, 5415R) for 10 min at maximal speed and 4°C. The supernatant was transferred to a new microfuge tube. 100 µl of the supernatant were removed as the input control and mixed with 20 µl 6x sample buffer (**chapter 2.1.**) in separate microfuge tube. 5 µl (2 µg) anti-FADD antibody (Santa Cruz, rabbit polyclonal, H-181, sc-5559) were added to the remaining supernatant and rocked overnight at 4°C. A 1:1 slurry of sepharose beads coated with protein G (Sigma) in 70% ethanol was washed three times in 500 µl lysis buffer. The beads were then blocked with 5% BSA in lysis buffer overnight at 4°C. The following day, the beads were washed three times with 500 µl lysis buffer. Finally, the beads were resuspended 1:1 in lysis buffer. 1 mM fresh PMSF and 40 µl of the BSA-blocked beads in lysis buffer were added to the immunoprecipitation samples. The samples were rocked for one hour at room temperature and subsequently spun in a bench top centrifuge for 1 min at 500 x g and 4°C. The supernatant was removed with gel loading tips. The beads were washed three times with 500 µl lysis buffer. After the third wash, the lysis buffer was carefully removed and 35 µl 6X sample buffer were added. The samples were boiled for 10 min. 8 µl of input and immunoprecipitation samples were run on a 13.5% polyacrylamide gel and probed with an anti-FADD antibody (**table 2.5.**). 15 µl sample were run on a 12% polyacrylamide gel and probed with anti-caspase-8 antibody (**table 2.5.**), and 10 µl sample were run on an 8% polyacrylamide gel and probed with an anti-HK1 antibody (**table 2.5.**) as described (**chapter 2.9.2 to 2.9.4.**).

2.13.4. Bax translocalization to the mitochondria and mitochondrial cytochrome c release.

2.25×10^5 HeLa cells were plated into each well of a six-well plate and transfected with siRNAs as described (**chapter 2.5.1.**). An entire six-well plate was set up for each experimental condition. Seventy two hours after transfection, cells were treated with 20 ng/ml TNF and 5 µg/ml CHX. All subsequent steps are identical with the protocol for cellular fractionation (**chapter 2.10.**).

The isolated fractions were probed for VDAC1, tubulin, Bax and cytochrome c in Western blot analysis (**chapter 2.9.2 to 2.9.4.**).

2.13.5. Bax oligomerization at the mitochondria.

2.25×10^5 HeLa cells were plated into each well of a six-well plate, transfected with siRNAs as described (**chapter 2.5.1.**), and incubated for seventy two hours. An entire six-well plate was set up for each experimental condition. The cells were treated with 20 ng/ml TNF and 5 μ g/ml CHX, harvested, lysed mechanically, and the heavy membrane/mitochondrial fraction was isolated as described in **chapter 2.10.** The mitochondrial fraction was only washed once and then lysed in 500 μ l lysis buffer 3 (**chapter 2.1.**) The samples were incubated for 30 min on ice and then spun in a bench top centrifuge (Eppendorf, 5415R) for 10 min at maximal speed and 4°C. The supernatant was transferred to a new microfuge tube. The protein concentrations in each sample were measured and equalized as described in **chapter 2.11.** Each of the samples was split in half, one of the samples was treated with 1 mM of the cross-linker bismaleimido-hexane (BMH; Thermo Scientific) and the other one with the BMH solvent DMSO. A fresh 20 mM BMH stock was prepared for every experiment. The samples were rocked for one hour at room temperature. Then the cross-linking reaction was terminated by rocking the samples with 25 mM DTT for 15 min. The samples were spun in a bench top centrifuge for 5 min at maximal speed to precipitate any large complexes that may have formed during cross-linking. The supernatants were concentrated by acetone precipitation. Four sample volumes of -20°C acetone were added and mixed by vortexing. The samples were incubated for one hour at -20°C and subsequently spun in a bench top centrifuge for 10 min at 15,000 x g and 4°C. The supernatant was aspirated, and the pellet was air-dried. 60 μ l 2X sample buffer containing double the amount of β -mercaptoethanol (**chapter 2.1.**) were added. The samples were boiled for 5 min, and 15 μ l were run on a 10% 0.75 mm polyacrylamide gel. Proteins were separated by SDS-PAGE and transferred to a nitrocellulose membrane by wet transfer (**chapter 2.9.2.** and **2.9.3.**).

2.13.6. TMRE assay for the detection of the IMM potential.

1 ml HeLa cells at a concentration of 4×10^5 cells/ml were plated into each well of a twelve-well plate if the TMRE assay was planned for the subsequent day. 1 ml HeLa cells at a concentration of 2×10^5 cells/ml were plated into each well of a twelve-well plate two days prior to the TMRE assay if the cells were transfected with expression constructs as described (**chapter 2.6.**). For experiments with siRNAs, 1.125×10^5 HeLa cells or 7.5×10^4 MEF cells were plated into each well of a twelve-well plate, transfected with siRNA as described (**chapter 2.5.1.**) and incubated for seventy two hours. One well of a twelve-well plate was set up for each experimental condition in addition to one well of cells as a negative control for TMRE staining. In experiments with GFP expression constructs a separate well was set up as a positive control for GFP fluorescence in the absence of TMRE fluorescence. If needed, apoptosis was induced with 20 ng/ml TNF and 5 μ g/ml CHX. In the last hour of the experiment, the cells were first incubated with 1 μ M tetramethylrhodamine ethyl ester (TMRE, Molecular Probes) for 30 min at 37°C in the incubator and then harvested. If the cells were not apoptotic, the culture medium was aspirated, and TMRE was added in fresh culture medium. If the cells were apoptotic and began to detach, the culture medium in the well was not aspirated and 2 μ M TMRE were added in a volume that equalled the volume of the culture medium in the well. After incubation with TMRE, the culture medium was collected into a 5 ml round bottom tube (12 x 75 mm, 352054; Fisher) suitable for flow cytometry. The wells were washed once in 500 μ l 37°C PBS, which was also collected in the tube. 250 μ l 37°C 0.25% Trypsin-EDTA were added to the cells. The cells were incubated for 5 to 10 min at 37°C in the incubator, and the detachment of the cells was confirmed with a light microscope (Zeiss, Axiovert 40C). The supernatant in the tube was used to wash the well and to transfer all cells to the tube. The tubes were spun in a multi-purpose centrifuge (Eppendorf, 5810R) for 2 min at 1,000 x g and room temperature. The supernatant was carefully aspirated with a glass Pasteur pipette attached to a vacuum aspiration system. The pellet was washed with 1 ml room temperature PBS, respun for 2 min at 1,000 x g, and resuspended in 500 μ l PBS. The percentage of cells with a lower than healthy range of TMRE fluorescence per cell, was determined by flow cytometry (FACScan, Becton Dickinson) in the Faculty of Medicine and Dentistry Flow Cytometry Facility at the

University of Alberta. In cases cells were transfected with GFP expression constructs, the TMRE fluorescence was measured for the GFP-positive population. The level of TMRE fluorescence was detected through the FL-2 channel equipped with a 585 nm filter (42 nm band pass) and the level of GFP fluorescence through the FL-1 channel equipped with a 530 nm filter (30 nm band pass). Data were acquired on 10,000 cells with fluorescence at logarithmic gain and analyzed with the CellQuest software (BD Biosciences). TMRE negative cells were used for calibration.

2.13.7. DEVDase assay for detection of caspase activity.

1.125×10^5 HeLa cells were plated into twelve-well plates and transfected with siRNAs as described (**chapter 2.5.1.**). One well of a twelve-well plate was set up for each experimental condition. The cells were treated with 20 ng/ml TNF and 5 μ g/ml CHX to induce caspase activity. The culture medium was collected into a microfuge tube. The cells were washed once in 500 μ l 37°C PBS, which was also collected in the microfuge tube. 250 μ l 37°C 0.25% Trypsin-EDTA (GIBCO) were added to the cells. The cells were incubated at 37°C in the incubator for 5 to 10 min. The detachment of cells was confirmed with a light microscope (Zeiss, Axiovert 40C). The mixture of detached cells, culture medium and PBS in the microfuge tube was spun in a bench top centrifuge (Eppendorf, 5415R) for 2 min at 1,000 x g and room temperature. The supernatant was aspirated until around 250 μ l supernatant remained in the microfuge tube. The 250 μ l of supernatant in the microfuge tube were used to wash the well and to transfer all cells into the microfuge tube. The microfuge tubes were then spun in a bench top centrifuge for 2 min at 1,000 x g and room temperature. The supernatant was carefully removed with a micropipette. The pellet was resuspended in 100 μ l lysis buffer 4 (**chapter 2.1.**) The lysates were incubated on ice for 10 min and spun in a bench top centrifuge (Eppendorf, 5415R) for 10 min at maximum speed and 4°C. The supernatant was transferred to a new microfuge tube. The protein content of each sample was determined in a ninety six-well Bradford assay as described in **chapter 2.11.** A sample containing 100 μ g protein was incubated with 50 μ M of the synthetic caspase substrate Ac-DEVD-AMC (N-Acetyl-Asp-Glu-Val-Asp-7-amido-4-methylcoumarin; Enzo Life Sciences) in reaction buffer (**chapter 2.1.**) for 1 h at 37°C. Each reaction was set up in triplicate in a ninety six-well plate.

The caspase activity resulted in substrate processing that was measured as AMC fluorescence with F355 excitation and F460 emission filter in the plate reader Wallac Victor2 1420 (PerkinElmer). The data were collected with the Wallac 1420 Workstation software, version 2.0, release 7 (PerkinElmer).

2.13.8. Caspase and caspase substrate processing.

1.125×10^5 HeLa cells, four thousand eight hundred seventy five U2OS cells, or four thousand eight hundred seventy five A549 cells were plated into each well of a twelve-well plate and reverse transfected with siRNA as described (**chapter 2.5.1.**). One well of a twelve-well plate was set up for each experimental condition. Three days after transfection, cells were treated with 20 ng/ml TNF and 5 μ g/ml CHX to induce caspase and caspase substrate processing. Cells were harvested and lysed as described in **chapter 2.9.1.** SDS-PAGE and Western blot were run as described in **chapter 2.9.2.** to **2.9.4.** Western blots were probed with antibodies against caspase-8, caspase-9, cleaved caspase-3 and caspase substrate PARP1 (**table 2.5.**)

CHAPTER 3. DEVELOPMENT OF A HIGH-THROUGHPUT siRNA ASSAY FOR MODIFIERS OF TNF-INDUCED DEATH.

A version of this chapter has been published:

Schindler A, Foley E: A functional RNAi screen identifies hexokinase 1 as a modifier of type II apoptosis. *Cell Signal*. 2010. 22(9):1330-40.

The assay was used in the following publications:

Parsons BD, Schindler A, Evans DH, Foley E: A direct phenotypic comparison of siRNA pools and multiple individual duplexes in a functional assay. *PLoS One* 2009. 4(12):e8471.

Merenuik TR, Maranchuk R, Schindler A, Penner-Chea J, Freschauf GK, Hegazy S, Lai R, Foley E, and Weinfeld M: Genetic screening for synthetic lethal partners of polynucleotide kinase/phosphatase: potential for targeting SHP-1 depleted cancers. *Cancer Res*. 2012. 72(22):5934-44.

3.1. HeLa cells are a suitable system to examine TNF-induced death.

Elevated or decreased levels of TNF-induced apoptosis are the cause of numerous inflammatory and cancerous diseases [20, 54, 457, 458]. Thus, there is a clear need to identify cellular proteins that regulate cell fate in the presence of TNF. siRNA technologies are an excellent tool to address that problem as siRNA allows the rapid generation of transient protein depletion “mutants” in cell culture, whose behaviour in the context of TNF can be examined.

To this end, I first sought a cellular system with TNF receptor expression and accessibility to siRNA that faithfully reproduced prominent features of signal transduction in response to TNF. My choice fell onto the first and most widely used human cancer cell line HeLa. HeLa cells originate from an adenocarcinoma, a rare cancer of the mucus-producing gland cells of the epithelium of the endocervix [459, 460]. They are characterized by high TNF receptor expression [461] and are easily accessible to siRNA transfections with lipid reagents [437]. Soluble TNF is an excellent tool to specifically activate TNF-R1, and not TNF-R2 signaling [69, 70].

I initially determined whether my stock of HeLa cells reproduced established features of the TNF-R1 signaling pathway. Specifically, I tested whether TNF activated NF- κ B, MAPK, and caspase signaling [52] and whether the activation of the caspases depended on weak NF- κ B-mediated gene expression [462].

In the absence of TNF, I- κ B- α sequesters dimers of NF- κ B in the cytoplasm by masking their nuclear localization signal [463-465]. TNF activates IKKs, which phosphorylate I- κ B- α at serine 32 and serine 36 [463, 465-468]. Phosphorylation of I- κ B- α triggers its ubiquitination and subsequent proteasomal degradation [465, 469]. Free NF- κ B dimers translocate to the nucleus and coordinate the transcription of a large number of target genes [97]. To test if TNF induced the NF- κ B signaling module, I stimulated HeLa cells with TNF and probed the lysates with an antibody specific for dual phosphorylated I- κ B- α on a Western blot (**figure 3.1.A**). As expected, TNF induced the rapid transient dual phosphorylation of I- κ B- α . I- κ B- α phosphorylation peaked ten minutes after the TNF stimulus and disappeared in the following ten minutes, most likely due to proteasomal degradation of I- κ B- α .

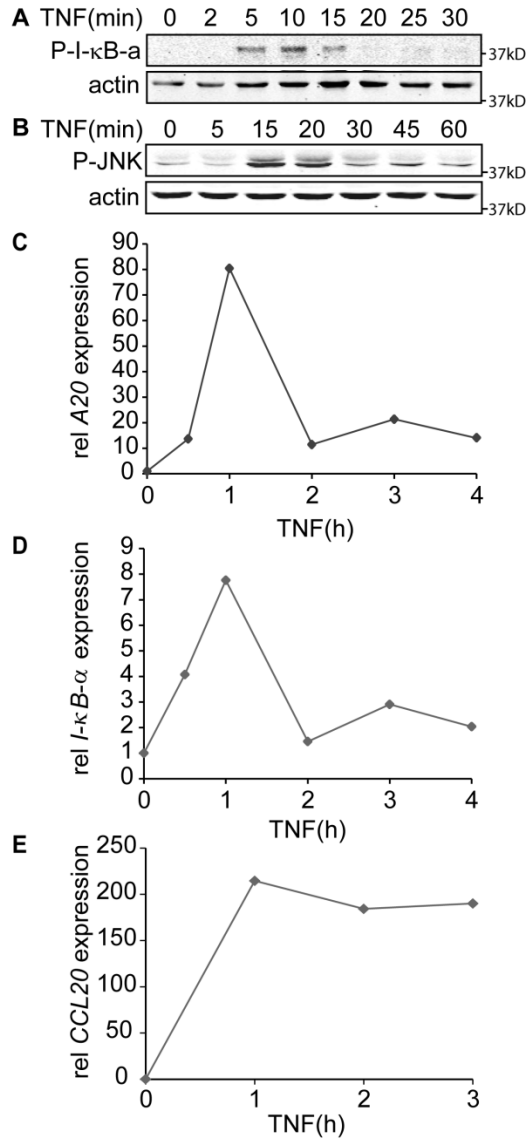


Figure 3.1. TNF activates NF-κB and JNK modules in HeLa cells. A-B: Western blots of the time course of I-κB-α (A) and JNK1 and JNK2 (B) phosphorylation after treatment of HeLa cells with TNF. Cell lysates were prepared at the indicated time points and probed with an antibody against phosphorylated I-κB-α (P-I-κB-α), phosphorylated JNK1 and JNK2 (P-JNK1/2), and actin as a loading control. **C-D:** Representative time courses of *A20* (C) and *IKBA* (D) gene expression after treatment of HeLa cells with TNF. Cellular cDNA was prepared at the indicated time points and probed with primers specific for *A20* and *IKBA* mRNA in quantitative real-time PCR. All values are expressed relative to actin mRNA levels. The basal gene expression level in untreated cells was assigned a value of one.

TNF also activates mitogen-activated protein kinase (MAPK) cascades, which includes activation of MKK7 and MKK4 [52] that in turn dually phosphorylate and activate JNK1 and JNK2 at threonine one hundred eighty three and tyrosine one hundred eighty five [130-133]. To test whether TNF induced JNK signaling in HeLa cells, I stimulated HeLa cells with TNF and probed the lysates with an antibody specific for phosphorylated JNK1 and JNK2 on a Western blot. As expected, TNF triggered the rapid transient phosphorylation of JNK1 and JNK2 (**figure 3.1.B**) [140, 470]. I observed maximum phosphorylation fifteen minutes after the TNF stimulus. Active JNK1 and JNK2 induce the AP-1 dependent expression of dual specificity protein phosphatases (DUSPs) that act in a negative feedback-loop to remove activating phosphate groups from JNK1 and JNK2 [471-475]. This is consistent with the gradual decline of phospho-JNK1 and JNK2 I observed over the forty five minutes that followed peak phosphorylation.

NF- κ B and AP-1 regulate the expression of a vast array of cell survival/anti-apoptotic, proliferatory, inflammatory, and auto-regulatory genes [104, 138]. Among the latter ones are the genes for I- κ B- α (*IKBA*) [476] and A20 (*A20*) [477]. A20 is a ubiquitin-editing enzyme that terminates NF- κ B activation [159]. It removes NEMO and RIPK1 K63-linked polyubiquitin chains and catalyses the formation of K48-linked polyubiquitin chains on RIPK1, which lead to RIPK1 proteasomal degradation [159]. To test whether TNF induced expression of these genes in HeLa cells, I stimulated the cells with TNF and isolated total cellular RNA. I then generated cDNA and probed it with primers specific for *A20* and *IKBA* mRNA by quantitative real-time PCR. **Figures 3.1.C** and **3.1.D** demonstrate the increased expression of *A20* and *IKBA* after continuous exposure of HeLa cells to TNF. In line with previous findings [478], both genes exhibited an expression profile typical for early response genes with peak expression at 1 hour after TNF stimulation. Furthermore, *A20* and *IKBA* were expressed in a cyclical manner, with a second minor peak expression at 3 hours, which is a typical gene expression pattern upon continuous TNF exposure [479].

TNF-induced NF- κ B and MAPK signals originate from the TNF receptor complex or 'complex I' at the cell membrane [47]. After receptor internalization, complex II forms at the endosome and acts as a platform for the induction of caspase signaling and apoptosis [149]. Diminished NF- κ B-mediated transcription decreases the level of anti-apoptotic gene products and permits activation of caspase-8 in complex II [47, 480]. As HeLa cells are type II cells, caspase-8 requires mitochondrial amplification of the pro-apoptotic signal to activate the apoptosome and downstream effector caspases [162-164]. Treatment with a combination of TNF and the translation inhibitor cycloheximide (CHX) is a common method to induce TNF-dependent apoptosis in cell culture. CHX attenuates the synthesis of NF- κ B dependent gene products and allows TNF to activate caspase signaling [111]. To test if TNF induces cell death after inhibition of translation, I treated HeLa cells with TNF and CHX and checked for typical hallmarks of apoptosis.

Decrease of mitochondrial integrity and inner membrane potential indicate activation of the caspase cascade in type I and type II cells [162]. Tetramethylrhodamine ethyl ester (TMRE) provides a convenient measure of the IMM potential in flow cytometric assays [481]. The cationic cell-permeable dye accumulates in the matrix of metabolically active mitochondria because of its relative negative charge [481]. Thus, healthy cells exhibit measurable levels of TMRE fluorescence, while apoptotic cells are characterized by reduced TMRE fluorescence.

To test the effect of a combined treatment of TNF and CHX on the fate of HeLa cells, I measured the percentage of cells with reduced TMRE fluorescence 8 hours after treatment with TNF and CHX (**figure 3.2.A, B**). Treatment with TNF or CHX alone did not elevate the percentage of cells with reduced TMRE fluorescence above the levels of a healthy population exposed to the same culture medium without TNF or CHX. These findings indicate that the dose of CHX used in these studies does not induce apoptosis. However, a combined treatment of cells with TNF and CHX led to a pronounced increase in the population with decreased IMM potential. Furthermore, pre-treatment of cells with the pan-caspase inhibitor z-VAD-fmk completely abrogated that effect.

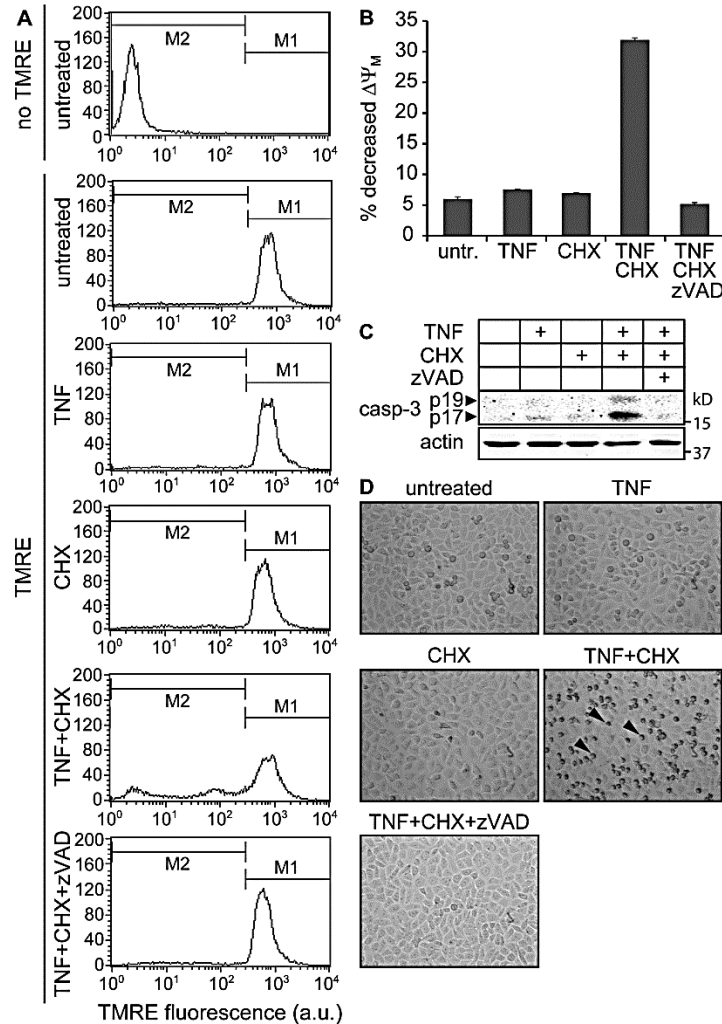


Figure 3.2. TNF combined with CHX induces apoptosis in HeLa cells. A: Histogram of TMRE fluorescence in HeLa cells after treatment with the indicated combinations of TNF and CHX for eight hours in comparison to cells that were not treated with TNF or CHX (untreated). All cells that did not receive z-VAD-fmk (zVAD) were pretreated with an equal volume of the zVAD-fmk solvent DMSO. All values are presented as the mean + S.E.M. of three technical replicates. **B:** Quantification of the population M2 in panel A, which represents the percentage of HeLa cells with a decreased IMM potential ($\Delta\Psi_M$) staining after treatment with the indicated combinations of TNF and CHX for eight hours in comparison to cells that were not treated with TNF or CHX (untr.). **C:** Western blot of caspase-3 cleavage in HeLa cells treated with the indicated combinations of TNF, CHX, and z-VAD-fmk (zVAD) for ten hours. All cells that did not receive z-VAD-fmk (zVAD) were pretreated with an equal volume of the zVAD-fmk solvent DMSO. Cell lysates were probed with an antibody against cleaved caspase-3 (casp-3 p19 and p17), and actin as a loading control. **D:** Light microscopic images of HeLa cells treated with the indicated combinations of TNF and CHX for ten hours. All cells that did not receive z-VAD-fmk (zVAD) were pretreated with an equal volume of the zVAD-fmk solvent DMSO. Arrowheads indicate representative cells with apoptotic morphology.

These observations confirm a need for gene translation for cell survival after exposure to TNF. They also demonstrate a requirement for caspase activity for the TNF-induced decrease of mitochondrial integrity in the presence of CHX.

Cleavage of the effector caspase caspase-3 is another hallmark of apoptosis and occurs downstream of mitochondrial apoptotic changes [162]. I detected alterations in the levels of cleaved caspase-3 after a combined treatment with TNF and CHX for ten hours (**figure 3.2.C**). Similar to the decrease of the IMM potential, processed caspase-3 only appeared in the presence of both TNF and CHX, and in the absence of the caspase inhibitor z-VAD-fmk. Light microscope images of the same cells just before cell lysis (**figure 3.2.D**) demonstrate that caspase-3 processing is paralleled by the morphological changes that are characteristic for apoptosis, including cell rounding and shrinkage, as well as membrane blebbing [1, 5].

In conclusion, TNF activates NF- κ B and JNK modules in HeLa cells and initiates the expression of auto-regulatory genes. In contrast, treatment of HeLa cells with TNF and the translation inhibitor CHX induces widespread caspase-mediated apoptosis. These findings are consistent with literature reports on the consequences of TNF-R1 activation by soluble TNF [52, 104, 111, 138].

3.2. HeLa cells are accessible to siRNA-mediated modification of TNF signals.

To determine if I could use siRNAs to modify cell fate decisions in response to TNF, I depleted two key TNF signaling molecules with opposing molecular functions. Caspase-8 is essential for activation of the caspase module [48], and depletion of caspase-8 disables the induction of apoptosis after TNF and CHX [48]. NEMO is the adapter protein that recruits the IKK complex to the TNF receptor complex at the membrane, and is crucially important for NF- κ B activation [90, 91]. Exposure of NEMO-depleted cells to TNF results in attenuated NF- κ B mediated gene expression and activation of the caspase module [482] like a combined treatment with TNF and CHX. Therefore, the combination of TNF and CHX on NEMO-depleted cells should result in an even more effective induction of apoptosis.

To test if caspase-8 depletion attenuated TNF-induced apoptosis, I transfected HeLa cells with a commercially available validated caspase-8 siRNA or a non-targeting control siRNA. I used a lipid-based forward transfection protocol to deliver the siRNA. To determine whether caspase-8 siRNA efficiently reduced caspase-8 mRNA levels, I isolated total cellular RNA three days after siRNA transfection. I generated cDNA and measured caspase-8 transcript levels in quantitative real-time PCR. Cells treated with caspase-8 siRNA exhibited greatly reduced levels of caspase-8 mRNA in comparison to control cells treated with a non-silencing siRNA (**figure 3.3.A**). The reduction of caspase-8 mRNA levels by around 70% indicates that the siRNA efficiently targeted caspase-8 mRNA. However, since my goal was to examine the effect of caspase-8 protein depletion on TNF signaling, I considered it even more important to monitor caspase-8 protein levels. Therefore, I also prepared cell lysates three days after the transfection of HeLa cells with caspase-8 siRNA, a control siRNA, or no siRNA and probed the cell lysates with an antibody against caspase-8 on a Western blot. I detected pronounced caspase-8 expression in cells treated with unspecific or no siRNA, and greatly reduced amounts of caspase-8 protein in cells treated with caspase-8 siRNA (**figure 3.3.B**).

With suitable siRNA transfection conditions in place, I examined whether depletion of caspase-8 modified the ability of TNF and CHX to induce apoptosis in target cells. For these experiments, I treated HeLa cells with either no siRNA, non-targeting siRNA or caspase-8 siRNA, incubated the cells for three days and induced apoptosis with TNF and CHX. I then examined several hallmarks of apoptosis. Five hours after treatment with TNF and CHX, I prepared cell lysates and incubated them with the artificial caspase substrate DEVD-AMC. Caspases generally cleave substrates after the tetrapeptide motif $X_4E_3X_2D_1$, in which position four and two regulate substrate affinity for specific caspases [9, 483, 484]. DEVD-AMC is best cleaved by the executioner caspases caspase-3 and to a lesser extent by caspase-7, but also by caspase-8 and 9 [485]. As such, DEVD-AMC cleavage provides a proxy measure of activity in the caspase cascade.

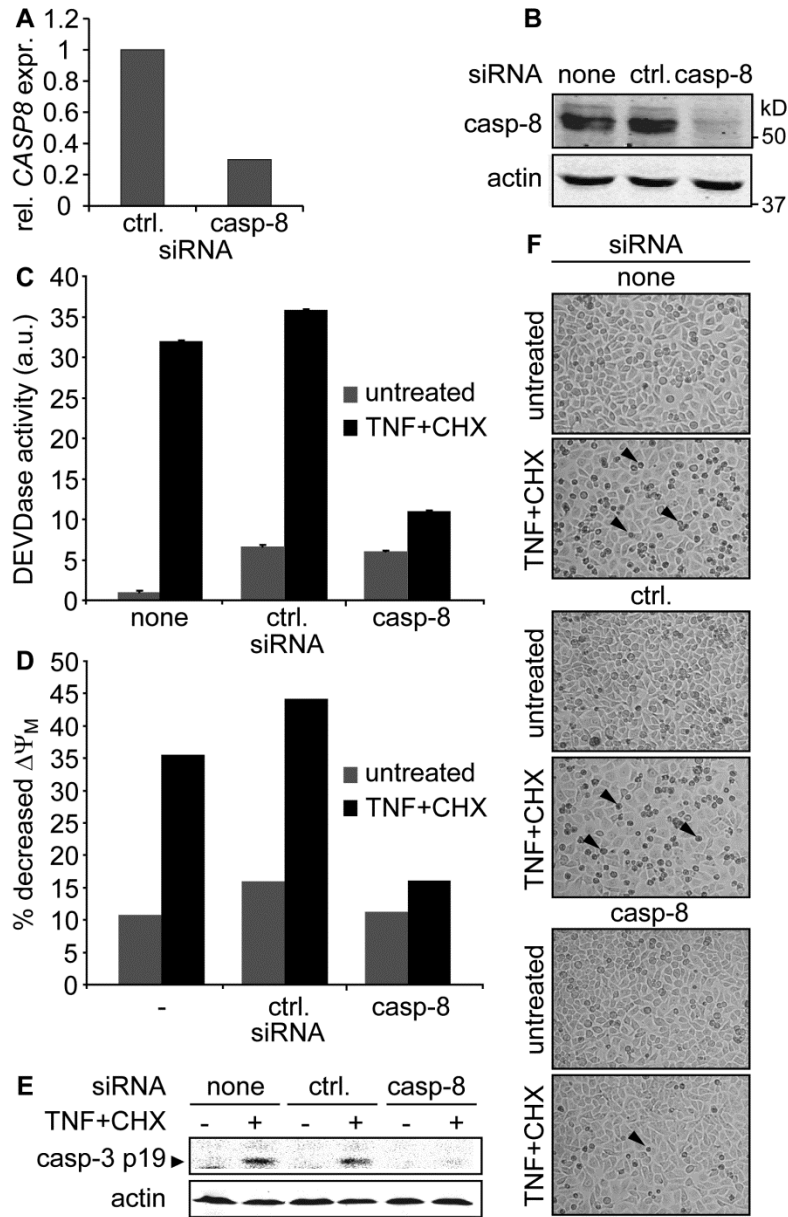


Figure 3.3. siRNA-mediated depletion of caspase-8 blocks apoptosis in HeLa cells treated with TNF and CHX. **A:** Relative expression levels of *CASP8* in HeLa cells treated with a non-silencing control siRNA (ctrl.), or caspase-8 siRNA (casp-8). Cellular cDNA was probed with Taqman primers specific for *CASP8* mRNA in quantitative real-time PCR. All values are expressed relative to *GAPDH* mRNA levels, and the basal gene expression level in untreated cells incubated with control siRNA was assigned a value of one. **B:** Western blot of HeLa cells treated with no siRNA (none), a non-silencing control siRNA (ctrl.), or caspase-8 siRNA (casp-8). Cell lysates were probed with an antibody against caspase-8, and actin as a loading control. **C:** Representative DEVD-specific caspase activity of HeLa cells incubated with TNF and CHX for five hours. HeLa cells were pretreated with no siRNA (none), a non-silencing control siRNA (ctrl.),

or caspase-8 (casp-8) siRNA. Cell lysates were incubated with the artificial caspase substrate DEVD-AMC, and AMC fluorescence resulting from caspase activity was measured and reported relative to basal fluorescence levels in untreated cells incubated without siRNA (none). All values are represented as the mean + S.E.M. of three technical replicates. **D:** Percentage of HeLa cells with decreased IMM potential ($\Delta\Psi_M$) in a representative cytometric TMRE assay after treatment with TNF and CHX for eight hours. HeLa cells were pretreated with no siRNA (none), a non-silencing control siRNA (ctrl.), or caspase-8 siRNA (casp-8). **E:** Western blot of cleaved caspase-3 (casp-3 p19) in HeLa cells treated with TNF and CHX for ten hours. Cells were pretreated with no siRNA (none), control siRNA (ctrl.), or caspase-8 siRNA (casp-8). Cell lysates were probed with an antibody specific for cleaved caspase-3, and actin as a loading control. **F:** Light microscopic images of HeLa cells treated with TNF and CHX for five hours. HeLa cells were pretreated with no siRNA (none), a non-silencing control siRNA (ctrl.), or caspase-8 siRNA (casp-8). Arrowheads indicate representative cells with apoptotic morphology.

Caspase-mediated DEVD-AMC processing results in the release of the fluorescent group 7-Amino-4-methylcoumarin (AMC). I detected AMC fluorescence with a fluorescence plate reader. Incubation of HeLa cells with TNF and CHX induced proteolytic cleavage of DEVD-AMC in cells transfected with a non-targeting siRNA or no siRNA (**figure 3.3.C**). In contrast, proteolytic cleavage of DEVD-AMC was greatly reduced in cells treated with caspase-8 siRNA. Similarly, TNF and CHX did not reduce the IMM potential in HeLa cells depleted of caspase-8 (**figure 3.3.D**). Additionally, reduced levels of caspase-8 hindered the production of caspase-3 cleavage products following exposure to TNF and CHX in comparison to HeLa cells transfected with a non-silencing siRNA or no siRNA (**figure 3.3.E**). Finally, depletion of caspase-8 resulted in a healthier morphological phenotype after treatment with TNF and CHX (**figure 3.3.D**). In conclusion, caspase-8 siRNA effectively depleted caspase-8 from HeLa cells, and hindered the induction of apoptosis induction by TNF and CHX. These data are consistent with a role for caspase-8 as the initiator caspase in the caspase cascade and as a central integrator of pro- and anti-apoptotic signals.

I then examined the consequences of NEMO depletion on TNF-induced death. NEMO is required for TNF-responsive transduction of pro-survival signals through NF- κ B [90, 91, 482]. siRNA-mediated depletion of NEMO in HeLa cells reduced TNF-induced phosphorylation of I- κ B- α in comparison to control cells (**figure 3.4.A**). However, cells with NEMO depletion were able to generate a significant amount of phosphorylated I- κ B- α . This finding may indicate that NEMO was not sufficiently depleted and that residual amounts of NEMO activated NF- κ B signaling or that alternate routes for NF- κ B activation, such as NEMO-independent non-canonical NF- κ B signaling, were unexpectedly available [97, 486]. Depletion of NEMO in HeLa cells attenuated but did not abrogate NF- κ B mediated gene transcription in the presence of TNF. In cells transfected with NEMO siRNA or a non-silencing control siRNA, TNF triggered a significant increase in *A20* and *IKBA* mRNA levels typical for early response genes [478]. NEMO depletion decreased the ability of TNF to induce *A20* and *IKBA* expression (**figures 3.4.B, C**).

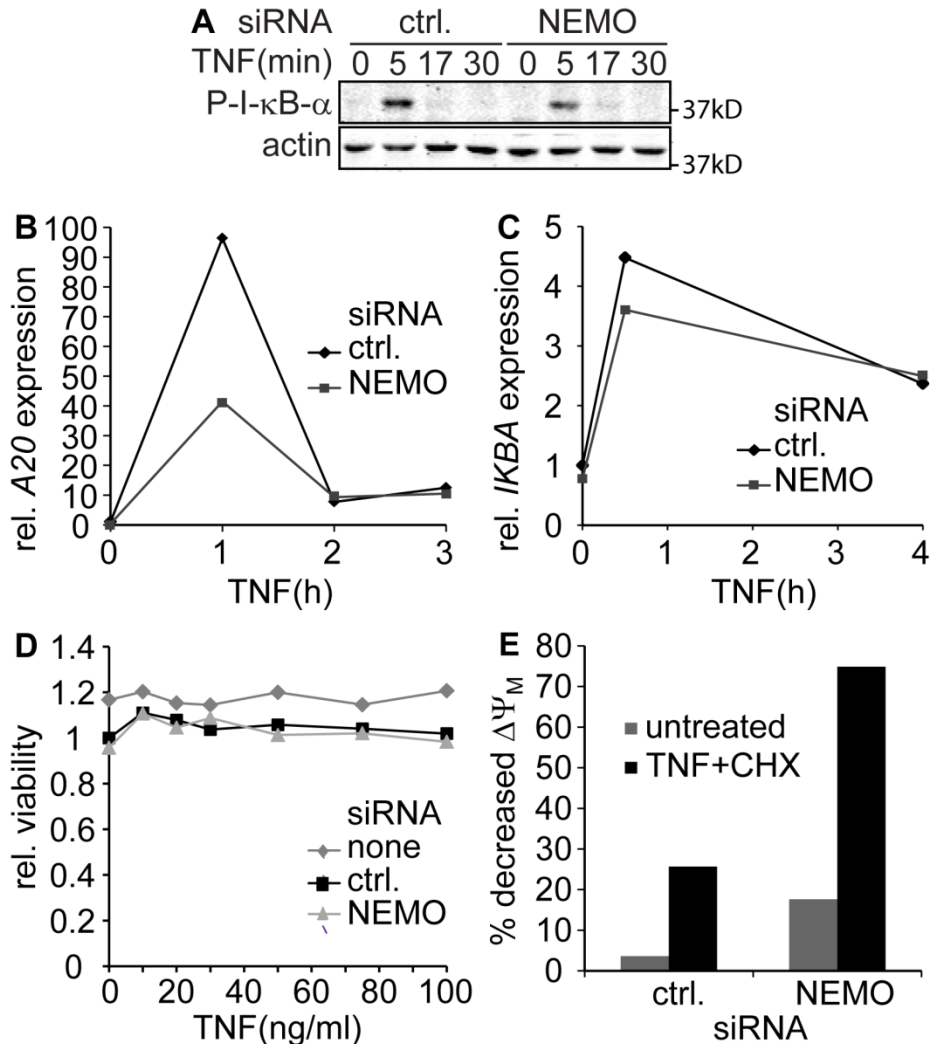


Figure 3.4. NEMO siRNA alters TNF-induced NF- κ B signaling. **A:** Western blot of the time course of I- κ B- α phosphorylation in HeLa cells pretreated with NEMO siRNA or a non-silencing control siRNA (ctrl.). Cells were incubated with TNF for the indicated time periods, and cellular lysates were probed with an antibody against phosphorylated I- κ B- α (P- I- κ B- α), and actin as a loading control. **B,C:** Representative time courses of *A20* (B) and *IKBA* (C) gene expression in HeLa cells pretreated with NEMO siRNA or a non-silencing control siRNA (ctrl.). Cells were treated with TNF for the indicated time periods, and cellular cDNA was probed with primers specific for *A20* and *IKBA* mRNA in quantitative real-time PCR. All values were expressed relative to actin mRNA levels, and the basal gene expression level in untreated cells incubated with control siRNA was assigned a value of one. **D:** Representative viability of HeLa cells depleted of NEMO after a treatment with TNF for fifteen hours. Control cells were treated with a non-silencing control siRNA (ctrl.) or no siRNA (none). Viability was determined in a resazurin viability assay. **E:** Percentage of HeLa cells with a decreased IMM potential ($\Delta\Psi_M$) in a representative cytometric assay with TMRE after treatment with TNF and CHX for eight hours. HeLa cells were pretreated with NEMO siRNA or non-silencing control siRNA (ctrl.).

I then asked if depletion of NEMO with siRNA shifted the balance of TNF-induced survival to TNF-induced apoptosis. For these experiments, I transfected HeLa cells with no siRNA, a non-silencing control siRNA or NEMO siRNA, and treated with various doses of TNF three days after transfection. I then measured the viability of the cells in a resazurin viability assay, which measures the metabolic activity of cells in a fluorimetric manner. Interestingly, the viability of NEMO-depleted cells is unchanged relative to the viability of control cells treated with an unspecific siRNA after fifteen hours incubation with TNF (**figure 3.4.D**). Cells that were mock transfected with water and transfection reagent exhibited slightly increased levels of viability, regardless of the dose of TNF. This was likely due to a reduced amount of non-specific siRNA-mediated toxic side effects of the transfection protocol. The inability of TNF to induce apoptosis in NEMO-depleted HeLa cells was unexpected [482], but may be explained by the residual NF- κ B transcriptional activity in NEMO-depleted cells.

To test if the depletion of NEMO from HeLa cells affected the induction of apoptosis by a combination of TNF and CHX. To test this, I exposed HeLa cells transfected with a non-silencing control siRNA or a NEMO siRNA to TNF and CHX and measured the percentage of cells with a decreased IMM potential in a TMRE assay. Depletion of NEMO alone led to a mild increase of the cell population with a decreased IMM potential in the absence of TNF and CHX (**figure 3.4.E**). In contrast, treatment of NEMO-depleted HeLa cells with TNF and CHX greatly increased the percentage of cells with a decreased IMM potential in comparison to control cells. Specifically, around 75% of NEMO-depleted cells exhibited a decreased IMM potential in contrast to around 25% of control cells. In summary, NEMO depletion in HeLa cells attenuated the TNF-induced activation of NF- κ B signaling. However, the level of reduction of NF- κ B signaling through NEMO depletion was not sufficient to shift the balance of the TNF-induced response from survival to apoptosis. In contrast, depletion of NEMO enhanced the ability of the TNF and CHX regime to induce apoptosis. These findings are consistent with the established pro-survival roles for NEMO.

In summary, I conclude that the depletion of key TNF signaling molecules with siRNA, modified the level of apoptosis induced by TNF and CHX.

siRNA-mediated depletion of pro-survival proteins, such as NEMO, enhanced cell death, while depletion of pro-apoptotic proteins, such as caspase-8, decreased TNF-induced death. These observations suggest that siRNA technology is a suitable tool to identify novel modifiers of TNF-induced death.

3.3. A high-throughput siRNA assay for modifiers of TNF-induced death.

To establish the conditions for a high-throughput siRNA assay for TNF-induced death, I first developed a functional assay to detect TNF-induced death. The selection criteria were high sensitivity, feasibility as a high-throughput assay, simplicity, availability of required instrumentation, and cost effectiveness. The resazurin viability assay (commercially available as Alamar Blue, CellTiter Blue, or Cell toxicity Colorimetric/Fluorometric Assay)[487] satisfied those criteria. The assay reports the viability of cells by the addition of a non-toxic resazurin solution to the culture medium and readout of a fluorescent signal in a plate reader [487]. The basis for the viability assay is the reduction of the blue resazurin to the pink, highly fluorescent resorufin in living cells [487]. The enzymatic reduction of resazurin occurs in mitochondria through flavin mononucleotide (FMN) dehydrogenase, flavin adenine dinucleotide (FAD) dehydrogenase, nicotinamide adenine dinucleotide (NAD⁺) dehydrogenase and cytochromes as well as in the cytosol or microsomes of the cell through NADPH:quinine oxidoreductase, flavin reductase, and cytochromes [487]. The assay is simple, sensitive, and can easily be executed in ninety six or three hundred eighty four-well format.

I then established a ninety six-well siRNA assay for modifiers of TNF-induced death in HeLa cells. Based on common screening practice and my success to deplete caspase-8 and NEMO, I set the incubation period with siRNAs to three days. This seems to be an ideal period to deplete residual amounts of most target proteins, while maintaining siRNA-mediated mRNA destruction [440, 488]. Based on recommendations by the siRNA manufacturer and the successful transfection of caspase-8 and NEMO siRNA, I set the siRNA concentration to 20 nM.

Subsequently, I visually determined the amount of HeLa cells I had to seed into each well of a ninety six-well plate to achieve a near confluent HeLa cell population three days later. This strategy ensured that I would examine a maximal amount of healthy HeLa cells in the exponential growth phase.

I used that cell number to determine the ideal lipid transfection reagent (Dharmafect I) and its concentration for siRNA delivery. I performed the titration experiment with a commercially available assay designed for RNAi optimization. Specifically, I transfected HeLa cells with a control siRNA or a validated siRNA that targets glyceraldehyde 3-phosphate dehydrogenase (GAPDH). On day three, I measured the GAPDH activity in the cell lysates of both groups in a fluorescence-based assay. I determined that an increasing concentration of transfection reagent decreased the GAPDH activity in control cells (**figure 3.5.A**). Lipid transfection reagents have cytotoxic side effects as they compromise the integrity of the cellular membranes. A visual inspection of the cells revealed that an increasing concentration of transfection reagent decreased the viability of the cells, which likely caused decreased GAPDH activity. However, an increasing concentration of transfection reagent also increased the loss of GAPDH activity through GAPDH siRNA (**figure 3.5.B**). I calculated the optimal compromise between cytotoxic effects of the transfection reagent and the transfection efficiency (the optimal balance factor) according to the instructions of the manufacturer as the product of the GAPDH activity in control cells and relative decrease of GAPDH activity through GAPDH siRNA (**figure 3.5.C**).

Next, I combined optimized siRNA delivery with the resazurin viability assay. I prepared a resazurin solution according to the concentration of commercially available solutions and added the recommended proportion [489] to the culture medium of cells treated with non-silencing control siRNA for three days. Incubation of cells with resazurin resulted in the accumulation of fluorescent resorufin that I detected with a fluorescence plate reader (**figure 3.6.A**). In the first two hours of the incubation, the resazurin fluorescence increased linearly with time. The increase of the resorufin fluorescence decelerated two hours after the resazurin treatment, and did not increase further five hours after the resazurin treatment. The saturation of the resorufin fluorescence may result from the decline of resazurin or from the conversion of the pink, fluorescent resorufin into transparent, non-fluorescent hydroresorufin [489]. To measure maximal unsaturated resorufin fluorescence, I set the incubation period with resazurin to 1.5 hours.

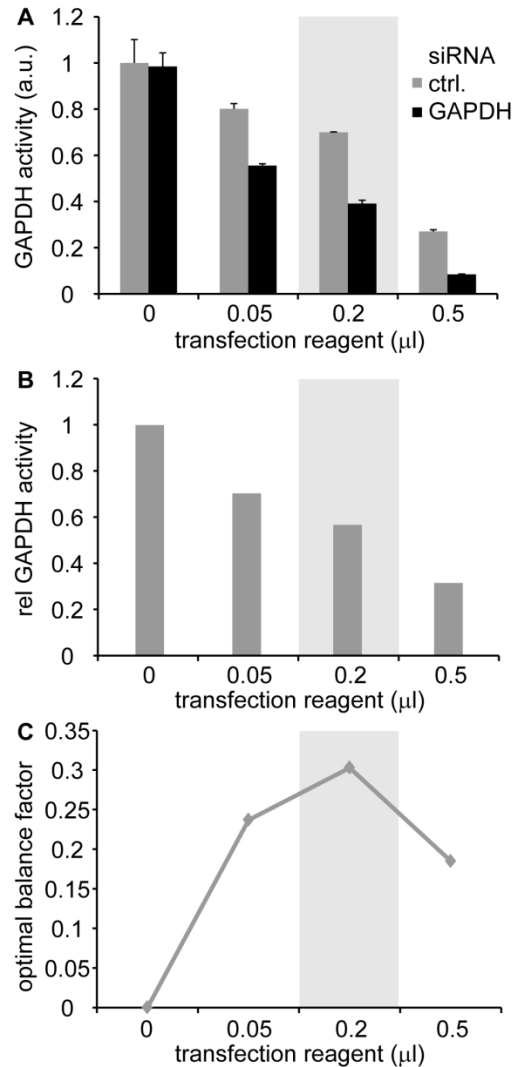


Figure 3.5. Optimization of siRNA delivery for the high-throughput siRNA assay. **A:** GAPDH activity in lysates of HeLa cells transfected with GAPDH siRNA or non-silencing control siRNA (ctrl.) with the indicated amounts of transfection reagent per condition. GAPDH activity was measured in a fluorescence-based assay and is presented as mean GAPDH activity + S.E.M. of two technical replicates. The shaded area marks the optimal amount of transfection reagent. **B:** Same experiment as in panel A. The relative GAPDH activity in lysates of HeLa cells transfected with a GAPDH siRNA is presented for the indicated amounts of transfection reagent. All values were normalized to the GAPDH activity in lysates of cells treated with a non-silencing control siRNA (ctrl.). The relative GAPDH activity in lysates of cells that were not treated with transfection reagent was assigned a value of one. All other values are presented relative to that value. The shaded area marks the optimal amount of transfection reagent. **C:** Same experiment as in panel A. Optimal balance factor or the mathematical product of GAPDH activity in lysates of HeLa cells transfected with non-silencing siRNA and the relative loss of GAPDH activity through the GAPDH siRNA. Cells were transfected with the indicated amounts of transfection reagent. The shaded area marks the optimal amount of transfection reagent.

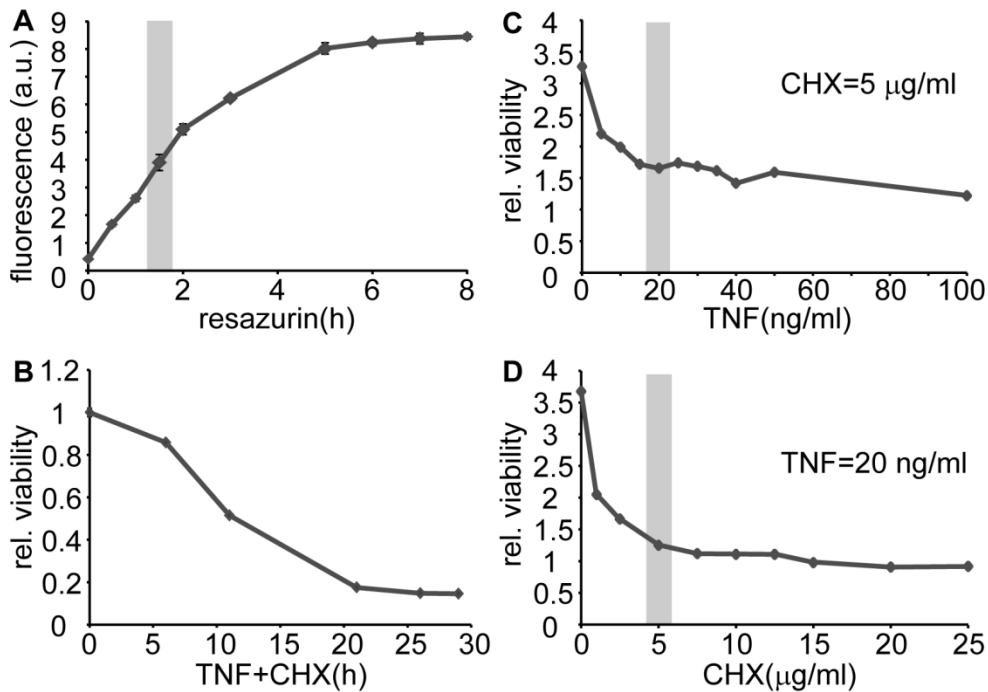


Figure 3.6. Optimization of the high-throughput viability assay. **A:** Time course of resorufin fluorescence in a near confluent population of HeLa cells. Cells were transfected with a non-silencing control siRNA and incubated resazurin for the indicated time periods. Resorufin fluorescence is presented as the mean fluorescence \pm S.E.M. of two technical replicates. The shaded area marks the optimal incubation period with resazurin. **B:** Time course of the viability of HeLa cells that were transfected with a non-silencing control siRNA and treated with TNF and CHX for the indicated time periods. Viability was measured in a resazurin viability assay. **C:** Viability of HeLa cells transfected with a non-silencing control siRNA and treated with a constant concentration of 5 μ g/ml CHX and the indicated concentrations of TNF for fifteen hours. Viability was determined in a resazurin viability assay. The shaded area marks the optimal concentration of TNF. **D:** Viability of HeLa cells transfected with a non-silencing control siRNA and treated with a constant concentration of 20 ng/ml TNF and the indicated concentrations of CHX for fifteen hours. Viability was determined in a resazurin viability assay. The shaded area marks the optimal concentration of CHX.

I then determined a time point that was ideal to observe siRNA-mediated modifications to the level of TNF-induced death in HeLa cells treated with a control siRNA. Incubation with TNF and CHX decreased the resorufin fluorescence with time (**figure 3.6.B**). This reflected decreased metabolic activity in dying HeLa cells. At twenty five hours after treatment with TNF and CHX, the resorufin fluorescence approached background levels suggesting that point all HeLa cells were metabolically dead at that time. I concluded that the ideal time frame to observe siRNA-mediated modification of the levels of TNF-induced death positioned between zero and twenty five hours incubation with TNF and CHX. As fifteen hours incubation with TNF and CHX resulted in approximately half maximal cell death, I reasoned that this time point was ideal for the identification of siRNAs that enhance or attenuate the induction of cell death by TNF and CHX.

Subsequently, I identified the concentrations of TNF and CHX required for optimal induction of cell death in HeLa cells treated with a control siRNA. To determine the optimal concentration of TNF, I kept the amount of CHX constant. Increasing concentrations of TNF decreased the viability of HeLa cells in this assay (**figure 3.6.C**), and HeLa cell death approached maximal levels at 20 ng/ml TNF. From these data, I concluded that 20 ng/ml TNF was sufficient to induce maximal cell death. Similarly, I determined that 5 μ g/ml CHX were sufficient to induce maximal cell death in combination with 20 ng/ml TNF (**figure 3.6.D**).

The optimization resulted in the following protocol for a high-throughput siRNA assay to identify modifiers of TNF-induced death (**figure 3.7.**): I transfected HeLa cells with individual siRNAs on day one. A subsequent 3 day incubation period allowed the depletion of the target protein in the cell. On day four, I treated duplicate cell populations with culture medium, or culture medium with TNF and CHX to induce apoptosis. I measured cell viability under both conditions in a resazurin viability assay.

To validate this approach, I tested the protocol with caspase-8 and NEMO control siRNAs detailed in **chapter 2.2**. Specifically, I transfected HeLa cells with no siRNA, a non-silencing siRNA, caspase-8, or NEMO siRNA in a ninety six-well plate and incubated the cells for three days.

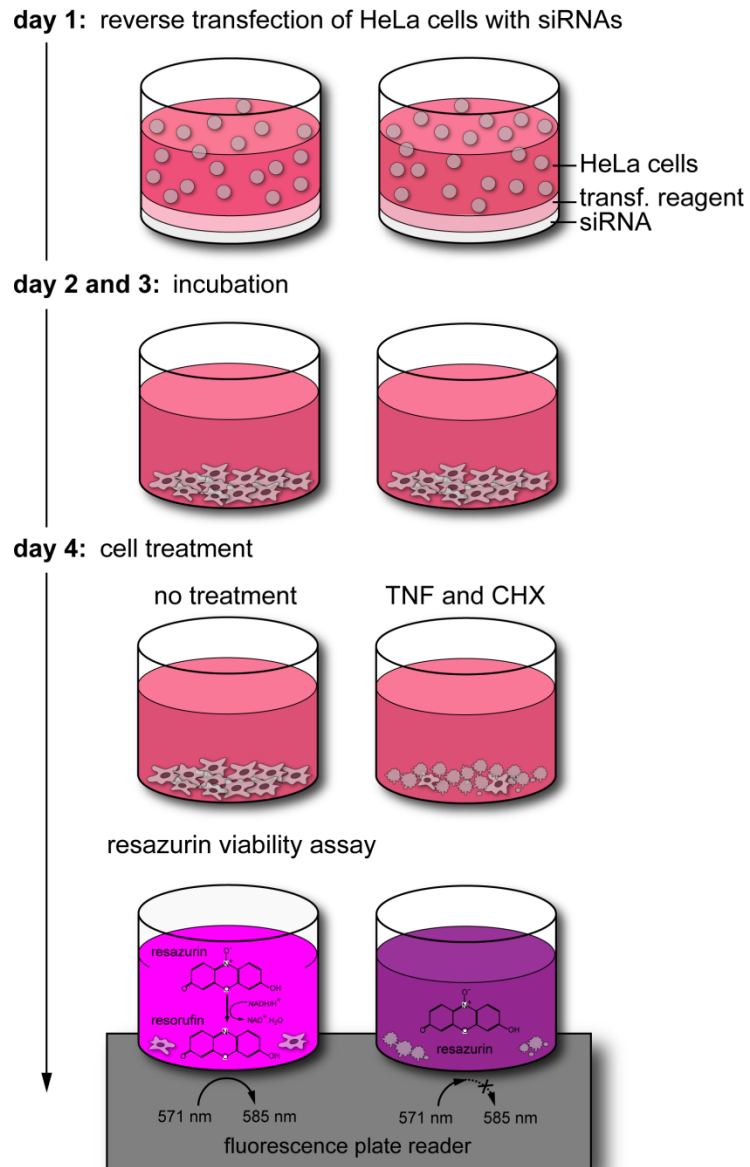


Figure 3.7. A high-throughput siRNA assay for modifiers of TNF-induced cell death. HeLa cells were transfected with individual siRNAs and incubated for three days. Duplicate cell populations remained untreated or were treated with TNF and CHX to induce apoptosis. The cell viability under both conditions was determined in a resazurin viability assay.

I then induced apoptosis with TNF and CHX and measured cell viability at defined intervals after treatment with TNF and CHX. Over the course of thirty hours cells transfected with non-targeting siRNA or no siRNA almost completely lost their reactivity towards resazurin (**figure 3.8.A**). The largest drop in cell viability occurred four hours after the treatment with TNF and CHX. In agreement with the results in **chapter 2.2.**, cells depleted of NEMO approached background levels of resazurin fluorescence faster than control cells, which is indicative of accelerated cell death. I measured the highest rate of death in NEMO depleted cells in the initial phase of the time course, after the first five hours of treatment with TNF and CHX. Caspase-8 depleted cells were still viable at thirty hours after begin of the treatment. At that point their original viability was reduced by 40%.

A photo of the assay plate after measurement of resorufin fluorescence demonstrates that the control siRNAs caspase-8 and NEMO generated visible phenotypes in the resazurin viability assay (**figure 3.8.B**). **Figure 3.8.C** shows the same ninety six-well plate following fixation of the cells and staining with nuclear acid stain SYTO red. Apoptosis leads to cell shrinkage, detachment from the plate, nuclear fragmentation, chromatin condensation and DNA fragmentation [1, 5], which are all factors that result in a reduced levels SYTO red staining in apoptotic cells. The SYTO red assay reflected the results of the resazurin viability assay. Cells treated with control siRNA or no siRNA showed a significant reduction in the level of staining with SYTO red over the course of the three hours treatment with TNF and CHX. In contrast, cells depleted of caspase-8 stained throughout the entire time period. Cells depleted of NEMO were characterized by accelerated reduction in staining intensity.

I conclude that the high-throughput resazurin assay is functional and detects TNF-induced cell death. Over the thirty hours, the viability of control cells decreased almost five-fold. Furthermore, the resazurin assay generated prominent siRNA phenotypes with the validated caspase-8 and NEMO control siRNAs. Due to the opposing roles that caspase-8 and NEMO play in TNF-induced apoptosis, they are ideal positive controls for pro-apoptotic and anti-apoptotic siRNA phenotypes in the high-throughput siRNA screen. Both siRNAs exhibited the greatest deviation from the level of TNF-induced death in control cells at fifteen hours.

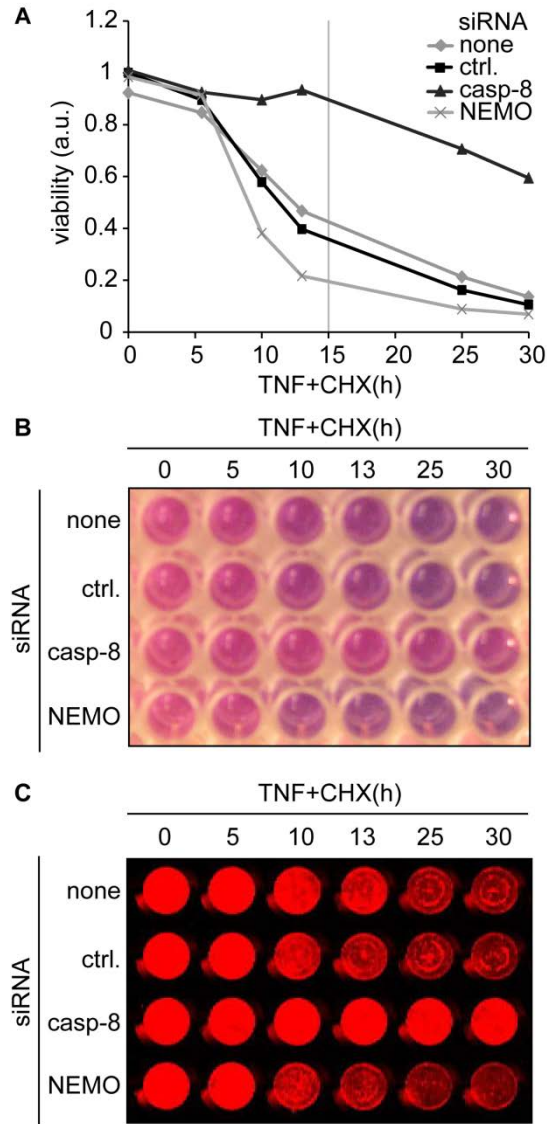


Figure 3.8. Depletion of caspase-8 or NEMO in the high-throughput siRNA assay modifies the rate of TNF-induced death. **A:** Representative time course of the viability of HeLa cells treated with TNF and CHX for the indicated time points in a resazurin viability assay. Cells were treated with caspase-8 (casp-8) siRNA or NEMO siRNA, respectively. Control cells were treated with a non-silencing control siRNA (ctrl.), or no siRNA (none). **B:** Photograph of the section of the corresponding ninety six-well plate for the results in panel A. **C:** Fluorescence scan of the same section of a ninety six-well plate as in panel B, but cells were washed and reprobred with the cell-permeable, fluorescent nucleic acid stain SYTO 60.

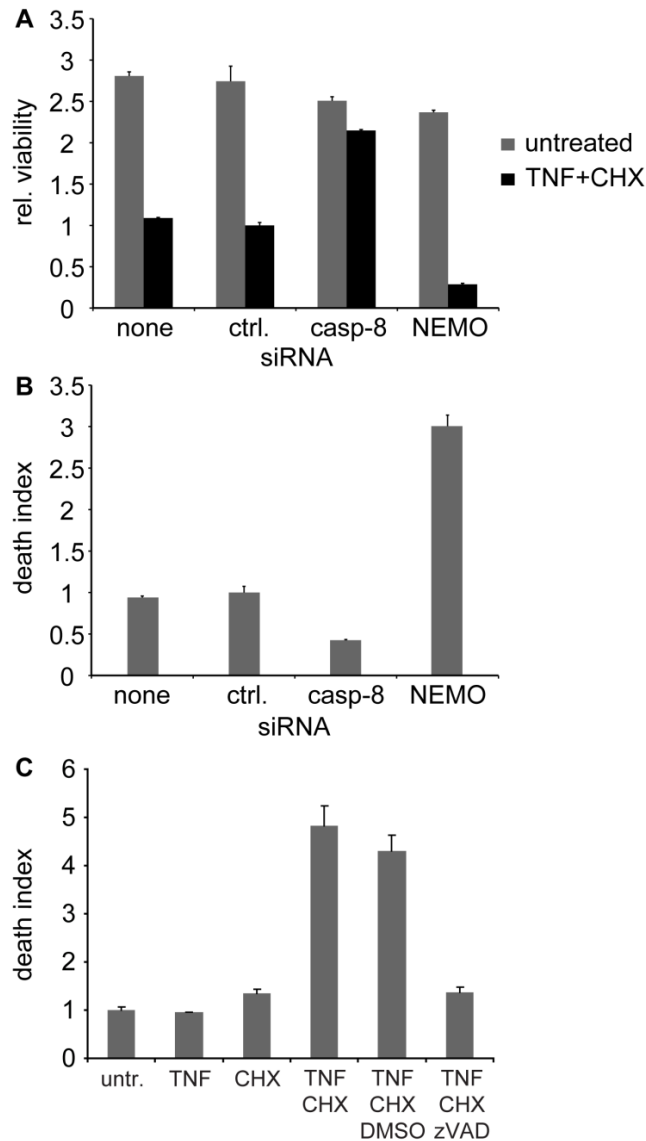


Figure 3.9. The high-throughput siRNA assay identifies TNF signaling components as modifiers of TNF-induced death. **A:** Viability of HeLa cells treated with no siRNA (none), a non-silencing control siRNA (ctrl.), caspase-8 (casp-8), or NEMO siRNA, and incubated with TNF and CHX for fifteen hours. Control cells were treated with the same siRNAs and no TNF or CHX. Viability was determined in a resazurin viability assay and expressed as the average viability + S.E.M. of two technical replicates. The viability of cells treated with control siRNA (ctrl.) in the presence of TNF and CHX was assigned a value of one. **B:** Corresponding death indices for panel A. The death index is expressed as the average death index + S.E.M. of two technical replicates. The death index of cells treated with a control siRNA (ctrl.) was assigned a value of one. **C:** Representative death indices of cells treated with the indicated combinations of TNF, CHX, DMSO, and z-VAD-fmk (zVAD) for fifteen hours. Death indices are presented as the mean values of three technical replicates + S.E.M. All values are reported relative to the death index of untreated cells (untr.), which was assigned a value of one.

I conclude that this is the ideal time point to identify novel modifiers of TNF-induced death. Therefore, I set the duration of the treatment with TNF and CHX in the high-throughput siRNA screen to fifteen hours, which includes incubation with resazurin for the last 1.5 hours.

To validate the assay conditions, I determined the viability of cells treated with non-silencing siRNA, in cells treated with caspase-8 siRNA or in cells treated with NEMO siRNA after fifteen hours incubation with TNF and CHX (**figure 3.9.A, B**). After a fifteen hour treatment with TNF and CHX, control cells exhibited a greater than 2.5 fold reduction in their original viability. Caspase-8 depleted cells exhibited less than half of that reduction, whereas NEMO-depleted cells exhibited around three times the reduction of control cells. A resazurin viability test on cells treated with CHX for fifteen hours confirmed that CHX alone did not decrease cell viability (**figure 3.9.C**). In summary, the assay reliably uncovered NEMO and caspase-8 as inhibitors and activators of TNF-induced cell death, respectively. From these observations, I conclude that the high-throughput siRNA assay is suited to identify novel modifiers of TNF-induced death.

CHAPTER 4. AN siRNA SCREEN FOR MODIFIERS OF TNF-INDUCED DEATH.

A version of this chapter has been published:

Schindler A, Foley E: A functional RNAi screen identifies hexokinase 1 as a modifier of type II apoptosis. *Cell Signal* 2010. 22(9):1330-40.

4.1. An siRNA screen for modifiers of TNF-induced death.

I conducted a high-throughput siRNA assay to identify novel modifiers of TNF-induced death. Specifically, I transfected HeLa cells with siRNAs that target nine hundred eighty six human kinases, phosphatases and associated proteins and monitored cell viability in the presence and absence of a combination of TNF and a sub-lethal dose of the translation inhibitor CHX. I chose to screen kinases and phosphatases, because they are a functional class of proteins with established roles in TNF-induced NF- κ B and JNK signaling [52]. All siRNAs originated from commercially available siRNA libraries that targeted each protein with three individual non-overlapping siRNAs to increase the likelihood of depletion phenotypes, and to include a means to identify possible off-target effects (OTE) [490].

The organization of each siRNA plate is outlined in **figure 4.1.A**. Each plate contained eighty or eighty eight experimental siRNAs and a number of control wells that included no siRNA, non-silencing siRNA, caspase-8, or NEMO siRNA. I assayed each plate in duplicate in the presence or absence of TNF and CHX to distinguish siRNAs that affected cell viability or cell numbers in general from siRNAs with a TNF-specific effect. I defined TNF-induced death or the 'death index' for each siRNA as the ratio of the average cell viability in the absence of TNF and CHX to the average cell viability in the presence of TNF and CHX (**figure 4.1.B**).

4.2. Analysis of the screen data.

The ranges of the raw resorufin fluorescence values from plates treated with TNF and CHX were clearly distinct and decreased in comparison to those of untreated plates (**figure 4.2.A**), which indicated the assay detected the induction of death by a regime of TNF and CHX. Replicate plates mostly exhibited very similar ranges of fluorescence values. However, there were prominent subset-to-subset variations in the fluorescence ranges across all one hundred fifty six plates, which is typical for siRNA screens performed in several (here ten) subsets [491].

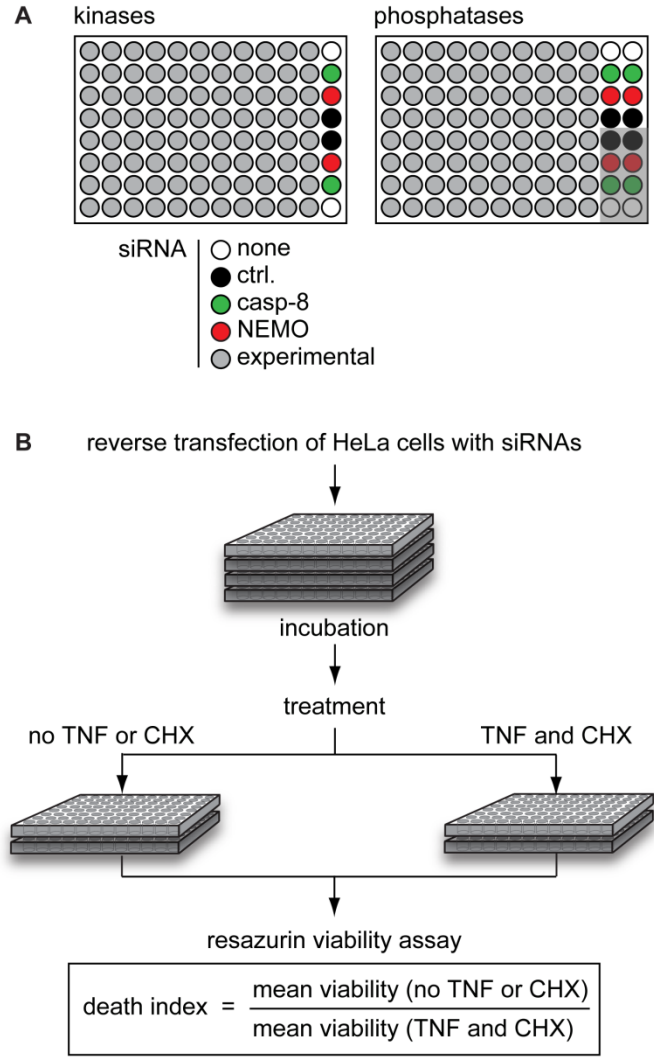


Figure 4.1. Plate layout and flow chart of the assay employed in the siRNA screen for modifiers of TNF-induced death. A: Locations of experimental and control siRNAs for kinase and phosphatase ninety six-well siRNA plates. Control siRNAs targeted caspase-8 (casp-8), NEMO, or were non-silencing (ctrl.). Half of the control wells in the phosphatase plates (grey area) were treated with culture medium or culture medium with TNF and CHX opposed to the general treatment of the plate. **B:** Flow chart of the siRNA screen assay. HeLa cells were transfected with each ninety six-well library plate in quadruplicate. After a three day incubation period, two of the four plates were treated with TNF and CHX in culture medium to induce apoptosis, and two plates were treated with culture medium only. Cell viability was determined in a resazurin viability assay. TNF-induced cell death (the death index) was determined as the ratio of the average viability without TNF or CHX treatment to the average viability with TNF and CHX treatment.

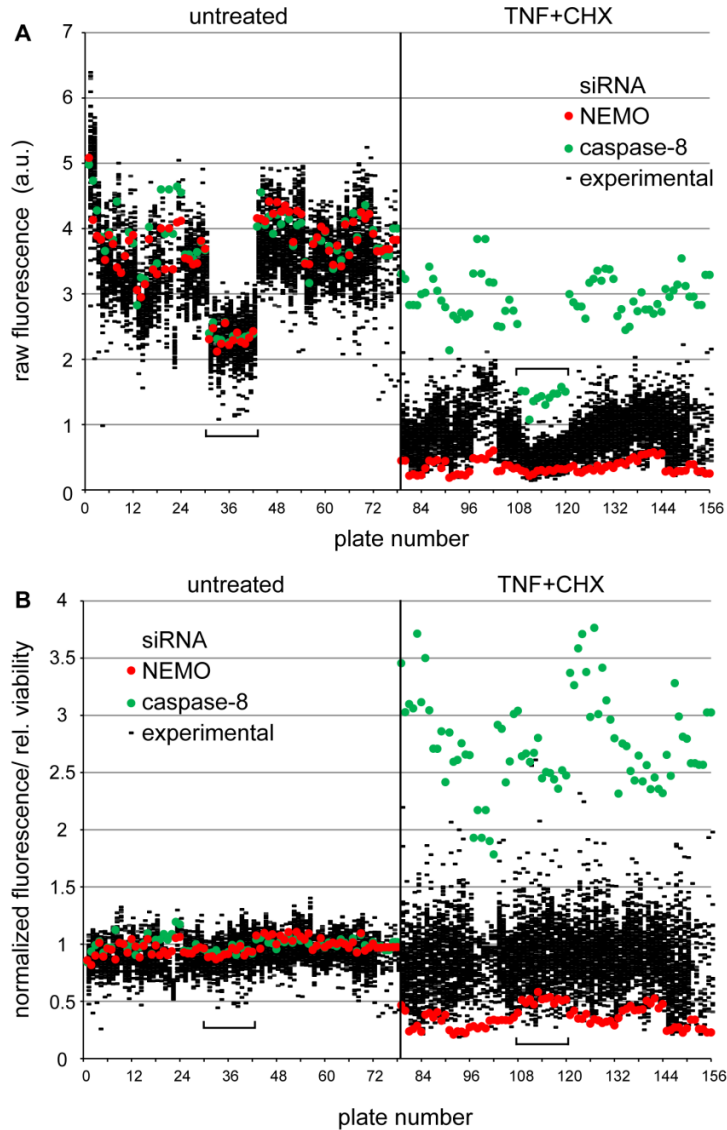


Figure 4.2. Normalization of screened plates. **A:** Distributions of the raw resorufin fluorescence values from all plates in the absence (plate one to seventy eight) and presence (plate seventy nine to one hundred fifty six) of TNF and CHX. Each vertical distribution of data values represents the raw resorufin fluorescence values for all experimental siRNAs on one plate (black lines). The raw fluorescence values for the control siRNAs caspase-8 (green circles) and NEMO (red circles) are also indicated for each plate. The order of the untreated plates corresponds to the order of the plates treated with TNF and CHX. For example, untreated plate one and treated plate seventy nine were screened on the same day. The brackets indicate plate set thirty one to forty two and one hundred nine to one hundred twenty with a major variation of the raw fluorescence ranges from the remaining plate sets. **B:** Plate normalization. The raw fluorescence values of cells treated with experimental and control siRNAs were normalized to the mean raw fluorescence value of the cells treated with non-silencing control siRNAs on each plate, which was assigned a value of one. All other fluorescence values are shown relative to that value.

For example, the subset that consisted of plates thirty one to forty two treated with fresh culture medium and plates one hundred nine to one hundred twenty treated with TNF and CHX exhibited significantly lower raw fluorescence values than other subsets (indicated with brackets).

I normalized each fluorescence value in one assay plate to the average fluorescence value of the plate-internal non-silencing siRNA controls (**figure 4.2.B**). Plate normalization with plate-internal controls is the recommended normalization method for a non-randomized distribution of siRNAs over siRNA plates, especially when the set of siRNAs covers only a specific class of proteins, like kinases and phosphatases, and a high density of hits is expected [492, 493]. I set the average viability of non-silencing control siRNAs to one, regardless of whether the plates received TNF treatment or not. As a result, death indices of non-silencing siRNA controls also obtained a value of one. Plate normalization mostly eliminated subset-to-subset variability and generated comparable viability values (**figure 4.2.B**).

4.3. Quality of the screen data.

To visualize the distribution of normalized viability values over the wells of the ninety six-well plates, I generated a combination of bubble chart and heat map for all one hundred fifty six screened plates (**appendix 3**). Overall, normalized viability values of cells untreated or treated with TNF and CHX fell into the expected ranges. I detected a few minor plate effects that mostly manifested as edge effects.

In general, viability scores were reproducible across replicate plates. I graphed duplicate values for all siRNAs in a scatter plot, in which each dot represents an siRNA with one replicate value on the x-axis and the second replicate value on the y-axis [491]. Replicates 1 and 2 are identical if they fall onto the identity line $y = 1x$. I determined a coefficient of determination R^2 of 0.6742 for replicate values to fall on the identity line (**figure 4.3**). This means the correlation r between replicate one and replicate two is around 82%, which indicates a significant degree of reproducibility between replicate measurements.

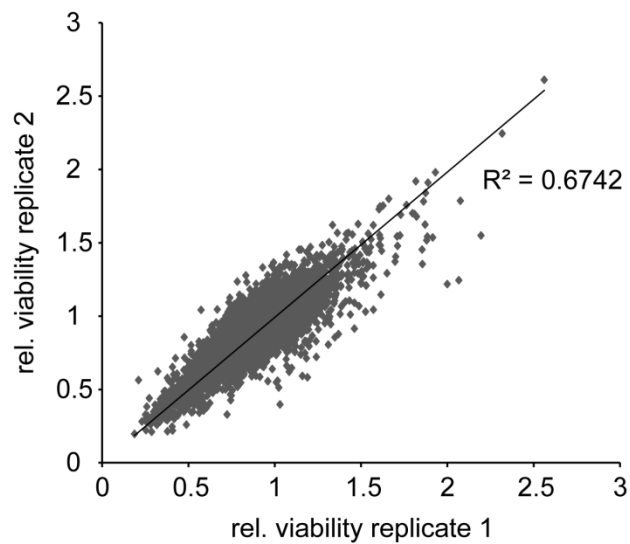


Figure 4.3. Level of identity between replicate plates in the screen. Scatter plot of the normalized viability of all cells treated with siRNAs from the phosphatase and kinase libraries in the absence and presence of TNF and CHX. All viability values from replicate one are plotted on the x-coordinate and the corresponding viability values for replicate two on the y-coordinate. The coefficient of determination (R^2) for identity of replicate one and replicate two ($y=1x$) is indicated.

Subsequently, I determined the mean normalized viability value for each replicate siRNA. The normalized viability values for each gene and siRNA are presented in **appendix 4**.

The performance of control siRNAs is another quality measure of siRNA screens [491]. In a good screen, positive controls should generate clear phenotypes that match to their established molecular functions. That phenotype should be distinct from the negative control siRNAs that do not have a phenotypic effect [491]. Positive controls with opposing phenotypes should not overlap [491]. To judge the dynamic ranges between siRNA controls in my screen, I visualized the distributions of the normalized viability values for caspase-8 and NEMO siRNAs. The normalized viability values of non-silencing siRNA controls did not have a distribution as they were set to one. I presented the distributions of the positive controls as Kernel density estimates [456], which are smoothed continuous histograms, built on the assumption that each data point is not just a point but the mean of a set of samples with normal distribution. All data point distributions are summed up to create the smoothed histogram.

As anticipated, caspase-8 and NEMO siRNA viability values distributed around one in the absence of TNF and CHX (**figure 4.4.A**). In fact, caspase-8 and NEMO siRNAs did not serve as positive controls for that condition. In contrast, cells treated with NEMO siRNA exhibited very low viability values of around 0.4 in the presence of TNF and CHX, whereas cells treated with caspase-8 siRNA exhibited high viability values of around 2.7 (**figure 4.4.B**). As a result, the death indices of cells treated with NEMO siRNA scattered around 3.0, and death indices of cells treated with caspase-8 siRNA around 0.3 (**figure 4.4.C**). The distributions of the two positive controls did not overlap with each other or the negative control, which indicated a very good dynamic range for my screen. These findings indicate that the screen allows discrimination between pro-survival and pro-death phenotypes.

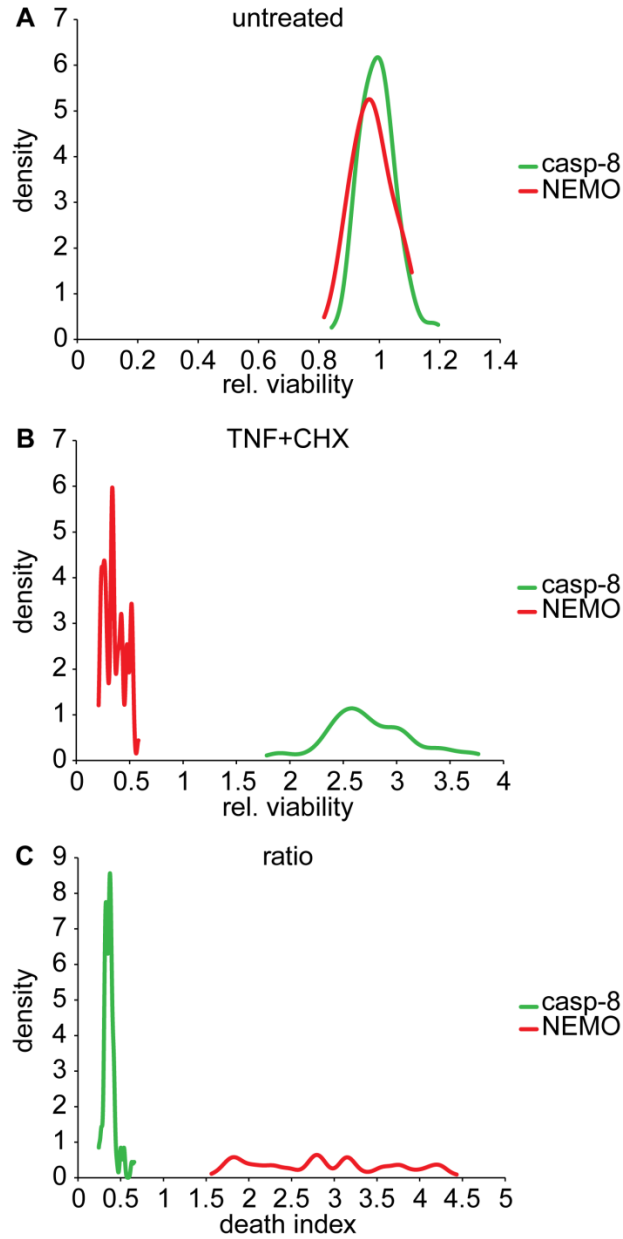


Figure 4.4. Behaviour of positive plate controls over all screened plates. A: Kernel density estimate of the distribution of the normalized basal viability values of all cells treated with caspase-8 (casp-8) or NEMO control siRNA. **B:** Kernel density estimate of the distribution of all normalized basal viability values of cells treated with caspase-8 (casp-8) or NEMO control siRNA and TNF and CHX. **C:** Kernel density estimate of the distribution of the death indices of all cells treated with caspase-8 (casp-8) or NEMO control siRNA.

4.4. Identification of high confidence modifiers of TNF-induced apoptosis and general cell viability.

I then determined the genes that modified viability in the presence and absence of TNF and CHX. The three non-overlapping siRNAs tested for each gene produced variable viability phenotypes (**figure 4.5.**). In line with the standard approach to exclude possible OTEs [490], I only considered a gene a modifier if a minimum of two of three gene-specific siRNAs had a significantly altered viability value or death index in comparison to control non-silencing siRNAs. To this end, I used the median of the three siRNA values to identify high confidence hits. This method ensured that a minimum of two siRNAs fell within the confidence interval of the median siRNA value.

I sorted and plotted the median siRNA viability values in the absence and presence of TNF and CHX and the median death indices for each gene relative to control non-silencing siRNAs (set to one) (**figure 4.6.**). Then I determined confidence intervals for the three distributions. Due to an asymmetric distribution of genes above and below the non-silencing control siRNAs, I determined independent confidence intervals for the upper and lower part of the distributions, respectively. I used the standard deviation of the median viability values/death indices from the non-silencing siRNA control to calculate confidence intervals. I considered genes within the 95% confidence intervals of all three distributions as high confidence hits.

Next, I classified hits into pro-survival and pro-death proteins and into proteins with a general or TNF-specific effect on cell viability (**figure 4.7., 4.8., 4.9.**). I reasoned that a decreased viability or an increased death index in the screen may result from the depletion of a pro-survival protein. Increased viability or a decreased death index in the screen may indicate the depletion of a pro-death protein. High confidence hits in the distribution of the median viability values in the absence of TNF and CHX were classified as proteins with a general effect on viability (**figure 4.7.**). I identified nineteen general pro-survival proteins. Four of these proteins also significantly enhanced TNF-induced death. I classified the latter proteins as general pro-survival proteins with TNF pathway-specific effect. I also identified eight general pro-death proteins (**figure 4.7.**).

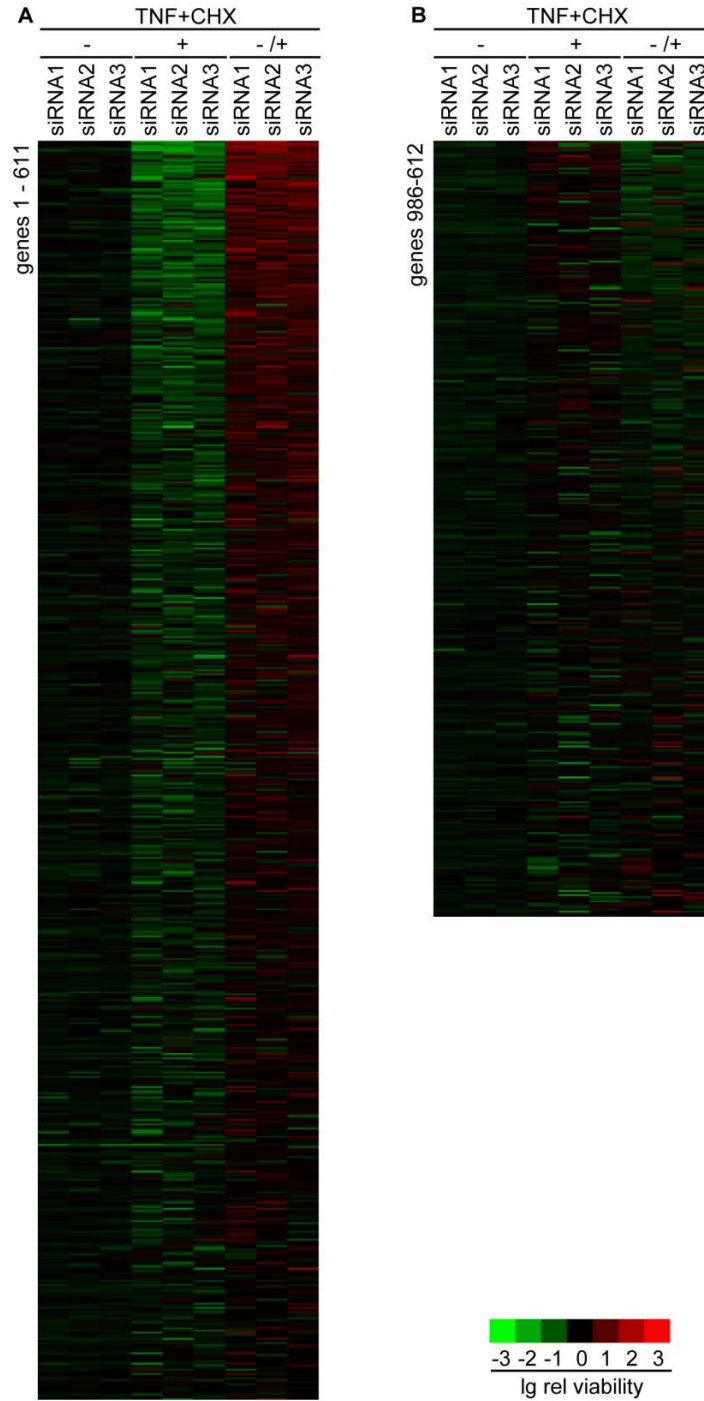


Figure 4.5. Heat map representation of all viability values and death indices in the screen. For each of the nine hundred eighty six screened genes, all three siRNAs are presented with their respective base two log-transformed cell viability in the absence (-) and presence of TNF and CHX (+) or with their base two log-transformed death indices (+/-) in form of a heat map. All genes are sorted according to the median death index in descending order for the top six hundred eleven pro-survival genes (left panel) and ascending order for the bottom three hundred seventy five pro-death genes (right panel).

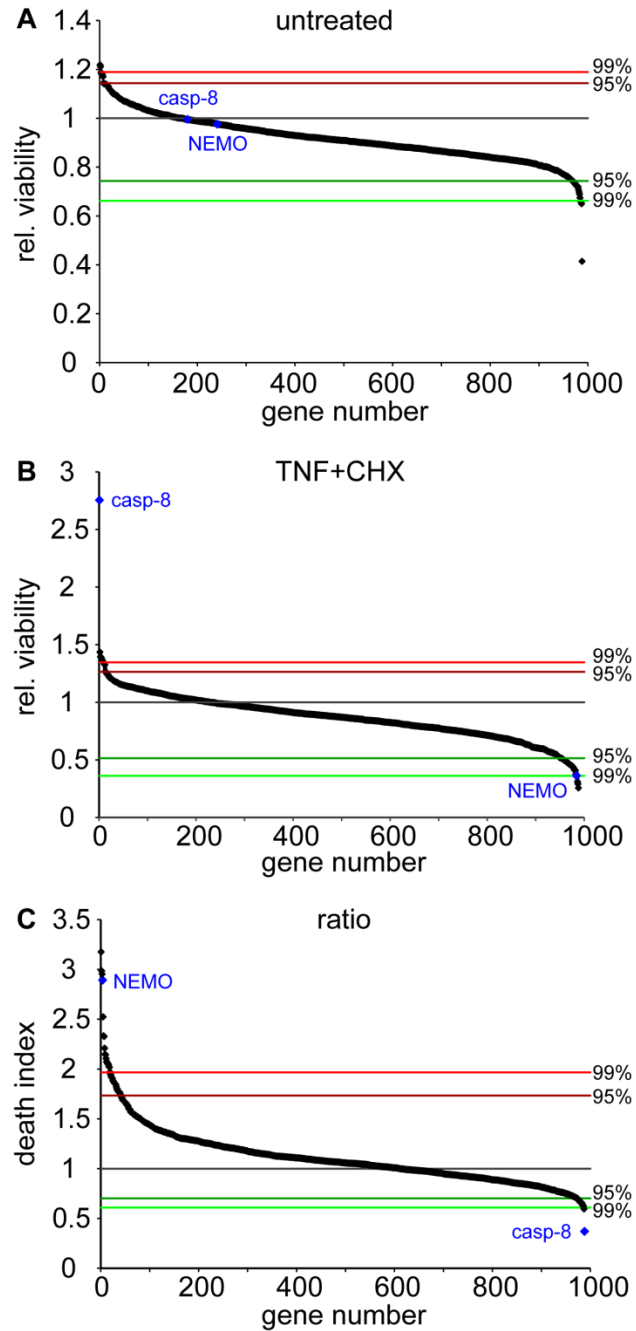


Figure 4.6. Distribution of the median viability values and death indices. A: Distribution of the median siRNA viability values in the absence of TNF or CHX. The median siRNA viability values were sorted in descending order. 99% and 95% confidence intervals are indicated for enhancers and suppressors of cell death. The mean viability of control cells treated with siRNAs that target NEMO or caspase-8 (casp-8) are indicated. **B:** Distribution of the median siRNA viability values after treatment with TNF and CHX. **C:** Distribution of the median siRNA death indices.

95% confidence general pro-survival proteins

a) not TNF-pathway specific

acc number	symbol	gene name	TNF+CHX		
			-	+	+/-
NM_005030	PLK1	polo-like kinase 1	green	black	red
NM_001248	ENTPD3	ectonucleoside triphosphate diphosphohydrolase 3	green	black	red
NM_030962	CMT4B2	myotubularin-related protein 13	green	black	red
NM_032124	HDHD2	haloacid dehalogenase-like hydrolase dom contain 2	green	black	red
NM_032483	HTPAP	phosphatidate phosphatase PPAPDC1B	green	black	red
NM_004687	MTMR4	myotubularin-related protein 4	green	black	red
NM_001610	ACP2	lysosomal acid phosphatase 2	green	black	red
NM_001948	DUT	dUTP pyrophosphatase	green	black	red
NM_138448	ACYP2	acylphosphatase 2	green	black	red
NM_014496	RPS6KA6	ribosomal protein S6 kinase alpha-6	green	black	red
NM_014214	IMPA2	inositolmonophosphatase 2	green	black	red
NM_080823	SRMS	tyrosine-protein kinase Srms	green	black	red
NM_014225	PPP2R1A	protein phosphatase 2A, 65kD reg su alpha	green	black	red
NM_001570	IRAK2	interleukin-1 receptor-associated kinase 2	green	black	red
NM_007181	MAP4K1	MEKKK1	green	black	red

b) TNF pathway-specific

acc number	symbol	gene name	TNF+CHX		
			-	+	+/-
NM_032728	C9orf67	probable lipid phosphate phosphatase PPAPDC3	green	black	red
NM_007174	CIT	citron rho-interacting kinase	green	black	red
NM_003681	PDXK	pyridoxal kinase	green	black	red
NM_002860	ALDH18A1	aldehyde dehydrogenase 18 family, member A1	green	black	red

95% confidence general pro-death proteins

a) not TNF-pathway specific

acc number	symbol	gene name	TNF+CHX		
			-	+	+/-
NM_016282	AK3L1	adenylate kinase 3 alpha-like 1	green	black	red
NM_139068	MAPK9	JNK2	green	black	red
NM_018323	PI4K2B	phosphatidylinositol 4-kinase, 2-beta	green	black	red
NM_002706	PPM1B	protein phosphatase 1B	green	black	red
NM_177983	PPM1G	protein phosphatase 1G	green	black	red
NM_177560	CSNK2A1	casein kinase 2, su alpha	green	black	red

b) TNF pathway-specific

acc number	symbol	gene name	TNF+CHX		
			-	+	+/-
NM_003648	DGKD	diacylglycerol kinase delta	green	black	red
NM_020438	DOLPP1	dolichyl pyrophosphate phosphatase 1	green	black	red

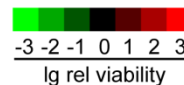


Figure 4.7. 95% confidence pro-survival and pro-death proteins in the absence of TNF. NCBI RefSeq gene accession number, symbol and name are shown for each gene. The heat map shows the base two log-transformed median viability values in the absence and presence of TNF and CHX and the base two log-transformed median death index for each gene. All genes are sorted according to the median viability in descending order for the pro-survival proteins, and ascending order for the pro-death proteins. Kinases are shown in black font and phosphatases in grey font.

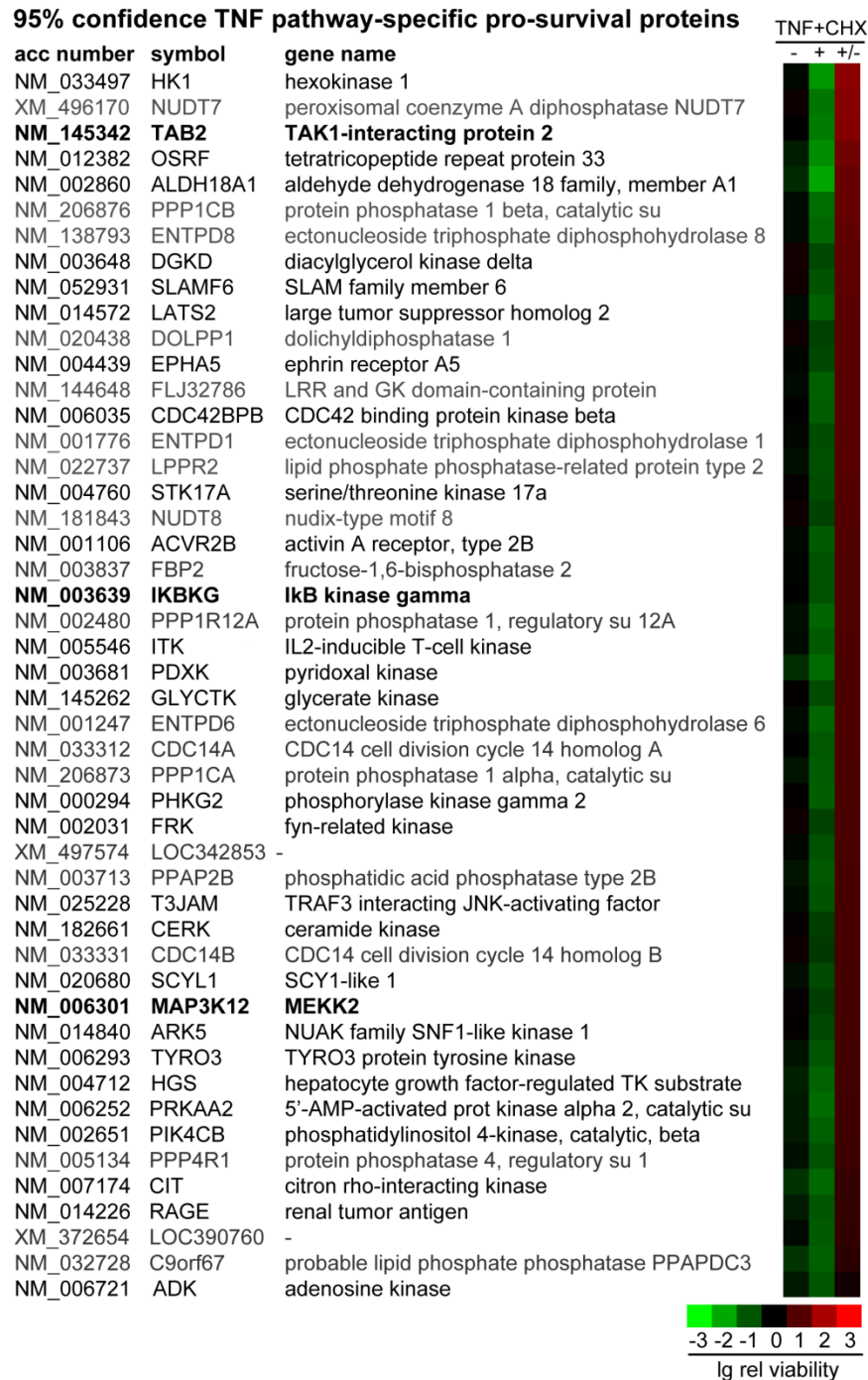


Figure 4.8. 95% confidence pro-survival proteins in TNF-induced death. NCBI RefSeq gene accession number, symbol and name are shown for each gene. The heat map shows the base two log-transformed median viability value in the absence and presence of TNF and CHX and the base two log-transformed median death index for each gene. All genes are sorted according to the median death index in descending order. Kinase-encoding genes are shown in black font and phosphatase-encoding genes in grey font. Key TNF signaling molecules are highlighted in bold.

95% confidence TNF pathway-specific pro-death proteins

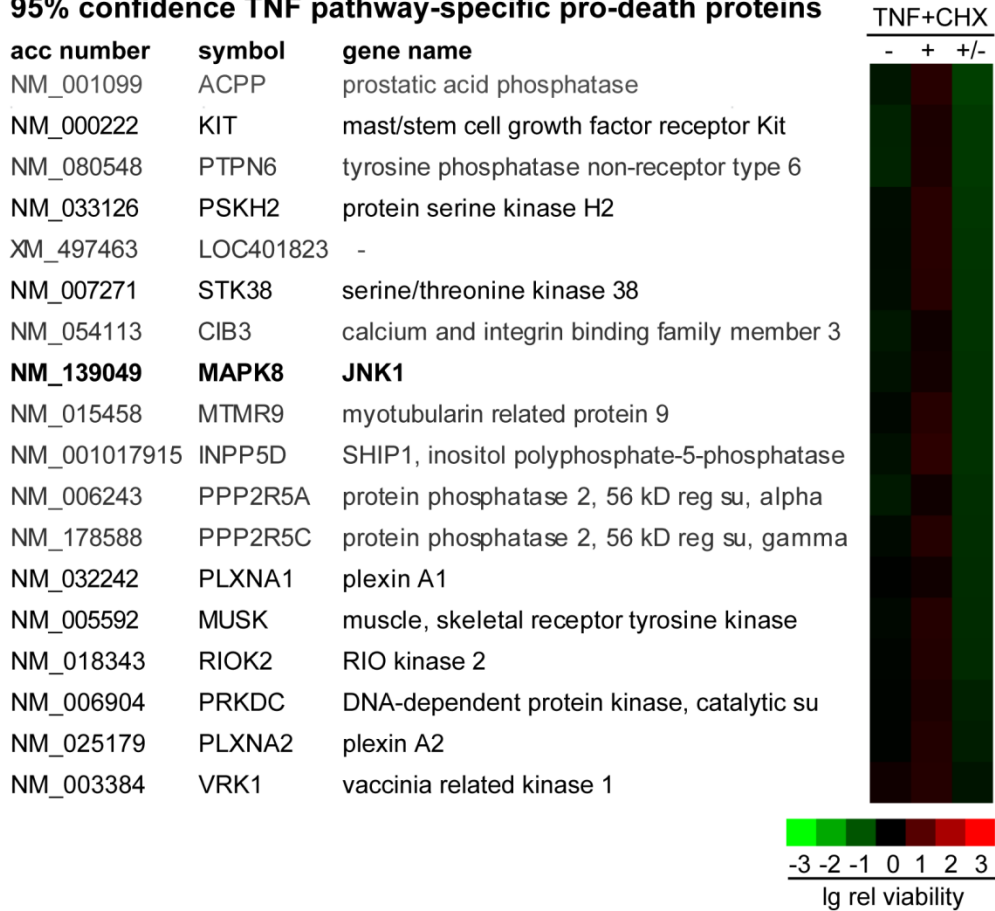


Figure 4.9. 95% confidence pro-death proteins in TNF-induced death. NCBI RefSeq gene accession number, symbol and name are shown for each gene. The heat map shows the base two log-transformed median viability value in the absence and presence of TNF and CHX and the base two log-transformed median death index for each gene. All genes are sorted according to the median death index in ascending order. Kinase-encoding genes are shown in black font and phosphatase-encoding genes in grey font. Key TNF signaling molecules are highlighted in bold.

Depletion of diacylglycerol kinase delta (DGKD) and dolichyl pyrophosphate phosphatase (DOLPP1) surprisingly also significantly enhanced TNF-induced death (**figure 4.7.**). It is possible that these counter-intuitive observations are the result of off-target effects (OTEs) for the specific siRNAs. I categorized the two proteins as general pro-death proteins with TNF-specific effect, with the caveat that both gene products require detailed molecular characterization to define their true biological functions.

I defined siRNA targets that had measurable impacts on cell viability only in the presence of TNF and CHX as proteins with a regulatory effect on TNF-induced death. I identified forty eight potential TNF-specific high confidence pro-survival proteins (**figure 4.8.**), and eighteen potential TNF-specific high confidence pro-death proteins (**figure 4.9.**).

4.5. Evaluation of screen results for established TNF pathway components.

The screen placed NEMO and caspase-8 into the 95% confidence intervals for pro-survival and pro-death proteins, respectively. Furthermore, I identified the established pro-survival NF- κ B activating proteins TAB2 [93] and NEMO [88, 90, 91, 482], and MEKK2 [103] (**figure 4.8.** and **figure 4.10.**) and the pro-death protein JNK1 [494] (**figure 4.9.**) in the anticipated groups with high confidence.

I then analyzed the primary screen data to determine the phenotypes identified for additional established TNF pathway components. I found that elements of the NF- κ B arm clustered as pro-survival proteins, while members of the JNK, caspase, and RIPK arms clustered as pro-death proteins (**figure 4.11.**). I note that these phenotypes are in line with the established roles of the NF- κ B [50, 462, 480], JNK [142, 494, 495], and caspase [48] modules in the regulation of TNF-responsive cell death.

Proteins with partial redundancies, such as TAK1 [463], appeared in lower confidence intervals than non-redundant proteins like TAB2 and NEMO [463]. In general, these findings demonstrate that the screen successfully categorized a cohort of known modifiers of TNF-responsive apoptosis.

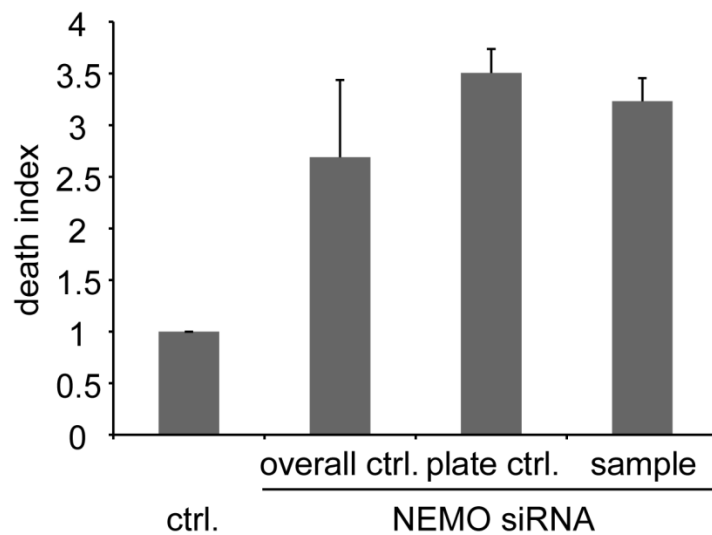


Figure 4.10. Confirmation of NEMO as a modifier of TNF-induced death in the screen. All death indices are reported relative to the screen-wide mean death index + S.E.M. of cells treated with a non-silencing siRNA control (ctrl.) in column one. Column two shows the mean death index + S.E.M. for all NEMO control siRNAs from the entire screen. Column three shows the mean death index + S.E.M. of the NEMO controls from the kinase plate that contained the identical NEMO siRNA as an experimental siRNA. The mean death index + S.E.M. of the NEMO experimental siRNAs is shown in column four.

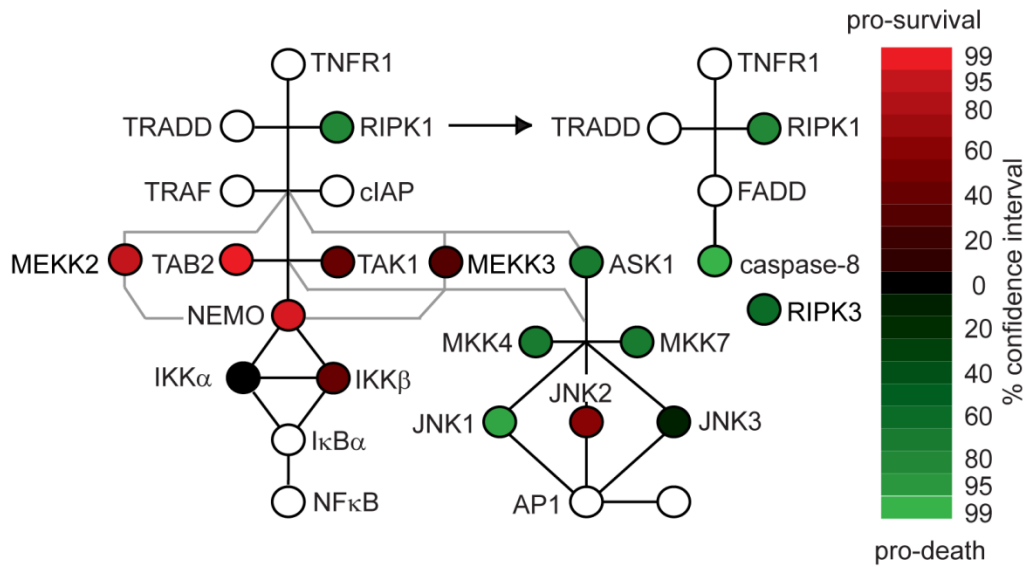


Figure 4.11. Heat map of the death indices of known TNF pathway components in the screen. Graphic representation of the TNF pathway interaction network. The color of the circle indicates the confidence interval of the median death index of the respective protein. White circles indicate proteins that were not tested in the screen.

4.6. HK1 is a negative regulator of TNF-induced death.

Of the approximately one thousand genes examined, hexokinase 1 (HK1) had the strongest TNF-specific pro-survival phenotype (**figure 4.12.A**). All three siRNAs tested in the primary screen produced phenotypes comparable to or greater than the pro-survival protein NEMO (**figure 4.12.B**) and suggest that HK1 has essential pro-survival functions in the TNF pathway. Two of the three siRNAs generated death indices that were greater than three-fold higher than the death indices of control cells and fell into the 99% confidence interval for pro-survival proteins. The death index of the third siRNA fell into the 90% confidence interval. Importantly, loss of HK1 did not have non-specific adverse effects on cell viability, which indicates that loss of HK1 enhances the induction of cell death by TNF (**figure 4.12.C**).

The pro-survival function appears specific to the HK1 isozyme as the siRNAs that target HK2, HK3 or HK4 had negligible impacts on TNF-induced death (**figure 4.12.B**). Only one of 3 siRNAs that target HK2 yielded a death index in the 95% confidence interval for pro-survival proteins. Given the extensive sequence identity between HK1 and HK2, I cannot exclude the possibility that the HK2 siRNA has unintended effects on the expression of HK1. As with all siRNA screens a conclusive statement about the impact of HK2, HK3, and HK4 on TNF signaling requires evaluation in secondary assays. I elected to focus on the characterization of HK1 in TNF signaling as it generated a reproducible, prominent TNF-dependent phenotype.

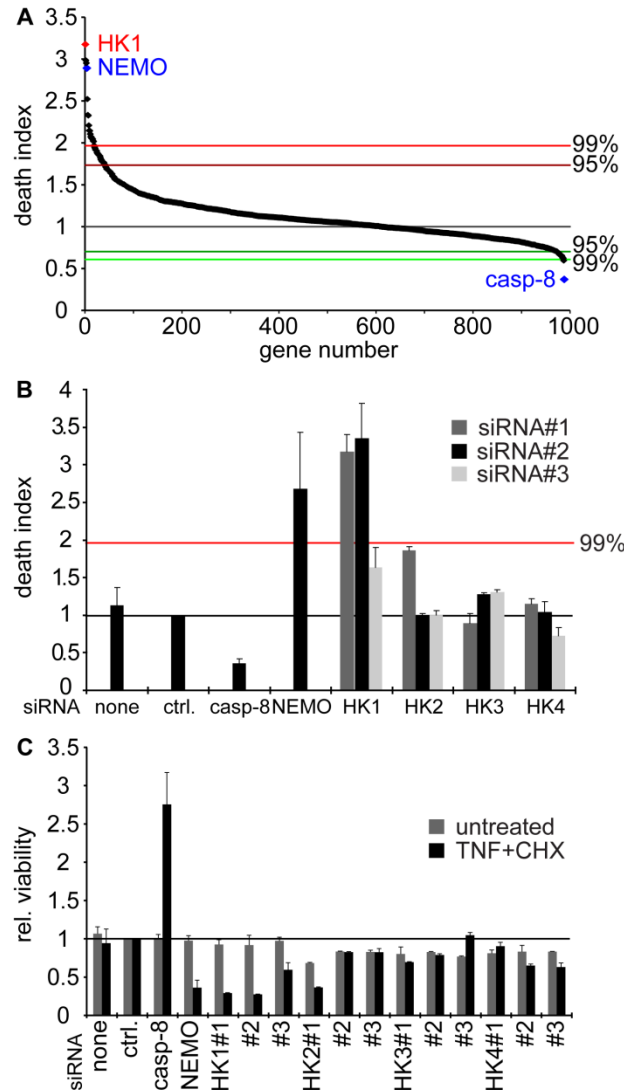


Figure 4.12. The siRNA screen revealed HK1 as a negative regulator of TNF-induced death. **A:** Distribution of the median siRNA death indices of all screened genes in descending order. 99% and 95% confidence intervals are indicated for enhancers and suppressors of cell death. The death index of cells treated with HK1 siRNA, NEMO control siRNA or caspase-8 (casp-8) control siRNA is indicated. **B:** Death indices of all 4 HK isoforms in the screen. The mean death index + S.E.M. is shown for each siRNA. All death indices are normalized to the death index of cells treated with a non-silencing control siRNA (ctrl.), which was assigned a value of one (black line). The death indices of control cells treated with caspase-8 (casp-8) siRNA, NEMO siRNA or no siRNA (none) are shown as the mean value + S.E.M. from all screen plates. The red line indicates the 99% confidence interval. **C:** Normalized cell viability for each HK isoform and the three specific siRNAs in the absence (untreated) and presence of TNF and CHX. The viability of cells treated with non-silencing control siRNA (ctrl.) under both conditions was assigned a value of one, and all other values are reported relative to that value.

CHAPTER 5. CHARACTERIZATION OF HK1 AS AN ANTI-APOPTOTIC PROTEIN.

A version of this chapter has been published:

Schindler A, Foley E: A functional RNAi screen identifies hexokinase 1 as a modifier of type II apoptosis. *Cell Signal* 2010. 22(9):1330-40.

5.1. Background.

In the siRNA screen for modulators of TNF-induced death, I identified HK1 as a pro-survival protein. HK1 [286] is one of four HK isozymes [293]. The isozymes are encoded by four different genes that result from gene duplication and fusion events [299, 300]. Of all four HK isozymes, I only identified HK1 as a high confidence regulator of TNF-induced death.

HKs are well known for their metabolic role in the phosphorylation of glucose [293]. Of the four isozymes, HK1 is most ubiquitously expressed and has the most clearly defined function [293]. HK1 predominantly channels glucose into the catabolic pathway of glycolysis, followed by the tricarboxylic acid cycle and oxidative phosphorylation to generate the energy equivalent ATP [293]. Together with HK2, HK1 assumes a dynamic and regulated interaction with the outer mitochondrial membrane [307]. Mitochondrial HK1 couples the rate of glycolysis with the rate of oxidative phosphorylation by using mitochondrial ATP to generate glucose 6-phosphate [293]. Interestingly, recent reports also ascribe anti-apoptotic roles to mitochondrial HKs. For example, mitochondrial HKs are believed to mediate anti-apoptotic effects of growth factors [340-342, 357, 368-370]. Data suggest that growth factors promote the interaction of HKs with mitochondria [360, 386, 388] and ultimately block apoptosis upstream of cytochrome c release [367]. The specific anti-apoptotic role of HK1 in that process has only been demonstrated in overexpression studies and with intrinsic apoptotic stimuli. Specifically, previous studies demonstrated that overexpression of HK1 countered cell-death induced by growth factor withdrawal alone [368] or growth factor withdrawal in combination with UV light [357], or oxidants [369].

In light of the reports of the anti-apoptotic role of mitochondrial HKs in growth factor signaling, I hypothesized that there are parallels between the anti-apoptotic role of HK1 in growth factor signaling and the pro-survival role for HK1 in the control of TNF-induced death. Consistent with this hypothesis, a previous study found that, Akt double knock-out (DKO) mouse embryonic fibroblasts (MEFs) are more sensitive to TNF-induced apoptosis [496]. Moreover, TNF-induced apoptosis requires mitochondrial amplification in type II HeLa cells [162-164]. Thus, I hypothesized:

(1) HK1 is a negative regulator of extrinsic death receptor-induced apoptosis.

(2) HK1 acts at the mitochondria to block TNF-dependent cell death.

5.2. Confirmation of HK1 as a negative regulator of TNF-induced death.

To validate HK1 as a pro-survival gene product, I retested the three HK1 siRNAs from the screen in addition to four independent HK1-specific siRNAs from a separate vendor for their respective impact on TNF-induced cell death. Six of the seven non-overlapping siRNAs led to clearly increased death indices (**figure 5.1.A, B**). In several cases, the death indices were comparable to or higher than those observed for NEMO siRNA. The enhanced cell death upon HK1 depletion is not an indirect consequence of exposure to CHX, as a combined regime of HK1 siRNA and CHX had minimal effects on cell viability (**figure 5.1.C**). These data confirm that HK1 is a negative regulator of TNF-induced cell death. However, almost all siRNAs, including the ones used in the screen, also mildly reduced cell viability in the absence of TNF and CHX (**figure 5.1.A**).

To confirm that the HK1 siRNAs effectively targeted HK1, I treated HeLa cells with the three HK1 siRNAs from the screen and monitored the relative expression of HK1 by Western blot analysis and quantitative real-time PCR. All siRNAs caused a pronounced reduction in HK1 protein levels (**figure 5.2.A**) and transcript levels (**figure 5.2.B**) after a three day incubation period. As HK1 and HK2 are paralogous genes with considerable overlaps in terms of sequence (73.4% sequence identity) and function [299], I tested whether the phenotype ascribed to HK1 may result from a parallel, off-target depletion of HK2. To this end, I measured the levels of HK2 transcripts in cells treated with the three HK1 siRNAs from the screen. Of the three siRNAs examined, only siRNA#3 also interfered with the expression of HK2 (**figure 5.2.C**). I consider the parallel knockdown of HK2 likely an OTE, as siRNA#3 shares a significant sequence similarity with HK2 (84% identity) (**figure 5.2.E**). As a consequence, I used siRNA#1 or #2 in subsequent assays. Interestingly, depletion of HK1 by siRNAs#1 and #2 was accompanied by increased HK2 mRNA levels (**figure 5.2.C**) and protein levels (**figure 5.2.D**), which may indicate mutual regulation of gene expression and redundant functions of HK1 and HK2.

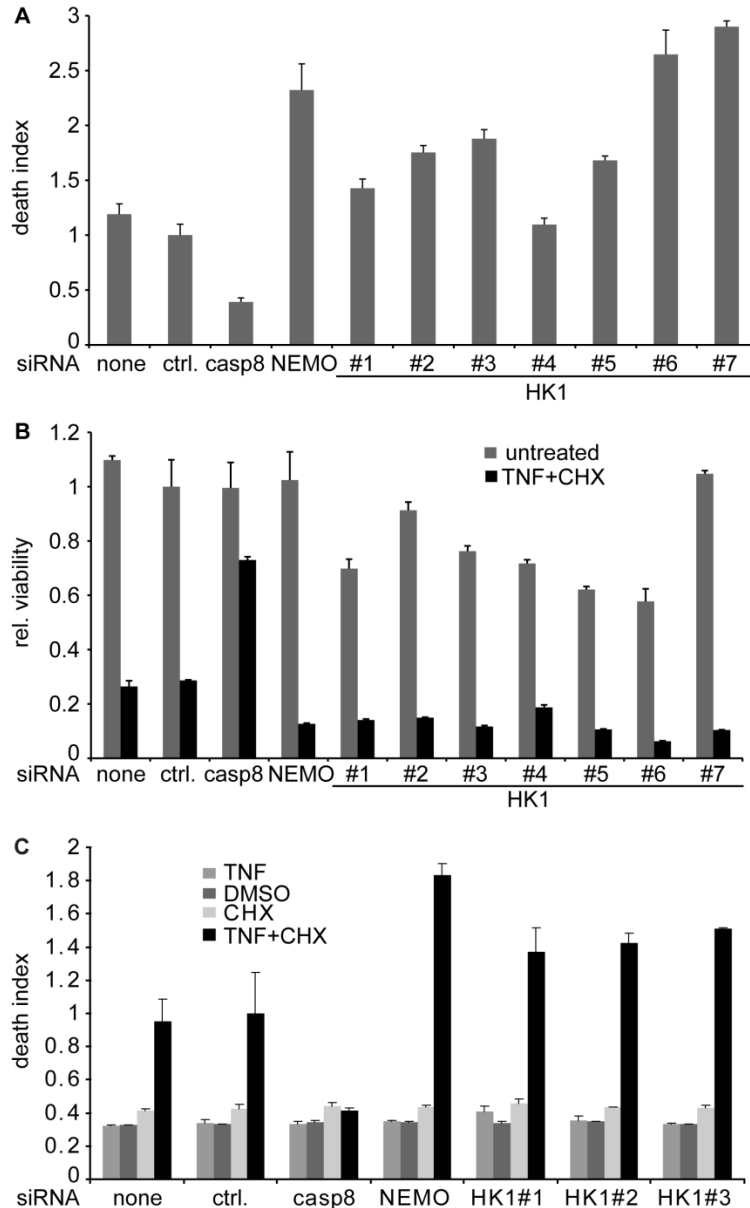


Figure 5.1. HK1 regulates TNF-induced death. **A:** Death indices of HeLa cells depleted of HK1 and treated with TNF and CHX. siRNAs #1 to #3 were used in the screen, #4 to #7 are independent siRNAs from a different vendor. Death indices were determined in a resazurin viability assay and are reported relative to the death index of cells treated with a non-silencing control siRNA (ctrl.). Control cells were treated with a caspase-8 (casp-8) siRNA, NEMO siRNA, or no siRNA (none). Data are representative of three independent experiments. **B:** Viability values of HeLa cells from panel A in the absence and presence of TNF and CHX. **C:** Death indices of HeLa cells depleted of HK1, NEMO, or caspase-8 (casp-8) and treated with TNF, CHX, the CHX solvent DMSO, or TNF and CHX. All death indices are reported as the mean + S.E.M. of two independent experiments and relative to the death index of cells treated with a non-silencing siRNA (ctrl.) and TNF and CHX. The death index of cells treated with a non-silencing siRNA and TNF and CHX was assigned a value of one.

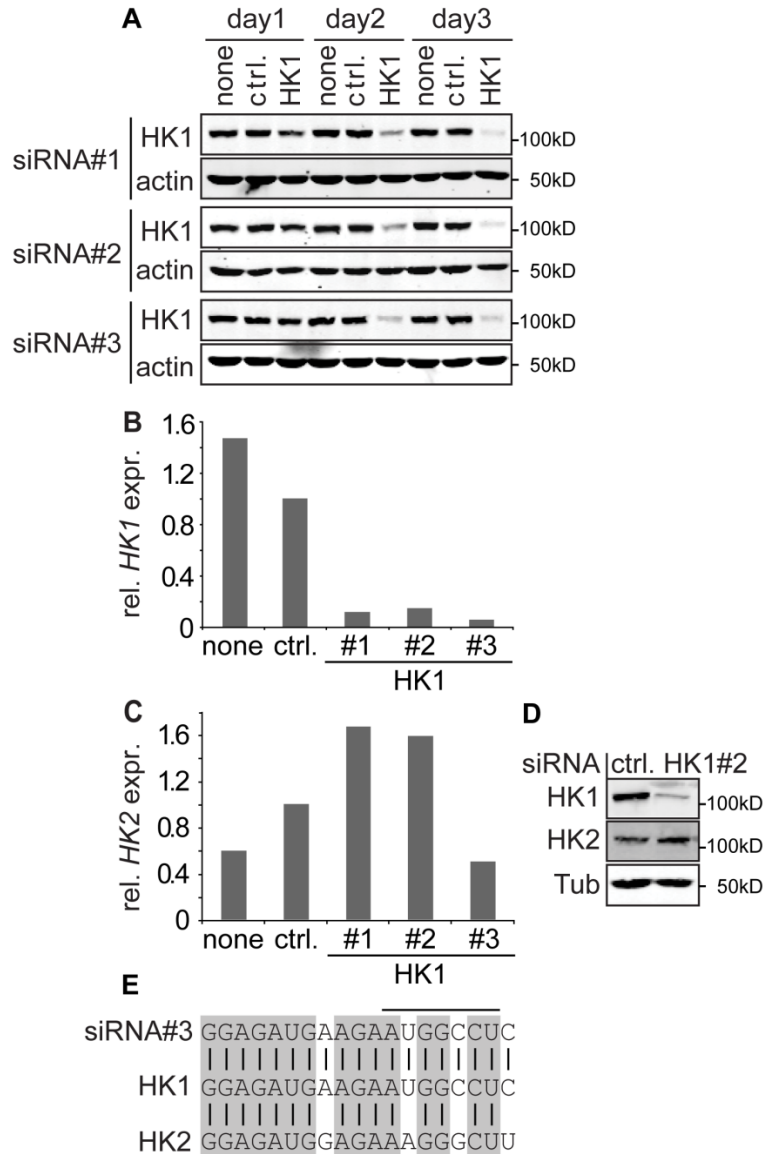


Figure 5.2. Confirmation of siRNA-mediated HK1 depletion. **A:** Western blot of HK1 expression in HeLa cells transfected with non-overlapping HK1 siRNAs #1 to #3, a non-silencing control siRNA (ctrl.), or no siRNA (none). For each day after the transfection, cell lysates were probed with an antibody against HK1, and actin as a loading control. **B,C:** Relative *HK1* (E) or *HK2* (F) expression levels in cells treated with HK1 siRNAs #1 to #3 as determined by quantitative real-time PCR. All values were normalized to the *HK* expression level in cells treated with a non-silencing control siRNA (ctrl.). **D:** Western blot of the expression of HK1 and HK2 after treatment of HeLa cells with HK1#2 siRNA for three days. Control cells were incubated with a non-silencing siRNA (ctrl.). Cellular lysates were probed with an antibody against HK1, HK2, and tubulin (Tub) as a loading control. **E:** Sequence alignment between HK1 siRNA#3 passenger strand, HK1 target sequence and HK2 off-target sequence. Identical nucleotides are highlighted in grey, and the complement of the seed region of the siRNA is labeled with a black line.

5.3. Effects of HK1 depletion on the TNF signaling modules.

5.3.1. HK1 depletion does not attenuate TNF-induced NF- κ B signaling.

To characterize the pro-survival role of HK1 in TNF-induced death, I first sought to identify the point, at which HK1 interacts with the TNF pathway. Given its pro-survival role in TNF-induced death, I reasoned that HK1 may be a positive regulator of NF- κ B pro-survival signaling or a negative regulator of JNK or caspase pro-apoptotic signaling. Reports on the anti-apoptotic role of mitochondrial HKs in growth factor signaling [341, 357, 368, 370] suggest an interaction of HK1 with TNF-induced cell death at the level of the mitochondria. However, to assure that I would not miss other potential interactions, I also tested for regulatory effects of HK1 on other TNF signaling modules.

To test if HK1 regulates the NF- κ B arm of the TNF pathway, I transfected HeLa cells with siRNAs, which deplete HK1 or the key NF- κ B signaling molecules NEMO and TAB2, and monitored several classic features of TNF-induced NF- κ B activation. TNF typically results in a rapid transient phosphorylation of I- κ B- α by the IKK complex [463, 465-468, 476], and loss of the IKK component NEMO [90, 91, 463] reduced the extent of I- κ B- α phosphorylation on a Western blot (**figure 5.3.A**). In contrast, depletion of HK1 did not affect the kinetics or reduce the extent of I- κ B- α phosphorylation. I also monitored the effect of HK1 loss on the expression of the NF- κ B responsive transcripts *A20* and *IKBA* in quantitative real-time PCR. Whereas depletion of NEMO diminished the expression of *A20* and *IKBA*, loss of HK1 did not alter *A20* or *IKBA* expression levels (**figure 5.3.B, C**). Finally, loss of the TNF receptor or its adaptor TAB2 [93] resulted in decreased NF- κ B reporter activity, whereas NF- κ B reporter activity was indistinguishable in control cells and cells treated with HK1 siRNA (**figure 5.3.D**). In combination, these data indicate that HK1 loss does not negatively affect the NF- κ B transcriptional pathway and suggest that HK1 is not a positive regulator of TNF-induced NF- κ B signaling.

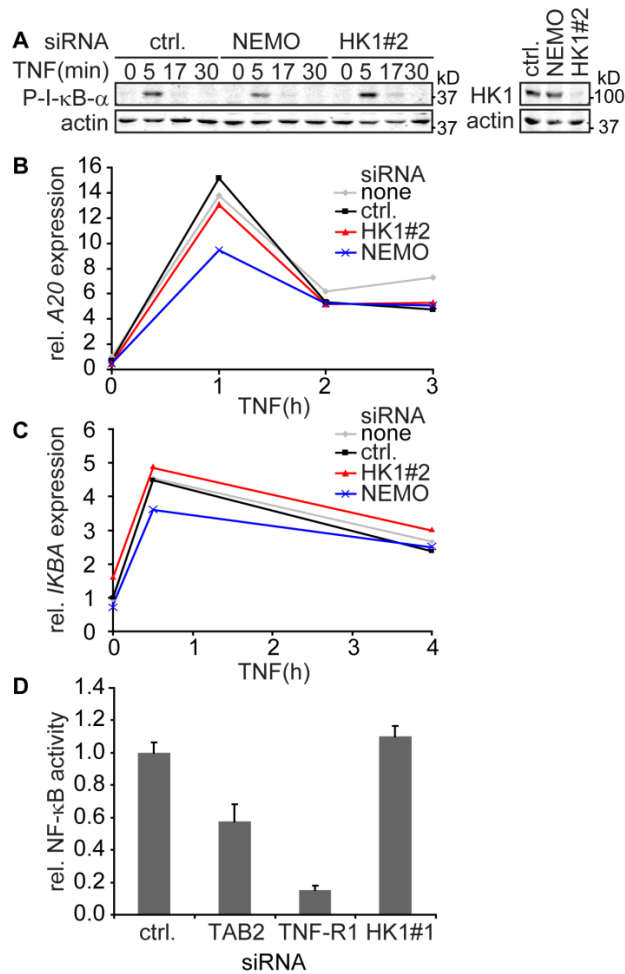


Figure 5.3. HK1 depletion does not attenuate NF-κB signaling. **A:** Western blot of the time course of I-κB-α phosphorylation after TNF stimulation. HeLa cells were treated with HK1 siRNA, NEMO siRNA, or a non-silencing control siRNA (ctrl.) and stimulated with TNF for the indicated time periods. The Western blot to the right shows the respective HK1 levels for the three siRNA treatments in unstimulated cells. Actin served as a loading control. **B,C:** Time course of the relative expression of *A20* (B) or *IKBA* (C) after TNF stimulation. HeLa cells were treated with HK1 siRNA, NEMO siRNA, a non-silencing control siRNA (ctrl.), or no siRNA (none) and stimulated with TNF for the indicated time periods. All values are reported relative to *A20* or *IKBA* expression in unstimulated cells treated with a non-silencing control siRNA. RNA from two independent experiments was pooled for quantitative real time PCR. **D:** Quantification of the TNF-induced NF-κB activity in an NF-κB reporter assay. HEK293T cells were treated with HK1 siRNA, TNF-R1 siRNA, TAB2 siRNA, or a non-silencing control siRNA (ctrl.) prior to stimulation with TNF. NF-κB activity is presented as the luminescence derived from the expression of an NF-κB dependent luciferase reporter relative to a control luciferase reporter. NF-κB activities are shown as the mean luminescence + S.E.M. of three replicate measurements. All values are reported relative to the NF-κB activity of cells treated with a non-silencing siRNA, which was assigned a value of one.

5.3.2. HK1 depletion accelerates TNF-induced apoptosis.

While secondary analyses indicated that HK1 does not interact with the NF- κ B module of the TNF pathway, I noticed that depletion of caspase-8 completely reverted the TNF-induced cell death seen upon loss of HK1 (**figure 5.4.**). These data indicate that loss of HK1 does not bypass caspase-mediated signals to reduce cell viability in the presence of TNF and CHX and that HK1 modifies the caspase signaling cascade to attenuate TNF-induced death.

To explore the link between HK1 and the apoptotic caspase cascade, I characterized the consequences of HK1 loss for progression through TNF-induced apoptosis. I initially examined the effect of HK1 depletion on a very distal event in apoptotic signaling: cleavage of the caspase substrate Poly [ADP-ribose] polymerase (PARP) [497-499]. PARP1 localizes to the nucleus and serves in DNA damage repair [500]. During apoptosis, activated effector caspases cleave 113 kD PARP1 into the 24 kD amino-terminal DNA-binding domain and the 89 kD carboxyl-terminal catalytic domain [497-499]. I detected the progressive accumulation of the carboxyl-terminal PARP1 cleavage product in lysates of HeLa cells treated with a non-silencing siRNA 5 to 9 hours after treatment with TNF and CHX (**figure 5.5.A**). Simultaneously, the levels of full-length PARP progressively decreased after treatment with TNF and CHX. As expected, interruption of TNF-induced caspase signaling by depletion of the initiator caspase caspase-8 prevented cleavage of PARP1. Depletion of NEMO attenuated TNF-induced NF- κ B signaling and enhanced TNF-induced caspase signaling (**figure 3.4.**). In line with those findings, NEMO depletion also greatly enhanced and accelerated PARP1 cleavage (**figure 5.5.A**). Five hours after the apoptotic stimulus, full-length PARP1 was no longer detectable, while the large cleavage fragment accumulated. Cells with a loss of HK1 essentially mirrored the NEMO phenotype. Depletion of HK1 with each of three independent siRNAs resulted in accelerated TNF-induced PARP cleavage. However, in contrast to NEMO depletion, loss of HK1 through two of the three siRNAs led to a minor level of PARP1 cleavage even in the absence of TNF and CHX, similarly to the slightly decreased viability in resazurin assays.

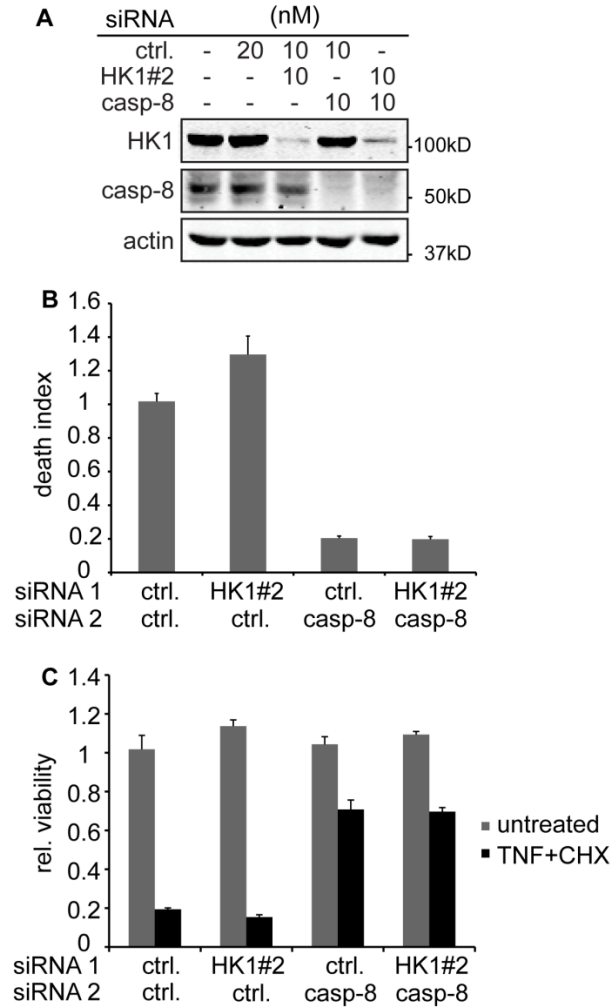


Figure 5.4. HK1 modifies TNF-signaling through the apoptotic cascade. A: Western blot of the expression of HK1 and caspase-8 in HeLa cells treated with combinations of a non-silencing control siRNA (ctrl.), HK1 siRNA, and caspase-8 siRNA (casp-8). Control cells were not treated with siRNA. The total siRNA concentration for all other cell populations was 20 nM. siRNAs were combined in the indicated concentrations. Cell lysates were probed with HK1, caspase-8 (casp-8), and actin antibody. Actin served as a loading control. **B:** Death indices of the cell populations in panel A treated with the combination of siRNA1 and siRNA2, and TNF and CHX in a resazurin viability assay. All death indices are presented as the mean of two technical replicates + S.E.M. and relative to the death index of cells treated with 20 nM control siRNA, which was assigned a value of one. **C:** Viability values of the cell populations in A in the absence and presence of TNF and CHX.

These data demonstrate that HK1 is a negative regulator of TNF-induced caspase signaling, with a phenotype comparable to established key anti-apoptotic regulators of TNF signaling.

Caspase processing occurs concomitantly with initiator caspase activation and is the pre-condition for effector caspase activation [25, 27]. TNF-induced apoptotic signals activate the initiator caspase caspase-8 at the TNF receptor complex II [47]. The dimerization of caspase-8 monomers at complex II induces the conformational changes for caspase activation [30, 31]. Dimerization is accompanied by proximity-induced auto-processing that disconnects the pro-domain and large and small catalytic subunits, but maintains and stabilizes the active dimer structure [30, 31].

In type II HeLa cells, active caspase-8 activates effector caspases through the mitochondrial apoptotic pathway [162-164]. Loss of mitochondrial integrity leads to the activation of caspase-9 in the apoptosome [180]. The processing mechanisms are similar for caspase-8 and caspase-9 [192]. Finally, caspase-9 activates effector caspases like caspase-3 [189, 194]. Inactive caspase-3 exists as a homodimer. Caspase-9 mediated processes the linker between the large and small subunit of caspase-3 to initiate the conformational changes required for caspase-3 activation [25, 27].

To examine the effects of HK1 depletion on TNF-induced caspase signaling, I transfected HeLa cells with HK1 siRNA or a non-silencing control siRNA. On day three after transfection, I treated cells with TNF and CHX to induce apoptosis and monitored processing of caspase-8, caspase-9 and caspase-3 via Western blot analysis of the cell lysates (**figure 5.5.B**). I detected processing of all three caspases in control cells three hours after the treatment with TNF and CHX. Processing of 55 kD caspase-8 resulted in the progressive accumulation of a roughly 43 kD fragment of the caspase-8 pro-domain and the large subunit p18, as well as the p18 cleavage product. Cleavage of 47 kD caspase-9 resulted in the accumulation of p37 and p35 cleavage products. Cleavage of caspase-3 resulted in accumulation of p19 and p17 large subunits. As the cleavage products accumulated, levels of full-length caspase-8 and 9 diminished.

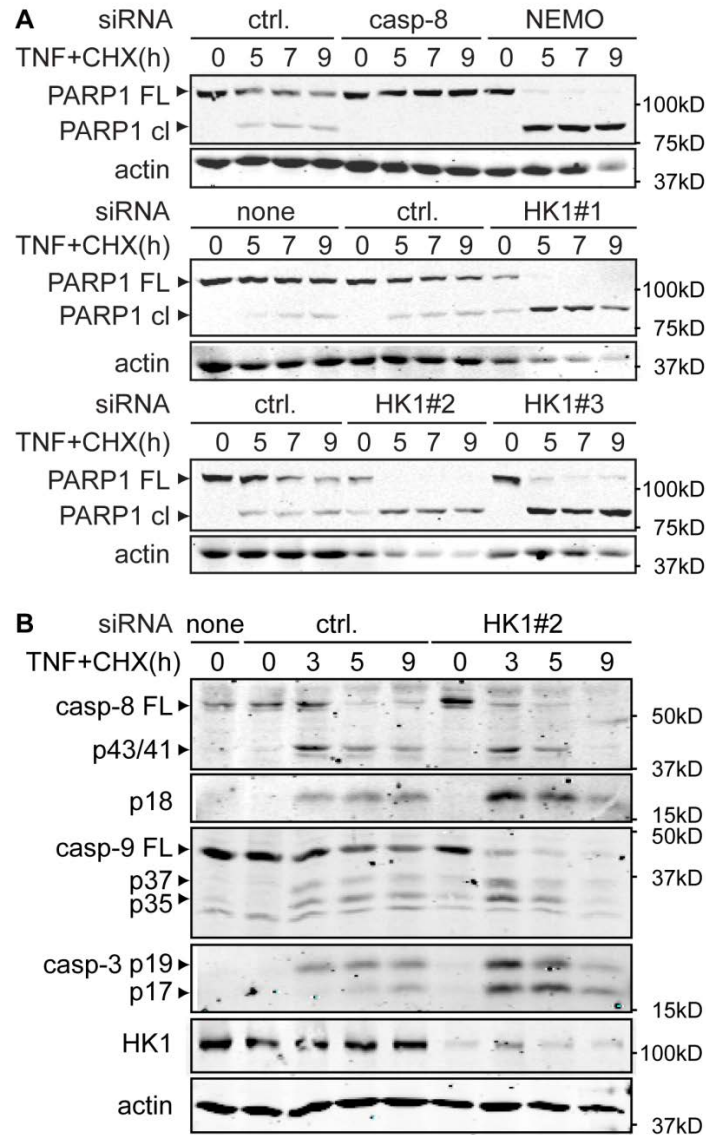


Figure 5.5. HK1 depletion accelerates TNF-induced caspase and caspase substrate processing. **A:** Western blot of the time course of the cleavage of full-length PARP1 (PARP1 FL) into the large 89 kD fragment of PARP1 (PARP1 cl) after incubation with TNF and CHX. HeLa cells were pretreated with three different HK1 siRNAs, caspase-8 siRNA, NEMO siRNA, a non-silencing control siRNA (ctrl.), or no siRNA (none). Cell lysates were probed with an antibody against PARP1, and actin as a loading control. **B:** Western blots of the time course of caspase cleavage after treatment with TNF and CHX. HeLa cells were treated with HK1 siRNA or a non-silencing control siRNA (ctrl.). Cell lysates were probed with an antibody that detects full-length caspase-8 (casp-8 FL) and p43/41 and p18 cleavage products, an antibody that detects full-length caspase-9 (casp-9 FL) and the p37 and p35 cleavage products, an antibody against the cleavage products p19 and p17 of caspase-3 (casp-3), an antibody against HK1, and actin as a loading control.

Full-length caspase-8 was hardly visible nine hours after TNF and CHX treatment, whereas full-length caspase-9 was still detectable. These processing patterns are consistent with the earlier involvement of caspase-8 in TNF-responsive apoptosis [47].

Loss of HK1 accelerated the processing of all three caspases. Full-length caspase-8 and 9 were almost completely processed three hours after incubation with TNF and CHX. In parallel, HK1 depletion enhanced the accumulation of the large active subunit of all caspases. Over the next six hours full-length caspase-8 and 9 and even the large subunits progressively diminished. In conclusion, depletion of HK1 accelerated processing of key caspases in the TNF-induced caspase signaling cascade. These findings are in line with accelerated processing of the effector caspase substrate PARP after HK1 depletion and suggest that loss of HK1 accelerated TNF-induced apoptosis.

I noticed a low level of caspase-9 and caspase-3 cleavage upon HK1 depletion prior to the addition of TNF and CHX. These observations are in line with the low level of PARP cleavage and mildly reduced viability observed after HK1 depletion. It is intriguing to speculate that these phenotypes may reflect a requirement for HK1 in the mitochondrial regulation of apoptosis.

In type II cells, loss of mitochondrial integrity is a pre-condition for the activation of caspase-9 and effector caspases. Disruptions to mitochondrial integrity are also critical elements of a feedback loop that potentiate caspase-8 contributions to apoptosis [162, 194]. Loss of OMM integrity occurs through the formation of Bak and Bax channels [170] and decreases the IMM potential. Specifically, loss of cytochrome c, influx of apoptotic effector caspases and the possible formation of MPTPs impede the activity of the electron transport chain and dissipate the IMM potential [170]. Therefore, I examined the effect of HK1 depletion on the TNF-induced decrease of the IMM potential. The cationic dye TMRE provides a convenient measure of the IMM potential in a flow-cytometric assay [481]. The IMM potential causes the accumulation of TMRE in the negatively charged mitochondrial matrix [481]. As TMRE fails to accumulate in the mitochondria of dead or dying cells, TMRE provides a reliable proxy measurement of mitochondrial function.

I used three independent HK1 siRNAs to test the effect of HK1 depletion on the TNF-induced decrease of the IMM potential. On day three after transfection, I treated with TNF and CHX to induce apoptosis and measured the IMM potential in a TMRE assay. As expected, cells treated with a non-silencing control siRNA, exhibited a steady growth of the population with decreased IMM potential over the course of eight hours treatment with TNF and CHX (**figure 5.6.A**). Depletion of caspase-8 completely abrogated the loss of the IMM potential. In contrast, depletion of NEMO resulted in a small population with a decreased IMM potential prior to addition of TNF and CHX. In addition, loss of NEMO resulted in a four-fold higher rate of apoptosis in TNF and CHX treated cells compared to a population of control cells treated with a non-silencing siRNA, TNF and CHX. Interestingly, loss of HK1 resulted in a dissipation of the IMM potential at rates that paralleled cells treated with NEMO siRNA. Similar to cells treated with NEMO siRNA, each HK1 siRNA increased the amount of cells with a decreased IMM potential prior to incubation with TNF and CHX.

As depletion of HK1 enhances the loss of the IMM potential by TNF and CHX, I asked if overexpression of HK1 impedes the ability of a TNF and CHX regime to disrupt mitochondrial function. For these experiments, I transfected HeLa cells with an expression construct for carboxyl-terminally GFP-tagged HK1 or GFP as a control. I then stimulated the transfected cells with TNF and CHX to induce apoptosis. Subsequently, I measured the size of the GFP-transfected population that displayed a reduced IMM potential in a TMRE assay. As expected, the percentage of GFP-transfected control cells with decreased IMM potential increased in response to TNF and CHX (**figure 5.6.B**). At all time points, the fraction of cells with a decreased IMM potential surpassed the one of cells treated with a control siRNA and TNF and CHX (**figure 5.6.A**), which might result from the higher toxicity of the transfection reagent in use. Interestingly, overexpression of HK1 reduced the population with decreased IMM potential to almost two thirds of the control population.

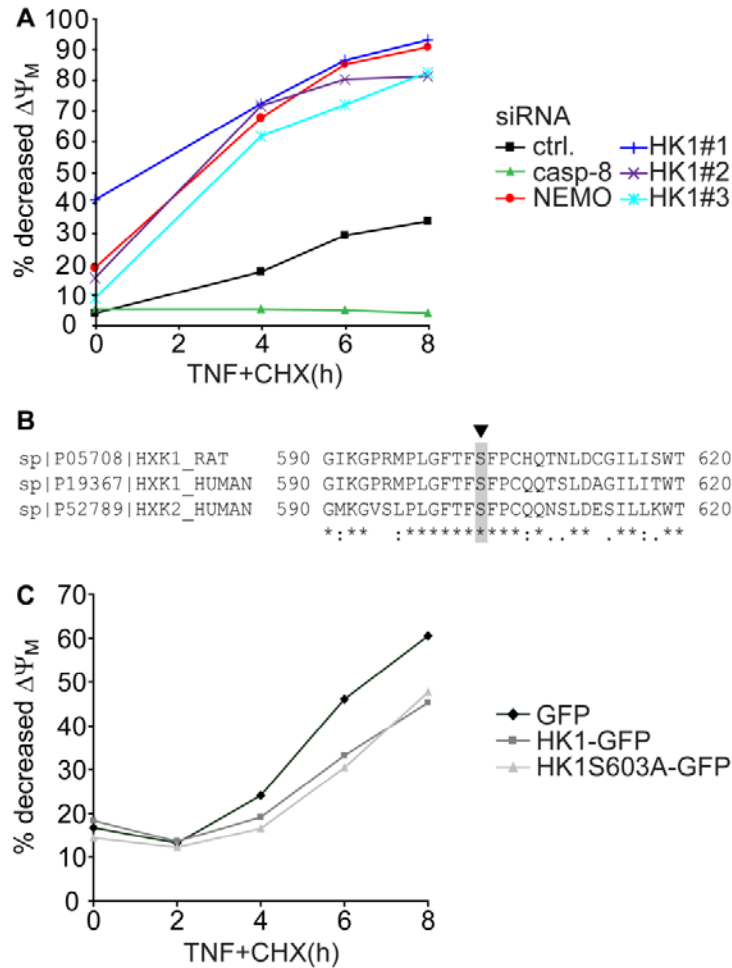


Figure 5.6. HK1 attenuates the TNF-induced decrease of the IMM potential.

A: Time course of the percentage of HeLa cells with decreased inner mitochondrial membrane potential ($\Delta\Psi_M$) after treatment with TNF and CHX. All values are presented as the percentage of cells with reduced TMRE fluorescence in a cell population that was treated with one of three HK1 siRNAs, caspase-8 siRNA, NEMO siRNA, or a non-silencing control siRNA (ctrl.). Data are representative of three independent experiments. **B:** ClustalW2 multiple sequence alignment of a fragment of the amino acid sequences of rat HK1, human HK1 and human HK2 from amino acids five hundred ninety to amino acids six hundred twenty. Identical amino acids are indicated by an asterisk (*), amino acid conservations between a group with strongly similar properties are indicated by a colon (:), amino acid conservations between a group with weakly similar properties are indicated by a colon (.). Serine six hundred three is indicated with an arrow head. **C:** Time course of the percentage of HeLa cells with a decrease of the inner mitochondrial membrane potential ($\Delta\Psi_M$) after treatment with TNF and CHX. All values are presented as the percentage of TMRE negative and GFP-positive cells in a cell population that was transiently transfected with HK1-GFP, HK1S603A-GFP, or a control GFP expression construct. Data are representative of six independent experiments.

I conclude that overexpression of HK1 stabilizes the IMM potential during TNF-induced apoptosis, whereas the depletion of HK1 accelerates the decrease of the IMM potential.

Ectopic expression of HK1 also mimics the anti-apoptotic effect of growth factors [357, 368, 369]. However, growth factors require glucose and HK activity to counter apoptotic insults [357, 368-370]. Serine six hundred three is essential for the catalytic activity of HK1 [298, 501] (**figure 5.6.B**). To test whether HK1 catalytic activity is required to modify TNF-induced apoptosis, I replaced serine six hundred three with an alanine to create catalytically inactive HK1. I expressed carboxyl-terminally GFP-tagged HK1S603A in HeLa cells and visualized the loss of the IMM potential by a combined TNF and CHX regime in GFP positive cells. HK1S603A blocked the dissipation of the IMM potential by TNF and CHX as efficiently as wild-type HK1 (**figure 5.6.C**). These data suggest that the catalytic activity of HK1 is not required to inhibit mitochondrial disruption by TNF.

These observations led me to examine the consequences of HK1 loss for complex II formation, which is the most upstream event in TNF-induced apoptosis signaling [47]. Complex II forms as a consequence of TNF-R1 internalization and is accompanied by the recruitment of caspase-8 and the adapter molecule FADD [47, 149]. Dimerization of caspase-8 monomers in complex II leads to rapid caspase-8 activation and proximity-induced auto-processing between the pro-domain and the large subunit p18, as well as p18 and the small subunit p11 [30, 31]. Processing stabilizes the dimer structure of caspase-8 in complex II [30, 31].

To examine the kinetics of TNF-induced complex II formation in control cells and HeLa cells depleted of HK1, I immunoprecipitated FADD and monitored the presence of caspase-8 on a Western blot. In line with previous precipitation studies [149], I detected the p43/41 fragment of caspase-8 pro-domain and large subunit p18 in FADD precipitates (**figure 5.7.A, B**), which indicates that caspase-8 was rapidly processed following recruitment into complex II. Loss of HK1 accelerated the appearance of p43/41 in FADD precipitates (**figure 5.7.B**), just as it accelerated the kinetics of cellular caspase-8 cleavage (**figure 5.7.A, 5.7.B**).

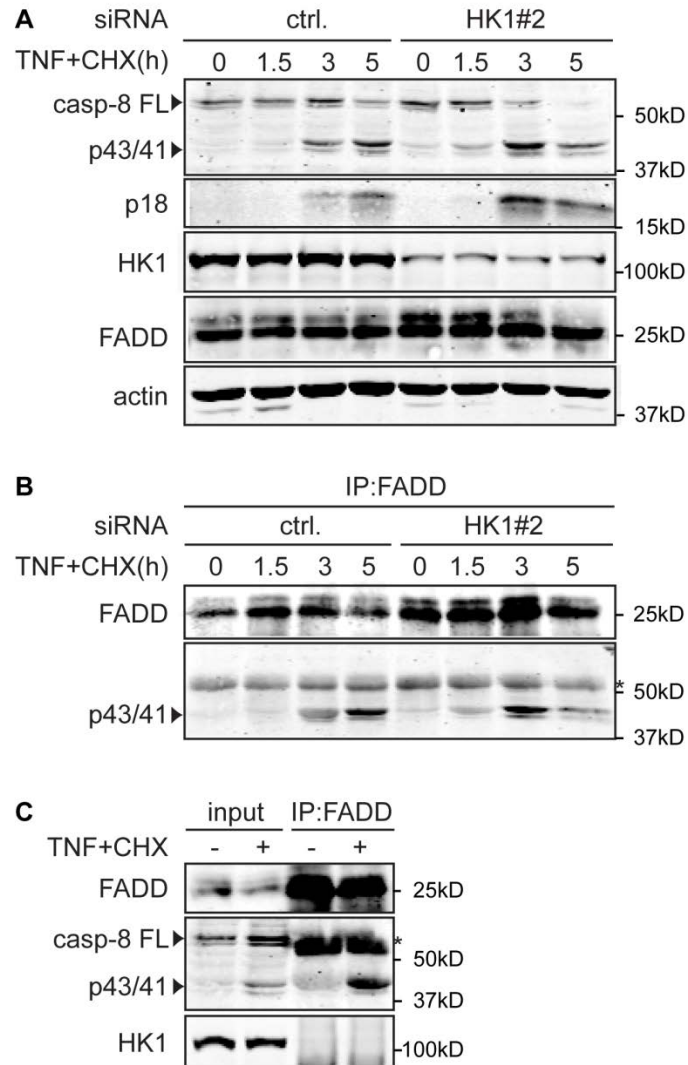


Figure 5.7. HK1 depletion accelerates the formation of complex II. A: Western blot of the time course of full-length caspase-8 (casp-8 FL) cleavage into p43/p41 and p18 variants after treatment with TNF and CHX for the indicated time periods. Cells were treated with HK1 siRNA or a non-silencing control siRNA (ctrl.) and probed with antibodies against caspase-8, HK1, FADD, and actin as a loading control. **B:** Western blot of the time course of complex II formation in HeLa cells from panel A. Cell lysates were precipitated for complex II with an anti-FADD antibody (IP:FADD). Each sample was probed with an anti-FADD and anti-caspase-8 (p43/41) antibody on a Western blot. Antibody heavy chains are labeled with *. **C:** Western blot of the immunoprecipitation of complex II. Complex II was precipitated with an anti-FADD antibody from lysates of untreated HeLa cells (-), or cells treated with TNF and CHX for five hours (+). Cell lysates (input) and precipitates (IP:FADD) were probed with antibodies against FADD, caspase-8 (casp-8), HK1, and actin as a loading control. Caspase-8 is shown as the full-length caspase-8 (casp-8 FL) and p43/41 cleavage product. Antibody heavy chains are labeled with *.

These findings underline that depletion of HK1 generates favourable conditions for the formation of the mature, active complex II.

The majority of caspase-8 activation and processing in type II cells requires inputs from the mitochondria following repression of XIAP and activation of caspase-3 and caspase-6 [162-164]. The results detailed above do not reveal if HK1 impacts caspase-8 cleavage upstream or downstream of the mitochondria.

To explore the possibility that HK1 interferes with TNF-induced caspase signaling upstream of the mitochondria, I looked for the incorporation of HK1 into complex II. FADD immunoprecipitates were repeatedly HK1-negative after incubation with TNF and CHX (**figure 5.7.C**). Thus, although I cannot exclude indirect interactions between HK1 and complex II, HK1 does not appear to be a constitutive element of complex II.

In summary, depletion of HK1 accelerated the kinetics of several features of TNF-induced apoptosis: complex II formation and caspase-8 cleavage, decrease of the IMM potential, caspase-9 and caspase-3 cleavage, and processing of the caspase substrate PARP1. HK1 overexpression decreased the rate of TNF-dependent cell death. These data argue that HK1 inhibits TNF-induced entry into and progression through the apoptotic program. The presence of apoptotic markers and the mildly reduced cell viability in the absence of TNF and CHX suggest that HK1 depletion unlocks apoptotic signals in the absence of TNF and CHX, and enables accelerated progression of apoptosis in the presence of TNF and CHX.

The pro-apoptotic phenotype of HK1 depletion is not restricted to HeLa cells, as I detected similar phenotypes in the type II U2OS osteosarcoma cell line [502] and the type II A549 lung carcinoma cell line [503] (**figure 5.8. A, B, C**). I used 3 independent siRNAs to deplete HK1 from U2OS cells and measured the levels of TNF-induced death in comparison to cells treated with non-silencing, caspase-8 or NEMO siRNA. Similar to my observations in HeLa cells (**figure 5.1.C**), depletion of caspase-8 strongly attenuated TNF-dependent death, whereas depletion of NEMO slightly accelerated TNF-induced death in U2OS cells (**figure 5.8.A**). All 3 siRNAs enhanced the induction of apoptosis by TNF and CHX. A combined treatment of CHX with any of the siRNAs did not result in an apoptotic phenotype, which indicates that the observed death in the presence of TNF and CHX is TNF-dependent. The pro-apoptotic phenotype of HK1 depletion was equally prominent in a PARP cleavage assay (**figure 5.8.B**). U2OS cells treated with a control siRNA exhibited PARP1 cleavage on a Western blot five hours after treatment with TNF and CHX. Over the course of the following four hours, the levels of PARP1 p89 continuously increased while the levels of full-length PARP1 decreased. In contrast, loss of HK1 accelerated PARP1 cleavage and resulted in complete degradation of full-length PARP1 five hours after TNF and CHX treatment. Similarly, HK1 depletion accelerated PARP cleavage in A549 cells (**figure 5.8.C**). In control cells, the levels of the full-length PARP1 decreased continuously, while the large cleavage fragment became detectable nine hours after TNF and CHX. HK1 depletion accelerated PARP1 cleavage and generated detectable levels of cleaved PARP1 p89 five hours after TNF and CHX treatment.

Moreover, I believe that the interactions between HK1 and the apoptotic machinery extend beyond TNF-specific responses, as I noticed similar effects of HK1 depletion on additional extrinsic apoptotic signals, such as Fas-crosslinking antibody or TRAIL (**figure 5.8.D, E**). Fas cross-linking antibody activates the Fas receptor [504], and soluble TRAIL activates TRAIL-R1 and TRAIL-R2 [505]. All 3 receptors belong to the class of FADD-recruiting death receptors [38]. Engagement of the receptors directly assembles a caspase-8 containing death-inducing signaling complex (DISC) at the cell membrane that grows with receptor internalization [38, 506, 507]. Thus, Fas and TRAIL receptors directly engage the apoptotic signaling cascade at the membrane receptor [38, 506, 507].

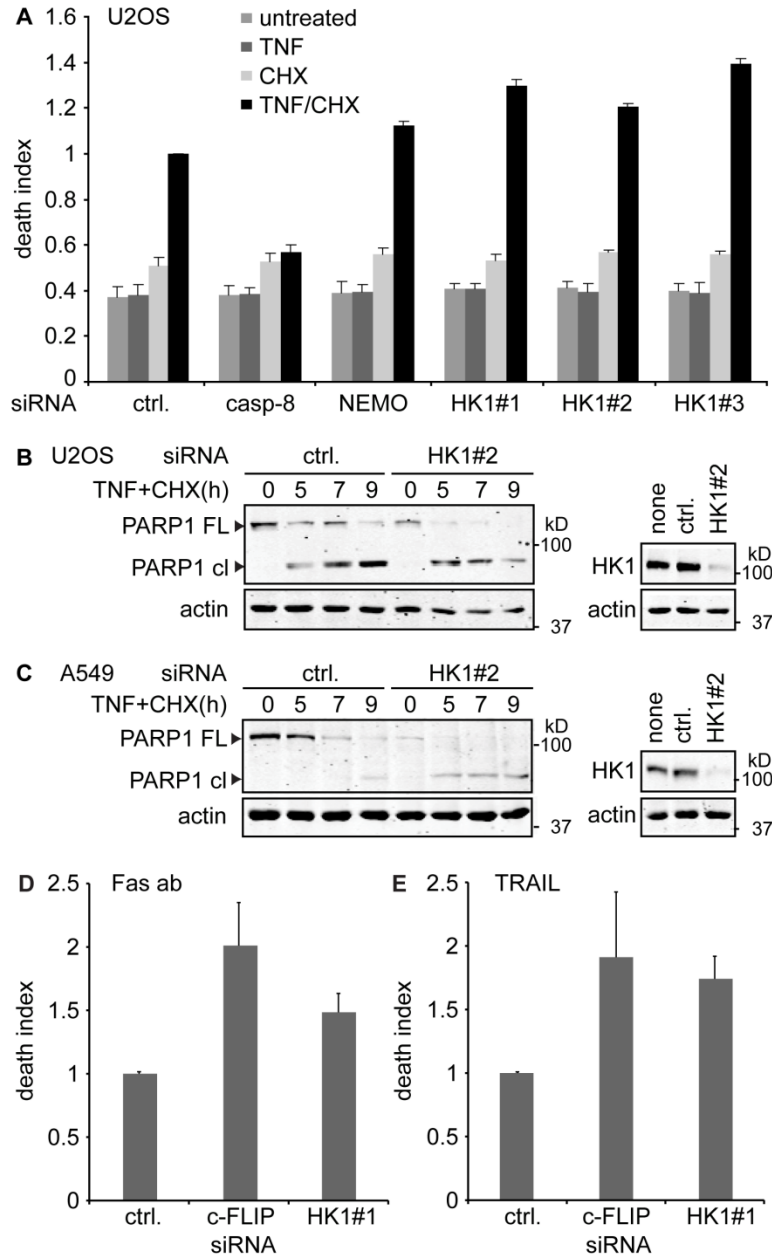


Figure 5.8. HK1 depletion accelerates death receptor-induced cell death. A: Death indices of U2OS cells depleted of HK1, NEMO, or caspase-8 (casp-8) and treated with TNF, DMSO, CHX, or TNF and CHX in a resazurin viability assay. All death indices are reported as the mean + S.E.M. of two independent experiments and normalized to the death index of cells treated with a non-silencing siRNA (ctrl.) and TNF and CHX, which was assigned a value of one. **B:** Western blot of the time course of PARP1 cleavage in U2OS cells treated with HK1 siRNA or a non-silencing control siRNA (ctrl.). Cells were incubated with TNF and CHX for the indicated time periods and lysates probed with an antibody that detects full-length PARP1 (PARP1 FL) and the large PARP1 fragment (PARP1 cl). The Western blot to the right shows the respective HK1 levels for the two siRNA treatments in unstimulated cells. Actin served as a loading control throughout. **C:** As in (B), but

for A549 cells. **D,E:** Death indices of HeLa cells depleted of HK1 and treated with an activating anti-Fas antibody (D) or recombinant TRAIL (E) in a resazurin viability assay. Death indices are reported relative to the death index of cells treated with a non-silencing control siRNA (ctrl.) and as the mean value + S.E.M. of three independent experiments. Death indices of cells treated with with a non-silencing siRNA were assigned a value of one. Cells treated with c-FLIP siRNA served as positive controls.

Importantly, the features of the apoptotic signaling cascade are conserved between TNF, Fas and TRAIL-R1 and TRAIL-R2 signaling [38, 506, 507]. As type II cells, HeLa cells recruit the mitochondrial apoptotic pathway [162-164] when stimulated with soluble TRAIL or with an antibody that cross-links Fas receptors to create a functional DISC. Both conditions led to a significant loss of cell viability in a resazurin viability assay. Depletion of HK1 increased the level of Fas receptor or TRAIL receptor-induced death to an extent comparable to the depletion of the key inhibitor of caspase-8 activation, c-FLIP [109, 113] (**figure 5.8.D, E**). These observations suggest that HK1 is a likely a general regulator of death receptor-induced apoptosis. These results are the first accounts of a specific role of HK1 in the inhibition of extrinsic death receptor signals.

5.4. HK1 localizes to the mitochondria.

As HK1 attenuated death receptor-induced apoptotic signals in type II cells, I tested if HK1 regulates cell death at the level of the mitochondria similar to its role in growth factor signaling. To this end, I first confirmed the mitochondrial localization of HK1. HK1 interacts with the OMM in a dynamic and regulated manner [307, 508]. Studies showed that the fifteen amino-terminal amino acids of HK1 (**figure 5.9.A**) are necessary and sufficient to mediate HK1-mitochondria interactions [311], even though the exact mechanism is unknown [360].

To validate those findings for HK1, I used fluorescence microscopy on fixed HeLa cells to examine the subcellular localization of HK1. I stained endogenous HK1 with specific primary antibodies that were recognized by fluorochrome-coupled secondary antibodies. I also stained the mitochondria with the fixable mitochondrial dye MitoTracker Red (**figure 5.9.B**). As expected, a large amount of HK1 localized to the mitochondria. However, another population of HK1 did not overlap with the mitochondria, and presumably resided in the cytoplasm.

I also performed cellular fractionation assays, and tested the mitochondrial (heavy membrane) fraction or the cytosolic fraction for the presence of HK1. I used the cytosolic protein tubulin [509] and the mitochondrial protein VDAC1 [204] as markers for the purity of the respective fractions.

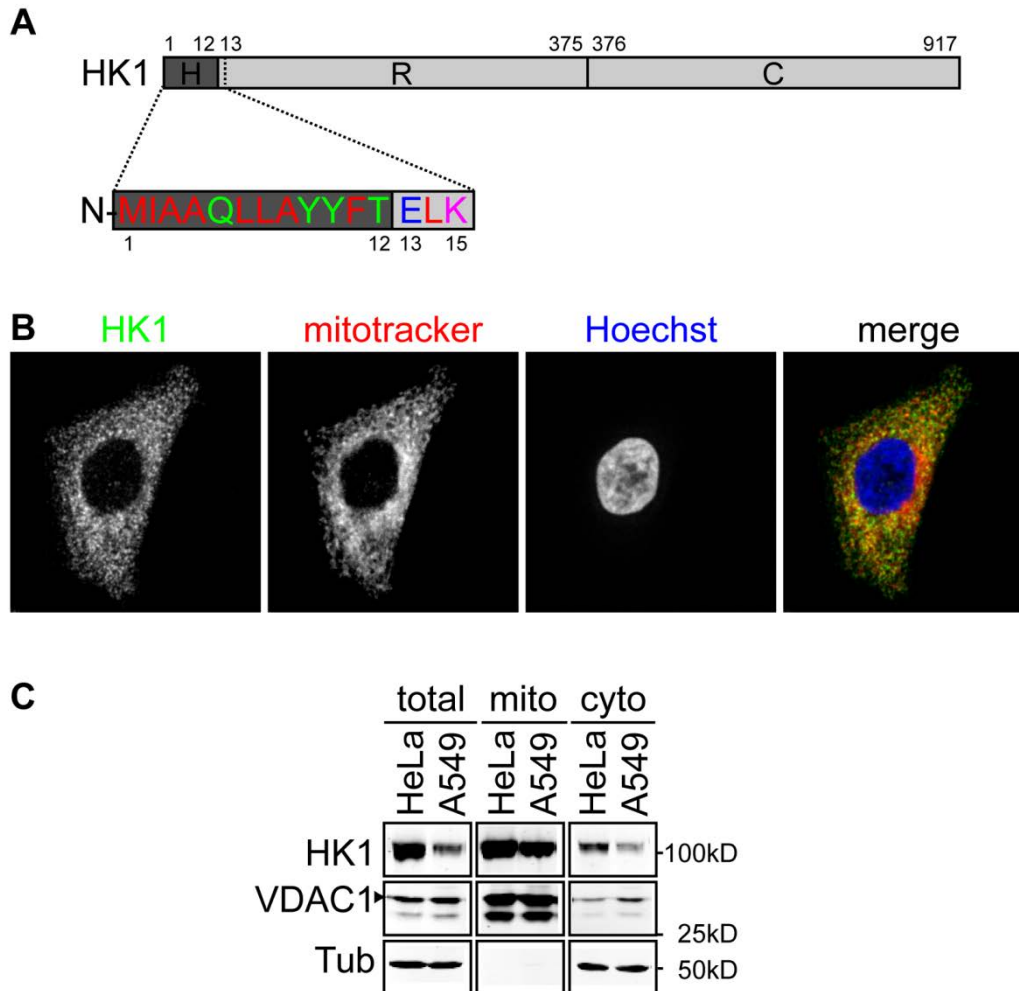


Figure 5.9. HK1 is predominantly mitochondrial. **A:** Illustration of the domain structure of HK1, including the hydrophobic N-terminus (H), the regulatory domain (R), and the C-terminal catalytic domain. The amino-terminal fifteen amino acids responsible for mitochondrial association of HK1 are highlighted. Red: hydrophobic amino acids, green: polar amino acids, blue: charged acidic amino acids, pink: charged basic amino acids. **B:** Fluorescence microscopic image of HeLa cells that were stained with an antibody against endogenous HK1, mitotracker red, and nucleic acid stain Hoechst. All single channel images were false-coloured (HK1 in green, mitotracker red in red, Hoechst in blue) and merged. **C:** Western blot of the cellular localization of HK1 in type II HeLa and A549 cells. Total lysate, mitochondrial and cytosolic fractions were probed for HK1, VDAC1 and Tubulin (Tub). Tubulin and VDAC1 served as markers for cytosolic and mitochondrial fractions, respectively.

The majority of HK1 co-fractionated with the mitochondria and only a portion localized to the cytoplasm in HeLa cells and A549 cells (**figure 5.9.C**).

5.5. HK1 siRNA depletes mitochondrial HK1.

Mitochondrial HKs are essential to mediate the anti-apoptotic effect of growth factors [340-342, 357, 370]. Given that HK1 plays an anti-apoptotic role in TNF-induced apoptosis signaling, and that depletion of HK1 potentiates apoptotic signaling, I hypothesized that HK1 depletion also depletes the mitochondrial HK1 pool and permits mitochondrial apoptotic signaling.

To examine the impact of HK1 siRNA on mitochondrial HK1, I transfected HeLa cells with HK1 siRNA or a non-silencing control siRNA. On day three, I ruptured the cells mechanically and separated the mitochondrial and cytosolic fractions. I detected a depletion of the mitochondrial and the cytosolic HK1 pool in separated fractions (**figure 5.10.**). I conclude that HK1 siRNA decreases the pool of HK1 at the mitochondria.

5.6. HK1 siRNA decreases the IMM potential.

As HK1 localizes to the OMM [304-306] and growth factors counter apoptosis through mitochondrial HKs [340-342, 357, 370] upstream of mitochondrial cytochrome c release [367], I hypothesized that reduction of the mitochondrial HK1 pool decreases mitochondrial integrity. In line with this hypothesis, I showed that depletion of HK1 from HeLa cells decreases the IMM potential in the absence of an apoptotic stimulus (**figure 5.6.A**).

To substantiate that finding, I re-examined the IMM potential after siRNA-mediated depletion of HK1. On day three after the transfection, I performed a cytometric TMRE assay to measure the proportion of cells with a decreased IMM potential. Cells that were depleted of HK1 (**figure 5.11.B**) had a two-fold larger population of cells with decreased IMM potential in comparison to cells treated with a non-silencing control siRNA (**figure 5.11.A**). The decrease of the IMM potential in cells treated with HK1 siRNA occurred specifically between day two and day three after siRNA transfection (**figure 5.11.D**) coincident with the depletion of HK1 protein (**figure 5.11.C**). I conclude that HK1 depletion, which includes HK1 depletion at the OMM, reduces the IMM potential.

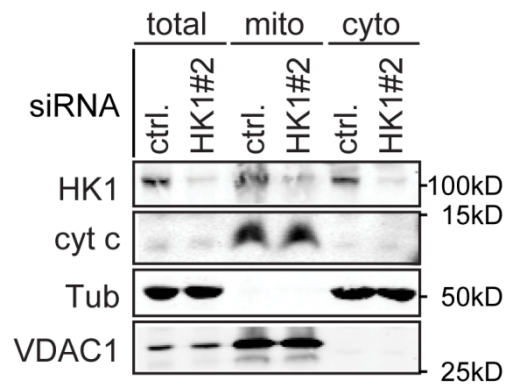


Figure 5.10. HK1 siRNA depletes mitochondrial HK1. Western blot of HK1 in cellular fractions of HeLa cells treated with HK1 siRNA or an unspecific control siRNA (ctrl.). Heavy membrane/mitochondrial (mito), and cytosolic (cyto) fractions were isolated. All fractions were blotted for HK1, cytochrome c (cyt c), tubulin and VDAC1. Tubulin and VDAC1 served as markers for cytosolic and mitochondrial fractions, respectively.

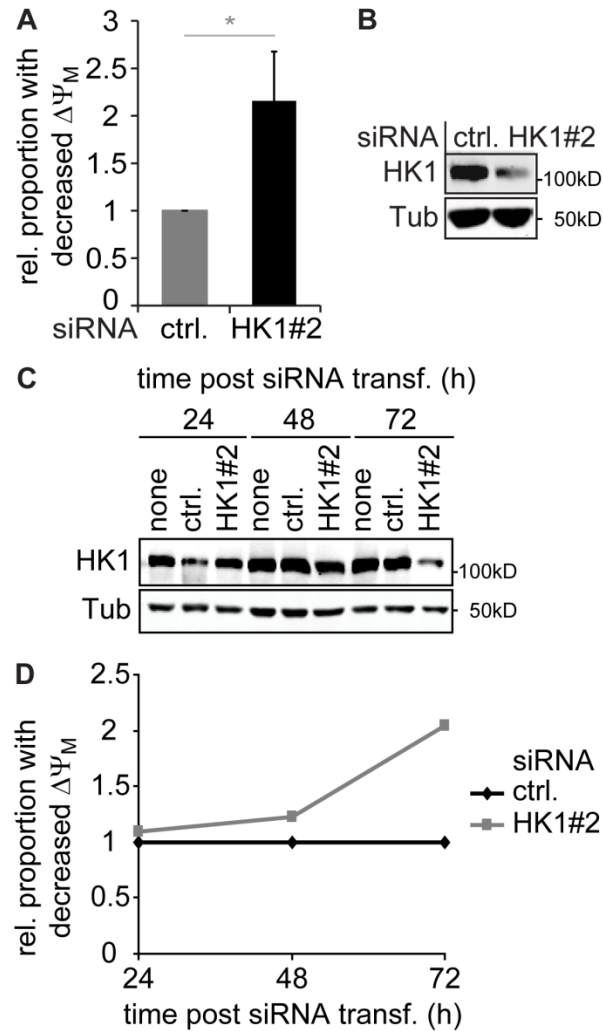


Figure 5.11. HK1 siRNA decreases the IMM potential. **A:** Plot of the relative amount of cells with a reduced IMM potential ($\Delta\Psi_M$)/TMRE staining in a population of HeLa cells treated with HK1 siRNA or a non-silencing control siRNA (ctrl.). All values are presented as relative values to the proportion of control cells with reduced IMM potential, which was assigned a value of one. Three independent experiments were performed and presented as the mean + S.E.M. A significant difference ($p < 0.05$) between the two experimental groups in the Student's T-test is indicated with *. **B:** Western blot of HK1 expression in HeLa cells from panel B. Cells were treated with HK1 siRNA or non-silencing control siRNA (ctrl.). Total cell lysates were blotted for HK1 and tubulin (Tub) as a loading control. **C:** Western blot of the time course of siRNA-mediated HK1 depletion in HeLa cells. Cells were treated with HK1 siRNA, non-silencing control siRNA (ctrl.), or no siRNA (none) and incubated for the indicated time periods. Cell lysates were blotted for HK1 and tubulin (Tub) as a loading control. **D:** Representative time course of the relative amount of cells with reduced IMM potential ($\Delta\Psi_M$)/TMRE staining in HeLa cells from panel C. Cells were transfected with HK1 siRNA or a non-silencing control siRNA (ctrl.) and incubated for the indicated time periods. All values are relative to the proportion of control cells with reduced IMM potential at each individual time point, which was set to one.

5.7. Mitochondrial detachment of HKs decreases the IMM potential and mitochondrial integrity.

To provide evidence for the link between mitochondrial HK1 and the IMM potential, I used a direct approach to detach HK1 from the mitochondria while keeping the total cellular levels of HK1 constant. To this end, I used the anti-fungal imidazole derivative clotrimazole (CTZ). Treatment of B16 melanoma cells with CTZ in the absence of serum reduces the levels of mitochondrial hexokinase activity [510] and protein [340-342]. The molecular mechanism of CTZ-mediated HK detachment from the mitochondria is not understood in detail, but it is thought that the amphipathic CTZ disturbs the interactions of charged membrane molecules with their binding partners, such as the interaction of HKs with VDAC in the OMM. CTZ seems unable to access pre-formed VDAC:HK complexes, but prevents the reformation of the interaction following HK detachment [315]. I believe that this is the reason why CTZ is usually administered in culture medium without growth factor-containing serum. As growth factor deprivation in the presence of sufficient energy and nutrient supply should allow the detachment of mitochondrial HKs, the simultaneous presence of CTZ presumably prevents the re-attachment of HKs to the mitochondria.

A caveat for these studies is that CTZ prohibits the re-attachment of both mitochondrial HK1 and HK2 [340, 341]. Accordingly, when I treated HeLa cells with 20 μM CTZ for 1 hour in the absence of serum, HK1 and HK2 levels decreased in the mitochondrial or heavy membrane fraction and increased in the cytosolic fraction (**figure 5.12.A**). In contrast, treatment with the CTZ solvent DMSO did not affect the localization of HK1 or HK2. I then used the TMRE assay to monitor the effect of HK detachment from the mitochondria on the IMM potential. Treatment of HeLa cells with CTZ decreased the IMM potential in a concentration-dependent fashion. Very low concentrations of CTZ did not affect the IMM potential, but as soon as a threshold of around 20 μM CTZ was reached, the amount of cells with a decreased IMM potential rapidly increased until saturation at around 60 μM CTZ (**figure 5.12.B**). A concentration of 100 μM CTZ rendered almost all cells TMRE negative, suggesting a collapse of the IMM potential in the majority of the mitochondria.

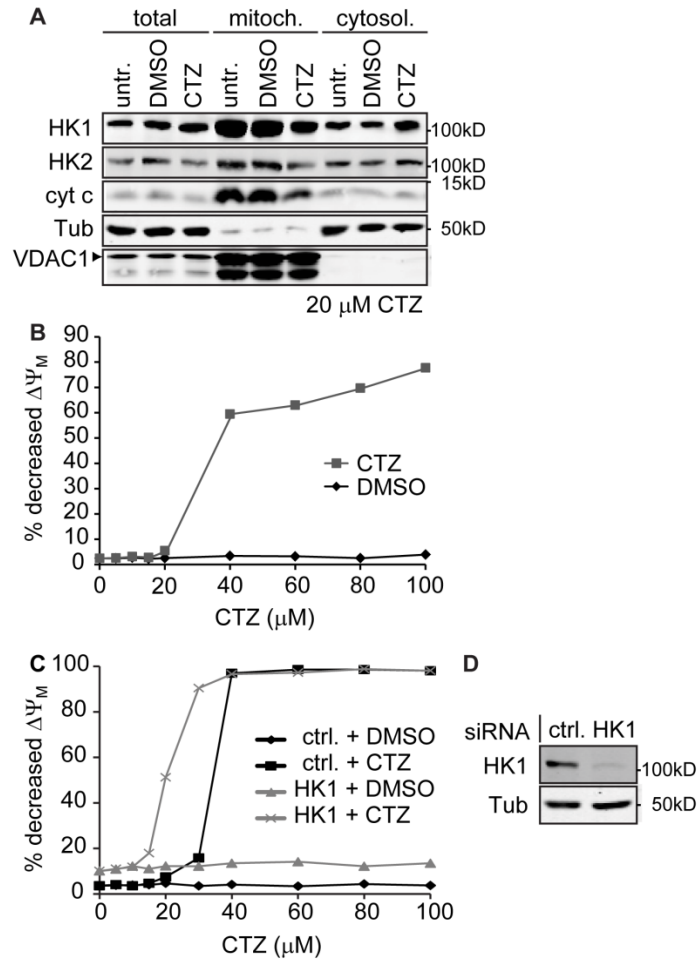


Figure 5.12. Mitochondrial detachment of HKs decreases the IMM potential and disrupts mitochondrial integrity. **A:** Western blot of the localization of mitochondrial HKs after treatment with CTZ. HeLa cells were treated with serum-free medium (SFM) (untr.), SFM with the solvent DMSO (DMSO), or SFM and 20 μ M CTZ (CTZ) for 1 hour. Total, heavy membrane/mitochondrial (mito), and cytosolic (cytosol.) fractions were isolated and probed with antibodies against HK1, HK2, cytochrome c (cyt c), tubulin, and VDAC1. Tubulin (Tub) and VDAC1 served as markers cytosolic and mitochondrial fractions, respectively. **B:** Representative graph of the percentage of cells with a reduced IMM potential ($\Delta\Psi_M$)/TMRE staining in a population of HeLa cells treated with increasing concentrations of CTZ. Cells were incubated with the indicated concentrations of CTZ or CTZ solvent DMSO for 1 hour. **C:** Representative graph of the percentage of cells with a reduced IMM potential ($\Delta\Psi_M$)/TMRE staining in a population of HeLa cells depleted of HK1 and treated with increasing concentrations of CTZ. HeLa cells were pretreated with HK1 siRNA or a non-silencing control siRNA (ctrl.) and incubated with the indicated concentrations of CTZ or its solvent DMSO for one hour in SFM. **D:** Western Blot of HK1 expression in HeLa cells from panel C. Cells were treated with HK1 siRNA or a non-silencing control siRNA (ctrl.). Cell lysates were blotted with an antibody for HK1 and tubulin (Tub) as a loading control.

Thus, the phenotype of CTZ treatment essentially mirrors the phenotype of siRNA-mediated HK1 depletion. Both treatments deplete the mitochondrial HK1 pool and decrease the IMM potential.

To test if the decrease of the IMM potential through CTZ was at least in part mediated by reduction of mitochondrial HK1 levels and not just by the reduction of mitochondrial HK2 levels, I generated another CTZ concentration curve for cells that were treated with HK1 siRNA and compared it to the one of cells treated with a non-silencing control siRNA (**figure 5.12.C, D**). HK1 depletion resulted in the typical increase in the population with a decreased IMM potential. The threshold concentration for CTZ to decrease the IMM potential halved in HK1-depleted cells from 20 μM to 10 μM . Likewise, the growth of the population with decreased IMM potential saturated at lower CTZ concentrations than in cells treated with a non-silencing control siRNA. These results demonstrate that depletion of HK1 facilitates the decrease of the IMM potential by CTZ. This finding prompts me to propose that mitochondrial HK1 is required to stabilize the IMM potential. The loss of mitochondrial cytochrome c after the detachment of mitochondrial HKs with a lower concentration of CTZ (**figure 5.12.A**) supports the notion that HK1 maintains not just the IMM potential, but also mitochondrial membrane integrity.

5.8. Mitochondrial detachment of HKs accelerates TNF-induced apoptosis.

I then asked if detachment of mitochondrial HKs with CTZ sensitizes HeLa cells to TNF-induced apoptosis. To this end, I induced apoptosis with TNF and CHX and treated cells with the lowest concentration of CTZ that caused a detectable decrease of the IMM potential (20 μM). CTZ generally only detaches mitochondrial HKs when given in serum-free medium [315, 340, 341]. However, prolonged incubation in serum-free medium is harmful to HeLa cells. Therefore, I exposed HeLa cells to serum-free medium from two to four hours after treatment with TNF and CHX. This time frame coincides with the arrival of the pro-apoptotic signal at the mitochondria. Six hours after treatment with TNF and CHX, I determined the size of the population with a decreased IMM potential in a TMRE assay. The combination of TNF and CHX alone only mildly increased the population with a decreased IMM potential (**figure 5.13.A**). In contrast, the combined treatment of CTZ and TNF and CHX decreased the IMM potential.

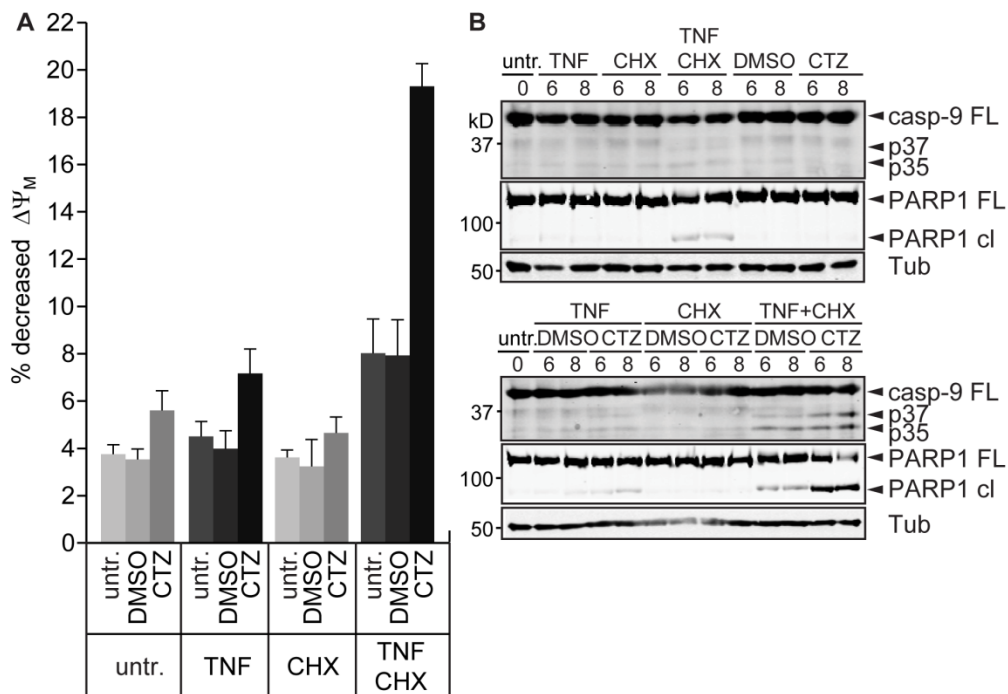


Figure 5.13. Mitochondrial detachment of HKs accelerates TNF-induced apoptosis. **A:** Graph of the percentage of cells with a reduced IMM potential ($\Delta\Psi_M$)/TMRE staining in a population of HeLa cells treated with a combination of a death receptor signal (TNF, TNF and CHX, CHX control, or untreated control (untr.)) for six hours and a chemical that detaches mitochondrial HKs (CTZ in serum-free medium (SFM), CTZ solvent DMSO control in SFM, or SFM control). Values are presented as the mean + S.E.M. of two independent experiments. **B:** Western blot of caspase-9 and PARP1 cleavage in HeLa cells from panel A. Cell lysates for zero, six, and eight hour time points were probed with antibodies that detected full-length caspase-9 (casp-9 FL) and p37 and p35 cleavage products, full-length PARP1 (PARP1 FL) and p89 cleavage product (PARP1 cl), and tubulin (Tub) as a loading control.

The population of cells with decreased IMM potential more than doubled in comparison to treatments with CTZ or combined TNF and CHX alone. Combined treatment with TNF and CTZ only mildly increased the size of the population with decreased IMM potential in comparison to single treatments. These results show that detachment of mitochondrial HKs sensitizes HeLa cells to TNF and CHX-induced decrease of the IMM potential.

I was interested whether CTZ accelerates the appearance of other apoptotic markers upon exposure to TNF and CHX. Therefore, I used the same combination of treatments and monitored the cleavage of caspase-9, as well as the cleavage of the caspase substrate PARP1 on a Western blot. I visualized those apoptotic markers six and eight hours after incubation with TNF and CHX, respectively. None of the individual treatments with TNF, CHX, CTZ or its solvent DMSO led to the cleavage of caspase-9 or PARP1 (**figure 5.13.B**). However, treatment with TNF and CHX resulted in a mild cleavage of caspase-9 and PARP1. When I administered TNF, CHX, or TNF and CHX in combination with CTZ, I observed a low level of cleavage in cells treated with TNF, and a pronounced cleavage in cells treated with TNF and CHX. The level of processing greatly exceeded the one in control cells treated with DMSO. I conclude that treatment with CTZ sensitizes cells to TNF-induced apoptosis. These findings argue that mitochondrial HKs counter TNF-induced apoptosis.

5.9. Bcl-2 proteins modify the decrease of the IMM potential after HK1 depletion.

5.9.1. Bcl-2 overexpression stabilizes the IMM potential after HK1 depletion.

Next, I examined the relationship between mitochondrial HK1 and the IMM potential. Others [340-342] and I (**figure 5.12.A**) observed that detachment of mitochondrial HKs through CTZ or HK2-specific peptides results in the release of cytochrome c, a hallmark of mitochondrial apoptotic signaling. Furthermore, detachment of mitochondrial HKs with CTZ or a HK2-specific peptide increased the amount of mitochondrial Bax [340]. Both findings suggest that loss of mitochondrial HKs leads to the release of cytochrome c through the formation of Bax and possibly Bak-regulated channels in the OMM [170, 511]. Anti-apoptotic Bcl-2 proteins, like Bcl-2, inhibit the formation of cytochrome c releasing channels

by sequestration of Bak and Bax-activating BH3-only proteins [259-262] or Bak and Bax themselves [218, 235, 239, 258].

To examine if pro-apoptotic Bcl-2 proteins are required to decrease the IMM potential after HK1 depletion, I tested, whether Bcl-2 overexpression attenuates the decrease of the IMM potential following HK1 depletion. To this end, I depleted HK1 (**figure 5.14.A**) and overexpressed Bcl-2 in HeLa cells. To obtain maximal amounts of HK1-depleted, Bcl-2 expressing cells, I transfected HeLa cells with HK1 siRNA or non-silencing control siRNA on day one and Bcl-2 or control plasmid on day three. As the major drop of HK1 protein levels and the IMM potential occurred between day three and four (**figure 5.2.A, 5.11.C**), I reasoned that expression of Bcl-2 from day three on is sufficient to examine its effect on the decrease of the IMM potential. siRNA-mediated depletion of HK1 resulted in the typical increase of the population with decreased IMM potential ($p < 0.01$) (**figure 5.14.B**). Interestingly, overexpression of Bcl-2 significantly blocked the increase of the population with a decreased IMM potential after HK1 depletion ($p < 0.01$). In fact, there was no significant difference in the IMM potential of cells that overexpressed Bcl-2 after treatment with a non-silencing siRNA or a HK1 siRNA. I conclude that pro-apoptotic Bcl-2 proteins are involved in the decrease of the IMM potential after loss of HK1.

5.8.2. HK1 depletion decreases the IMM potential in a manner that requires Bak and Bax.

Bcl-2 controls the formation of Bak and Bax-regulated channels in the OMM [218, 235, 258-260, 262]. Given that Bcl-2 overexpression blocked the decrease of the IMM potential after HK1 depletion, I examined if the formation of Bak and Bax-regulated channels in the OMM is the molecular basis for the loss of mitochondrial integrity after HK1 depletion. Specifically, I used mouse embryonal fibroblast (MEF) cells with a deletion in the genomic *bak* and *bax* genes that hinders the expression of functional Bak and Bax [512, 513]. Both wild type (wt) and DKO cells expressed HK1 and exhibited a cellular HK1 localization pattern comparable to HeLa cells (**figure 5.15.A**). The majority of cellular HK1 attached to the mitochondria, and a minor amount resided in the cytoplasm. In contrast, HK2 was hardly expressed. Low amounts of HK2 exclusively localized to the mitochondria.

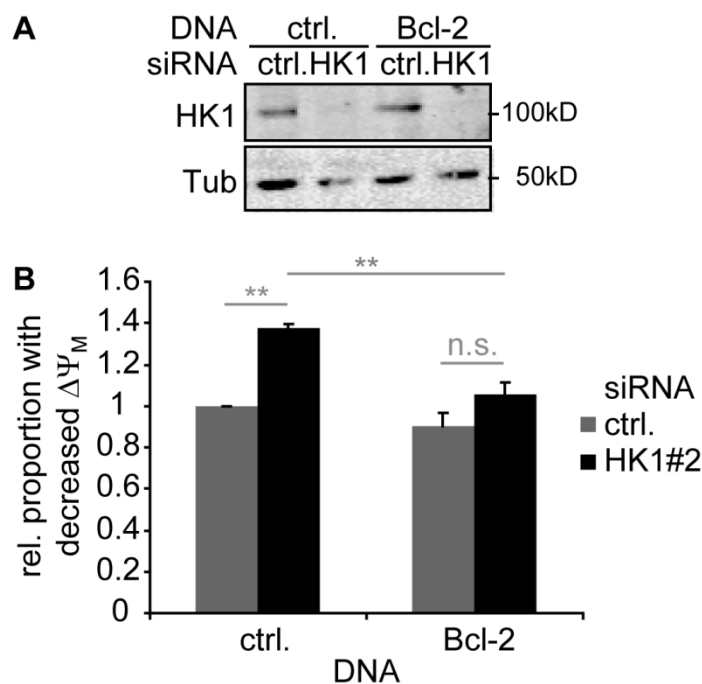


Figure 5.14. Bcl-2 overexpression stabilizes the IMM potential after HK1 depletion. **A:** Western Blot of HK1 expression in HeLa cells transfected HK1 siRNA or a non-silencing control siRNA and a Bcl-2 expression construct or a control plasmid (ctrl.). Cell lysates were blotted for HK1 and tubulin (Tub) as a loading control. **B:** Plot of the relative proportion of HeLa cells with a reduced IMM potential ($\Delta\Psi_M$)/TMRE staining after transfection with HK1 siRNA or a non-silencing control siRNA (ctrl.) and a Bcl-2 expression construct or control plasmid (ctrl.). All values are reported relative to the proportion of cells with reduced IMM potential in the cell population transfected with control siRNA and plasmid and presented as the mean + S.E.M of three independent experiments. A significant difference between experimental groups in a Student's T-test with $p < 0.01$ is indicated with **, and a non-significant difference with n.s.

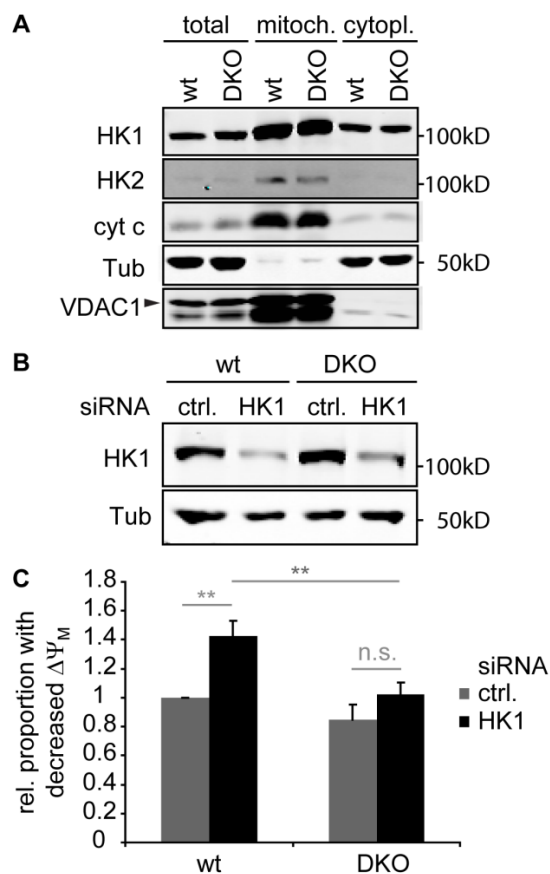


Figure 5.15. The absence of Bak and Bax stabilizes the IMM potential after HK1 depletion. **A:** Western blot of the expression and localization of HKs and cytochrome c in wild type (wt) and Bax/Bak double knock-out (DKO) MEFs. Total, heavy membrane/mitochondrial (mito), and cytosolic (cyto) fractions were isolated and blotted for HK1, HK2, cytochrome c (cyt c), tubulin and VDAC1. Tubulin (Tub) and VDAC1 served as markers for cytosolic and mitochondrial fractions, respectively. **B:** Western Blot of the expression of HK1 in wild type (wt) and Bax/Bak double knock-out (DKO) MEF cells transfected with HK1 siRNA or a non-silencing control siRNA (ctrl.). Cell lysates were blotted for HK1 and tubulin as a loading control. **C:** Plot of the relative proportion of cells with a reduced IMM potential ($\Delta\Psi_M$)/TMRE staining in wild type (wt) and Bax/Bak double knock-out (Bax/Bak DKO) MEFs after treatment with HK1 siRNA or a non-silencing control siRNA (ctrl.). All values are presented as the mean + S.E.M of four independent experiments. A significant difference between experimental groups in the Student's T-test with $p < 0.01$ is indicated with **, and a non-significant difference with n.s.

I then depleted HK1 with an siRNA specific for mouse HK1 (**figure 5.15.B**), and monitored whether the reduction of the IMM potential occurred in wt and Bak/Bax DKO cells. HK1 depletion significantly ($p < 0.01$) reduced the IMM potential in wt cells. However, the loss of Bak and Bax blocked the decrease of the IMM potential after HK1 depletion ($p < 0.01$), and did not significantly change the IMM potential in DKO cells (**figure 5.15.C**). These results indicate a requirement for Bak and/or Bax for the decrease of the IMM potential following depletion of HK1, most likely through the formation of Bak and/or Bax channels in the OMM and release of pro-apoptotic molecules. I conclude that HK1 stabilizes the IMM potential through the inhibition of Bak and/or Bax at the mitochondria.

5.8.3. HK1 depletion initiates and accelerates Bax activation.

The previous chapter showed that the decrease of the IMM in the absence of HK1 is mediated at least in part by Bak and Bax. These findings prompted me to ask, if HK1 depletion allows Bax translocation from the cytoplasm to the mitochondria, Bax oligomerization at the mitochondria and mitochondrial cytochrome c release in the absence of an apoptotic stimulus. I also asked if a combination of TNF, CHX, and HK1 depletion accelerated mitochondrial apoptotic events.

To monitor Bax translocation and cytochrome c release, I transfected HeLa cells with HK1 or control siRNA. On day three, I treated the cells with TNF and CHX and performed cellular fractionation to examine the presence of Bax and cytochrome c in the mitochondrial (heavy membrane) or cytosolic fraction, respectively. Interestingly, loss of HK1 elevated mitochondrial Bax levels in the absence of an apoptotic stimulus and further increased them in the presence of TNF and CHX (**figure 5.16.A**). In line with my previous findings (**figure 5.10.**), I did not detect alterations in the levels of mitochondrial or cytosolic cytochrome c in the absence of an apoptotic cue. However, the release of mitochondrial cytochrome c into the cytoplasm was accelerated when HK1-depleted cells were exposed to TNF and CHX.

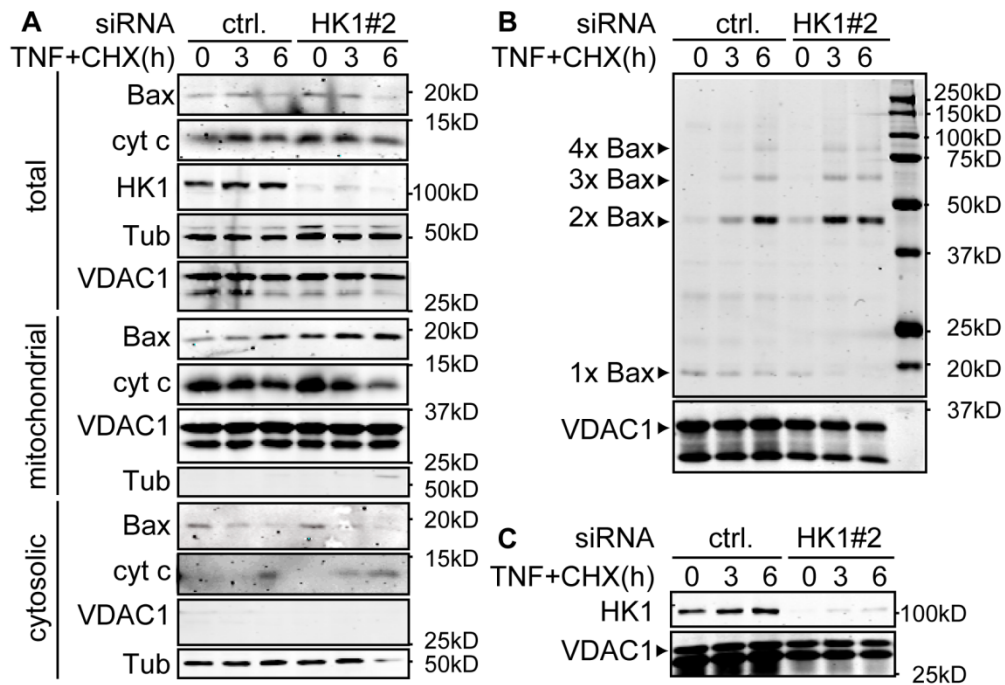


Figure 5.16. HK1 depletion initiates and accelerates Bax activation. **A:** Western blot of the time course of Bax translocation to the mitochondria and release of cytochrome c from the mitochondria during TNF-induced apoptosis. HeLa cells were treated with HK1 siRNA or a non-silencing control siRNA and incubated with TNF and CHX for the indicated time periods. Total lysates, heavy membrane/mitochondrial and cytosolic fractions were probed for Bax, cytochrome c (cyt c), HK1, Tubulin (Tub) and VDAC1. Tubulin and VDAC1 served as markers for cytosolic and mitochondrial fractions, respectively. **B:** Western blot of Bax oligomerization in HeLa cells after treatment with TNF and CHX for the indicated time periods. Cells were treated with HK1 siRNA or a non-silencing control siRNA. Lysates of the heavy membrane/mitochondrial fractions were incubated with the cross-linker BMH and probed with an antibody against Bax and VDAC1. Bax mono- and multimers are indicated. VDAC1 served as a loading control. **C:** Western blot of HK1 depletion in the cell populations from B. Cells were depleted of HK1 or treated with a non-silencing control siRNA. Both populations were treated with TNF and CHX for the indicated time periods, lysed and probed with an antibody against HK1 and VDAC1. VDAC1 served as a loading control.

To examine the effect of HK1 depletion on the oligomerization of Bax, I treated HeLa cells with HK1 or control siRNA. On day three, I treated the cells with TNF and CHX to induce Bax oligomerization. I then performed cellular fractionation to isolate the mitochondrial (heavy membrane) fraction. I lysed the mitochondrial fraction and exposed the lysates to the cross-linker bismaleimido-hexane (BMH) to covalently link possible Bax oligomers and to render them resistant to the denaturing conditions of SDS-polyacrylamide gel electrophoresis. In the absence of TNF and CHX, the majority of mitochondrial Bax was monomeric in control cells (**figure 5.16.B**). Over the course of six hours treatment with TNF and CHX the amount of monomeric Bax decreased and the amount of dimeric, trimeric and tetrameric Bax increased steadily. As oligomerization of Bax begins with dimerization [236], and continues with the oligomerization of Bax dimers [240], the presence of trimeric Bax indicates incomplete cross-linking and suggests that the actual size of the oligomers was larger than the detected fragments on the Western blot. Loss of HK1 (**figure 5.16.C**) was accompanied by lower levels of monomeric Bax and higher levels of dimeric Bax in the absence of TNF and CHX (**figure 5.16.B**). This indicates that loss of HK1 not only increases the amounts of mitochondrial Bax, but also activates and oligomerizes Bax at least to the dimeric state. Strikingly, incubation with TNF and CHX accelerated the formation of higher state Bax oligomers in cells treated with HK1 siRNA in comparison to control cells. Due to the possibility of incomplete cross-linking, conclusions on the formation of functional, cytochrome c permeable Bax pores cannot be drawn. These data demonstrate that cellular HK1 inhibits access of Bax to the mitochondria and Bax oligomerization at the mitochondria and provides at least a partial mechanistic explanation for the loss of the IMM potential after HK1 depletion. I cannot exclude that HK1 depletion also affects Bak or other mitochondrial components.

CHAPTER 6. DISCUSSION.

6.1. A high-throughput siRNA assay for modifiers of TNF-induced death.

In the present study, I examined the regulation of cell viability in response to TNF. TNF serves as a second messenger in inflammation to coordinate a meaningful response to an infection or tissue damage [19, 51, 54]. It triggers an array of reactions in cells at the inflammation site that include the secretion of additional pro-inflammatory cytokines, cell differentiation and proliferation, and the induction of cell death [19, 51, 54]. In an ideal situation, inflammation confines and eliminates the danger from the organism [19, 51, 54]. However, the beneficial effects of TNF and inflammation are often accompanied by undesirable effects such as tissue damage [19, 20, 54]. A similar “balance act” between life and death in the inflammatory environment accompanies tumor development. Many tumors are characterized by a low level of inflammation that results from the infiltration with cells of the innate and the adaptive immune system [15]. A low level of inflammation is advantageous for tumor progression as it promotes angiogenesis, cancer cell proliferation, tissue invasion, and metastasis [457]. In contrast, a full-blown inflammation can lead to tumor regression due to its cytotoxic side effects, including the capability of TNF to induce cell death [457, 458]. Given the medical relevance, it is essential to establish a good understanding of the intracellular molecular mechanisms that regulate cell viability in the presence of TNF.

TNF provokes physiological responses through NF- κ B, MAPK, and caspase modules [47, 52]. There is considerable cross-talk between the individual modules, and there are still major gaps in our understanding of the activation and integration of signals from each module [50, 52, 140, 146, 147, 462, 480]. I sought to address these questions with an siRNA screen for regulators of TNF-induced cell death. I reasoned that siRNA will help identify the most important and non-redundant players in the pathway. These could be valuable candidates for the treatment of inflammatory diseases and diseases with a disturbed balance of survival or death signaling such as cancer.

In the present study, I developed and executed the first siRNA screen for modifiers of TNF-induced death. Specifically, I screened nine hundred eighty six human kinases, phosphatases and associated proteins and identified key signaling elements and novel candidate modifiers of TNF-induced death.

6.1.1. Development of a high-throughput siRNA assay for modifiers of TNF-induced death.

The development of RNAi technology makes it possible to address complex questions, such as “What are the modifiers of TNF-induced death?”, in a reasonable time frame. No more than fifteen years ago, a systematic and unbiased approach to that question did not even exist. At the time, potential modifiers had to be tested by overexpression of wild-type or mutant constructs or by the time-consuming process of generating knock-out animals. While these techniques remain standard techniques for in-depth secondary analysis, RNAi is a very potent gene discovery tool prior to detailed molecular analysis.

In 1998, Fire and Mello discovered the causative agent and mechanism behind observations that were generally labeled as post-transcriptional gene silencing [514]. For their pioneering work on RNAi in the nematode *Caenorhabditis elegans*, they were awarded the nobel prize in Physiology or Medicine in 2006.

The power of RNAi as a tool for the rapid generation of depletion “mutants” in cell culture or even specific areas of entire organisms was immediately recognized. However, a hurdle for the application of RNAi in mammalian systems still had to be overcome. The use of long dsRNAs as the basis for RNAi, which worked wonderfully in invertebrates, provoked an innate immune response in mammalian cells [436]. Elbashir and colleagues overcame those difficulties in 2001 with their discovery that mammalian systems tolerate small interfering RNA duplexes (siRNAs) of roughly twenty one base pairs [437]. That breakthrough paved the way for the establishment of the first siRNA and plasmid-based shRNA libraries [441, 442, 515-518].

To establish a high-throughput siRNA screen for protein modifiers of TNF-induced death, I sought a cellular system that responds to siRNA and faithfully reproduces prominent features of signal transduction in response to TNF. I demonstrated that the human epithelial adenocarcinoma line HeLa [459, 460] activates NF- κ B, JNK and caspase modules after treatment with TNF (**figure 3.1.** and **3.2.**). Furthermore, I confirmed that the caspase module is active in the absence of TNF-induced gene translation (**figure 3.2.**).

Therefore, I combined TNF and the translation inhibitor CHX to induce apoptosis. As anticipated, I observed that siRNA-mediated depletion of the pro-apoptotic protein caspase-8 prevented the induction of apoptosis by TNF and CHX (**figure 3.3.**). Depletion of the anti-apoptotic NF- κ B activator NEMO mildly inhibited prominent hallmarks of TNF-induced NF- κ B signaling (**figure 3.4.**). I believe that the weak phenotype may be a result of inefficient protein depletion by the specific NEMO siRNA, which should be validated in future quantitative real-time PCR and Western blot studies. However, loss of NEMO greatly accelerated the induction of TNF-induced death (**figure 3.4.**) and therefore served as a valid positive control for the modification of TNF-induced death.

I then established a simple and sensitive ninety six-well viability assay for the quantification of cell death in response to a combined TNF and CHX regime (**figure 3.6.**). I also established a high-throughput protocol to efficiently deplete target proteins with siRNA (**figure 3.5.**). Depletion of caspase-8 or NEMO resulted in the anticipated response to treatment with TNF and CHX in the viability assay (**figure 3.7. to 3.9.**). These findings suggest that the assay was sufficiently robust to identify novel modifiers of cell death.

6.2. An siRNA screen for modifiers of TNF-induced death.

6.2.1. Analysis of the screen data.

6.2.1.1. Data normalization.

A major challenge for the execution of large-scale RNAi screens is to keep the error rate minimal to allow data comparison between individual samples [519, 520]. Therefore, the goal is to execute the entire screen in a minimal time frame, with minimal reagent variability, the same batch of cells, and to process each plate in exactly the same way. These criteria are broadly satisfied by the relatively uncomplicated high-throughput resazurin assay described above.

As I performed the screen manually, I was limited by the amount of plates I could handle in a day and processed all one hundred fifty six ninety six-well plates in ten subsets.

Figure 4.2. shows that there were prominent subset-to-subset variations in the fluorescence ranges across all one hundred fifty six plates and smaller but significant plate-to-plate variations, which made comparison of raw fluorescence values across plates impossible. For example, plates thirty one to forty two, which were not treated with TNF and CHX, and the corresponding plates one hundred nine to one hundred twenty, which were treated with TNF and CHX (indicated with a bracket), exhibited significantly lower raw resorufin fluorescence values than the rest of the plates. The lower fluorescence values result from reduced cell numbers in the specific subset, due to cell counting errors. However, as the low cell numbers did not affect general cell viability, the plate subset contributed a valuable data set to the screen. In the future, automated cell counting can be used to circumvent issues with variable cell numbers.

To eliminate plate-to-plate variations I normalized fluorescence values from each plate to the average fluorescence value of the plate-internal non-silencing siRNA controls (**figure 4.2.**). Commercially available non-silencing siRNAs are designed to have no homology with any human transcript. The non-silencing siRNA that I used in the screen (AllStars negative control siRNA, Qiagen) has been validated in microarray assays to have no impact on the expression of genes involved in interferon signaling, cell cycle, apoptosis signaling, and Jak/Stat signaling in standard human cell lines [521]. Moreover, cell number, cell viability, cell cycle profile, DNA synthesis, and nuclear size did not significantly vary from untransfected cells [521]. Importantly, the siRNA successfully entered the RISC complex [521]. In my assays, the non-silencing siRNA behaved as a reliable negative control with a TNF-dependent death index that was clearly distinct from the caspase-8 and NEMO positive controls.

The siRNA kinase and phosphatase library plates are organized in a non-randomized manner. For example, the eight MAPKs, MAPK3 (ERK1), MAPK8 (JNK1), MAPK11 (p38 β), MAPK13 (p38 δ), MAP3K13 (MLK), MAP2K7 (MKK7), MAPK12 (p38 γ), MAP4K1 (HPK1) are all positioned on one siRNA plate. Six of the MAPKs modify TNF pathway signaling [52](**figure 1.5.**). The same plate also contains the NF- κ B modifiers TAB2, I- κ B- ϵ and RIPK1 [52, 463].

The non-stochastic arrangement of experimental siRNA duplexes in the assay plates precludes the use of normalization procedures that report experimental values relative to the plate mean or median [492, 493].

While normalization to a defined value like the average of the negative controls centers all plate distributions, alternative normalization methods also correct for variability in the distribution of values between plates. For example, the transformation of all raw fluorescence values into dimensionless standard or z-scores centers all plate distributions and sets the plate standard deviations to one [520]. The standard or z-score is calculated by dividing the difference of the individual raw fluorescence values and the plate mean by the plate standard deviation [520]. I defined the plate mean as the mean raw fluorescence value of the negative controls and the standard deviation as the standard deviation from the negative controls. That way, each siRNA obtained a value that expressed the number of standard deviations between itself and the plate negative controls.

In general, z-scores are superior to plate normalization to the negative controls, as z-scores account for variation in the distribution of the fluorescence values across the plate [520]. However, the specific set-up of my screen made z-score calculations disadvantageous. I wished to calculate a TNF-dependent death index for each siRNA based on the ratio of viability without TNF and CHX and viability with TNF and CHX. In my screen, raw viability values originated from different plates that were not comparable without normalization. z-scores made all viability values comparable to each other. However, it adjusted plate standard deviations of plates that were not treated with TNF and CHX to the ones that were treated with TNF and CHX. Thus, it amplified small differences in the viability of cells in the absence of TNF and CHX to adjust it to the high variability of viability values in the presence of TNF and CHX. The subsequent calculation of death indices yielded unreasonable death indices for known modifiers of TNF-induced death. Therefore, I refrained from the use of z-scores to identify novel modifiers of TNF-dependent cell death.

In the future, it is preferable to examine individual siRNAs in the presence and absence of TNF and CHX on the same plate. This plate organization permits the calculation of death indices before the calculation of z-scores.

Plate effects are another source of error in siRNA screens [433, 491, 522]. Plate effects are differences in the viability values across a plate that derive from the position of each well on the plate irrespective of the siRNA under examination [522]. Cells on the edges of plates are exposed to slightly different conditions than cells in the center of the plate [522]. For example, media evaporation, availability of oxygen, and humidity are factors that vary with the well position. Other plate effects might result from systematic pipetting errors. I created heat maps of the viability values across plates to test for potential plate effects (**appendix 3**). Kinase and phosphatase plates that were not treated with TNF and CHX were characterized by a relatively even distribution of viability values across plates. However, there were some plate effects in the edge columns and rows, which resulted in higher viability at the edge and lower viability in the center of the plate. Kinase and phosphatase plates that were treated with TNF and CHX were characterized by highly variable viability values. There was no obvious abnormal spatial distribution of viability values. Given that the overall plate effects for the screen were insubstantial, I did not account for plate effects in my evaluation of data from the primary screen.

6.2.1.2. Data scoring.

The accurate identification of hits that are true modifiers of TNF-induced death requires reliable scoring criteria. One of the first issues I encountered in the process of setting reliable scoring criteria was the question of how to rank gene products that were assayed with three siRNAs. Non-overlapping siRNA duplexes that target a single gene often generate phenotypes of different severities in quantitative assays [523]. Phenotypic variability derives from the ability of the siRNA to deplete the target gene [443]. Another undesired factor for phenotypic variability between individual siRNAs is the possibility of off-target effects (OTEs) [490, 524, 525]. OTEs arise from unintended interactions of an siRNA with the target cell, whether they are sequence-dependent or not [490, 524, 525]. Sequence-specific OTEs are caused by the unintentional depletion of a protein other than the targeted one [490, 524, 525]. While experimental siRNA duplexes perfectly match the target mRNA, there are instances of near perfect matches between the experimental duplex and the open reading frame of a second “bystander mRNA” [526].

Experimental siRNA duplexes may also display imperfect matches with the untranslated regions of a non-targeted mRNA and induce translational silencing of the bystander transcript [422, 524, 526, 527]. The most significant factor for an imperfect match is a sequence match with the siRNA seed region, which comprises nucleotides two to eight from the 5' end of the single strand siRNA [422, 524, 526].

In addition, OTEs may arise from the incorporation of the non-guide or passenger strand of the experimental siRNA duplex into the RISC [433]. Some siRNA vendors introduce chemical modifications into the siRNA backbone that greatly reduce the entry of the siRNA passenger strand into the RISC complex to eliminate passenger strand-mediated OTEs [528, 529]. The siRNA duplexes of the kinase and phosphatase library had no chemical modifications. In short, it seems reasonable to assume the assignment of ranks to genes examined with three individual siRNAs is complicated by phenotypic penetrance of individual siRNAs and confounding OTEs. To mitigate against OTEs [490] and to assign a representative functional phenotype to each siRNA, I ranked genes according to the value of the median siRNA.

These criteria provided me with three distributions, a distribution of median viability values in the absence of TNF and CHX, a distribution of median viability values in the presence of TNF and CHX, and a distribution of median death indices (**figure 4.6.**). These distributions covered large ranges of viability values and death indices to each side of the non-silencing siRNA control and were framed by the values of caspase-8 and NEMO siRNAs in the distributions that resulted from the treatment with TNF and CHX. These findings suggest that the screen detected enhancer and suppressor type siRNA phenotypes and not only experimental variance.

The distributions of the median viability values were skewed in the absence and presence of TNF and CHX (**figure 4.6.**). 83% and 77% of the genes qualified as pro-survival proteins in the absence or presence of TNF and CHX, respectively. Their corresponding viability values spread with three-fold and 1.5 fold greater variability than the ones of the remaining pro-death proteins, respectively.

Similarly, the distribution of the median death indices was skewed towards the pro-survival proteins. 62% of all proteins qualified as pro-survival proteins and covered a 5.5 fold larger range of death indices than the pro-death proteins. I speculate that a major reason for the data asymmetry in my screen derives from the fact that I screened a specific subset of proteins and not the entire genome. Many protein kinases and phosphatases have essential functions in the absence of TNF [530] and established pro-survival roles in TNF signaling [52]. This may be an underlying reason for the overrepresentation of pro-survival proteins in the screen.

Setting symmetric scoring thresholds on skewed distributions is problematic. It leads to an underrepresentation of hits on the side of the distribution with the narrower distribution of values. In the case of the screen described in this thesis, symmetric scoring thresholds on the distribution of median death indices excluded established pro-death proteins as valid “hits” in the screen. For example, the established TNF-dependent pro-death protein JNK1 was not identified as a pro-death protein, despite the low death indices of 0.34, 0.66, and 0.74 identified for the individual siRNAs.

To accommodate the asymmetric distribution of viability values and death indices I set separate significance thresholds for pro-survival and pro-death proteins. Specifically, I assigned significance thresholds by defining independent confidence intervals (CI) for the two groups. The confidence threshold for normally distributed data sets is calculated as the product of the standard deviation of the distribution and the tabulated x-values of the Gaussian density function according to the desired level of confidence [531]. I assumed that the viability values and death indices were normally distributed on the respective sides of the non-silencing siRNA control. I then calculated standard deviations and confidence thresholds for the values on either side of the non-silencing control. This is mathematically possible because the standard deviation of the distribution depends on the squared distances of each individual value from the non-silencing siRNA control and is independent of the side, on which the values are located [531].

I set a 95% CI as the threshold for pro-survival and pro-death proteins in the presence and absence of TNF. By definition, these criteria mean, that my confidence that those hits were significantly different from the rest of the distribution was 95% [531]. Preliminary evaluation of the screen data showed that the scoring criteria correctly identified the established modifiers of TNF-induced death caspase-8, NEMO, TAB2, MEKK2, and JNK1 in the respective intervals. In addition, I identified a number of novel modifiers of TNF-induced death (**figure 4.7. to 4.9.**). These lists of candidate pro-survival and pro-death proteins should be interpreted with care as two types of dangers are associated with numerical thresholds setting in high-throughput screens [520]. A high threshold increases the risk of false-negatives and the attendant possibility of excluding valid modifiers of TNF responses from secondary evaluation [520]. Likewise, a low threshold increases the risk of false-positives and may result in the labour-intensive evaluation of irrelevant gene products [520].

A number of experimental factors such as experimental variability, screen bias, and off-target effects (OTEs) lead to the erroneous identification of false-positives [520, 524]. To mitigate against potential OTEs, I screened each gene product with three non-overlapping siRNAs [490]. As I determined CIs for the median viability value or death index of each gene product, I ensured that a minimum of two of the three viability values or death indices fell within the respective CI. This course of action increased my confidence that the proteins were classified according to their true phenotype.

As selected hits can be evaluated in secondary assays for false positives, I consider the inclusion of false-positives less harmful than the exclusion of false-negatives. However, the evaluation of many hits is a costly and labour-intensive procedure. Typically, secondary assays are designed to confirm target depletion with several non-overlapping siRNAs and to validate the phenotype in the primary assay and in more specific secondary assays [433, 490]. Secondary assays may include the expression and phenotypic evaluation of wild type, constitutively active or dominant negative variants of the candidate gene [433].

Any gene that does not appear in the 95% confidence list of general or TNF-specific pro-survival or pro-death proteins may be a true negative or a false-negative [520]. A lack of screen sensitivity and variability in the depletion efficiency of different siRNA duplexes are major sources of false-negatives in siRNA-based screens [524]. Residual target protein may obscure a depletion phenotype, or generate a weak phenotype that is excluded under stringent hit selection criteria [524]. False-negatives are a cause for concern, as the exclusion of false negatives from primary data prevents the identification and characterization of potentially interesting gene products in secondary assays [524].

To increase the likelihood of siRNA phenotypes, I used multiple siRNAs to target one protein. However, in the future I recommend researchers to perform screens with a pool of individual siRNAs to increase the phenotypic impact of the siRNAs. Upon completion of this project, we found that the siRNA phenotype of a pool of 3 individual siRNAs had greater phenotypic penetrance than the individual siRNAs [523]. The enhanced efficiency of knock-down phenotypes attributed to pools of siRNAs is consistent with the efficient knock-down phenotypes typically observed in invertebrate siRNA screens. Invertebrate cells tolerate and introduce long double stranded RNAs into the RNAi pathway [414, 437]. Invertebrate dicer cleaves the long double stranded RNAs to generate a pool of twenty one to twenty three nucleotide siRNAs [412-414]. Our survey of pooled and single siRNA duplexes suggests that a combination of independent siRNA duplexes is more likely to deplete a target transcript than a single siRNA, even if their individual concentrations constitute a fraction of the constant total siRNA concentration [523]. In addition, the reduced concentrations of individual siRNAs duplexes in vertebrate siRNA pools and invertebrate long double stranded RNAs minimize OTEs.

In some cases, functional redundancy of the target gene product prevents the manifestation of depletion phenotypes [524]. For example, depletion of a component of the TNF pathway will not result in a detectable phenotype if an ancillary protein functionally substitutes for the target.

This issue is particularly germane to the relatively complex human genome where gene duplication events resulted in distinct isoforms for numerous genes. For example, recent studies suggest that the human genome encodes approximately three isoforms per gene [532]. The lack of phenotypes for functionally redundant genes is a disadvantage for the identification of all elements of a specific pathway. If one of the redundant elements is established, siRNA screens for modifiers of its depletion phenotype may identify additional redundant elements [533].

Finally, I want to note that the rank order of hits in the lists of candidate pro-survival and pro-death proteins is not a rank order of importance in the pathway. Rank order is influenced by siRNA penetrance and functional redundancy.

6.2.2. Quality of the screen.

Duplicate measurements of each siRNA in the screen demonstrate that majority of the siRNA phenotypes were reproducible in replicate assays (**figure 4.3.**). Therefore, I am confident in the primary phenotype that was attributed to the individual siRNAs. However, as elaborated in the previous chapter this phenotype is the result of a complex set of factors including target and off-target effects, phenotypic penetrance and functional redundancy [524].

The negative non-silencing control as well as the positive controls caspase-8 and NEMO in this screen had distinct phenotypes in the 95% CIs throughout (**figure 4.4.** and **4.2.**), which indicates that the screen reliably discriminated between pro-survival and pro-death phenotypes, and control siRNAs were reliable measures of phenotypic penetrance for experimental duplexes. The skewed distribution of phenotypes in the primary assay leads to an apparent unequal variability in the phenotypes observed for the positive controls. For example, viability values for cells treated with caspase-8 siRNA, TNF and CHX and death indices for cells treated with NEMO siRNAs appear more variable than the ones of the corresponding cells treated with NEMO or caspase-8 siRNA, respectively. In reality, the viability values and the death indices varied by a magnitude of two and three-fold for both control siRNAs, respectively.

A comparison of anticipated hits with actual hits gives an approximate sense of the extent to which false negatives impair interpretation of the primary screen data. In my case, I reliably identified core TNF pathway members such as caspase-8, NEMO, TAB2, MEKK2, and JNK1 as critical modifiers of cellular responses to TNF. In fact, the mean death index for the NEMO control siRNA was almost identical to the death index attributed to the corresponding siRNA in the screen. My screen also correctly ranked proteins that are not part of TNF-signaling. For example, IKK- α is not required for canonical NF- κ B signaling [463]. The screen assigned the three IKK- α siRNA duplexes neutral phenotypes (death indices: 1.00, 1.03, 1.08).

As a caveat, I note that my screen did not saturate the entire TNF pathway. For example, our primary data did not implicate IKK- β , TAK1, ASK1, MKK4 and MKK7 as essential modifiers of the TNF pathway [52]. TAK1, ASK1, MKK4 and MKK7 belong to the group of redundant proteins in the TNF pathway. For example, TAK1 is redundant with MEKK2 and MEKK3 to activate NF- κ B [92, 101, 103, 463](**figure 1.10.**). ASK1 is redundant with the MAP3Ks TAK1 and MEKK3 to activate pro-apoptotic JNK signaling [120], and MKK4 and MKK7 are redundant MAP2Ks for JNK [120]. Most likely, the functional redundancy is the reason why those proteins are not classified as high-confidence modifiers of TNF-induced death [524]. Despite redundancy, these proteins appear with the anticipated phenotypes in lower CIs. For example, I identified TAK1 and MEKK3 as 40%, and 30% CI pro-survival proteins, respectively. ASK1, MKK4, and MKK7 were all classified as 70% CI pro-death proteins.

IKK- β is a non-redundant activator of canonical NF- κ B [99, 463] signaling that I identified as a 40% CI pro-survival protein with death indices of 1.13, 1.22, and 1.96. As stated earlier, CI classification is based on the condition that at least two siRNAs belong to the respective CI. One of the IKK- β siRNA duplexes qualifies for the 95% CI. I speculate that the other two siRNAs result in a milder phenotype because they only partially deplete IKK- β protein [524].

These examples illustrate that my screen did not saturate the TNF pathway because many of those pathway components are functionally redundant. A few non-redundant modifiers fell below the detection criteria most likely due to non-penetrant siRNA phenotypes. However, the siRNA phenotypes of the majority of established pathway components were in agreement with their established role. Therefore, I believe that some novel modifiers of TNF-induced death can be found below the 95% confidence interval for pro-survival and pro-death proteins. Some of those modifiers could be identified through the use of bioinformatics tools. For example, in combination with existing knowledge bases, several of those tools identify interaction networks for a large fraction of the human proteome [534, 535]. Established components of the screened pathway and the identified novel modifiers could be used to construct such an interaction network and then be compared to the list of proteins classified as non-modifiers. Other bioinformatics tools use the information of the entire screen to identify pathways that were significantly modified [536]. Components of those pathways may be unidentified hits. In addition, searches for protein interaction motifs or functional domains may help identify false-negatives [537, 538].

The apparent pro-death phenotype attributed to RIPK1 (80% CI pro-death, death indices: 0.63, 0.78, 1.17) is counter-intuitive given the established involvement of RIPK1 in TNF-induced NF- κ B signaling [539-541]. As two out of three siRNAs support the pro-death phenotype, I would consider it a candidate pro-death gene product based on the stringency conditions I used in the evaluation of the primary screen data. Recent studies established that caspase-8 generates a RIPK1 cleavage product at the TNF-receptosome that actively promotes complex II assembly and apoptosis [542]. Furthermore, RIPK1 mediates TNF-induced necrosis in conjunction with RIPK3 that I identified as a 60% CI pro-death protein in the primary screen [543-545]. These reports support requirements for RIPK1 in the induction of cell death by TNF and are consistent with the phenotypes observed for RIPK1 duplexes in this thesis. However, only a clear validation in secondary assays can give certainty about this result and rule out possible OTEs.

6.2. Characterization of HK1 as an anti-apoptotic protein.

I was particularly intrigued by the identification of HK1 as a pro-survival gene product. Of nine hundred eighty six gene products tested, HK1 had the greatest pro-survival phenotype. HK1 fell into the 99% CI of pro-survival gene products with death indices of 3.18, 3.36, and 1.64, respectively (**figure 4.12.**) In secondary evaluations of the three original siRNAs and four independent HK1 siRNAs, I observed identical results for six of the seven siRNAs (**figure 5.1.**). I confirmed that the three HK1 siRNAs (#1 to #3) used in the screen depleted HK1 from HeLa cells. All siRNAs efficiently reduced HK1 mRNA (**figure 5.2.B**) and protein levels (**figure 5.2.A**). Furthermore, HK1 siRNA#1 and siRNA#2 specifically depleted HK1 and not HK2 (**figure 5.2.C,D**). These results rule out the primary screen phenotype as an OTE and indicate that HK1 is a potent inhibitor of TNF-induced cell death.

HKs are well known for their metabolic role in the phosphorylation of glucose [293]. HK1 predominantly channels glucose into the catabolic pathway of glycolysis, followed by the tricarboxylic acid cycle and oxidative phosphorylation to generate the energy equivalent ATP [293]. HK1 interacts with the OMM in a dynamic manner [307]. Mitochondrial HK1 couples the rate of glycolysis with the rate of phosphorylative oxidation as it uses mitochondrial ATP to generate glucose 6-phosphate [293]. Recent reports ascribed anti-apoptotic roles to mitochondrial HKs in response to growth factor signaling [340-342, 357, 368-370]. These data suggest that growth factors promote the interaction of HKs with mitochondria through mostly unknown mechanisms [360, 386, 388] that ultimately block apoptosis upstream of cytochrome c release [367]. The anti-apoptotic role attributed to HK1 in growth factor signaling is consistent with the pro-survival role I observed for HK1 in TNF-signaling. Thus, I hypothesized that HK1 acts at the OMM to attenuate TNF-dependent cell death.

In the present study, I demonstrated that HK1 has an anti-apoptotic role in TNF-induced apoptosis. I found that HK1 attached to the OMM to stabilize mitochondrial integrity and the IMM potential. I showed that HK1 exerts anti-apoptotic effects at the mitochondria through the antagonism of pro-apoptotic Bcl-2 effector proteins.

6.2.1. HK1 has an anti-apoptotic role in TNF signaling.

I showed that the depletion of HK1 accelerated TNF-induced death. I demonstrated that depletion of HK1 with six out of seven independent siRNAs decreased TNF-dependent viability of HeLa cells in a resazurin assay. Next, I showed that depletion of HK1 with a validated HK1 siRNA accelerated TNF-dependent induction of several hallmarks of apoptosis. Specifically, loss of HK1 accelerated complex II formation and caspase-8 processing at complex II (**figure 5.7.**), the translocation of Bax from the cytoplasm to the mitochondria (**figure 5.16.A**) and Bax oligomerization at the mitochondria (**figure 5.16.B,C**), cytochrome c release from the mitochondria (**figure 5.16.A**), the decrease of the IMM potential (**figure 5.6.**), processing of caspase-9 (**figure 5.5.B**) and caspase-3 (**figure 5.5.B**), as well as the caspase substrate PARP1 (**figure 5.5.A**). In a complementary experiment, I showed that overexpression of HK1 attenuated TNF-induced loss of the IMM potential (**figure 5.6.**).

In short, the most parsimonious interpretation of the loss-of-function and overexpression data is that HK1 is a negative regulator of TNF-induced apoptosis.

6.2.2. HK1 is a general anti-apoptotic protein.

I believe that HK1 is a general modifier of TNF-induced death, as I detected similar apoptotic phenotypes of HK1 depletion in the U2OS osteosarcoma cell line and the A549 lung carcinoma cell line. In all three cell lines, loss of HK1 led to accelerated TNF-induced death (**figure 5.8.A**) and processing of caspase substrate PARP (**figure 5.8.B,C**).

I do not believe that interactions between HK1 and the apoptotic machinery are restricted to TNF responses, as I noticed similar pro-death phenotypes upon additional extrinsic apoptotic signals such as Fas cross-linking antibody or soluble TRAIL (**figure 5.8.D,E**).

6.2.3. HK1 attenuates TNF-induced apoptosis at the mitochondria.

I then sought to identify the interaction point between HK1 and the TNF pathway.

I considered several possibilities for these experiments: a negative regulatory interaction of HK1 with the anti-apoptotic NF- κ B module or a positive regulatory interaction with the pro-apoptotic caspase module. My secondary analyses demonstrated that NF- κ B signaling was not attenuated by loss of HK1 (**figure 5.3.**). Instead, I showed that loss of HK1 accelerated TNF-induced pro-apoptotic caspase signaling (**figure 5.4. to 5.8., 5.16.**). Extrinsic apoptotic signals, like TNF, drive caspase-8 mediated activation of effector caspases [38, 43, 47, 506]. In type II cells, caspase-8 signals to the mitochondria to induce caspase-9 dependent activation of effector caspases [162-164]. The pro-apoptotic feedback signaling loop that connects activated effector caspases and the initiator caspase caspase-8 [195, 196] complicated the identification of the exact point at which HK1 influences extrinsic apoptotic cues.

As HK1 has a predominantly mitochondrial localization (**figure 5.9.**) and TNF-induced apoptosis signaling in type II HeLa cells inevitably engages the mitochondria [162-164], I hypothesized that HK1 impedes TNF-induced apoptosis at the mitochondria.

To examine mitochondrial requirements for HK1 in the control of apoptosis, I treated cells with clotrimazole (CTZ), an antifungal agent that displaces HK1 and HK2 from the outer mitochondrial membrane [340-342, 510]. CTZ induced the relocalization of HK1 to the cytoplasm (**figure 5.12.A**) and generated the same pro-apoptotic phenotype as siRNA-mediated HK1 depletion. Specifically, incubation of cells with CTZ and a standard TNF and CHX regime accelerated the decrease of the IMM potential (**figure 5.13.A**) and processing of caspase-9 and PARP (**figure 5.13.B**) compared to treatment with TNF and CHX alone. These data support an anti-apoptotic function of HK1 at the mitochondria.

Treatment of cells with CTZ simultaneously detached HK1 and HK2 from the mitochondria (**figure 5.12.A**), which raises the question whether the phenotype resulted from detachment of HK1, HK2, or both. Furthermore, three previous studies established a pro-apoptotic function for a peptide with sequence identity to the amino-terminus of HK2 that displaces HK2 from mitochondria. The HK2 amino-terminal peptide led to the release of mitochondrial cytochrome c, decreased the IMM potential, induced nuclear fragmentation [340-342] and accelerated apoptosis induced by Bax-dependent indomethacin [340], or a combination of growth factor withdrawal and sublethal UV irradiation [341].

It was not examined whether the HK2-specific peptide has any effect on the localization of HK1. According to Kurokawa *et al.* HK1 and HK2 compete for binding to the mitochondria and therefore likely bind the same site on the OMM [339]. Thus, there is no *a priori* reason to assume that the HK2 amino-terminal peptide does not simultaneously displace HK1 and HK2 from the mitochondrial OMM. The data in this thesis and overexpression data for HK2 (**figure A3.1.**) [340, 370] suggest that HK1 and HK2 both have anti-apoptotic functions at the mitochondria. In the primary siRNA screen HK1 exerted greater anti-apoptotic effects than HK2 in HeLa cells. An unbiased evaluation of screen data positioned HK2 in the 10% CI of pro-survival proteins with death indices of 1.00, 1.01, and 1.87. The death index of 1.87 landed within the 95% CI. It is possible that the other siRNA duplexes generated false-negative phenotypes due to impaired depletion of HK2 transcript or protein. Additional experiments with validated HK2 siRNAs that do not alter HK1 protein levels are required to test this hypothesis.

To distinguish the roles of HK1 and HK2 in the regulation of apoptosis, I generated a synthetic cell-permeable peptide that mimics the amino-terminus of HK1. The peptide was a fusion of the first sixteen amino acids of HK1 and the cell-penetrating sequence of the HIV-1 transactivator of transcription (TAT) (**figure A3.2.A**). The amino-terminus of the peptide was acetylated to match HK1 sequencing studies by Bienvenut *et al.* [546] However, the synthetic peptide was toxic at high doses (**figure A3.2.C**) and failed to induce a mitochondrial displacement of HK1 (or HK2) at low doses (**figure A3.2.B**).

I also attempted to examine the role of mitochondrial HK1 by expressing a HK1 that lacked the amino-terminal twenty one amino acids (HK1 Δ 21). In this assay, I wanted to test if the expression of cytosolic HK1 Δ 21 in HeLa cells attenuates TNF-induced apoptosis. However, cellular fractionation assays demonstrated that a portion of HK1 Δ 21 localized to mitochondria (**figure A3.2.D.**) and undermined the purpose of the assay. I believe that heterotetramerization of endogenous HK1 and HK1 Δ 21 may have caused the mitochondrial localization of HK1 Δ 21.

6.2.4. Attachment of HK1 to the mitochondria attenuates TNF-induced apoptosis.

The parallels between the pro-apoptotic depletion phenotype of HK1 (**figure 5.4 to 5.8, 5.16**) and the pro-apoptotic phenotype of mitochondrial HK detachment with CTZ (**figure 5.13.**) suggest that HK1 blocks apoptosis at the mitochondrion. However, the non-specific nature of CTZ prevents unambiguous interpretation of mitochondrial requirements for HK1 in the control of apoptosis. As both conditions depleted mitochondrial stores of HK1 (**figure 5.10., 5.12.A**) and led to an accelerated induction of apoptosis, I consider it very likely that the depletion of mitochondrial HK1 accelerates the induction of apoptosis by TNF. This hypothesis is supported by prior observations that growth factors induce mitochondrial attachment of HKs to block apoptosis [341].

6.2.5. A catalytically inactive HK1 attenuates TNF-induced death.

Glucose and HK1 activity are required for the anti-apoptotic effects of growth factors [357, 368-370]. However, it has not been tested whether a catalytically inactive HK1 has anti-apoptotic activity [295].

To address this question, I generated an expression construct for catalytically inactive HK1. The location of the active center has not been reported for human HK1. I used sequence alignment between rat HK1, human HK2, and human HK1 to determine that the active center of human HK1 contains the essential and conserved serine 603 (**figure 5.6.B**) [501, 547]. To create an inactive HK1 I replaced serine 603 with alanine. The same mutation reduced the activity of human HK2 to 6% of the wild type HK2 [298, 501]. However, I note that future studies are required to confirm the reduced catalytic activity of HK1S603A.

Overexpression of HK1 or HK1S603A attenuated the TNF and CHX-responsive decrease of the IMM potential in equal measures. This experiment demonstrates that the anti-apoptotic and metabolic roles of HK1 are molecularly distinct.

6.2.6. Metabolic and anti-apoptotic functions of HK1 are distinct.

Loss of HK1 induced a low level of Bax activation (**figure 5.16.**), caspase-9 and PARP cleavage (**figure 5.5.**), and mildly decreased general cell viability (**figure 5.1.**). In addition, loss of HK1 accelerated the rate of TNF-induced apoptosis (**figure 5.4 to 5.8, 5.16**). I believe that these observations are manifestations of the anti-apoptotic activity of HK1 at the mitochondrion, and not the result of the loss of HK1 metabolic activity.

As stated in the previous chapter, wild-type HK1 and catalytically inactive HK1S603A equally protect against TNF-induced apoptosis (**figure 5.6.B**). These findings show that there is a distinction between the metabolic and the anti-apoptotic function of HK1.

In addition, a CTZ-mediated relocalization of HK1 from the mitochondria to the cytoplasm has an overlapping pro-apoptotic phenotype with the siRNA-mediated depletion of HK1 (**figure 5.13.**). Unlike HK1 siRNA, CTZ does not alter the cellular HK1 levels or the metabolic capacity of the cell. These findings are another indication that the anti-apoptotic activity and the metabolic activity of HK1 are separate functions.

I have also demonstrated that HK1 affects cell death through the apoptotic caspase cascade. The pro-death phenotype of HK1 depletion in the presence of TNF and CHX was completely reverted by the parallel depletion of caspase-8. The pro-death phenotype of HK1 depletion in the absence of TNF and CHX was inhibited by the absence Bak and Bax and the overexpression of Bcl-2. These findings suggest that loss of HK1 has a very specific activating effect on the pro-apoptotic caspase cascade. Therefore, I do not believe that the decreased viability observed upon HK1 loss is the result of a general metabolic weakness.

6.2.7. HK1 stabilizes mitochondrial integrity and the IMM potential.

Depletion of HK1 with siRNAs and detachment of mitochondrial HKs with CTZ led to a significant decrease of the IMM potential (**figure 5.11.A,B and 5.12.B**).

HK1 siRNA decreased the IMM potential in a manner that paralleled the drop of HK1 protein levels 2 days after siRNA transfection (**figure 5.11.**). The decrease of the IMM potential occurred consistently in about 10% to 20% of cells. Treatment with CTZ led to a rapid decrease of the IMM potential in a concentration dependent manner (**figure 5.12.B**). Concentrations of more than 40 μM decreased the IMM potential in nearly all cells. Importantly, loss of HK1 facilitated the decrease of the IMM potential by CTZ (**figure 5.12.C,D**). This implies that the drop in mitochondrial HK1 facilitates the CTZ-responsive decrease of the IMM potential. From these data, I conclude that detachment of HK1 from the mitochondria decreases the IMM potential. A mitochondrial detachment of HK2 likely decreases the IMM potential as well, which I believe is the reason why CTZ decreases the IMM potential more potently than HK1 siRNA alone.

Detachment of mitochondrial HKs by CTZ resulted in a loss of mitochondrial cytochrome c (**figure 5.12.A**), which I did not observe when I depleted HK1 only (**figure 5.10.**). The apparent inability of HK1 siRNA to induce loss of mitochondrial reserves of cytochrome c may be due to the compensatory action of HK2.

6.2.8. HK1 stabilizes the IMM potential against Bcl-2 effector proteins.

The IMM potential dissipates when OMM integrity is compromised during apoptosis [171]. The decrease in the IMM potential is partially caused by the loss of cytochrome c from IMS and ICS with significant contributions from effector caspases [171]. Effector caspases reach the IMM through the compromised OMM and proteolytically destroy complexes of the respiratory chain in the IMM [171]. Disruptions to the respiratory chain dissipate the IMM potential [171].

I showed that the detachment of mitochondrial HKs with CTZ compromises OMM integrity and leads to the release of cytochrome c (**figure 5.12.A**). The release of cytochrome c requires a considerable reorganization of the mitochondria and includes remodeling of the IMM and opening of cristae junctions [170, 171, 548, 549]. As depletion of HK1 decreases the IMM potential to a minor extent, I believe that loss of HK1 induces a decrease in OMM integrity that does not result in detectable release of cytochrome c.

The release of cytochrome c is a typical feature of mitochondrially induced apoptosis [170, 171, 550]. Thus, I asked whether the loss of mitochondrial HKs led to the formation of pro-apoptotic channels in the OMM that are regulated by Bcl-2 proteins.

I showed that overexpression of the anti-apoptotic protein Bcl-2 or absence of the Bcl-2 effector proteins Bak and Bax blocked HK1 siRNA-mediated decrease of the IMM potential (**figure 5.14.B** and **5.15.C**). The former experiment was performed in HeLa cells and the latter one in Bak and Bax DKO MEFs that reproduced the decrease of the IMM potential after HK1 depletion with a mouse-specific HK1 siRNA (**figure 5.15.C**).

These findings suggest that HK1 depletion leads to a decrease of the IMM potential through the formation of Bak and Bax channels in the OMM. In line with that hypothesis I found that HK1 siRNA caused an increase of mitochondrial Bax (**figure 5.16.A**), a weak increase in Bax oligomerization in the absence of TNF and CHX (**figure 5.16.B,C**), and a pronounced acceleration of Bax oligomerization in cells that were incubated with TNF and CHX (**figure 5.16.A**).

A modification of Bax activation by mitochondrial HKs has been described elsewhere. Pastorino *et al.* demonstrated that displacement of HK2 from mitochondria with CTZ or a specific HK2 peptide allowed Bax binding, cytochrome c release and apoptosis [340]. Ectopic expression of HK2 had the opposite effect [340]. In other studies, the ectopic expression of HK1 or the amino-terminal hemidomain of HK2 attenuated the exposure of the Bax amino-terminus, while the decrease of mitochondrial HK activity under glucose deprivation led to increased Bax oligomerization at the mitochondria [368, 370].

6.2.9. Model.

In summary, I propose the following model (**figure 6.1.**): mitochondrial HK1 antagonizes the activation and oligomerization of the Bcl-2 effector protein Bax and possibly Bak and stabilizes OMM integrity and IMM potential. Loss of mitochondrial HK1 through siRNA or CTZ leads to the activation of Bax and possibly Bak, which results in the decrease of OMM integrity and IMM potential.

The engagement of death receptors in the absence of HK1 potentiates the activation of Bax and Bak and thereby accelerates the decrease of OMM integrity, the dissipation of the IMM potential, and the rate of pro-apoptotic caspase signaling.

6.2.10. Future perspectives.

An understanding of the regulatory mechanisms that affect HK1 subcellular localization and the consequences of HK1 localization for apoptosis and metabolism will allow us to modify those mechanisms to our advantage.

Therefore, I see great interest in future studies that address the specific mechanisms of the anti-apoptotic role of HK1 at the mitochondria. In particular, studies that address the relationships between the mitochondrial localization of HK1 and the stability of the IMM potential may clarify the manner by which HK1 attenuates the induction of apoptosis. My study focused on the interaction of HK1 with Bcl-2 proteins. However, there are indications that other factors, such as the OMM channel VDAC and the IMM channel ANT may be involved in the cross-membrane talk from HK1 [295].

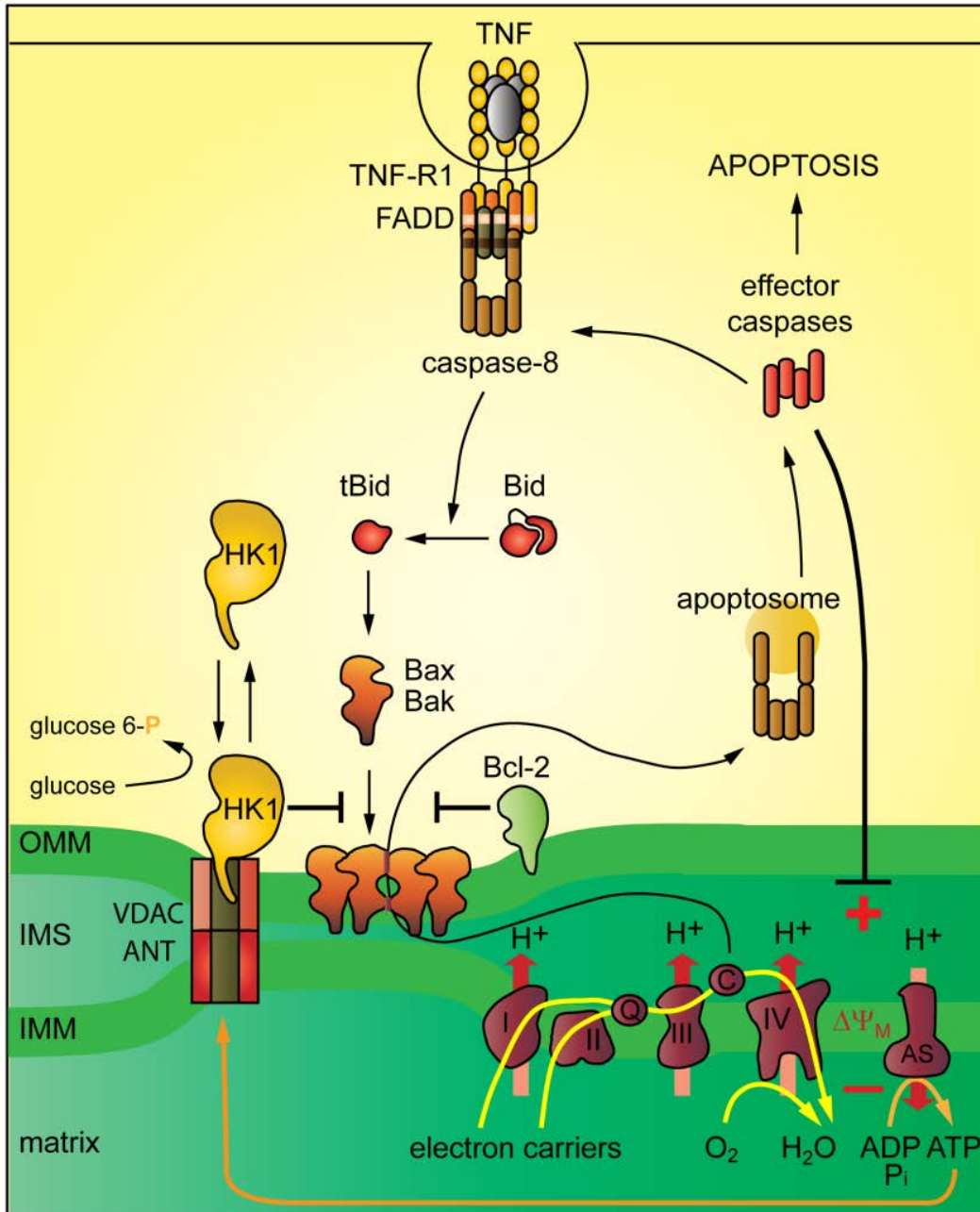


Figure 6.1. Model of HK1 anti-apoptotic activity at the mitochondrion. OMM: outer mitochondrial membrane, IMS: intermembrane space, IMM: inner mitochondrial membrane, I, II, III, and IV: complexes I to IV of the electron transport chain, AS: ATP-synthase, Q: ubiquinone, C: cytochrome c.

Identification of the regulatory mechanisms that determine the cellular localization of HK1 are also interesting subjects to study. Growth factor signals promote the mitochondrial localization of HK1, even though the exact mechanisms are mostly unknown. This study reveals HK1 as an important anti-apoptotic factor at the mitochondria. It would be interesting to examine whether apoptotic signals in type II cells are required to regulate the subcellular localization of HK1 to successfully induce apoptosis and whether such a regulatory mechanism may depend on cross-talk with growth factor signaling.

6.3. Significance.

In the present study I developed and executed the first systematic siRNA screen for modifiers of TNF-induced death. I screened nine hundred eighty six human kinases, phosphatases and associated proteins and identified key signaling elements and novel non-redundant candidate modifiers of TNF-induced death. These data are a valuable source for TNF and apoptosis researchers and represent potential pharmacological targets for inflammatory and cancerous diseases with imbalances in cell viability. HK1 had the greatest pro-survival phenotype in TNF-induced death signaling. The four human HKs are known for their essential metabolic function in glycolysis, gluconeogenesis and the pentose phosphate pathway [293]. However, in recent years it has been shown that the mitochondrial HKs, HK1 and HK2, also transduce anti-apoptotic signals from growth factors [340-342, 357, 368-370]. An anti-apoptotic role for HK1 has only been demonstrated in overexpression studies and with intrinsic apoptotic stimuli [357, 368, 369]. I performed the first HK1 depletion study that examined the anti-apoptotic role of HK1 in the context of death receptor signaling. I showed that the anti-apoptotic mechanism of HK1 in death receptor signaling is similar to the one in growth factor signaling. Interaction of HK1 with the mitochondria antagonizes TNF-induced mitochondrial apoptotic signals in type II cells. However, contrary to the anti-apoptotic role in growth factor signaling, HK1 did not require catalytic activity to attenuate TNF-induced death. HK1 attaches to the OMM to stabilize mitochondrial integrity and the IMM potential. One of the mechanisms of HK1 to stabilize the IMM potential is the antagonism of pro-apoptotic Bcl-2 effector proteins. Reagents that modify the interaction of HK1 with the mitochondria would be valid candidate drugs to promote or restrict cell viability, respectively.

CHAPTER 7. BIBLIOGRAPHY.

1. Kerr JF, Wyllie AH, Currie AR: **Apoptosis: a basic biological phenomenon with wide-ranging implications in tissue kinetics.** *British journal of cancer* 1972, **26**(4):239-257.
2. Lawen A: **Apoptosis-an introduction.** *BioEssays : news and reviews in molecular, cellular and developmental biology* 2003, **25**(9):888-896.
3. Danial NN, Korsmeyer SJ: **Cell death: critical control points.** *Cell* 2004, **116**(2):205-219.
4. Hengartner MO: **The biochemistry of apoptosis.** *Nature* 2000, **407**(6805):770-776.
5. Taylor RC, Cullen SP, Martin SJ: **Apoptosis: controlled demolition at the cellular level.** *Nature reviews Molecular cell biology* 2008, **9**(3):231-241.
6. Wyllie AH: **Glucocorticoid-induced thymocyte apoptosis is associated with endogenous endonuclease activation.** *Nature* 1980, **284**(5756):555-556.
7. Nicholson DW, Thornberry NA: **Caspases: killer proteases.** *Trends in biochemical sciences* 1997, **22**(8):299-306.
8. Li J, Yuan J: **Caspases in apoptosis and beyond.** *Oncogene* 2008, **27**(48):6194-6206.
9. Timmer JC, Salvesen GS: **Caspase substrates.** *Cell death and differentiation* 2007, **14**(1):66-72.
10. Galluzzi L, Vitale I, Abrams JM, Alnemri ES, Baehrecke EH, Blagosklonny MV, Dawson TM, Dawson VL, El-Deiry WS, Fulda S *et al*: **Molecular definitions of cell death subroutines: recommendations of the Nomenclature Committee on Cell Death 2012.** *Cell death and differentiation* 2012, **19**(1):107-120.
11. Jacobson MD, Weil M, Raff MC: **Programmed cell death in animal development.** *Cell* 1997, **88**(3):347-354.
12. Cohen JJ: **Programmed cell death in the immune system.** *Advances in immunology* 1991, **50**:55-85.
13. Feig C, Peter ME: **How apoptosis got the immune system in shape.** *European journal of immunology* 2007, **37** Suppl 1:S61-70.
14. Rudin CM, Thompson CB: **Apoptosis and disease: regulation and clinical relevance of programmed cell death.** *Annual review of medicine* 1997, **48**:267-281.
15. Hanahan D, Weinberg RA: **Hallmarks of cancer: the next generation.** *Cell* 2011, **144**(5):646-674.
16. Mattson MP: **Apoptosis in neurodegenerative disorders.** *Nature reviews Molecular cell biology* 2000, **1**(2):120-129.
17. Friedlander RM: **Apoptosis and caspases in neurodegenerative diseases.** *The New England journal of medicine* 2003, **348**(14):1365-1375.
18. Hotchkiss RS, Nicholson DW: **Apoptosis and caspases regulate death and inflammation in sepsis.** *Nature reviews Immunology* 2006, **6**(11):813-822.
19. Nathan C: **Points of control in inflammation.** *Nature* 2002, **420**(6917):846-852.
20. Nathan C, Ding A: **Nonresolving inflammation.** *Cell* 2010, **140**(6):871-882.
21. Mahoney JA, Rosen A: **Apoptosis and autoimmunity.** *Current opinion in immunology* 2005, **17**(6):583-588.

22. Alnemri ES, Livingston DJ, Nicholson DW, Salvesen G, Thornberry NA, Wong WW, Yuan J: **Human ICE/CED-3 protease nomenclature.** *Cell* 1996, **87**(2):171.
23. Stennicke HR, Salvesen GS: **Catalytic properties of the caspases.** *Cell death and differentiation* 1999, **6**(11):1054-1059.
24. Shi Y: **Mechanisms of caspase activation and inhibition during apoptosis.** *Molecular cell* 2002, **9**(3):459-470.
25. Boatright KM, Salvesen GS: **Mechanisms of caspase activation.** *Current opinion in cell biology* 2003, **15**(6):725-731.
26. Fuentes-Prior P, Salvesen GS: **The protein structures that shape caspase activity, specificity, activation and inhibition.** *The Biochemical journal* 2004, **384**(Pt 2):201-232.
27. MacKenzie SH, Clark AC: **Death by caspase dimerization.** *Advances in experimental medicine and biology* 2012, **747**:55-73.
28. Hofmann K: **The modular nature of apoptotic signaling proteins.** *Cellular and molecular life sciences : CMLS* 1999, **55**(8-9):1113-1128.
29. Hofmann K, Bucher P, Tschopp J: **The CARD domain: a new apoptotic signalling motif.** *Trends in biochemical sciences* 1997, **22**(5):155-156.
30. Boatright KM, Renatus M, Scott FL, Sperandio S, Shin H, Pedersen IM, Ricci JE, Edris WA, Sutherlin DP, Green DR *et al*: **A unified model for apical caspase activation.** *Molecular cell* 2003, **11**(2):529-541.
31. Donepudi M, Mac Sweeney A, Briand C, Grutter MG: **Insights into the regulatory mechanism for caspase-8 activation.** *Molecular cell* 2003, **11**(2):543-549.
32. Luthi AU, Martin SJ: **The CASBAH: a searchable database of caspase substrates.** *Cell death and differentiation* 2007, **14**(4):641-650.
33. Bhardwaj A, Aggarwal BB: **Receptor-mediated choreography of life and death.** *Journal of clinical immunology* 2003, **23**(5):317-332.
34. Locksley RM, Killeen N, Lenardo MJ: **The TNF and TNF receptor superfamilies: integrating mammalian biology.** *Cell* 2001, **104**(4):487-501.
35. Naismith JH, Sprang SR: **Modularity in the TNF-receptor family.** *Trends in biochemical sciences* 1998, **23**(2):74-79.
36. Tartaglia LA, Ayres TM, Wong GH, Goeddel DV: **A novel domain within the 55 kd TNF receptor signals cell death.** *Cell* 1993, **74**(5):845-853.
37. Itoh N, Nagata S: **A novel protein domain required for apoptosis. Mutational analysis of human Fas antigen.** *The Journal of biological chemistry* 1993, **268**(15):10932-10937.
38. Lavrik I, Golks A, Krammer PH: **Death receptor signaling.** *Journal of cell science* 2005, **118**(Pt 2):265-267.
39. Loetscher H, Pan YC, Lahm HW, Gentz R, Brockhaus M, Tabuchi H, Lesslauer W: **Molecular cloning and expression of the human 55 kd tumor necrosis factor receptor.** *Cell* 1990, **61**(2):351-359.
40. Schall TJ, Lewis M, Koller KJ, Lee A, Rice GC, Wong GH, Gatanaga T, Granger GA, Lentz R, Raab H *et al*: **Molecular cloning and expression of a receptor for human tumor necrosis factor.** *Cell* 1990, **61**(2):361-370.
41. Chinnaiyan AM, O'Rourke K, Tewari M, Dixit VM: **FADD, a novel death domain-containing protein, interacts with the death domain of Fas and initiates apoptosis.** *Cell* 1995, **81**(4):505-512.

42. Eberstadt M, Huang B, Chen Z, Meadows RP, Ng SC, Zheng L, Lenardo MJ, Fesik SW: **NMR structure and mutagenesis of the FADD (Mort1) death-effector domain.** *Nature* 1998, **392**(6679):941-945.
43. Peter ME, Krammer PH: **The CD95(APO-1/Fas) DISC and beyond.** *Cell death and differentiation* 2003, **10**(1):26-35.
44. Wang J, Chun HJ, Wong W, Spencer DM, Lenardo MJ: **Caspase-10 is an initiator caspase in death receptor signaling.** *Proceedings of the National Academy of Sciences of the United States of America* 2001, **98**(24):13884-13888.
45. Sprick MR, Rieser E, Stahl H, Grosse-Wilde A, Weigand MA, Walczak H: **Caspase-10 is recruited to and activated at the native TRAIL and CD95 death-inducing signalling complexes in a FADD-dependent manner but can not functionally substitute caspase-8.** *The EMBO journal* 2002, **21**(17):4520-4530.
46. Hsu H, Shu HB, Pan MG, Goeddel DV: **TRADD-TRAF2 and TRADD-FADD interactions define two distinct TNF receptor 1 signal transduction pathways.** *Cell* 1996, **84**(2):299-308.
47. Micheau O, Tschopp J: **Induction of TNF receptor I-mediated apoptosis via two sequential signaling complexes.** *Cell* 2003, **114**(2):181-190.
48. Varfolomeev EE, Schuchmann M, Luria V, Chiannikulchai N, Beckmann JS, Mett IL, Rebrikov D, Brodianski VM, Kemper OC, Kollet O *et al*: **Targeted disruption of the mouse Caspase 8 gene ablates cell death induction by the TNF receptors, Fas/Apo1, and DR3 and is lethal prenatally.** *Immunity* 1998, **9**(2):267-276.
49. Yeh WC, Pompa JL, McCurrach ME, Shu HB, Elia AJ, Shahinian A, Ng M, Wakeham A, Khoo W, Mitchell K *et al*: **FADD: essential for embryo development and signaling from some, but not all, inducers of apoptosis.** *Science* 1998, **279**(5358):1954-1958.
50. Van Antwerp DJ, Martin SJ, Kafri T, Green DR, Verma IM: **Suppression of TNF-alpha-induced apoptosis by NF-kappaB.** *Science* 1996, **274**(5288):787-789.
51. Sherwood ER, Toliver-Kinsky T: **Mechanisms of the inflammatory response.** *Best practice & research Clinical anaesthesiology* 2004, **18**(3):385-405.
52. Wajant H, Pfizenmaier K, Scheurich P: **Tumor necrosis factor signaling.** *Cell death and differentiation* 2003, **10**(1):45-65.
53. Laster SM, Wood JG, Gooding LR: **Tumor necrosis factor can induce both apoptic and necrotic forms of cell lysis.** *Journal of immunology* 1988, **141**(8):2629-2634.
54. Medzhitov R: **Inflammation 2010: new adventures of an old flame.** *Cell* 2010, **140**(6):771-776.
55. Beutler B, Greenwald D, Hulmes JD, Chang M, Pan YC, Mathison J, Ulevitch R, Cerami A: **Identity of tumour necrosis factor and the macrophage-secreted factor cachectin.** *Nature* 1985, **316**(6028):552-554.

56. Cherix S, Speiser M, Matter M, Raffoul W, Lienard D, Theumann N, Mouhsine E, Mirimanoff RO, Leyvraz S, Lejeune FJ *et al*: **Isolated limb perfusion with tumor necrosis factor and melphalan for non-resectable soft tissue sarcomas: long-term results on efficacy and limb salvage in a selected group of patients.** *Journal of surgical oncology* 2008, **98**(3):148-155.
57. Verhoef C, de Wilt JH, Grunhagen DJ, van Geel AN, ten Hagen TL, Eggermont AM: **Isolated limb perfusion with melphalan and TNF-alpha in the treatment of extremity sarcoma.** *Current treatment options in oncology* 2007, **8**(6):417-427.
58. Wong M, Ziring D, Korin Y, Desai S, Kim S, Lin J, Gjertson D, Braun J, Reed E, Singh RR: **TNFalpha blockade in human diseases: mechanisms and future directions.** *Clinical immunology* 2008, **126**(2):121-136.
59. Lin J, Ziring D, Desai S, Kim S, Wong M, Korin Y, Braun J, Reed E, Gjertson D, Singh RR: **TNFalpha blockade in human diseases: an overview of efficacy and safety.** *Clinical immunology* 2008, **126**(1):13-30.
60. Pennica D, Nedwin GE, Hayflick JS, Seeburg PH, Derynck R, Palladino MA, Kohr WJ, Aggarwal BB, Goeddel DV: **Human tumour necrosis factor: precursor structure, expression and homology to lymphotoxin.** *Nature* 1984, **312**(5996):724-729.
61. Carswell EA, Old LJ, Kassel RL, Green S, Fiore N, Williamson B: **An endotoxin-induced serum factor that causes necrosis of tumors.** *Proceedings of the National Academy of Sciences of the United States of America* 1975, **72**(9):3666-3670.
62. Ruff MR, Gifford GE: **Rabbit tumor necrosis factor: mechanism of action.** *Infection and immunity* 1981, **31**(1):380-385.
63. Aggarwal BB: **Signalling pathways of the TNF superfamily: a double-edged sword.** *Nature reviews Immunology* 2003, **3**(9):745-756.
64. Kriegler M, Perez C, DeFay K, Albert I, Lu SD: **A novel form of TNF/cachectin is a cell surface cytotoxic transmembrane protein: ramifications for the complex physiology of TNF.** *Cell* 1988, **53**(1):45-53.
65. Tang P, Hung MC, Klostergaard J: **Human pro-tumor necrosis factor is a homotrimer.** *Biochemistry* 1996, **35**(25):8216-8225.
66. Black RA, Rauch CT, Kozlosky CJ, Peschon JJ, Slack JL, Wolfson MF, Castner BJ, Stocking KL, Reddy P, Srinivasan S *et al*: **A metalloproteinase disintegrin that releases tumour-necrosis factor-alpha from cells.** *Nature* 1997, **385**(6618):729-733.
67. Solomon KA, Pesti N, Wu G, Newton RC: **Cutting edge: a dominant negative form of TNF-alpha converting enzyme inhibits proTNF and TNFRII secretion.** *Journal of immunology* 1999, **163**(8):4105-4108.
68. Kolb WP, Granger GA: **Lymphocyte in vitro cytotoxicity: characterization of human lymphotoxin.** *Proceedings of the National Academy of Sciences of the United States of America* 1968, **61**(4):1250-1255.
69. Grell M, Wajant H, Zimmermann G, Scheurich P: **The type 1 receptor (CD120a) is the high-affinity receptor for soluble tumor necrosis factor.** *Proceedings of the National Academy of Sciences of the United States of America* 1998, **95**(2):570-575.

70. Grell M, Douni E, Wajant H, Lohden M, Clauss M, Maxeiner B, Georgopoulos S, Lesslauer W, Kollias G, Pfizenmaier K *et al*: **The transmembrane form of tumor necrosis factor is the prime activating ligand of the 80 kDa tumor necrosis factor receptor.** *Cell* 1995, **83**(5):793-802.
71. Chan FK, Chun HJ, Zheng L, Siegel RM, Bui KL, Lenardo MJ: **A domain in TNF receptors that mediates ligand-independent receptor assembly and signaling.** *Science* 2000, **288**(5475):2351-2354.
72. Banner DW, D'Arcy A, Janes W, Gentz R, Schoenfeld HJ, Broger C, Loetscher H, Lesslauer W: **Crystal structure of the soluble human 55 kd TNF receptor-human TNF beta complex: implications for TNF receptor activation.** *Cell* 1993, **73**(3):431-445.
73. Jiang Y, Woronicz JD, Liu W, Goeddel DV: **Prevention of constitutive TNF receptor 1 signaling by silencer of death domains.** *Science* 1999, **283**(5401):543-546.
74. Hsu H, Xiong J, Goeddel DV: **The TNF receptor 1-associated protein TRADD signals cell death and NF-kappa B activation.** *Cell* 1995, **81**(4):495-504.
75. Hsu H, Huang J, Shu HB, Baichwal V, Goeddel DV: **TNF-dependent recruitment of the protein kinase RIP to the TNF receptor-1 signaling complex.** *Immunity* 1996, **4**(4):387-396.
76. Tada K, Okazaki T, Sakon S, Koburai T, Kurosawa K, Yamaoka S, Hashimoto H, Mak TW, Yagita H, Okumura K *et al*: **Critical roles of TRAF2 and TRAF5 in tumor necrosis factor-induced NF-kappa B activation and protection from cell death.** *The Journal of biological chemistry* 2001, **276**(39):36530-36534.
77. Varfolomeev E, Goncharov T, Fedorova AV, Dynek JN, Zobel K, Deshayes K, Fairbrother WJ, Vucic D: **c-IAP1 and c-IAP2 are critical mediators of tumor necrosis factor alpha (TNFalpha)-induced NF-kappaB activation.** *The Journal of biological chemistry* 2008, **283**(36):24295-24299.
78. Silke J: **The regulation of TNF signalling: what a tangled web we weave.** *Current opinion in immunology* 2011, **23**(5):620-626.
79. Tsao DH, McDonagh T, Telliez JB, Hsu S, Malakian K, Xu GY, Lin LL: **Solution structure of N-TRADD and characterization of the interaction of N-TRADD and C-TRAF2, a key step in the TNFR1 signaling pathway.** *Molecular cell* 2000, **5**(6):1051-1057.
80. Mace PD, Smits C, Vaux DL, Silke J, Day CL: **Asymmetric recruitment of cIAPs by TRAF2.** *Journal of molecular biology* 2010, **400**(1):8-15.
81. Vince JE, Pantaki D, Feltham R, Mace PD, Cordier SM, Schmukle AC, Davidson AJ, Callus BA, Wong WW, Gentle IE *et al*: **TRAF2 must bind to cellular inhibitors of apoptosis for tumor necrosis factor (tnf) to efficiently activate nf-{kappa}b and to prevent tnf-induced apoptosis.** *The Journal of biological chemistry* 2009, **284**(51):35906-35915.
82. Zheng C, Kabaleeswaran V, Wang Y, Cheng G, Wu H: **Crystal structures of the TRAF2: cIAP2 and the TRAF1: TRAF2: cIAP2 complexes: affinity, specificity, and regulation.** *Molecular cell* 2010, **38**(1):101-113.
83. Walczak H: **TNF and ubiquitin at the crossroads of gene activation, cell death, inflammation, and cancer.** *Immunological reviews* 2011, **244**(1):9-28.

84. Pickart CM: **Back to the future with ubiquitin.** *Cell* 2004, **116**(2):181-190.
85. Bertrand MJ, Milutinovic S, Dickson KM, Ho WC, Boudreault A, Durkin J, Gillard JW, Jaquith JB, Morris SJ, Barker PA: **ciAP1 and ciAP2 facilitate cancer cell survival by functioning as E3 ligases that promote RIP1 ubiquitination.** *Molecular cell* 2008, **30**(6):689-700.
86. Mahoney DJ, Cheung HH, Mrad RL, Plenchette S, Simard C, Enwere E, Arora V, Mak TW, Lacasse EC, Waring J *et al.*: **Both ciAP1 and ciAP2 regulate TNFalpha-mediated NF-kappaB activation.** *Proceedings of the National Academy of Sciences of the United States of America* 2008, **105**(33):11778-11783.
87. Dynek JN, Goncharov T, Dueber EC, Fedorova AV, Izrael-Tomasevic A, Phu L, Helgason E, Fairbrother WJ, Deshayes K, Kirkpatrick DS *et al.*: **c-IAP1 and Ubch5 promote K11-linked polyubiquitination of RIP1 in TNF signalling.** *The EMBO journal* 2010, **29**(24):4198-4209.
88. Ea CK, Deng L, Xia ZP, Pineda G, Chen ZJ: **Activation of IKK by TNFalpha requires site-specific ubiquitination of RIP1 and polyubiquitin binding by NEMO.** *Molecular cell* 2006, **22**(2):245-257.
89. Zandi E, Rothwarf DM, Delhase M, Hayakawa M, Karin M: **The IkappaB kinase complex (IKK) contains two kinase subunits, IKKalpha and IKKbeta, necessary for IkappaB phosphorylation and NF-kappaB activation.** *Cell* 1997, **91**(2):243-252.
90. Yamaoka S, Courtois G, Bessia C, Whiteside ST, Weil R, Agou F, Kirk HE, Kay RJ, Israel A: **Complementation cloning of NEMO, a component of the IkappaB kinase complex essential for NF-kappaB activation.** *Cell* 1998, **93**(7):1231-1240.
91. Rothwarf DM, Zandi E, Natoli G, Karin M: **IKK-gamma is an essential regulatory subunit of the IkappaB kinase complex.** *Nature* 1998, **395**(6699):297-300.
92. Wang C, Deng L, Hong M, Akkaraju GR, Inoue J, Chen ZJ: **TAK1 is a ubiquitin-dependent kinase of MKK and IKK.** *Nature* 2001, **412**(6844):346-351.
93. Kanayama A, Seth RB, Sun L, Ea CK, Hong M, Shaito A, Chiu YH, Deng L, Chen ZJ: **TAB2 and TAB3 activate the NF-kappaB pathway through binding to polyubiquitin chains.** *Molecular cell* 2004, **15**(4):535-548.
94. Rahighi S, Ikeda F, Kawasaki M, Akutsu M, Suzuki N, Kato R, Kensche T, Uejima T, Bloor S, Komander D *et al.*: **Specific recognition of linear ubiquitin chains by NEMO is important for NF-kappaB activation.** *Cell* 2009, **136**(6):1098-1109.
95. Lo YC, Lin SC, Rospigliosi CC, Conze DB, Wu CJ, Ashwell JD, Eliezer D, Wu H: **Structural basis for recognition of diubiquitins by NEMO.** *Molecular cell* 2009, **33**(5):602-615.
96. Komander D, Reyes-Turcu F, Licchesi JD, Odenwaelde P, Wilkinson KD, Barford D: **Molecular discrimination of structurally equivalent Lys 63-linked and linear polyubiquitin chains.** *EMBO reports* 2009, **10**(5):466-473.
97. Gilmore TD: **Introduction to NF-kappaB: players, pathways, perspectives.** *Oncogene* 2006, **25**(51):6680-6684.
98. Hayden MS, Ghosh S: **Shared principles in NF-kappaB signaling.** *Cell* 2008, **132**(3):344-362.

99. Li ZW, Chu W, Hu Y, Delhase M, Deerinck T, Ellisman M, Johnson R, Karin M: **The IKKbeta subunit of IkappaB kinase (IKK) is essential for nuclear factor kappaB activation and prevention of apoptosis.** *The Journal of experimental medicine* 1999, **189**(11):1839-1845.
100. Senftleben U, Li ZW, Baud V, Karin M: **IKKbeta is essential for protecting T cells from TNFalpha-induced apoptosis.** *Immunity* 2001, **14**(3):217-230.
101. Yang J, Lin Y, Guo Z, Cheng J, Huang J, Deng L, Liao W, Chen Z, Liu Z, Su B: **The essential role of MEKK3 in TNF-induced NF-kappaB activation.** *Nature immunology* 2001, **2**(7):620-624.
102. Huang Q, Yang J, Lin Y, Walker C, Cheng J, Liu ZG, Su B: **Differential regulation of interleukin 1 receptor and Toll-like receptor signaling by MEKK3.** *Nature immunology* 2004, **5**(1):98-103.
103. Schmidt C, Peng B, Li Z, Scwabas GM, Fujioka S, Niu J, Schmidt-Supprian M, Evans DB, Abbruzzese JL, Chiao PJ: **Mechanisms of proinflammatory cytokine-induced biphasic NF-kappaB activation.** *Molecular cell* 2003, **12**(5):1287-1300.
104. Tian B, Nowak DE, Jamaluddin M, Wang S, Brasier AR: **Identification of direct genomic targets downstream of the nuclear factor-kappaB transcription factor mediating tumor necrosis factor signaling.** *The Journal of biological chemistry* 2005, **280**(17):17435-17448.
105. Song HY, Rothe M, Goeddel DV: **The tumor necrosis factor-inducible zinc finger protein A20 interacts with TRAF1/TRAF2 and inhibits NF-kappaB activation.** *Proceedings of the National Academy of Sciences of the United States of America* 1996, **93**(13):6721-6725.
106. Jaattela M, Mouritzen H, Elling F, Bastholm L: **A20 zinc finger protein inhibits TNF and IL-1 signaling.** *Journal of immunology* 1996, **156**(3):1166-1173.
107. Lee EG, Boone DL, Chai S, Libby SL, Chien M, Lodolce JP, Ma A: **Failure to regulate TNF-induced NF-kappaB and cell death responses in A20-deficient mice.** *Science* 2000, **289**(5488):2350-2354.
108. Thome M, Tschopp J: **Regulation of lymphocyte proliferation and death by FLIP.** *Nature reviews Immunology* 2001, **1**(1):50-58.
109. Krueger A, Schmitz I, Baumann S, Krammer PH, Kirchhoff S: **Cellular FLICE-inhibitory protein splice variants inhibit different steps of caspase-8 activation at the CD95 death-inducing signaling complex.** *The Journal of biological chemistry* 2001, **276**(23):20633-20640.
110. Micheau O, Lens S, Gaide O, Alevizopoulos K, Tschopp J: **NF-kappaB signals induce the expression of c-FLIP.** *Molecular and cellular biology* 2001, **21**(16):5299-5305.
111. Kreuz S, Siegmund D, Scheurich P, Wajant H: **NF-kappaB inducers upregulate cFLIP, a cycloheximide-sensitive inhibitor of death receptor signaling.** *Molecular and cellular biology* 2001, **21**(12):3964-3973.
112. Yeh WC, Itie A, Elia AJ, Ng M, Shu HB, Wakeham A, Mirtsos C, Suzuki N, Bonnard M, Goeddel DV *et al*: **Requirement for Casper (c-FLIP) in regulation of death receptor-induced apoptosis and embryonic development.** *Immunity* 2000, **12**(6):633-642.
113. Irmiler M, Thome M, Hahne M, Schneider P, Hofmann K, Steiner V, Bodmer JL, Schroter M, Burns K, Mattmann C *et al*: **Inhibition of death receptor signals by cellular FLIP.** *Nature* 1997, **388**(6638):190-195.

114. Zong WX, Edelstein LC, Chen C, Bash J, Gelinas C: **The prosurvival Bcl-2 homolog Bfl-1/A1 is a direct transcriptional target of NF-kappaB that blocks TNFalpha-induced apoptosis.** *Genes & development* 1999, **13**(4):382-387.
115. Tamatani M, Che YH, Matsuzaki H, Ogawa S, Okado H, Miyake S, Mizuno T, Tohyama M: **Tumor necrosis factor induces Bcl-2 and Bcl-x expression through NFkappaB activation in primary hippocampal neurons.** *The Journal of biological chemistry* 1999, **274**(13):8531-8538.
116. Chen C, Edelstein LC, Gelinas C: **The Rel/NF-kappaB family directly activates expression of the apoptosis inhibitor Bcl-x(L).** *Molecular and cellular biology* 2000, **20**(8):2687-2695.
117. Stehlik C, de Martin R, Kumabashiri I, Schmid JA, Binder BR, Lipp J: **Nuclear factor (NF)-kappaB-regulated X-chromosome-linked iap gene expression protects endothelial cells from tumor necrosis factor alpha-induced apoptosis.** *The Journal of experimental medicine* 1998, **188**(1):211-216.
118. Deveraux QL, Roy N, Stennicke HR, Van Arsdale T, Zhou Q, Srinivasula SM, Alnemri ES, Salvesen GS, Reed JC: **IAPs block apoptotic events induced by caspase-8 and cytochrome c by direct inhibition of distinct caspases.** *The EMBO journal* 1998, **17**(8):2215-2223.
119. Deveraux QL, Takahashi R, Salvesen GS, Reed JC: **X-linked IAP is a direct inhibitor of cell-death proteases.** *Nature* 1997, **388**(6639):300-304.
120. Kyriakis JM, Avruch J: **Mammalian MAPK signal transduction pathways activated by stress and inflammation: a 10-year update.** *Physiological reviews* 2012, **92**(2):689-737.
121. Sato S, Sanjo H, Takeda K, Ninomiya-Tsuji J, Yamamoto M, Kawai T, Matsumoto K, Takeuchi O, Akira S: **Essential function for the kinase TAK1 in innate and adaptive immune responses.** *Nature immunology* 2005, **6**(11):1087-1095.
122. Baud V, Liu ZG, Bennett B, Suzuki N, Xia Y, Karin M: **Signaling by proinflammatory cytokines: oligomerization of TRAF2 and TRAF6 is sufficient for JNK and IKK activation and target gene induction via an amino-terminal effector domain.** *Genes & development* 1999, **13**(10):1297-1308.
123. Yan M, Dai T, Deak JC, Kyriakis JM, Zon LI, Woodgett JR, Templeton DJ: **Activation of stress-activated protein kinase by MEKK1 phosphorylation of its activator SEK1.** *Nature* 1994, **372**(6508):798-800.
124. Iriyama T, Takeda K, Nakamura H, Morimoto Y, Kuroiwa T, Mizukami J, Umeda T, Noguchi T, Naguro I, Nishitoh H *et al*: **ASK1 and ASK2 differentially regulate the counteracting roles of apoptosis and inflammation in tumorigenesis.** *The EMBO journal* 2009, **28**(7):843-853.
125. Ceci JD, Patriotis CP, Tsatsanis C, Makris AM, Kovatch R, Swing DA, Jenkins NA, Tsichlis PN, Copeland NG: **Tpl-2 is an oncogenic kinase that is activated by carboxy-terminal truncation.** *Genes & development* 1997, **11**(6):688-700.
126. Salmeron A, Ahmad TB, Carlile GW, Pappin D, Narsimhan RP, Ley SC: **Activation of MEK-1 and SEK-1 by Tpl-2 proto-oncoprotein, a novel MAP kinase kinase kinase.** *The EMBO journal* 1996, **15**(4):817-826.

127. Dumitru CD, Ceci JD, Tsatsanis C, Kontoyiannis D, Stamatakis K, Lin JH, Patriotis C, Jenkins NA, Copeland NG, Kollias G *et al*: **TNF-alpha induction by LPS is regulated posttranscriptionally via a Tpl2/ERK-dependent pathway.** *Cell* 2000, **103**(7):1071-1083.
128. Sanchez I, Hughes RT, Mayer BJ, Yee K, Woodgett JR, Avruch J, Kyriakis JM, Zon LI: **Role of SAPK/ERK kinase-1 in the stress-activated pathway regulating transcription factor c-Jun.** *Nature* 1994, **372**(6508):794-798.
129. Derijard B, Raingeaud J, Barrett T, Wu IH, Han J, Ulevitch RJ, Davis RJ: **Independent human MAP-kinase signal transduction pathways defined by MEK and MKK isoforms.** *Science* 1995, **267**(5198):682-685.
130. Lu X, Nemoto S, Lin A: **Identification of c-Jun NH2-terminal protein kinase (JNK)-activating kinase 2 as an activator of JNK but not p38.** *The Journal of biological chemistry* 1997, **272**(40):24751-24754.
131. Tournier C, Whitmarsh AJ, Cavanagh J, Barrett T, Davis RJ: **Mitogen-activated protein kinase kinase 7 is an activator of the c-Jun NH2-terminal kinase.** *Proceedings of the National Academy of Sciences of the United States of America* 1997, **94**(14):7337-7342.
132. Wu Z, Wu J, Jacinto E, Karin M: **Molecular cloning and characterization of human JNKK2, a novel Jun NH2-terminal kinase-specific kinase.** *Molecular and cellular biology* 1997, **17**(12):7407-7416.
133. Yao Z, Diener K, Wang XS, Zukowski M, Matsumoto G, Zhou G, Mo R, Sasaki T, Nishina H, Hui CC *et al*: **Activation of stress-activated protein kinases/c-Jun N-terminal protein kinases (SAPKs/JNKs) by a novel mitogen-activated protein kinase kinase.** *The Journal of biological chemistry* 1997, **272**(51):32378-32383.
134. Cuenda A, Alonso G, Morrice N, Jones M, Meier R, Cohen P, Nebreda AR: **Purification and cDNA cloning of SAPKK3, the major activator of RK/p38 in stress- and cytokine-stimulated monocytes and epithelial cells.** *The EMBO journal* 1996, **15**(16):4156-4164.
135. Cuenda A, Cohen P, Buee-Scherrer V, Goedert M: **Activation of stress-activated protein kinase-3 (SAPK3) by cytokines and cellular stresses is mediated via SAPKK3 (MKK6); comparison of the specificities of SAPK3 and SAPK2 (RK/p38).** *The EMBO journal* 1997, **16**(2):295-305.
136. Raingeaud J, Whitmarsh AJ, Barrett T, Derijard B, Davis RJ: **MKK3- and MKK6-regulated gene expression is mediated by the p38 mitogen-activated protein kinase signal transduction pathway.** *Molecular and cellular biology* 1996, **16**(3):1247-1255.
137. Raman M, Chen W, Cobb MH: **Differential regulation and properties of MAPKs.** *Oncogene* 2007, **26**(22):3100-3112.
138. Shaulian E, Karin M: **AP-1 as a regulator of cell life and death.** *Nature cell biology* 2002, **4**(5):E131-136.
139. Karin M, Gallagher E: **From JNK to pay dirt: jun kinases, their biochemistry, physiology and clinical importance.** *IUBMB life* 2005, **57**(4-5):283-295.
140. Ventura JJ, Hubner A, Zhang C, Flavell RA, Shokat KM, Davis RJ: **Chemical genetic analysis of the time course of signal transduction by JNK.** *Molecular cell* 2006, **21**(5):701-710.

141. Liu H, Lo CR, Czaja MJ: **NF-kappaB inhibition sensitizes hepatocytes to TNF-induced apoptosis through a sustained activation of JNK and c-Jun.** *Hepatology* 2002, **35**(4):772-778.
142. Deng Y, Ren X, Yang L, Lin Y, Wu X: **A JNK-dependent pathway is required for TNFalpha-induced apoptosis.** *Cell* 2003, **115**(1):61-70.
143. Chang L, Kamata H, Solinas G, Luo JL, Maeda S, Venuprasad K, Liu YC, Karin M: **The E3 ubiquitin ligase itch couples JNK activation to TNFalpha-induced cell death by inducing c-FLIP(L) turnover.** *Cell* 2006, **124**(3):601-613.
144. Puthalakath H, Huang DC, O'Reilly LA, King SM, Strasser A: **The proapoptotic activity of the Bcl-2 family member Bim is regulated by interaction with the dynein motor complex.** *Molecular cell* 1999, **3**(3):287-296.
145. Lei K, Davis RJ: **JNK phosphorylation of Bim-related members of the Bcl2 family induces Bax-dependent apoptosis.** *Proceedings of the National Academy of Sciences of the United States of America* 2003, **100**(5):2432-2437.
146. Papa S, Bubici C, Zazzeroni F, Pham CG, Kuntzen C, Knabb JR, Dean K, Franzoso G: **The NF-kappaB-mediated control of the JNK cascade in the antagonism of programmed cell death in health and disease.** *Cell death and differentiation* 2006, **13**(5):712-729.
147. Tang G, Minemoto Y, Dibling B, Purcell NH, Li Z, Karin M, Lin A: **Inhibition of JNK activation through NF-kappaB target genes.** *Nature* 2001, **414**(6861):313-317.
148. Javelaud D, Besancon F: **NF-kappa B activation results in rapid inactivation of JNK in TNF alpha-treated Ewing sarcoma cells: a mechanism for the anti-apoptotic effect of NF-kappa B.** *Oncogene* 2001, **20**(32):4365-4372.
149. Schneider-Brachert W, Tchikov V, Neumeyer J, Jakob M, Winoto-Morbach S, Held-Feindt J, Heinrich M, Merkel O, Ehrenschwender M, Adam D *et al*: **Compartmentalization of TNF receptor 1 signaling: internalized TNF receptosomes as death signaling vesicles.** *Immunity* 2004, **21**(3):415-428.
150. Tchikov V, Bertsch U, Fritsch J, Edelmann B, Schutze S: **Subcellular compartmentalization of TNF receptor-1 and CD95 signaling pathways.** *European journal of cell biology* 2011, **90**(6-7):467-475.
151. Mosselmans R, Hepburn A, Dumont JE, Fiers W, Galand P: **Endocytic pathway of recombinant murine tumor necrosis factor in L-929 cells.** *Journal of immunology* 1988, **141**(9):3096-3100.
152. Bradley JR, Johnson DR, Pober JS: **Four different classes of inhibitors of receptor-mediated endocytosis decrease tumor necrosis factor-induced gene expression in human endothelial cells.** *Journal of immunology* 1993, **150**(12):5544-5555.
153. Schutze S, Machleidt T, Adam D, Schwandner R, Wiegmann K, Kruse ML, Heinrich M, Wickel M, Kronke M: **Inhibition of receptor internalization by monodansylcadaverine selectively blocks p55 tumor necrosis factor receptor death domain signaling.** *The Journal of biological chemistry* 1999, **274**(15):10203-10212.
154. Higuchi M, Aggarwal BB: **TNF induces internalization of the p60 receptor and shedding of the p80 receptor.** *Journal of immunology* 1994, **152**(7):3550-3558.

155. Mahul-Mellier AL, Strappazzon F, Petiot A, Chatellard-Causse C, Torch S, Blot B, Freeman K, Kuhn L, Garin J, Verna JM *et al*: **Alix and ALG-2 are involved in tumor necrosis factor receptor 1-induced cell death.** *The Journal of biological chemistry* 2008, **283**(50):34954-34965.
156. Boldin MP, Goncharov TM, Goltsev YV, Wallach D: **Involvement of MACH, a novel MORT1/FADD-interacting protease, in Fas/APO-1- and TNF receptor-induced cell death.** *Cell* 1996, **85**(6):803-815.
157. Lin Y, Devin A, Rodriguez Y, Liu ZG: **Cleavage of the death domain kinase RIP by caspase-8 prompts TNF-induced apoptosis.** *Genes & development* 1999, **13**(19):2514-2526.
158. Martinon F, Holler N, Richard C, Tschopp J: **Activation of a pro-apoptotic amplification loop through inhibition of NF-kappaB-dependent survival signals by caspase-mediated inactivation of RIP.** *FEBS letters* 2000, **468**(2-3):134-136.
159. Wertz IE, O'Rourke KM, Zhou H, Eby M, Aravind L, Seshagiri S, Wu P, Wiesmann C, Baker R, Boone DL *et al*: **De-ubiquitination and ubiquitin ligase domains of A20 downregulate NF-kappaB signalling.** *Nature* 2004, **430**(7000):694-699.
160. Liao W, Xiao Q, Tchikov V, Fujita K, Yang W, Wincovitch S, Garfield S, Conze D, El-Deiry WS, Schutze S *et al*: **CARP-2 is an endosome-associated ubiquitin ligase for RIP and regulates TNF-induced NF-kappaB activation.** *Current biology : CB* 2008, **18**(9):641-649.
161. Liao W, Xiao Q, Fujita K, Tchikov V, Yang W, Gunsor M, Garfield S, Goldsmith P, El-Deiry W, Schutze S *et al*: **CARP-1 regulates TNF-induced NF- κ B activation by targeting RIP for proteasomal degradation.** *Current biology : CB* 2008(19):R17-R19.
162. Scaffidi C, Fulda S, Srinivasan A, Friesen C, Li F, Tomaselli KJ, Debatin KM, Krammer PH, Peter ME: **Two CD95 (APO-1/Fas) signaling pathways.** *The EMBO journal* 1998, **17**(6):1675-1687.
163. Barnhart BC, Alappat EC, Peter ME: **The CD95 type I/type II model.** *Seminars in immunology* 2003, **15**(3):185-193.
164. Kaufmann T, Strasser A, Jost PJ: **Fas death receptor signalling: roles of Bid and XIAP.** *Cell death and differentiation* 2012, **19**(1):42-50.
165. Jost PJ, Grabow S, Gray D, McKenzie MD, Nachbur U, Huang DC, Bouillet P, Thomas HE, Borner C, Silke J *et al*: **XIAP discriminates between type I and type II FAS-induced apoptosis.** *Nature* 2009, **460**(7258):1035-1039.
166. Wang K, Yin XM, Chao DT, Milliman CL, Korsmeyer SJ: **BID: a novel BH3 domain-only death agonist.** *Genes & development* 1996, **10**(22):2859-2869.
167. Li H, Zhu H, Xu CJ, Yuan J: **Cleavage of BID by caspase 8 mediates the mitochondrial damage in the Fas pathway of apoptosis.** *Cell* 1998, **94**(4):491-501.
168. Luo X, Budihardjo I, Zou H, Slaughter C, Wang X: **Bid, a Bcl2 interacting protein, mediates cytochrome c release from mitochondria in response to activation of cell surface death receptors.** *Cell* 1998, **94**(4):481-490.
169. Yin XM, Wang K, Gross A, Zhao Y, Zinkel S, Klocke B, Roth KA, Korsmeyer SJ: **Bid-deficient mice are resistant to Fas-induced hepatocellular apoptosis.** *Nature* 1999, **400**(6747):886-891.

170. Kroemer G, Galluzzi L, Brenner C: **Mitochondrial membrane permeabilization in cell death.** *Physiological reviews* 2007, **87**(1):99-163.
171. Tait SW, Green DR: **Mitochondria and cell death: outer membrane permeabilization and beyond.** *Nature reviews Molecular cell biology* 2010, **11**(9):621-632.
172. Brenner C, Grimm S: **The permeability transition pore complex in cancer cell death.** *Oncogene* 2006, **25**(34):4744-4756.
173. Joza N, Susin SA, Daugas E, Stanford WL, Cho SK, Li CY, Sasaki T, Elia AJ, Cheng HY, Ravagnan L *et al*: **Essential role of the mitochondrial apoptosis-inducing factor in programmed cell death.** *Nature* 2001, **410**(6828):549-554.
174. Susin SA, Lorenzo HK, Zamzami N, Marzo I, Snow BE, Brothers GM, Mangion J, Jacotot E, Costantini P, Loeffler M *et al*: **Molecular characterization of mitochondrial apoptosis-inducing factor.** *Nature* 1999, **397**(6718):441-446.
175. Li LY, Luo X, Wang X: **Endonuclease G is an apoptotic DNase when released from mitochondria.** *Nature* 2001, **412**(6842):95-99.
176. Buttner S, Eisenberg T, Carmona-Gutierrez D, Ruli D, Knauer H, Ruckenstuhl C, Sigrist C, Wissing S, Kollroser M, Frohlich KU *et al*: **Endonuclease G regulates budding yeast life and death.** *Molecular cell* 2007, **25**(2):233-246.
177. Du C, Fang M, Li Y, Li L, Wang X: **Smac, a mitochondrial protein that promotes cytochrome c-dependent caspase activation by eliminating IAP inhibition.** *Cell* 2000, **102**(1):33-42.
178. Gray CW, Ward RV, Karran E, Turconi S, Rowles A, Viglienghi D, Southan C, Barton A, Fantom KG, West A *et al*: **Characterization of human HtrA2, a novel serine protease involved in the mammalian cellular stress response.** *European journal of biochemistry / FEBS* 2000, **267**(18):5699-5710.
179. Faccio L, Fusco C, Chen A, Martinotti S, Bonventre JV, Zervos AS: **Characterization of a novel human serine protease that has extensive homology to bacterial heat shock endoprotease HtrA and is regulated by kidney ischemia.** *The Journal of biological chemistry* 2000, **275**(4):2581-2588.
180. Riedl SJ, Salvesen GS: **The apoptosome: signalling platform of cell death.** *Nature reviews Molecular cell biology* 2007, **8**(5):405-413.
181. Acehan D, Jiang X, Morgan DG, Heuser JE, Wang X, Akey CW: **Three-dimensional structure of the apoptosome: implications for assembly, procaspase-9 binding, and activation.** *Molecular cell* 2002, **9**(2):423-432.
182. Yu X, Acehan D, Menetret JF, Booth CR, Ludtke SJ, Riedl SJ, Shi Y, Wang X, Akey CW: **A structure of the human apoptosome at 12.8 Å resolution provides insights into this cell death platform.** *Structure* 2005, **13**(11):1725-1735.
183. Zou H, Henzel WJ, Liu X, Lutschg A, Wang X: **Apaf-1, a human protein homologous to C. elegans CED-4, participates in cytochrome c-dependent activation of caspase-3.** *Cell* 1997, **90**(3):405-413.
184. Srinivasula SM, Ahmad M, Fernandes-Alnemri T, Alnemri ES: **Autoactivation of procaspase-9 by Apaf-1-mediated oligomerization.** *Molecular cell* 1998, **1**(7):949-957.

185. Hu Y, Ding L, Spencer DM, Nunez G: **WD-40 repeat region regulates Apaf-1 self-association and procaspase-9 activation.** *The Journal of biological chemistry* 1998, **273**(50):33489-33494.
186. Hu Y, Benedict MA, Ding L, Nunez G: **Role of cytochrome c and dATP/ATP hydrolysis in Apaf-1-mediated caspase-9 activation and apoptosis.** *The EMBO journal* 1999, **18**(13):3586-3595.
187. Saleh A, Srinivasula SM, Acharya S, Fishel R, Alnemri ES: **Cytochrome c and dATP-mediated oligomerization of Apaf-1 is a prerequisite for procaspase-9 activation.** *The Journal of biological chemistry* 1999, **274**(25):17941-17945.
188. Kim HE, Du F, Fang M, Wang X: **Formation of apoptosome is initiated by cytochrome c-induced dATP hydrolysis and subsequent nucleotide exchange on Apaf-1.** *Proceedings of the National Academy of Sciences of the United States of America* 2005, **102**(49):17545-17550.
189. Li P, Nijhawan D, Budihardjo I, Srinivasula SM, Ahmad M, Alnemri ES, Wang X: **Cytochrome c and dATP-dependent formation of Apaf-1/caspase-9 complex initiates an apoptotic protease cascade.** *Cell* 1997, **91**(4):479-489.
190. Qin H, Srinivasula SM, Wu G, Fernandes-Alnemri T, Alnemri ES, Shi Y: **Structural basis of procaspase-9 recruitment by the apoptotic protease-activating factor 1.** *Nature* 1999, **399**(6736):549-557.
191. Renatus M, Stennicke HR, Scott FL, Liddington RC, Salvesen GS: **Dimer formation drives the activation of the cell death protease caspase 9.** *Proceedings of the National Academy of Sciences of the United States of America* 2001, **98**(25):14250-14255.
192. Pop C, Timmer J, Sperandio S, Salvesen GS: **The apoptosome activates caspase-9 by dimerization.** *Molecular cell* 2006, **22**(2):269-275.
193. Stennicke HR, Deveraux QL, Humke EW, Reed JC, Dixit VM, Salvesen GS: **Caspase-9 can be activated without proteolytic processing.** *The Journal of biological chemistry* 1999, **274**(13):8359-8362.
194. Cullen SP, Martin SJ: **Caspase activation pathways: some recent progress.** *Cell death and differentiation* 2009, **16**(7):935-938.
195. Inoue S, Browne G, Melino G, Cohen GM: **Ordering of caspases in cells undergoing apoptosis by the intrinsic pathway.** *Cell death and differentiation* 2009, **16**(7):1053-1061.
196. Slee EA, Harte MT, Kluck RM, Wolf BB, Casiano CA, Newmeyer DD, Wang HG, Reed JC, Nicholson DW, Alnemri ES *et al*: **Ordering the cytochrome c-initiated caspase cascade: hierarchical activation of caspases-2, -3, -6, -7, -8, and -10 in a caspase-9-dependent manner.** *The Journal of cell biology* 1999, **144**(2):281-292.
197. Chai J, Du C, Wu JW, Kyin S, Wang X, Shi Y: **Structural and biochemical basis of apoptotic activation by Smac/DIABLO.** *Nature* 2000, **406**(6798):855-862.
198. Yang QH, Church-Hajduk R, Ren J, Newton ML, Du C: **Omi/HtrA2 catalytic cleavage of inhibitor of apoptosis (IAP) irreversibly inactivates IAPs and facilitates caspase activity in apoptosis.** *Genes & development* 2003, **17**(12):1487-1496.

199. Srinivasula SM, Gupta S, Datta P, Zhang Z, Hegde R, Cheong N, Fernandes-Alnemri T, Alnemri ES: **Inhibitor of apoptosis proteins are substrates for the mitochondrial serine protease Omi/HtrA2.** *The Journal of biological chemistry* 2003, **278**(34):31469-31472.
200. Vande Walle L, Van Damme P, Lamkanfi M, Saelens X, Vandekerckhove J, Gevaert K, Vandenabeele P: **Proteome-wide Identification of HtrA2/Omi Substrates.** *Journal of proteome research* 2007, **6**(3):1006-1015.
201. Hegde R, Srinivasula SM, Zhang Z, Wassell R, Mukattash R, Cilenti L, DuBois G, Lazebnik Y, Zervos AS, Fernandes-Alnemri T *et al*: **Identification of Omi/HtrA2 as a mitochondrial apoptotic serine protease that disrupts inhibitor of apoptosis protein-caspase interaction.** *The Journal of biological chemistry* 2002, **277**(1):432-438.
202. Frey TG, Mannella CA: **The internal structure of mitochondria.** *Trends in biochemical sciences* 2000, **25**(7):319-324.
203. Hackenbrock CR: **Ultrastructural bases for metabolically linked mechanical activity in mitochondria. I. Reversible ultrastructural changes with change in metabolic steady state in isolated liver mitochondria.** *The Journal of cell biology* 1966, **30**(2):269-297.
204. Colombini M: **VDAC: the channel at the interface between mitochondria and the cytosol.** *Molecular and cellular biochemistry* 2004, **256-257**(1-2):107-115.
205. Hiller S, Garces RG, Malia TJ, Orekhov VY, Colombini M, Wagner G: **Solution structure of the integral human membrane protein VDAC-1 in detergent micelles.** *Science* 2008, **321**(5893):1206-1210.
206. Bayrhuber M, Meins T, Habeck M, Becker S, Giller K, Villinger S, Vonrhein C, Griesinger C, Zweckstetter M, Zeth K: **Structure of the human voltage-dependent anion channel.** *Proceedings of the National Academy of Sciences of the United States of America* 2008, **105**(40):15370-15375.
207. Saraste M: **Oxidative phosphorylation at the fin de siecle.** *Science* 1999, **283**(5407):1488-1493.
208. Mitchell P: **Chemiosmotic coupling in oxidative and photosynthetic phosphorylation.** *Biological reviews of the Cambridge Philosophical Society* 1966, **41**(3):445-502.
209. Mitchell P, Moyle J: **Evidence discriminating between the chemical and the chemiosmotic mechanisms of electron transport phosphorylation.** *Nature* 1965, **208**(5016):1205-1206.
210. Mitchell P, Moyle J: **Stoichiometry of proton translocation through the respiratory chain and adenosine triphosphatase systems of rat liver mitochondria.** *Nature* 1965, **208**(5006):147-151.
211. Beutner G, Ruck A, Riede B, Brdiczka D: **Complexes between porin, hexokinase, mitochondrial creatine kinase and adenylate translocator display properties of the permeability transition pore. Implication for regulation of permeability transition by the kinases.** *Biochimica et biophysica acta* 1998, **1368**(1):7-18.
212. Beutner G, Ruck A, Riede B, Welte W, Brdiczka D: **Complexes between kinases, mitochondrial porin and adenylate translocator in rat brain resemble the permeability transition pore.** *FEBS letters* 1996, **396**(2-3):189-195.

213. Gumaa KA, McLean P: **A possible interrelationship between binding of hexokinase and the site of ATP formation in Krebs ascites cells.** *Biochemical and biophysical research communications* 1969, **36**(5):771-779.
214. Chipuk JE, Moldoveanu T, Llambi F, Parsons MJ, Green DR: **The BCL-2 family reunion.** *Molecular cell* 2010, **37**(3):299-310.
215. Youle RJ, Strasser A: **The BCL-2 protein family: opposing activities that mediate cell death.** *Nature reviews Molecular cell biology* 2008, **9**(1):47-59.
216. Wei MC, Zong WX, Cheng EH, Lindsten T, Panoutsakopoulou V, Ross AJ, Roth KA, MacGregor GR, Thompson CB, Korsmeyer SJ: **Proapoptotic BAX and BAK: a requisite gateway to mitochondrial dysfunction and death.** *Science* 2001, **292**(5517):727-730.
217. Kvaisakul M, Yang H, Fairlie WD, Czabotar PE, Fischer SF, Perugini MA, Huang DC, Colman PM: **Vaccinia virus anti-apoptotic F1L is a novel Bcl-2-like domain-swapped dimer that binds a highly selective subset of BH3-containing death ligands.** *Cell death and differentiation* 2008, **15**(10):1564-1571.
218. Oltvai ZN, Milliman CL, Korsmeyer SJ: **Bcl-2 heterodimerizes in vivo with a conserved homolog, Bax, that accelerates programmed cell death.** *Cell* 1993, **74**(4):609-619.
219. Farrow SN, White JH, Martinou I, Raven T, Pun KT, Grinham CJ, Martinou JC, Brown R: **Cloning of a bcl-2 homologue by interaction with adenovirus E1B 19K.** *Nature* 1995, **374**(6524):731-733.
220. Chittenden T, Harrington EA, O'Connor R, Flemington C, Lutz RJ, Evan GI, Guild BC: **Induction of apoptosis by the Bcl-2 homologue Bak.** *Nature* 1995, **374**(6524):733-736.
221. Kiefer MC, Brauer MJ, Powers VC, Wu JJ, Umansky SR, Tomei LD, Barr PJ: **Modulation of apoptosis by the widely distributed Bcl-2 homologue Bak.** *Nature* 1995, **374**(6524):736-739.
222. Hsu SY, Kaipia A, McGee E, Lomeli M, Hsueh AJ: **Bok is a pro-apoptotic Bcl-2 protein with restricted expression in reproductive tissues and heterodimerizes with selective anti-apoptotic Bcl-2 family members.** *Proceedings of the National Academy of Sciences of the United States of America* 1997, **94**(23):12401-12406.
223. Ke F, Voss A, Kerr JB, O'Reilly LA, Tai L, Echeverry N, Bouillet P, Strasser A, Kaufmann T: **BCL-2 family member BOK is widely expressed but its loss has only minimal impact in mice.** *Cell death and differentiation* 2012, **19**(6):915-925.
224. Wolter KG, Hsu YT, Smith CL, Nechushtan A, Xi XG, Youle RJ: **Movement of Bax from the cytosol to mitochondria during apoptosis.** *The Journal of cell biology* 1997, **139**(5):1281-1292.
225. Hsu YT, Wolter KG, Youle RJ: **Cytosol-to-membrane redistribution of Bax and Bcl-X(L) during apoptosis.** *Proceedings of the National Academy of Sciences of the United States of America* 1997, **94**(8):3668-3672.
226. Goping IS, Gross A, Lavoie JN, Nguyen M, Jemmerson R, Roth K, Korsmeyer SJ, Shore GC: **Regulated targeting of BAX to mitochondria.** *The Journal of cell biology* 1998, **143**(1):207-215.

227. Letai A, Bassik MC, Walensky LD, Sorcinelli MD, Weiler S, Korsmeyer SJ: **Distinct BH3 domains either sensitize or activate mitochondrial apoptosis, serving as prototype cancer therapeutics.** *Cancer cell* 2002, **2**(3):183-192.
228. Kuwana T, Bouchier-Hayes L, Chipuk JE, Bonzon C, Sullivan BA, Green DR, Newmeyer DD: **BH3 domains of BH3-only proteins differentially regulate Bax-mediated mitochondrial membrane permeabilization both directly and indirectly.** *Molecular cell* 2005, **17**(4):525-535.
229. Chipuk JE, Green DR: **How do BCL-2 proteins induce mitochondrial outer membrane permeabilization?** *Trends in cell biology* 2008, **18**(4):157-164.
230. Du H, Wolf J, Schafer B, Moldoveanu T, Chipuk JE, Kuwana T: **BH3 domains other than Bim and Bid can directly activate Bax/Bak.** *The Journal of biological chemistry* 2011, **286**(1):491-501.
231. Walensky LD, Gavathiotis E: **BAX unleashed: the biochemical transformation of an inactive cytosolic monomer into a toxic mitochondrial pore.** *Trends in biochemical sciences* 2011, **36**(12):642-652.
232. Krajewski S, Krajewska M, Reed JC: **Immunohistochemical analysis of in vivo patterns of Bak expression, a proapoptotic member of the Bcl-2 protein family.** *Cancer research* 1996, **56**(12):2849-2855.
233. Lazarou M, Stojanovski D, Frazier AE, Kotevski A, Dewson G, Craigen WJ, Kluck RM, Vaux DL, Ryan MT: **Inhibition of Bak activation by VDAC2 is dependent on the Bak transmembrane anchor.** *The Journal of biological chemistry* 2010, **285**(47):36876-36883.
234. Cheng EH, Sheiko TV, Fisher JK, Craigen WJ, Korsmeyer SJ: **VDAC2 inhibits BAK activation and mitochondrial apoptosis.** *Science* 2003, **301**(5632):513-517.
235. Willis SN, Chen L, Dewson G, Wei A, Naik E, Fletcher JI, Adams JM, Huang DC: **Proapoptotic Bak is sequestered by Mcl-1 and Bcl-xL, but not Bcl-2, until displaced by BH3-only proteins.** *Genes & development* 2005, **19**(11):1294-1305.
236. Dewson G, Ma S, Frederick P, Hockings C, Tan I, Kratina T, Kluck RM: **Bax dimerizes via a symmetric BH3:groove interface during apoptosis.** *Cell death and differentiation* 2012, **19**(4):661-670.
237. Dewson G, Kratina T, Sim HW, Puthalakath H, Adams JM, Colman PM, Kluck RM: **To trigger apoptosis, Bak exposes its BH3 domain and homodimerizes via BH3:groove interactions.** *Molecular cell* 2008, **30**(3):369-380.
238. Dewson G, Kratina T, Czabotar P, Day CL, Adams JM, Kluck RM: **Bak activation for apoptosis involves oligomerization of dimers via their alpha6 helices.** *Molecular cell* 2009, **36**(4):696-703.
239. Ding J, Zhang Z, Roberts GJ, Falcone M, Miao Y, Shao Y, Zhang XC, Andrews DW, Lin J: **Bcl-2 and Bax interact via the BH1-3 groove-BH3 motif interface and a novel interface involving the BH4 motif.** *The Journal of biological chemistry* 2010, **285**(37):28749-28763.
240. Zhang Z, Zhu W, Lapolla SM, Miao Y, Shao Y, Falcone M, Boreham D, McFarlane N, Ding J, Johnson AE *et al*: **Bax forms an oligomer via separate, yet interdependent, surfaces.** *The Journal of biological chemistry* 2010, **285**(23):17614-17627.

241. Epand RF, Martinou JC, Montessuit S, Epand RM, Yip CM: **Direct evidence for membrane pore formation by the apoptotic protein Bax.** *Biochemical and biophysical research communications* 2002, **298**(5):744-749.
242. Schlesinger PH, Gross A, Yin XM, Yamamoto K, Saito M, Waksman G, Korsmeyer SJ: **Comparison of the ion channel characteristics of proapoptotic BAX and antiapoptotic BCL-2.** *Proceedings of the National Academy of Sciences of the United States of America* 1997, **94**(21):11357-11362.
243. Antonsson B, Conti F, Ciavatta A, Montessuit S, Lewis S, Martinou I, Bernasconi L, Bernard A, Mermoud JJ, Mazzei G *et al*: **Inhibition of Bax channel-forming activity by Bcl-2.** *Science* 1997, **277**(5324):370-372.
244. Jurgensmeier JM, Xie Z, Deveraux Q, Ellerby L, Bredesen D, Reed JC: **Bax directly induces release of cytochrome c from isolated mitochondria.** *Proceedings of the National Academy of Sciences of the United States of America* 1998, **95**(9):4997-5002.
245. Yang J, Liu X, Bhalla K, Kim CN, Ibrado AM, Cai J, Peng TI, Jones DP, Wang X: **Prevention of apoptosis by Bcl-2: release of cytochrome c from mitochondria blocked.** *Science* 1997, **275**(5303):1129-1132.
246. Hockenbery D, Nunez G, Millman C, Schreiber RD, Korsmeyer SJ: **Bcl-2 is an inner mitochondrial membrane protein that blocks programmed cell death.** *Nature* 1990, **348**(6299):334-336.
247. Monaghan P, Robertson D, Amos TA, Dyer MJ, Mason DY, Greaves MF: **Ultrastructural localization of bcl-2 protein.** *The journal of histochemistry and cytochemistry : official journal of the Histochemistry Society* 1992, **40**(12):1819-1825.
248. Krajewski S, Tanaka S, Takayama S, Schibler MJ, Fenton W, Reed JC: **Investigation of the subcellular distribution of the bcl-2 oncoprotein: residence in the nuclear envelope, endoplasmic reticulum, and outer mitochondrial membranes.** *Cancer research* 1993, **53**(19):4701-4714.
249. Nguyen M, Millar DG, Yong VW, Korsmeyer SJ, Shore GC: **Targeting of Bcl-2 to the mitochondrial outer membrane by a COOH-terminal signal anchor sequence.** *The Journal of biological chemistry* 1993, **268**(34):25265-25268.
250. Nguyen M, Branton PE, Walton PA, Oltvai ZN, Korsmeyer SJ, Shore GC: **Role of membrane anchor domain of Bcl-2 in suppression of apoptosis caused by E1B-defective adenovirus.** *The Journal of biological chemistry* 1994, **269**(24):16521-16524.
251. Akao Y, Otsuki Y, Kataoka S, Ito Y, Tsujimoto Y: **Multiple subcellular localization of bcl-2: detection in nuclear outer membrane, endoplasmic reticulum membrane, and mitochondrial membranes.** *Cancer research* 1994, **54**(9):2468-2471.
252. Lithgow T, van Driel R, Bertram JF, Strasser A: **The protein product of the oncogene bcl-2 is a component of the nuclear envelope, the endoplasmic reticulum, and the outer mitochondrial membrane.** *Cell growth & differentiation : the molecular biology journal of the American Association for Cancer Research* 1994, **5**(4):411-417.
253. Tsujimoto Y, Finger LR, Yunis J, Nowell PC, Croce CM: **Cloning of the chromosome breakpoint of neoplastic B cells with the t(14;18) chromosome translocation.** *Science* 1984, **226**(4678):1097-1099.

254. Bakhshi A, Jensen JP, Goldman P, Wright JJ, McBride OW, Epstein AL, Korsmeyer SJ: **Cloning the chromosomal breakpoint of t(14;18) human lymphomas: clustering around JH on chromosome 14 and near a transcriptional unit on 18.** *Cell* 1985, **41**(3):899-906.
255. Cleary ML, Sklar J: **Nucleotide sequence of a t(14;18) chromosomal breakpoint in follicular lymphoma and demonstration of a breakpoint-cluster region near a transcriptionally active locus on chromosome 18.** *Proceedings of the National Academy of Sciences of the United States of America* 1985, **82**(21):7439-7443.
256. Vaux DL, Cory S, Adams JM: **Bcl-2 gene promotes haemopoietic cell survival and cooperates with c-myc to immortalize pre-B cells.** *Nature* 1988, **335**(6189):440-442.
257. McDonnell TJ, Deane N, Platt FM, Nunez G, Jaeger U, McKearn JP, Korsmeyer SJ: **bcl-2-immunoglobulin transgenic mice demonstrate extended B cell survival and follicular lymphoproliferation.** *Cell* 1989, **57**(1):79-88.
258. Sattler M, Liang H, Nettesheim D, Meadows RP, Harlan JE, Eberstadt M, Yoon HS, Shuker SB, Chang BS, Minn AJ *et al*: **Structure of Bcl-xL-Bak peptide complex: recognition between regulators of apoptosis.** *Science* 1997, **275**(5302):983-986.
259. Cheng EH, Wei MC, Weiler S, Flavell RA, Mak TW, Lindsten T, Korsmeyer SJ: **BCL-2, BCL-X(L) sequester BH3 domain-only molecules preventing BAX- and BAK-mediated mitochondrial apoptosis.** *Molecular cell* 2001, **8**(3):705-711.
260. Chen L, Willis SN, Wei A, Smith BJ, Fletcher JI, Hinds MG, Colman PM, Day CL, Adams JM, Huang DC: **Differential targeting of prosurvival Bcl-2 proteins by their BH3-only ligands allows complementary apoptotic function.** *Molecular cell* 2005, **17**(3):393-403.
261. Kim H, Rafiuddin-Shah M, Tu HC, Jeffers JR, Zambetti GP, Hsieh JJ, Cheng EH: **Hierarchical regulation of mitochondrion-dependent apoptosis by BCL-2 subfamilies.** *Nature cell biology* 2006, **8**(12):1348-1358.
262. Certo M, Del Gaizo Moore V, Nishino M, Wei G, Korsmeyer S, Armstrong SA, Letai A: **Mitochondria primed by death signals determine cellular addiction to antiapoptotic BCL-2 family members.** *Cancer cell* 2006, **9**(5):351-365.
263. Yang E, Zha J, Jockel J, Boise LH, Thompson CB, Korsmeyer SJ: **Bad, a heterodimeric partner for Bcl-XL and Bcl-2, displaces Bax and promotes cell death.** *Cell* 1995, **80**(2):285-291.
264. Ricci JE, Munoz-Pinedo C, Fitzgerald P, Bailly-Maitre B, Perkins GA, Yadava N, Scheffler IE, Ellisman MH, Green DR: **Disruption of mitochondrial function during apoptosis is mediated by caspase cleavage of the p75 subunit of complex I of the electron transport chain.** *Cell* 2004, **117**(6):773-786.
265. Ricci JE, Gottlieb RA, Green DR: **Caspase-mediated loss of mitochondrial function and generation of reactive oxygen species during apoptosis.** *The Journal of cell biology* 2003, **160**(1):65-75.
266. Zhao Y, Wang ZB, Xu JX: **Effect of cytochrome c on the generation and elimination of O₂⁻ and H₂O₂ in mitochondria.** *The Journal of biological chemistry* 2003, **278**(4):2356-2360.

267. Zorov DB, Filburn CR, Klotz LO, Zweier JL, Sollott SJ: **Reactive oxygen species (ROS)-induced ROS release: a new phenomenon accompanying induction of the mitochondrial permeability transition in cardiac myocytes.** *The Journal of experimental medicine* 2000, **192**(7):1001-1014.
268. Kowaltowski AJ, Castilho RF, Vercesi AE: **Mitochondrial permeability transition and oxidative stress.** *FEBS letters* 2001, **495**(1-2):12-15.
269. Hunter DR, Haworth RA, Southard JH: **Relationship between configuration, function, and permeability in calcium-treated mitochondria.** *The Journal of biological chemistry* 1976, **251**(16):5069-5077.
270. Vander Heiden MG, Chandel NS, Williamson EK, Schumacker PT, Thompson CB: **Bcl-xL regulates the membrane potential and volume homeostasis of mitochondria.** *Cell* 1997, **91**(5):627-637.
271. Green DR, Kroemer G: **The pathophysiology of mitochondrial cell death.** *Science* 2004, **305**(5684):626-629.
272. Faustin B, Rossignol R, Rocher C, Benard G, Malgat M, Letellier T: **Mobilization of adenine nucleotide translocators as molecular bases of the biochemical threshold effect observed in mitochondrial diseases.** *The Journal of biological chemistry* 2004, **279**(19):20411-20421.
273. Brdiczka D: **Contact sites between mitochondrial envelope membranes. Structure and function in energy- and protein-transfer.** *Biochimica et biophysica acta* 1991, **1071**(3):291-312.
274. Crompton M: **Mitochondrial intermembrane junctional complexes and their role in cell death.** *The Journal of physiology* 2000, **529 Pt 1**:11-21.
275. Bernardi P: **The permeability transition pore. Control points of a cyclosporin A-sensitive mitochondrial channel involved in cell death.** *Biochimica et biophysica acta* 1996, **1275**(1-2):5-9.
276. Friberg H, Wieloch T: **Mitochondrial permeability transition in acute neurodegeneration.** *Biochimie* 2002, **84**(2-3):241-250.
277. Halestrap AP: **Mitochondrial permeability: dual role for the ADP/ATP translocator?** *Nature* 2004, **430**(7003):1 p following 983.
278. Le Bras M, Clement MV, Pervaiz S, Brenner C: **Reactive oxygen species and the mitochondrial signaling pathway of cell death.** *Histology and histopathology* 2005, **20**(1):205-219.
279. Crompton M, Virji S, Ward JM: **Cyclophilin-D binds strongly to complexes of the voltage-dependent anion channel and the adenine nucleotide translocase to form the permeability transition pore.** *European journal of biochemistry / FEBS* 1998, **258**(2):729-735.
280. Kokoszka JE, Waymire KG, Levy SE, Sligh JE, Cai J, Jones DP, MacGregor GR, Wallace DC: **The ADP/ATP translocator is not essential for the mitochondrial permeability transition pore.** *Nature* 2004, **427**(6973):461-465.
281. Baines CP, Kaiser RA, Sheiko T, Craigen WJ, Molkentin JD: **Voltage-dependent anion channels are dispensable for mitochondrial-dependent cell death.** *Nature cell biology* 2007, **9**(5):550-555.
282. Nakagawa T, Shimizu S, Watanabe T, Yamaguchi O, Otsu K, Yamagata H, Inohara H, Kubo T, Tsujimoto Y: **Cyclophilin D-dependent mitochondrial permeability transition regulates some necrotic but not apoptotic cell death.** *Nature* 2005, **434**(7033):652-658.

283. Halestrap A: **Biochemistry: a pore way to die.** *Nature* 2005, **434**(7033):578-579.
284. Schneider MD: **Cyclophilin D: knocking on death's door.** *Science's STKE : signal transduction knowledge environment* 2005, **2005**(287):pe26.
285. Zamzami N, Larochette N, Kroemer G: **Mitochondrial permeability transition in apoptosis and necrosis.** *Cell death and differentiation* 2005, **12 Suppl 2**:1478-1480.
286. Nishi S, Seino S, Bell GI: **Human hexokinase: sequences of amino- and carboxyl-terminal halves are homologous.** *Biochemical and biophysical research communications* 1988, **157**(3):937-943.
287. Deeb SS, Malkki M, Laakso M: **Human hexokinase II: sequence and homology to other hexokinases.** *Biochemical and biophysical research communications* 1993, **197**(1):68-74.
288. Furuta H, Nishi S, Le Beau MM, Fernald AA, Yano H, Bell GI: **Sequence of human hexokinase III cDNA and assignment of the human hexokinase III gene (HK3) to chromosome band 5q35.2 by fluorescence in situ hybridization.** *Genomics* 1996, **36**(1):206-209.
289. Tanizawa Y, Koranyi LI, Welling CM, Permutt MA: **Human liver glucokinase gene: cloning and sequence determination of two alternatively spliced cDNAs.** *Proceedings of the National Academy of Sciences of the United States of America* 1991, **88**(16):7294-7297.
290. Koranyi LI, Tanizawa Y, Welling CM, Rabin DU, Permutt MA: **Human islet glucokinase gene. Isolation and sequence analysis of full-length cDNA.** *Diabetes* 1992, **41**(7):807-811.
291. Tanizawa Y, Matsutani A, Chiu KC, Permutt MA: **Human glucokinase gene: isolation, structural characterization, and identification of a microsatellite repeat polymorphism.** *Molecular endocrinology* 1992, **6**(7):1070-1081.
292. Nishi S, Stoffel M, Xiang K, Shows TB, Bell GI, Takeda J: **Human pancreatic beta-cell glucokinase: cDNA sequence and localization of the polymorphic gene to chromosome 7, band p 13.** *Diabetologia* 1992, **35**(8):743-747.
293. Wilson JE: **Isozymes of mammalian hexokinase: structure, subcellular localization and metabolic function.** *The Journal of experimental biology* 2003, **206**(Pt 12):2049-2057.
294. Xu LZ, Harrison RW, Weber IT, Pilkis SJ: **Human beta-cell glucokinase. Dual role of Ser-151 in catalysis and hexose affinity.** *The Journal of biological chemistry* 1995, **270**(17):9939-9946.
295. Robey RB, Hay N: **Mitochondrial hexokinases, novel mediators of the antiapoptotic effects of growth factors and Akt.** *Oncogene* 2006, **25**(34):4683-4696.
296. Wilson JE, vol. 1. Boca Raton: CRC Press; 1985.
297. Marcus F, Ureta T: **Amino acid sequence homology between yeast hexokinases and rat hexokinase C.** *Biochemical and biophysical research communications* 1986, **139**(2):714-719.
298. Schirch DM, Wilson JE: **Rat brain hexokinase: amino acid sequence at the substrate hexose binding site is homologous to that of yeast hexokinase.** *Archives of biochemistry and biophysics* 1987, **257**(1):1-12.

299. Cardenas ML, Cornish-Bowden A, Ureta T: **Evolution and regulatory role of the hexokinases.** *Biochimica et biophysica acta* 1998, **1401**(3):242-264.
300. Colowick SP. In: *The enzymes*. Edited by Boyer PD, vol. 9B, 3 edn. New York: Academic Press; 1973: 1-84.
301. Wilson JE: **Hexokinases.** *Reviews of physiology, biochemistry and pharmacology* 1995, **126**:65-198.
302. Katzen HM, Schimke RT: **Multiple forms of hexokinase in the rat: tissue distribution, age dependency, and properties.** *Proceedings of the National Academy of Sciences of the United States of America* 1965, **54**(4):1218-1225.
303. Rogers PA, Fisher RA, Harris H: **An electrophoretic study of the distribution and properties of human hexokinases.** *Biochemical genetics* 1975, **13**(11-12):857-866.
304. Crane RK, Sols A: **The association of hexokinase with particulate fractions of brain and other tissue homogenates.** *The Journal of biological chemistry* 1953, **203**(1):273-292.
305. Johnson MK: **The intracellular distribution of glycolytic and other enzymes in rat-brain homogenates and mitochondrial preparations.** *The Biochemical journal* 1960, **77**:610-618.
306. Rose IA, Warms JV: **Mitochondrial hexokinase. Release, rebinding, and location.** *The Journal of biological chemistry* 1967, **242**(7):1635-1645.
307. Wilson JE: **Ambiguous enzymes: Variation in intracellular distribution as a regulatory mechanism.** *Trends in biochemical sciences* 1978(3):124-125.
308. Kropp ES, Wilson JE: **Hexokinase binding sites on mitochondrial membranes.** *Biochemical and biophysical research communications* 1970, **38**(1):74-79.
309. Kurokawa M, Yokoyama K, Kaneko M, Ishibashi S: **Difference in hydrophobicity between mitochondria-bindable and non-bindable forms of hexokinase purified from rat brain.** *Biochemical and biophysical research communications* 1983, **115**(3):1101-1107.
310. Polakis PG, Wilson JE: **An intact hydrophobic N-terminal sequence is critical for binding of rat brain hexokinase to mitochondria.** *Archives of biochemistry and biophysics* 1985, **236**(1):328-337.
311. Gelb BD, Adams V, Jones SN, Griffin LD, MacGregor GR, McCabe ER: **Targeting of hexokinase 1 to liver and hepatoma mitochondria.** *Proceedings of the National Academy of Sciences of the United States of America* 1992, **89**(1):202-206.
312. Sui D, Wilson JE: **Structural determinants for the intracellular localization of the isozymes of mammalian hexokinase: intracellular localization of fusion constructs incorporating structural elements from the hexokinase isozymes and the green fluorescent protein.** *Archives of biochemistry and biophysics* 1997, **345**(1):111-125.
313. Xie GC, Wilson JE: **Rat brain hexokinase: the hydrophobic N-terminus of the mitochondrially bound enzyme is inserted in the lipid bilayer.** *Archives of biochemistry and biophysics* 1988, **267**(2):803-810.
314. Felgner PL, Wilson JE: **Effect of neutral salts on the interaction of rat brain hexokinase with the outer mitochondrial membrane.** *Archives of biochemistry and biophysics* 1977, **182**(1):282-294.

315. Azoulay-Zohar H, Aflalo C: **Binding of rat brain hexokinase to recombinant yeast mitochondria: identification of necessary physico-chemical determinants.** *European journal of biochemistry / FEBS* 2000, **267**(10):2973-2980.
316. Felgner PL, Messer JL, Wilson JE: **Purification of a hexokinase-binding protein from the outer mitochondrial membrane.** *The Journal of biological chemistry* 1979, **254**(12):4946-4949.
317. Linden M, Gellerfors P, Nelson BD: **Pore protein and the hexokinase-binding protein from the outer membrane of rat liver mitochondria are identical.** *FEBS letters* 1982, **141**(2):189-192.
318. Fiek C, Benz R, Roos N, Brdiczka D: **Evidence for identity between the hexokinase-binding protein and the mitochondrial porin in the outer membrane of rat liver mitochondria.** *Biochimica et biophysica acta* 1982, **688**(2):429-440.
319. Dorbani L, Jancsik V, Linden M, Leterrier JF, Nelson BD, Rendon A: **Subfractionation of the outer membrane of rat brain mitochondria: evidence for the existence of a domain containing the porin-hexokinase complex.** *Archives of biochemistry and biophysics* 1987, **252**(1):188-196.
320. Kottke M, Adam V, Riesinger I, Bremm G, Bosch W, Brdiczka D, Sandri G, Panfili E: **Mitochondrial boundary membrane contact sites in brain: points of hexokinase and creatine kinase location, and control of Ca²⁺ transport.** *Biochimica et biophysica acta* 1988, **935**(1):87-102.
321. Adams V, Bosch W, Schlegel J, Wallimann T, Brdiczka D: **Further characterization of contact sites from mitochondria of different tissues: topology of peripheral kinases.** *Biochimica et biophysica acta* 1989, **981**(2):213-225.
322. Blachly-Dyson E, Zambronicz EB, Yu WH, Adams V, McCabe ER, Adelman J, Colombini M, Forte M: **Cloning and functional expression in yeast of two human isoforms of the outer mitochondrial membrane channel, the voltage-dependent anion channel.** *The Journal of biological chemistry* 1993, **268**(3):1835-1841.
323. Ha H, Hajek P, Bedwell DM, Burrows PD: **A mitochondrial porin cDNA predicts the existence of multiple human porins.** *The Journal of biological chemistry* 1993, **268**(16):12143-12149.
324. Rahmani Z, Maunoury C, Siddiqui A: **Isolation of a novel human voltage-dependent anion channel gene.** *European journal of human genetics : EJHG* 1998, **6**(4):337-340.
325. Sukumaran SK, Fu NY, Tin CB, Wan KF, Lee SS, Yu VC: **A soluble form of the pilus protein FimA targets the VDAC-hexokinase complex at mitochondria to suppress host cell apoptosis.** *Molecular cell* 2010, **37**(6):768-783.
326. Shoshan-Barmatz V, Keinan N, Zaid H: **Uncovering the role of VDAC in the regulation of cell life and death.** *Journal of bioenergetics and biomembranes* 2008, **40**(3):183-191.
327. Azoulay-Zohar H, Aflalo C: **Binding of rat brain hexokinase to recombinant yeast mitochondria: identification of necessary molecular determinants.** *Journal of bioenergetics and biomembranes* 1999, **31**(6):569-579.

328. Neumann D, Buckers J, Kastrup L, Hell SW, Jakobs S: **Two-color STED microscopy reveals different degrees of colocalization between hexokinase-I and the three human VDAC isoforms.** *PMC biophysics* 2010, **3**(1):4.
329. Zaid H, Abu-Hamad S, Israelson A, Nathan I, Shoshan-Barmatz V: **The voltage-dependent anion channel-1 modulates apoptotic cell death.** *Cell death and differentiation* 2005, **12**(7):751-760.
330. De Pinto V, al Jamal JA, Palmieri F: **Location of the dicyclohexylcarbodiimide-reactive glutamate residue in the bovine heart mitochondrial porin.** *The Journal of biological chemistry* 1993, **268**(17):12977-12982.
331. Rosano C: **Molecular model of hexokinase binding to the outer mitochondrial membrane porin (VDAC1): Implication for the design of new cancer therapies.** *Mitochondrion* 2011, **11**(3):513-519.
332. Osawa H, Printz RL, Whitesell RR, Granner DK: **Regulation of hexokinase II gene transcription and glucose phosphorylation by catecholamines, cyclic AMP, and insulin.** *Diabetes* 1995, **44**(12):1426-1432.
333. Riddle SR, Ahmad A, Ahmad S, Deeb SS, Malkki M, Schneider BK, Allen CB, White CW: **Hypoxia induces hexokinase II gene expression in human lung cell line A549.** *American journal of physiology Lung cellular and molecular physiology* 2000, **278**(2):L407-416.
334. Shinohara Y, Hino M, Ishida T, Yamanaka Y, Terada H: **Growth condition-dependent synchronized changes in transcript levels of type II hexokinase and type 1 glucose transporter in tumor cells.** *Biochimica et biophysica acta* 2001, **1499**(3):242-248.
335. Taneja N, Coy PE, Lee I, Bryson JM, Robey RB: **Proinflammatory interleukin-1 cytokines increase mesangial cell hexokinase activity and hexokinase II isoform abundance.** *American journal of physiology Cell physiology* 2004, **287**(2):C548-557.
336. Pedersen PL, Mathupala S, Rempel A, Geschwind JF, Ko YH: **Mitochondrial bound type II hexokinase: a key player in the growth and survival of many cancers and an ideal prospect for therapeutic intervention.** *Biochimica et biophysica acta* 2002, **1555**(1-3):14-20.
337. Katzen HM, Soderman DD, Wiley CE: **Multiple forms of hexokinase. Activities associated with subcellular particulate and soluble fractions of normal and streptozotocin diabetic rat tissues.** *The Journal of biological chemistry* 1970, **245**(16):4081-4096.
338. Kosow DP, Rose IA: **Ascites tumor mitochondrial hexokinase II. Effect of binding on kinetic properties.** *The Journal of biological chemistry* 1968, **243**(13):3623-3630.
339. Kurokawa M, Oda S, Tsubotani E, Fujiwara H, Yokoyama K, Ishibashi S: **Characterization of hexokinase isoenzyme types I and II in ascites tumor cells by an interaction with mitochondrial membrane.** *Molecular and cellular biochemistry* 1982, **45**(3):151-157.
340. Pastorino JG, Shulga N, Hoek JB: **Mitochondrial binding of hexokinase II inhibits Bax-induced cytochrome c release and apoptosis.** *The Journal of biological chemistry* 2002, **277**(9):7610-7618.

341. Majewski N, Nogueira V, Bhaskar P, Coy PE, Skeen JE, Gottlob K, Chandel NS, Thompson CB, Robey RB, Hay N: **Hexokinase-mitochondria interaction mediated by Akt is required to inhibit apoptosis in the presence or absence of Bax and Bak.** *Molecular cell* 2004, **16**(5):819-830.
342. Chiara F, Castellaro D, Marin O, Petronilli V, Brusilow WS, Juhaszova M, Sollott SJ, Forte M, Bernardi P, Rasola A: **Hexokinase II detachment from mitochondria triggers apoptosis through the permeability transition pore independent of voltage-dependent anion channels.** *PLoS one* 2008, **3**(3):e1852.
343. Granner D, Pilkis S: **The genes of hepatic glucose metabolism.** *The Journal of biological chemistry* 1990, **265**(18):10173-10176.
344. Iynedjian PB, Mobius G, Seitz HJ, Wollheim CB, Renold AE: **Tissue-specific expression of glucokinase: identification of the gene product in liver and pancreatic islets.** *Proceedings of the National Academy of Sciences of the United States of America* 1986, **83**(7):1998-2001.
345. Iynedjian PB, Pilot PR, Nospikel T, Milburn JL, Quaade C, Hughes S, Ucla C, Newgard CB: **Differential expression and regulation of the glucokinase gene in liver and islets of Langerhans.** *Proceedings of the National Academy of Sciences of the United States of America* 1989, **86**(20):7838-7842.
346. Hughes SD, Quaade C, Milburn JL, Cassidy L, Newgard CB: **Expression of normal and novel glucokinase mRNAs in anterior pituitary and islet cells.** *The Journal of biological chemistry* 1991, **266**(7):4521-4530.
347. Shiota C, Coffey J, Grimsby J, Grippo JF, Magnuson MA: **Nuclear import of hepatic glucokinase depends upon glucokinase regulatory protein, whereas export is due to a nuclear export signal sequence in glucokinase.** *The Journal of biological chemistry* 1999, **274**(52):37125-37130.
348. Bosco D, Meda P, Iynedjian PB: **Glucokinase and glucokinase regulatory protein: mutual dependence for nuclear localization.** *The Biochemical journal* 2000, **348 Pt 1**:215-222.
349. Danial NN, Gramm CF, Scorrano L, Zhang CY, Krauss S, Ranger AM, Datta SR, Greenberg ME, Licklider LJ, Lowell BB *et al.*: **BAD and glucokinase reside in a mitochondrial complex that integrates glycolysis and apoptosis.** *Nature* 2003, **424**(6951):952-956.
350. Arden C, Baltrusch S, Agius L: **Glucokinase regulatory protein is associated with mitochondria in hepatocytes.** *FEBS letters* 2006, **580**(8):2065-2070.
351. Clarke DD, Sokoloff L: **Circulation and energy metabolism in the brain.**, 6 edn. Lippincott: Williams & Wilkins; 1998.
352. BeltrandelRio H, Wilson JE: **Hexokinase of rat brain mitochondria: relative importance of adenylate kinase and oxidative phosphorylation as sources of substrate ATP, and interaction with intramitochondrial compartments of ATP and ADP.** *Archives of biochemistry and biophysics* 1991, **286**(1):183-194.
353. BeltrandelRio H, Wilson JE: **Coordinated regulation of cerebral glycolytic and oxidative metabolism, mediated by mitochondrially bound hexokinase dependent on intramitochondrially generated ATP.** *Archives of biochemistry and biophysics* 1992, **296**(2):667-677.

354. BeltrandelRio H, Wilson JE: **Interaction of mitochondrially bound rat brain hexokinase with intramitochondrial compartments of ATP generated by oxidative phosphorylation and creatine kinase.** *Archives of biochemistry and biophysics* 1992, **299**(1):116-124.
355. de Cerqueira Cesar M, Wilson JE: **Application of a double isotopic labeling method to a study of the interaction of mitochondrially bound rat brain hexokinase with intramitochondrial compartments of ATP generated by oxidative phosphorylation.** *Archives of biochemistry and biophysics* 1995, **324**(1):9-14.
356. Cesar Mde C, Wilson JE: **Further studies on the coupling of mitochondrially bound hexokinase to intramitochondrially compartmented ATP, generated by oxidative phosphorylation.** *Archives of biochemistry and biophysics* 1998, **350**(1):109-117.
357. Gottlob K, Majewski N, Kennedy S, Kandel E, Robey RB, Hay N: **Inhibition of early apoptotic events by Akt/PKB is dependent on the first committed step of glycolysis and mitochondrial hexokinase.** *Genes & development* 2001, **15**(11):1406-1418.
358. Wilson JE: **Rapid purification of mitochondrial hexokinase from rat brain by a single affinity chromatography step on Affi-Gel blue.** *Preparative biochemistry* 1989, **19**(1):13-21.
359. Kabir F, Wilson JE: **Mitochondrial hexokinase in brain of various species: differences in sensitivity to solubilization by glucose 6-phosphate.** *Archives of biochemistry and biophysics* 1993, **300**(2):641-650.
360. Pastorino JG, Hoek JB: **Regulation of hexokinase binding to VDAC.** *Journal of bioenergetics and biomembranes* 2008, **40**(3):171-182.
361. Miccoli L, Oudard S, Sureau F, Poirson F, Dutrillaux B, Poupon MF: **Intracellular pH governs the subcellular distribution of hexokinase in a glioma cell line.** *The Biochemical journal* 1996, **313 (Pt 3)**:957-962.
362. Miccoli L, Beurdeley-Thomas A, De Pinieux G, Sureau F, Oudard S, Dutrillaux B, Poupon MF: **Light-induced photoactivation of hypericin affects the energy metabolism of human glioma cells by inhibiting hexokinase bound to mitochondria.** *Cancer research* 1998, **58**(24):5777-5786.
363. Sebastian S, Horton JD, Wilson JE: **Anabolic function of the type II isozyme of hexokinase in hepatic lipid synthesis.** *Biochemical and biophysical research communications* 2000, **270**(3):886-891.
364. Kaselonis GL, McCabe ER, Gray SM: **Expression of hexokinase 1 and hexokinase 2 in mammary tissue of nonlactating and lactating rats: evaluation by RT-PCR.** *Molecular genetics and metabolism* 1999, **68**(3):371-374.
365. Arora KK, Pedersen PL: **Functional significance of mitochondrial bound hexokinase in tumor cell metabolism. Evidence for preferential phosphorylation of glucose by intramitochondrially generated ATP.** *The Journal of biological chemistry* 1988, **263**(33):17422-17428.
366. Postic C, Shiota M, Magnuson MA: **Cell-specific roles of glucokinase in glucose homeostasis.** *Recent progress in hormone research* 2001, **56**:195-217.

367. Kennedy SG, Kandel ES, Cross TK, Hay N: **Akt/Protein kinase B inhibits cell death by preventing the release of cytochrome c from mitochondria.** *Molecular and cellular biology* 1999, **19**(8):5800-5810.
368. Rathmell JC, Fox CJ, Plas DR, Hammerman PS, Cinalli RM, Thompson CB: **Akt-directed glucose metabolism can prevent Bax conformation change and promote growth factor-independent survival.** *Molecular and cellular biology* 2003, **23**(20):7315-7328.
369. Bryson JM, Coy PE, Gottlob K, Hay N, Robey RB: **Increased hexokinase activity, of either ectopic or endogenous origin, protects renal epithelial cells against acute oxidant-induced cell death.** *The Journal of biological chemistry* 2002, **277**(13):11392-11400.
370. Majewski N, Nogueira V, Robey RB, Hay N: **Akt inhibits apoptosis downstream of BID cleavage via a glucose-dependent mechanism involving mitochondrial hexokinases.** *Molecular and cellular biology* 2004, **24**(2):730-740.
371. Rostovtseva T, Colombini M: **VDAC channels mediate and gate the flow of ATP: implications for the regulation of mitochondrial function.** *Biophysical journal* 1997, **72**(5):1954-1962.
372. Vander Heiden MG, Chandel NS, Li XX, Schumacker PT, Colombini M, Thompson CB: **Outer mitochondrial membrane permeability can regulate coupled respiration and cell survival.** *Proceedings of the National Academy of Sciences of the United States of America* 2000, **97**(9):4666-4671.
373. Gottlieb E, Armour SM, Harris MH, Thompson CB: **Mitochondrial membrane potential regulates matrix configuration and cytochrome c release during apoptosis.** *Cell death and differentiation* 2003, **10**(6):709-717.
374. Azoulay-Zohar H, Israelson A, Abu-Hamad S, Shoshan-Barmatz V: **In self-defence: hexokinase promotes voltage-dependent anion channel closure and prevents mitochondria-mediated apoptotic cell death.** *The Biochemical journal* 2004, **377**(Pt 2):347-355.
375. Ardail D, Privat JP, Egret-Charlier M, Levrat C, Lerme F, Louisot P: **Mitochondrial contact sites. Lipid composition and dynamics.** *The Journal of biological chemistry* 1990, **265**(31):18797-18802.
376. Lutter M, Fang M, Luo X, Nishijima M, Xie X, Wang X: **Cardiolipin provides specificity for targeting of tBid to mitochondria.** *Nature cell biology* 2000, **2**(10):754-761.
377. Lutter M, Perkins GA, Wang X: **The pro-apoptotic Bcl-2 family member tBid localizes to mitochondrial contact sites.** *BMC cell biology* 2001, **2**:22.
378. Epand RF, Martinou JC, Fornallaz-Mulhauser M, Hughes DW, Epand RM: **The apoptotic protein tBid promotes leakage by altering membrane curvature.** *The Journal of biological chemistry* 2002, **277**(36):32632-32639.
379. Kuwana T, Mackey MR, Perkins G, Ellisman MH, Latterich M, Schneider R, Green DR, Newmeyer DD: **Bid, Bax, and lipids cooperate to form supramolecular openings in the outer mitochondrial membrane.** *Cell* 2002, **111**(3):331-342.

380. Petit PX, Dupaigne P, Pariselli F, Gonzalvez F, Etienne F, Rameau C, Bernard S: **Interaction of the alpha-helical H6 peptide from the pro-apoptotic protein tBid with cardiolipin.** *The FEBS journal* 2009, **276**(21):6338-6354.
381. Shimizu S, Narita M, Tsujimoto Y: **Bcl-2 family proteins regulate the release of apoptogenic cytochrome c by the mitochondrial channel VDAC.** *Nature* 1999, **399**(6735):483-487.
382. Malia TJ, Wagner G: **NMR structural investigation of the mitochondrial outer membrane protein VDAC and its interaction with antiapoptotic Bcl-xL.** *Biochemistry* 2007, **46**(2):514-525.
383. Xie G, Wilson JE: **Tetrameric structure of mitochondrially bound rat brain hexokinase: a crosslinking study.** *Archives of biochemistry and biophysics* 1990, **276**(1):285-293.
384. Wicker U, Bucheler K, Gellerich FN, Wagner M, Kapischke M, Brdiczka D: **Effect of macromolecules on the structure of the mitochondrial intermembrane space and the regulation of hexokinase.** *Biochimica et biophysica acta* 1993, **1142**(3):228-239.
385. Vyssokikh MY, Goncharova NY, Zhuravlyova AV, Zorova LD, Kirichenko VV, Krasnikov BF, Kuzminova AE, Melikov KC, Melik-Nubarov NS, Samsonov AV *et al*: **Proteinaceous complexes from mitochondrial contact sites.** *Biochemistry Biokhimiia* 1999, **64**(4):390-398.
386. Pastorino JG, Hoek JB, Shulga N: **Activation of glycogen synthase kinase 3beta disrupts the binding of hexokinase II to mitochondria by phosphorylating voltage-dependent anion channel and potentiates chemotherapy-induced cytotoxicity.** *Cancer research* 2005, **65**(22):10545-10554.
387. Cross DA, Alessi DR, Cohen P, Andjelkovich M, Hemmings BA: **Inhibition of glycogen synthase kinase-3 by insulin mediated by protein kinase B.** *Nature* 1995, **378**(6559):785-789.
388. Miyamoto S, Murphy AN, Brown JH: **Akt mediates mitochondrial protection in cardiomyocytes through phosphorylation of mitochondrial hexokinase-II.** *Cell death and differentiation* 2008, **15**(3):521-529.
389. Bustamante E, Pedersen PL: **High aerobic glycolysis of rat hepatoma cells in culture: role of mitochondrial hexokinase.** *Proceedings of the National Academy of Sciences of the United States of America* 1977, **74**(9):3735-3739.
390. Bustamante E, Morris HP, Pedersen PL: **Energy metabolism of tumor cells. Requirement for a form of hexokinase with a propensity for mitochondrial binding.** *The Journal of biological chemistry* 1981, **256**(16):8699-8704.
391. Shinohara Y, Ichihara J, Terada H: **Remarkably enhanced expression of the type II hexokinase in rat hepatoma cell line AH130.** *FEBS letters* 1991, **291**(1):55-57.
392. Shinohara Y, Yamamoto K, Kogure K, Ichihara J, Terada H: **Steady state transcript levels of the type II hexokinase and type 1 glucose transporter in human tumor cell lines.** *Cancer letters* 1994, **82**(1):27-32.

393. Rempel A, Bannasch P, Mayer D: **Differences in expression and intracellular distribution of hexokinase isoenzymes in rat liver cells of different transformation stages.** *Biochimica et biophysica acta* 1994, **1219**(3):660-668.
394. Rempel A, Mathupala SP, Griffin CA, Hawkins AL, Pedersen PL: **Glucose catabolism in cancer cells: amplification of the gene encoding type II hexokinase.** *Cancer research* 1996, **56**(11):2468-2471.
395. Smith TA: **Mammalian hexokinases and their abnormal expression in cancer.** *British journal of biomedical science* 2000, **57**(2):170-178.
396. Warburg O: **On the origin of cancer cells.** *Science* 1956, **123**(3191):309-314.
397. Vander Heiden MG, Cantley LC, Thompson CB: **Understanding the Warburg effect: the metabolic requirements of cell proliferation.** *Science* 2009, **324**(5930):1029-1033.
398. Braun RD, Lanzen JL, Snyder SA, Dewhirst MW: **Comparison of tumor and normal tissue oxygen tension measurements using OxyLite or microelectrodes in rodents.** *American journal of physiology Heart and circulatory physiology* 2001, **280**(6):H2533-2544.
399. Yasuda S, Aarii S, Mori A, Isobe N, Yang W, Oe H, Fujimoto A, Yonenaga Y, Sakashita H, Imamura M: **Hexokinase II and VEGF expression in liver tumors: correlation with hypoxia-inducible factor 1 alpha and its significance.** *Journal of hepatology* 2004, **40**(1):117-123.
400. Wyatt E, Wu R, Rabeh W, Park HW, Ghanefar M, Ardehali H: **Regulation and cytoprotective role of hexokinase III.** *PloS one* 2010, **5**(11):e13823.
401. Reivich M, Kuhl D, Wolf A, Greenberg J, Phelps M, Ido T, Casella V, Fowler J, Hoffman E, Alavi A *et al*: **The [¹⁸F]fluorodeoxyglucose method for the measurement of local cerebral glucose utilization in man.** *Circulation research* 1979, **44**(1):127-137.
402. Valencia-Sanchez MA, Liu J, Hannon GJ, Parker R: **Control of translation and mRNA degradation by miRNAs and siRNAs.** *Genes & development* 2006, **20**(5):515-524.
403. Carthew RW, Sontheimer EJ: **Origins and Mechanisms of miRNAs and siRNAs.** *Cell* 2009, **136**(4):642-655.
404. Friedman RC, Farh KK, Burge CB, Bartel DP: **Most mammalian mRNAs are conserved targets of microRNAs.** *Genome research* 2009, **19**(1):92-105.
405. Lee Y, Jeon K, Lee JT, Kim S, Kim VN: **MicroRNA maturation: stepwise processing and subcellular localization.** *The EMBO journal* 2002, **21**(17):4663-4670.
406. Kim VN: **MicroRNA biogenesis: coordinated cropping and dicing.** *Nature reviews Molecular cell biology* 2005, **6**(5):376-385.
407. Lee Y, Ahn C, Han J, Choi H, Kim J, Yim J, Lee J, Provost P, Radmark O, Kim S *et al*: **The nuclear RNase III Drosha initiates microRNA processing.** *Nature* 2003, **425**(6956):415-419.
408. Denli AM, Tops BB, Plasterk RH, Ketting RF, Hannon GJ: **Processing of primary microRNAs by the Microprocessor complex.** *Nature* 2004, **432**(7014):231-235.
409. Lund E, Guttinger S, Calado A, Dahlberg JE, Kutay U: **Nuclear export of microRNA precursors.** *Science* 2004, **303**(5654):95-98.

410. Yi R, Qin Y, Macara IG, Cullen BR: **Exportin-5 mediates the nuclear export of pre-microRNAs and short hairpin RNAs.** *Genes & development* 2003, **17**(24):3011-3016.
411. Hutvagner G, McLachlan J, Pasquinelli AE, Balint E, Tuschl T, Zamore PD: **A cellular function for the RNA-interference enzyme Dicer in the maturation of the let-7 small temporal RNA.** *Science* 2001, **293**(5531):834-838.
412. Bernstein E, Caudy AA, Hammond SM, Hannon GJ: **Role for a bidentate ribonuclease in the initiation step of RNA interference.** *Nature* 2001, **409**(6818):363-366.
413. Meister G, Tuschl T: **Mechanisms of gene silencing by double-stranded RNA.** *Nature* 2004, **431**(7006):343-349.
414. Tomari Y, Zamore PD: **Perspective: machines for RNAi.** *Genes & development* 2005, **19**(5):517-529.
415. Gregory RI, Chendrimada TP, Cooch N, Shiekhattar R: **Human RISC couples microRNA biogenesis and posttranscriptional gene silencing.** *Cell* 2005, **123**(4):631-640.
416. Carmell MA, Xuan Z, Zhang MQ, Hannon GJ: **The Argonaute family: tentacles that reach into RNAi, developmental control, stem cell maintenance, and tumorigenesis.** *Genes & development* 2002, **16**(21):2733-2742.
417. Song JJ, Liu J, Tolia NH, Schneiderman J, Smith SK, Martienssen RA, Hannon GJ, Joshua-Tor L: **The crystal structure of the Argonaute2 PAZ domain reveals an RNA binding motif in RNAi effector complexes.** *Nature structural biology* 2003, **10**(12):1026-1032.
418. Song JJ, Smith SK, Hannon GJ, Joshua-Tor L: **Crystal structure of Argonaute and its implications for RISC slicer activity.** *Science* 2004, **305**(5689):1434-1437.
419. Khvorova A, Reynolds A, Jayasena SD: **Functional siRNAs and miRNAs exhibit strand bias.** *Cell* 2003, **115**(2):209-216.
420. Schwarz DS, Hutvagner G, Du T, Xu Z, Aronin N, Zamore PD: **Asymmetry in the assembly of the RNAi enzyme complex.** *Cell* 2003, **115**(2):199-208.
421. Matranga C, Tomari Y, Shin C, Bartel DP, Zamore PD: **Passenger-strand cleavage facilitates assembly of siRNA into Ago2-containing RNAi enzyme complexes.** *Cell* 2005, **123**(4):607-620.
422. Bartel DP: **MicroRNAs: target recognition and regulatory functions.** *Cell* 2009, **136**(2):215-233.
423. Lewis BP, Burge CB, Bartel DP: **Conserved seed pairing, often flanked by adenosines, indicates that thousands of human genes are microRNA targets.** *Cell* 2005, **120**(1):15-20.
424. Lewis BP, Shih IH, Jones-Rhoades MW, Bartel DP, Burge CB: **Prediction of mammalian microRNA targets.** *Cell* 2003, **115**(7):787-798.
425. Krek A, Grun D, Poy MN, Wolf R, Rosenberg L, Epstein EJ, MacMenamin P, da Piedade I, Gunsalus KC, Stoffel M *et al*: **Combinatorial microRNA target predictions.** *Nature genetics* 2005, **37**(5):495-500.
426. Brennecke J, Stark A, Russell RB, Cohen SM: **Principles of microRNA-target recognition.** *PLoS biology* 2005, **3**(3):e85.
427. Doench JG, Sharp PA: **Specificity of microRNA target selection in translational repression.** *Genes & development* 2004, **18**(5):504-511.

428. Lai EC: **Micro RNAs are complementary to 3' UTR sequence motifs that mediate negative post-transcriptional regulation.** *Nature genetics* 2002, **30**(4):363-364.
429. Liu J, Carmell MA, Rivas FV, Marsden CG, Thomson JM, Song JJ, Hammond SM, Joshua-Tor L, Hannon GJ: **Argonaute2 is the catalytic engine of mammalian RNAi.** *Science* 2004, **305**(5689):1437-1441.
430. Hammond SM, Boettcher S, Caudy AA, Kobayashi R, Hannon GJ: **Argonaute2, a link between genetic and biochemical analyses of RNAi.** *Science* 2001, **293**(5532):1146-1150.
431. Meister G, Landthaler M, Patkaniowska A, Dorsett Y, Teng G, Tuschl T: **Human Argonaute2 mediates RNA cleavage targeted by miRNAs and siRNAs.** *Molecular cell* 2004, **15**(2):185-197.
432. Saxena S, Jonsson ZO, Dutta A: **Small RNAs with imperfect match to endogenous mRNA repress translation. Implications for off-target activity of small inhibitory RNA in mammalian cells.** *The Journal of biological chemistry* 2003, **278**(45):44312-44319.
433. Falschlehner C, Steinbrink S, Erdmann G, Boutros M: **High-throughput RNAi screening to dissect cellular pathways: a how-to guide.** *Biotechnology journal* 2010, **5**(4):368-376.
434. Caplen NJ, Fleenor J, Fire A, Morgan RA: **dsRNA-mediated gene silencing in cultured Drosophila cells: a tissue culture model for the analysis of RNA interference.** *Gene* 2000, **252**(1-2):95-105.
435. Clemens JC, Worby CA, Simonson-Leff N, Muda M, Maehama T, Hemmings BA, Dixon JE: **Use of double-stranded RNA interference in Drosophila cell lines to dissect signal transduction pathways.** *Proceedings of the National Academy of Sciences of the United States of America* 2000, **97**(12):6499-6503.
436. Gil J, Esteban M: **Induction of apoptosis by the dsRNA-dependent protein kinase (PKR): mechanism of action.** *Apoptosis : an international journal on programmed cell death* 2000, **5**(2):107-114.
437. Elbashir SM, Harborth J, Lendeckel W, Yalcin A, Weber K, Tuschl T: **Duplexes of 21-nucleotide RNAs mediate RNA interference in cultured mammalian cells.** *Nature* 2001, **411**(6836):494-498.
438. Paddison PJ, Caudy AA, Bernstein E, Hannon GJ, Conklin DS: **Short hairpin RNAs (shRNAs) induce sequence-specific silencing in mammalian cells.** *Genes & development* 2002, **16**(8):948-958.
439. Rubinson DA, Dillon CP, Kwiatkowski AV, Sievers C, Yang L, Kopinja J, Rooney DL, Zhang M, Ibragimov MM, McManus MT *et al*: **A lentivirus-based system to functionally silence genes in primary mammalian cells, stem cells and transgenic mice by RNA interference.** *Nature genetics* 2003, **33**(3):401-406.
440. McManus MT, Sharp PA: **Gene silencing in mammals by small interfering RNAs.** *Nature reviews Genetics* 2002, **3**(10):737-747.
441. Kittler R, Putz G, Pelletier L, Poser I, Heninger AK, Drechsel D, Fischer S, Konstantinova I, Habermann B, Grabner H *et al*: **An endoribonuclease-prepared siRNA screen in human cells identifies genes essential for cell division.** *Nature* 2004, **432**(7020):1036-1040.
442. Paddison PJ, Silva JM, Conklin DS, Schlabach M, Li M, Aruleba S, Balija V, O'Shaughnessy A, Gnoj L, Scobie K *et al*: **A resource for large-scale RNA-interference-based screens in mammals.** *Nature* 2004, **428**(6981):427-431.

443. Reynolds A, Leake D, Boese Q, Scaringe S, Marshall WS, Khvorova A: **Rational siRNA design for RNA interference.** *Nature biotechnology* 2004, **22**(3):326-330.
444. Silva JM, Li MZ, Chang K, Ge W, Golding MC, Rickles RJ, Siolas D, Hu G, Paddison PJ, Schlabach MR *et al.*: **Second-generation shRNA libraries covering the mouse and human genomes.** *Nature genetics* 2005, **37**(11):1281-1288.
445. Huesken D, Lange J, Mickanin C, Weiler J, Asselbergs F, Warner J, Melloon B, Engel S, Rosenberg A, Cohen D *et al.*: **Design of a genome-wide siRNA library using an artificial neural network.** *Nature biotechnology* 2005, **23**(8):995-1001.
446. Giuliano KA, Haskins JR, Taylor DL: **Advances in high content screening for drug discovery.** *Assay and drug development technologies* 2003, **1**(4):565-577.
447. **The RNAi Consortium - Broad Institute of MIT and Harvard** [<http://www.broadinstitute.org/rnai/trc>]
448. **RNAi libraries - System Biosciences** [<http://www.systembio.com/rnai-libraries>]
449. Boutros M, Kiger AA, Armknecht S, Kerr K, Hild M, Koch B, Haas SA, Paro R, Perrimon N, Heidelberg Fly Array C: **Genome-wide RNAi analysis of growth and viability in Drosophila cells.** *Science* 2004, **303**(5659):832-835.
450. Foley E, O'Farrell PH: **Functional dissection of an innate immune response by a genome-wide RNAi screen.** *PLoS biology* 2004, **2**(8):E203.
451. Kamath RS, Ahringer J: **Genome-wide RNAi screening in Caenorhabditis elegans.** *Methods* 2003, **30**(4):313-321.
452. Kamath RS, Fraser AG, Dong Y, Poulin G, Durbin R, Gotta M, Kanapin A, Le Bot N, Moreno S, Sohrmann M *et al.*: **Systematic functional analysis of the Caenorhabditis elegans genome using RNAi.** *Nature* 2003, **421**(6920):231-237.
453. Sonnichsen B, Koski LB, Walsh A, Marschall P, Neumann B, Brehm M, Alleaume AM, Artelt J, Bettencourt P, Cassin E *et al.*: **Full-genome RNAi profiling of early embryogenesis in Caenorhabditis elegans.** *Nature* 2005, **434**(7032):462-469.
454. **Heatmap Tables with Excel - Revisited.** In., vol. 2013: Blog of XLCubed Ltd. ; 2011.
455. **Kernel Bandwidth Optimization** [<http://176.32.89.45/~hideaki/res/kernel.html>]
456. Shimazaki H, Shinomoto S: **Kernel bandwidth optimization in spike rate estimation.** *Journal of computational neuroscience* 2010, **29**(1-2):171-182.
457. Grivennikov SI, Greten FR, Karin M: **Immunity, inflammation, and cancer.** *Cell* 2010, **140**(6):883-899.
458. Balkwill F: **Tumour necrosis factor and cancer.** *Nature reviews Cancer* 2009, **9**(5):361-371.
459. Jones HW, Jr., McKusick VA, Harper PS, Wu KD: **George Otto Gey. (1899-1970). The HeLa cell and a reappraisal of its origin.** *Obstetrics and gynecology* 1971, **38**(6):945-949.

460. Gey GO, Coffman WD, Kubicek MT: **Tissue culture studies of the proliferative capacity of cervical carcinoma and normal epithelium.** *Cancer research* 1952(12):264-265.
461. Brockhaus M, Schoenfeld HJ, Schlaeger EJ, Hunziker W, Lesslauer W, Loetscher H: **Identification of two types of tumor necrosis factor receptors on human cell lines by monoclonal antibodies.** *Proceedings of the National Academy of Sciences of the United States of America* 1990, **87**(8):3127-3131.
462. Dutta J, Fan Y, Gupta N, Fan G, Gelinas C: **Current insights into the regulation of programmed cell death by NF-kappaB.** *Oncogene* 2006, **25**(51):6800-6816.
463. Wajant H, Scheurich P: **TNFR1-induced activation of the classical NF-kappaB pathway.** *The FEBS journal* 2011, **278**(6):862-876.
464. Baeuerle PA, Baltimore D: **I kappa B: a specific inhibitor of the NF-kappa B transcription factor.** *Science* 1988, **242**(4878):540-546.
465. Karin M, Ben-Neriah Y: **Phosphorylation meets ubiquitination: the control of NF-[kappa]B activity.** *Annual review of immunology* 2000, **18**:621-663.
466. Brown K, Gerstberger S, Carlson L, Franzoso G, Siebenlist U: **Control of I kappa B-alpha proteolysis by site-specific, signal-induced phosphorylation.** *Science* 1995, **267**(5203):1485-1488.
467. Brockman JA, Scherer DC, McKinsey TA, Hall SM, Qi X, Lee WY, Ballard DW: **Coupling of a signal response domain in I kappa B alpha to multiple pathways for NF-kappa B activation.** *Molecular and cellular biology* 1995, **15**(5):2809-2818.
468. Traenckner EB, Pahl HL, Henkel T, Schmidt KN, Wilk S, Baeuerle PA: **Phosphorylation of human I kappa B-alpha on serines 32 and 36 controls I kappa B-alpha proteolysis and NF-kappa B activation in response to diverse stimuli.** *The EMBO journal* 1995, **14**(12):2876-2883.
469. Finco TS, Beg AA, Baldwin AS, Jr.: **Inducible phosphorylation of I kappa B alpha is not sufficient for its dissociation from NF-kappa B and is inhibited by protease inhibitors.** *Proceedings of the National Academy of Sciences of the United States of America* 1994, **91**(25):11884-11888.
470. Zhang P, Miller BS, Rosenzweig SA, Bhat NR: **Activation of C-jun N-terminal kinase/stress-activated protein kinase in primary glial cultures.** *Journal of neuroscience research* 1996, **46**(1):114-121.
471. Davis RJ: **Signal transduction by the JNK group of MAP kinases.** *Cell* 2000, **103**(2):239-252.
472. Wu JJ, Roth RJ, Anderson EJ, Hong EG, Lee MK, Choi CS, Neuffer PD, Shulman GI, Kim JK, Bennett AM: **Mice lacking MAP kinase phosphatase-1 have enhanced MAP kinase activity and resistance to diet-induced obesity.** *Cell metabolism* 2006, **4**(1):61-73.
473. Chi H, Barry SP, Roth RJ, Wu JJ, Jones EA, Bennett AM, Flavell RA: **Dynamic regulation of pro- and anti-inflammatory cytokines by MAPK phosphatase 1 (MKP-1) in innate immune responses.** *Proceedings of the National Academy of Sciences of the United States of America* 2006, **103**(7):2274-2279.

474. Zhao Q, Wang X, Nelin LD, Yao Y, Matta R, Manson ME, Baliga RS, Meng X, Smith CV, Bauer JA *et al*: **MAP kinase phosphatase 1 controls innate immune responses and suppresses endotoxic shock.** *The Journal of experimental medicine* 2006, **203**(1):131-140.
475. Zhang Y, Blattman JN, Kennedy NJ, Duong J, Nguyen T, Wang Y, Davis RJ, Greenberg PD, Flavell RA, Dong C: **Regulation of innate and adaptive immune responses by MAP kinase phosphatase 5.** *Nature* 2004, **430**(7001):793-797.
476. Brown K, Park S, Kanno T, Franzoso G, Siebenlist U: **Mutual regulation of the transcriptional activator NF-kappa B and its inhibitor, I kappa B-alpha.** *Proceedings of the National Academy of Sciences of the United States of America* 1993, **90**(6):2532-2536.
477. Krikos A, Laherty CD, Dixit VM: **Transcriptional activation of the tumor necrosis factor alpha-inducible zinc finger protein, A20, is mediated by kappa B elements.** *The Journal of biological chemistry* 1992, **267**(25):17971-17976.
478. Tian B, Nowak DE, Brasier AR: **A TNF-induced gene expression program under oscillatory NF-kappaB control.** *BMC genomics* 2005, **6**:137.
479. Nelson DE, Ihekwaba AE, Elliott M, Johnson JR, Gibney CA, Foreman BE, Nelson G, See V, Horton CA, Spiller DG *et al*: **Oscillations in NF-kappaB signaling control the dynamics of gene expression.** *Science* 2004, **306**(5696):704-708.
480. Beg AA, Baltimore D: **An essential role for NF-kappaB in preventing TNF-alpha-induced cell death.** *Science* 1996, **274**(5288):782-784.
481. Scaduto RC, Jr., Grotyohann LW: **Measurement of mitochondrial membrane potential using fluorescent rhodamine derivatives.** *Biophysical journal* 1999, **76**(1 Pt 1):469-477.
482. Rudolph D, Yeh WC, Wakeham A, Rudolph B, Nallainathan D, Potter J, Elia AJ, Mak TW: **Severe liver degeneration and lack of NF-kappaB activation in NEMO/IKKgamma-deficient mice.** *Genes & development* 2000, **14**(7):854-862.
483. Thornberry NA, Rano TA, Peterson EP, Rasper DM, Timkey T, Garcia-Calvo M, Houtzager VM, Nordstrom PA, Roy S, Vaillancourt JP *et al*: **A combinatorial approach defines specificities of members of the caspase family and granzyme B. Functional relationships established for key mediators of apoptosis.** *The Journal of biological chemistry* 1997, **272**(29):17907-17911.
484. Talanian RV, Quinlan C, Trautz S, Hackett MC, Mankovich JA, Banach D, Ghayur T, Brady KD, Wong WW: **Substrate specificities of caspase family proteases.** *The Journal of biological chemistry* 1997, **272**(15):9677-9682.
485. McStay GP, Salvesen GS, Green DR: **Overlapping cleavage motif selectivity of caspases: implications for analysis of apoptotic pathways.** *Cell death and differentiation* 2008, **15**(2):322-331.
486. Senftleben U, Cao Y, Xiao G, Greten FR, Krahn G, Bonizzi G, Chen Y, Hu Y, Fong A, Sun SC *et al*: **Activation by IKKalpha of a second, evolutionary conserved, NF-kappa B signaling pathway.** *Science* 2001, **293**(5534):1495-1499.
487. Czekanska EM: **Assessment of cell proliferation with resazurin-based fluorescent dye.** *Methods in molecular biology* 2011, **740**:27-32.

488. Choi I, Cho BR, Kim D, Miyagawa S, Kubo T, Kim JY, Park CG, Hwang WS, Lee JS, Ahn C: **Choice of the adequate detection time for the accurate evaluation of the efficiency of siRNA-induced gene silencing.** *Journal of biotechnology* 2005, **120**(3):251-261.
489. O'Brien J, Wilson I, Orton T, Pognan F: **Investigation of the Alamar Blue (resazurin) fluorescent dye for the assessment of mammalian cell cytotoxicity.** *European journal of biochemistry / FEBS* 2000, **267**(17):5421-5426.
490. Echeverri CJ, Beachy PA, Baum B, Boutros M, Buchholz F, Chanda SK, Downward J, Ellenberg J, Fraser AG, Hacohen N *et al.*: **Minimizing the risk of reporting false positives in large-scale RNAi screens.** *Nature methods* 2006, **3**(10):777-779.
491. Boutros M, Bras LP, Huber W: **Analysis of cell-based RNAi screens.** *Genome biology* 2006, **7**(7):R66.
492. Birmingham A, Selfors LM, Forster T, Wrobel D, Kennedy CJ, Shanks E, Santoyo-Lopez J, Dunican DJ, Long A, Kelleher D *et al.*: **Statistical methods for analysis of high-throughput RNA interference screens.** *Nature methods* 2009, **6**(8):569-575.
493. Brideau C, Gunter B, Pikounis B, Liaw A: **Improved statistical methods for hit selection in high-throughput screening.** *Journal of biomolecular screening* 2003, **8**(6):634-647.
494. Liu J, Minemoto Y, Lin A: **c-Jun N-terminal protein kinase 1 (JNK1), but not JNK2, is essential for tumor necrosis factor alpha-induced c-Jun kinase activation and apoptosis.** *Molecular and cellular biology* 2004, **24**(24):10844-10856.
495. Ventura JJ, Cogswell P, Flavell RA, Baldwin AS, Jr., Davis RJ: **JNK potentiates TNF-stimulated necrosis by increasing the production of cytotoxic reactive oxygen species.** *Genes & development* 2004, **18**(23):2905-2915.
496. Chen WS, Xu PZ, Gottlob K, Chen ML, Sokol K, Shiyanova T, Roninson I, Weng W, Suzuki R, Tobe K *et al.*: **Growth retardation and increased apoptosis in mice with homozygous disruption of the Akt1 gene.** *Genes & development* 2001, **15**(17):2203-2208.
497. Kaufmann SH, Desnoyers S, Ottaviano Y, Davidson NE, Poirier GG: **Specific proteolytic cleavage of poly(ADP-ribose) polymerase: an early marker of chemotherapy-induced apoptosis.** *Cancer research* 1993, **53**(17):3976-3985.
498. Lazebnik YA, Kaufmann SH, Desnoyers S, Poirier GG, Earnshaw WC: **Cleavage of poly(ADP-ribose) polymerase by a proteinase with properties like ICE.** *Nature* 1994, **371**(6495):346-347.
499. Nicholson DW, Ali A, Thornberry NA, Vaillancourt JP, Ding CK, Gallant M, Gareau Y, Griffin PR, Labelle M, Lazebnik YA *et al.*: **Identification and inhibition of the ICE/CED-3 protease necessary for mammalian apoptosis.** *Nature* 1995, **376**(6535):37-43.
500. de Murcia JM, Niedergang C, Trucco C, Ricoul M, Dutrillaux B, Mark M, Oliver FJ, Masson M, Dierich A, LeMeur M *et al.*: **Requirement of poly(ADP-ribose) polymerase in recovery from DNA damage in mice and in cells.** *Proceedings of the National Academy of Sciences of the United States of America* 1997, **94**(14):7303-7307.

501. Arora KK, Filburn CR, Pedersen PL: **Glucose phosphorylation. Site-directed mutations which impair the catalytic function of hexokinase.** *The Journal of biological chemistry* 1991, **266**(9):5359-5362.
502. Ponten J, Saksela E: **Two established in vitro cell lines from human mesenchymal tumours.** *International journal of cancer Journal internationale du cancer* 1967, **2**(5):434-447.
503. Lieber M, Smith B, Szakal A, Nelson-Rees W, Todaro G: **A continuous tumor-cell line from a human lung carcinoma with properties of type II alveolar epithelial cells.** *International journal of cancer Journal internationale du cancer* 1976, **17**(1):62-70.
504. Dhein J, Daniel PT, Trauth BC, Oehm A, Moller P, Krammer PH: **Induction of apoptosis by monoclonal antibody anti-APO-1 class switch variants is dependent on cross-linking of APO-1 cell surface antigens.** *Journal of immunology* 1992, **149**(10):3166-3173.
505. Wu M, Das A, Tan Y, Zhu C, Cui T, Wong MC: **Induction of apoptosis in glioma cell lines by TRAIL/Apo-2l.** *Journal of neuroscience research* 2000, **61**(4):464-470.
506. Wajant H: **Death receptors.** *Essays in biochemistry* 2003, **39**:53-71.
507. Thorburn A: **Death receptor-induced cell killing.** *Cellular signalling* 2004, **16**(2):139-144.
508. Wilson JE: **"Ambiguous" behavior of brain hexokinase: rapid and reversible interaction of hexokinase with the outer mitochondrial membrane.** *Biophysical journal* 1982, **37**(1):18-19.
509. Weber K, Pollack R, Bibring T: **Antibody against tubulin: the specific visualization of cytoplasmic microtubules in tissue culture cells.** *Proceedings of the National Academy of Sciences of the United States of America* 1975, **72**(2):459-463.
510. Penso J, Beitner R: **Clotrimazole and bifonazole detach hexokinase from mitochondria of melanoma cells.** *European journal of pharmacology* 1998, **342**(1):113-117.
511. Ow YP, Green DR, Hao Z, Mak TW: **Cytochrome c: functions beyond respiration.** *Nature reviews Molecular cell biology* 2008, **9**(7):532-542.
512. Knudson CM, Tung KS, Tourtellotte WG, Brown GA, Korsmeyer SJ: **Bax-deficient mice with lymphoid hyperplasia and male germ cell death.** *Science* 1995, **270**(5233):96-99.
513. Lindsten T, Ross AJ, King A, Zong WX, Rathmell JC, Shiels HA, Ulrich E, Waymire KG, Mahar P, Frauwirth K *et al*: **The combined functions of proapoptotic Bcl-2 family members bak and bax are essential for normal development of multiple tissues.** *Molecular cell* 2000, **6**(6):1389-1399.
514. Fire A, Xu S, Montgomery MK, Kostas SA, Driver SE, Mello CC: **Potent and specific genetic interference by double-stranded RNA in *Caenorhabditis elegans*.** *Nature* 1998, **391**(6669):806-811.
515. Berns K, Hijmans EM, Mullenders J, Brummelkamp TR, Velds A, Heimerikx M, Kerkhoven RM, Madiredjo M, Nijkamp W, Weigelt B *et al*: **A large-scale RNAi screen in human cells identifies new components of the p53 pathway.** *Nature* 2004, **428**(6981):431-437.

516. Hsieh AC, Bo R, Manola J, Vazquez F, Bare O, Khvorova A, Scaringe S, Sellers WR: **A library of siRNA duplexes targeting the phosphoinositide 3-kinase pathway: determinants of gene silencing for use in cell-based screens.** *Nucleic acids research* 2004, **32**(3):893-901.
517. Aza-Blanc P, Cooper CL, Wagner K, Batalov S, Deveraux QL, Cooke MP: **Identification of modulators of TRAIL-induced apoptosis via RNAi-based phenotypic screening.** *Molecular cell* 2003, **12**(3):627-637.
518. Zheng L, Liu J, Batalov S, Zhou D, Orth A, Ding S, Schultz PG: **An approach to genomewide screens of expressed small interfering RNAs in mammalian cells.** *Proceedings of the National Academy of Sciences of the United States of America* 2004, **101**(1):135-140.
519. Stone DJ, Marine S, Majercak J, Ray WJ, Espeseth A, Simon A, Ferrer M: **High-throughput screening by RNA interference: control of two distinct types of variance.** *Cell cycle* 2007, **6**(8):898-901.
520. Malo N, Hanley JA, Cerquozzi S, Pelletier J, Nadon R: **Statistical practice in high-throughput screening data analysis.** *Nature biotechnology* 2006, **24**(2):167-175.
521. **Qiagen - Sample & Assay Technologies - AllStars Negative Control siRNAs**
[<https://b2b.qiagen.com/products/genesilencing/allstarrnacontrols/allstarsnegativecontrols.aspx>]
522. Lundholt BK, Scudder KM, Pagliaro L: **A simple technique for reducing edge effect in cell-based assays.** *Journal of biomolecular screening* 2003, **8**(5):566-570.
523. Parsons BD, Schindler A, Evans DH, Foley E: **A direct phenotypic comparison of siRNA pools and multiple individual duplexes in a functional assay.** *PloS one* 2009, **4**(12):e8471.
524. Sigoillot FD, King RW: **Vigilance and validation: Keys to success in RNAi screening.** *ACS chemical biology* 2011, **6**(1):47-60.
525. Martin SE, Caplen NJ: **Applications of RNA interference in mammalian systems.** *Annual review of genomics and human genetics* 2007, **8**:81-108.
526. Birmingham A, Anderson EM, Reynolds A, Ilesley-Tyree D, Leake D, Fedorov Y, Baskerville S, Maksimova E, Robinson K, Karpilow J *et al*: **3' UTR seed matches, but not overall identity, are associated with RNAi off-targets.** *Nature methods* 2006, **3**(3):199-204.
527. Shin C, Nam JW, Farh KK, Chiang HR, Shkumatava A, Bartel DP: **Expanding the microRNA targeting code: functional sites with centered pairing.** *Molecular cell* 2010, **38**(6):789-802.
528. Chen PY, Weinmann L, Gaidatzis D, Pei Y, Zavolan M, Tuschl T, Meister G: **Strand-specific 5'-O-methylation of siRNA duplexes controls guide strand selection and targeting specificity.** *Rna* 2008, **14**(2):263-274.
529. **Life Technologies - Silencer Select chemical modifications enhance guide strand bias.** [<http://www.invitrogen.com/site/us/en/home/Products-and-Services/Applications/rnai/Synthetic-RNAi-Analysis/Ambion-Silencer-Select-siRNAs/Enhanced-Guide-Strand-Bias.html>]

530. Grueneberg DA, Degot S, Pearlberg J, Li W, Davies JE, Baldwin A, Endege W, Doench J, Sawyer J, Hu Y *et al*: **Kinase requirements in human cells: I. Comparing kinase requirements across various cell types.** *Proceedings of the National Academy of Sciences of the United States of America* 2008, **105**(43):16472-16477.
531. Moore DS, McCabe GP, Craig BA: **Introduction to the Practice of Statistics.**, 7 edn: Freeman, W.H.; 2010.
532. Xing Y, Resch A, Lee C: **The multiassembly problem: reconstructing multiple transcript isoforms from EST fragment mixtures.** *Genome research* 2004, **14**(3):426-441.
533. Mereniuk TR, Maranchuk RA, Schindler A, Penner-Chea J, Freschauf GK, Hegazy S, Lai R, Foley E, Weinfeld M: **Genetic screening for synthetic lethal partners of polynucleotide kinase/phosphatase: potential for targeting SHP-1-depleted cancers.** *Cancer research* 2012, **72**(22):5934-5944.
534. Agapito G, Guzzi PH, Cannataro M: **Visualization of protein interaction networks: problems and solutions.** *BMC bioinformatics* 2013, **14** Suppl 1:S1.
535. Cannataro M, Guzzi PH, Veltri P: **Protein-to-protein interactions: Technologies, databases, and algorithms.** *ACM Computing Surveys* 2010, **43**(1):1:1-1:36.
536. Khatri P, Sirota M, Butte AJ: **Ten years of pathway analysis: current approaches and outstanding challenges.** *PLoS computational biology* 2012, **8**(2):e1002375.
537. Finn RD, Mistry J, Tate J, Coghill P, Heger A, Pollington JE, Gavin OL, Gunasekaran P, Ceric G, Forslund K *et al*: **The Pfam protein families database.** *Nucleic acids research* 2010, **38**(Database issue):D211-222.
538. Marchler-Bauer A, Lu S, Anderson JB, Chitsaz F, Derbyshire MK, DeWeese-Scott C, Fong JH, Geer LY, Geer RC, Gonzales NR *et al*: **CDD: a Conserved Domain Database for the functional annotation of proteins.** *Nucleic acids research* 2011, **39**(Database issue):D225-229.
539. Ting AT, Pimentel-Muinos FX, Seed B: **RIP mediates tumor necrosis factor receptor 1 activation of NF-kappaB but not Fas/APO-1-initiated apoptosis.** *The EMBO journal* 1996, **15**(22):6189-6196.
540. Li H, Kobayashi M, Blonska M, You Y, Lin X: **Ubiquitination of RIP is required for tumor necrosis factor alpha-induced NF-kappaB activation.** *The Journal of biological chemistry* 2006, **281**(19):13636-13643.
541. Lee TH, Shank J, Cusson N, Kelliher MA: **The kinase activity of Rip1 is not required for tumor necrosis factor-alpha-induced I kappa B kinase or p38 MAP kinase activation or for the ubiquitination of Rip1 by Traf2.** *The Journal of biological chemistry* 2004, **279**(32):33185-33191.
542. Kim JW, Choi EJ, Joe CO: **Activation of death-inducing signaling complex (DISC) by pro-apoptotic C-terminal fragment of RIP.** *Oncogene* 2000, **19**(39):4491-4499.
543. Vandenabeele P, Declercq W, Van Herreweghe F, Vanden Berghe T: **The role of the kinases RIP1 and RIP3 in TNF-induced necrosis.** *Science signaling* 2010, **3**(115):re4.
544. Vandenabeele P, Galluzzi L, Vanden Berghe T, Kroemer G: **Molecular mechanisms of necroptosis: an ordered cellular explosion.** *Nature reviews Molecular cell biology* 2010, **11**(10):700-714.

545. Zhang DW, Shao J, Lin J, Zhang N, Lu BJ, Lin SC, Dong MQ, Han J: **RIP3, an energy metabolism regulator that switches TNF-induced cell death from apoptosis to necrosis.** *Science* 2009, **325**(5938):332-336.
546. Bienvenut WV, Waridel P, Quadroni M: **protein sequence of human HK1.** In., March 2009 edn; 2009.
547. Baijal M, Wilson JE: **Functional consequences of mutation of highly conserved serine residues, found at equivalent positions in the N- and C-terminal domains of mammalian hexokinases.** *Archives of biochemistry and biophysics* 1992, **298**(1):271-278.
548. Sun MG, Williams J, Munoz-Pinedo C, Perkins GA, Brown JM, Ellisman MH, Green DR, Frey TG: **Correlated three-dimensional light and electron microscopy reveals transformation of mitochondria during apoptosis.** *Nature cell biology* 2007, **9**(9):1057-1065.
549. Garrido C, Galluzzi L, Brunet M, Puig PE, Didelot C, Kroemer G: **Mechanisms of cytochrome c release from mitochondria.** *Cell death and differentiation* 2006, **13**(9):1423-1433.
550. Li K, Li Y, Shelton JM, Richardson JA, Spencer E, Chen ZJ, Wang X, Williams RS: **Cytochrome c deficiency causes embryonic lethality and attenuates stress-induced apoptosis.** *Cell* 2000, **101**(4):389-399.

APPENDIX 1. SEQUENCE ALIGNMENT OF HUMAN HKs.

(sp|P52789|HXK2_HUMAN), HK3 (sp|P52790|HXK4_HUMAN), and HK4 (sp|P35557|HXK4_HUMAN). Hydrophobic amino acids are shown in red, polar amino acids in green, charged acidic amino acids in blue, charged basic amino acids in pink. Identical amino acids are indicated by an asterisk (*), amino acid conservations between a group with strongly similar properties are indicated by a colon (:), amino acid conservations between a group with weakly similar properties are indicated by a colon (.).

**APPENDIX 2: DNA SEQUENCE OF THE HK1 EXPRESSION
CONSTRUCT.**

1 TAGTTATTAATAGTAATCAATTACGGGGTCATTAGTTCATAGCCCATATATGGAGTTCGCGGTACATAA
71 CTTACGGTAAATGGCCCGCTGGCTGACCGCCCAACGACCCCGCCCATTTGACGTCAATAATGACGTATG
141 TTCCCATAGTAACGCCAATAGGGACTTCCATTGACGTCAATGGGTGGAGTATTTACGGTAAATGCCCA
211 CTTGGCAGTACATCAAGTGTATCATATGCCAAGTACGCCCCCTATTGACGTCAATGACGGTAAATGGCCC
281 GCCTGGCATTATGCCAGTACATGACCTTATGGGACTTCTACTTGGCAGTACATCTACGTATTAGTCA
351 TCGCTATTACCATGGTGTATGCGGTTTTGGCAGTACATCAATGGGCGTGGATAGCGGTTTACTCACGGGG
421 ATTTCCAAGTCCACCCCATGACGTCAATGGGAGTTGTTTTGGCACCAAATCAACGGGACTTTCCA
491 AAATGTCGTAACAACCTCCGCCCATGACGCAAAATGGGCGGTAGGCGTGTACGGTGGGAGGTCTATATAA
561 GCAGAGCTGGTTTAGTGAACCGTCAGATCCGCTAGCGCTACCGACTCAGATCTCGAGCTCatgatcgcc
631 ggcgagctcctggcctattacttcacggagctgaaggatgaccaggtcaaaaagattgacaagtatctct
701 atgccatcgggctctccgatgaaactctcatagatatcatgactcgcttcaggaaggagatgagaatgg
771 cctctccgggattttaaaccacagccacagtcgaagatgttgccaacattcgtaaggtccattccctgat
841 ggctctgaaaaggagatttcatgtccctggatcttgggtgggtctctcttccgaattctcggggtgcaag
911 tgaatcatgagaaaaaccagaatgttcacatggagtcagggtttatgacacccagagaaacatcgtgca
981 cggcagtggaagccagcttttggatcatggtgctgagtgctgggagatttcatggagaaaaggaaagatc
1051 aaggacaagaagttaactgtgggattcctgttcttcttcttcccttgccaacaatccaaaatagatgagggca
1121 tctgatcacctggacaaagcatttaaagcagcggagtggaaggagcagatgtggtcaaacctgcttaa
1191 caaagccatcaaaaagcaggggactatgatgccaacatcgtagctgtggtgaaatgacacagtgggcacc
1261 atgatgaactgtggctatgacgaccagcactgtgaagtcggcctgatcatcggcactggcacaatgctt
1331 gctacatcgggaaactgagccacattgctggggaaggagacgaggggaggtatgatatcaatacaga
1401 atggggagccttggagacgatggatcattagaagacatccggacagagtttgacagggagatagaccgg
1471 ggatccctcaaccctggaaaaacagctgttggagaagatggtcagtggtgacttctgggagagctgggtc
1541 gactgatcctagtcaagatggccaaggagggcctcttatttgaagggggatcaccctggagctgctcac
1611 ccggagcaagttaaaccagctgatgtgctcagccatcgaaaagaaaggaaggcctccacaacgcaaaa
1681 gaaatcctgacccgctgggagtgagcgcctcggatgatgactgtgtctcagtcacgacgcttggacca
1751 ttgtctcatttcgctcagccaacttgggtggctgccacactggcgccatcttgaaccgctcgggtataa
1821 caagggcacaccagctgcccagcaggttgggtgctcagcggatctcttacaagacgacccacagat
1891 tcccggcttccacaagactctaagggccttgggtgcccagactccgatgtgctcctcctcctcctcggaga
1961 gtggcagcggcaaggggctgccatggtagcggcgtggcctaccgcttggcggagcagcaccggcagat
2031 agaggagaccctggctcatttccacctcaccacaggacatgctgctggaggtgagaagaggatgcgggcc
2101 gagatggagctgggctgaggaagcagacgcacaacaatgcccgtggttaagatgctgcctcctcctgctc
2171 ggagaactcccagcgggaccgagaatgggtgacttcttggcctcggatcttgaggaaaccaatctccggt
2241 gctgctgggtaaaaatccgtagtgggaaaaagagaaacgggtggaatgcacaacaagatctacgccattcct
2311 attgaaatcatgcaggcactggggaagagctgttggatcacattgtctcctcctgcatctctgacttcttgg
2381 actacatggggatcaaaggcccaggatgctcctgggcttccagttctcatttccctgcccagcagacgag
2451 tctggagcgggaaatcttgatcacctgggcaaaagggtttaaaggcaacagactgctgctggcagctgta
2521 gtcacctactaagggatgagataaaaaggagaggaatttgacctggacgtgggtggctgtggtcaacg
2591 acacagtgggcaccatgatgacctgtgcttatgaggagccacctgtgaggtggactcattggtgggac
2661 cggcagcaatgctgctacatggaggagatgaagaacgtggagatgggtggagggggaccaggggagatg
2731 tgcatacaatggagtggggcttggggaacaaagggtgtctggatgatcaggagacaacaaatctccggt
2801 gactggtggacgaatatccctaaatgctgggaaacaaaggatgagaagatgatcagtggtatgtacct
2871 ggggtgaaatcgtccgcaacatcttaatcgacttcaccaagaaggatctcctcctccgagggcagatctct
2941 gagacgctgaagaccggggcatcttggagaccaagttctctcctcagatcgagagtgaccgattagcac
3011 tctccaggtccgggctatcctccagcagctaggtctgaaatagcactgagatgacagatcctcgtcaa
3081 gacagtgctgggggtggtgtccaggagggccgcacagctgtgtggcgcaggcatggctgcggttgggat
3151 aagatccgagagaacagaggactggaccgtctgaaatgtgactgtgggagtgagcgggacactctacaagc
3221 ttcatccacacttctccagaatcatgaccagacggtgaaggaactgtcaccaaaatgtaacgtgtcctt
3291 cctcctgtgaggtgagcagcggcagggcgcctcctcagcggcctgagggctgaggttacgcaca
3361 gaggcaagcagcCTGCACTCGACGGTACCGCGGCCCGGATCCACCGGTCGCCACCATGGTGAGCAAGG
3431 GCGAGGAGCTGTTACCGGGGTGGTGCCCATCCTGGTTCGAGCTGGACGGCGACGTAACCGGCCACAAGTT
3501 CAGCGTGTCCGGCAGGGCGAGGGCGATGCCACCTACGGCAAGCTGACCTGAAGTTTCATCTGCACCACC
3571 GGCAAGCTGCCCGTGCCTGGGCCACCTCGTGACCAACCTGACCTACGGCGTGCAGTGTTCAGCCGCT
3641 ACCCCGACCACATGAAGCAGCAGACTTCTTCAAGTCCGCCATGCCGAAGGCTACGTCCAGGAGCGCAC
3711 CATCTTCTTCAAGGACGACGGCAACTACAAGACCCGCGCGAGGTGAAGTTTCGAGGGCGACACCCCTGGTG
3781 AACCGCATCGAGCTGAAGGGCATCGACTTCAAGGAGGACGGCAACTCCTGGGGCACAAGCTGGAGTACA
3851 ACTACAACAGCCACAACGCTATATCATGGCCGACAAGCAGAAGAACCGGCATCAAGGTGAACCTTCAAGAT
3921 CCGCCACAACATCGAGGACGGCAGCGTGCAGCTCGCCGACCACTACCAGCAGAACACCCCATCGCGAC
3991 GGCCCGTGTGCTGCTGCCGACAACTACCTGAGCACCCAGTCCGCCCTGAGCAAAGACCCCAACGAGA
4061 AGCCCGATCACATGGTCTGCTGGAGTTCGTGACCGCCCGCGGATCACTCTCGGCATGGCAGGAGCTGTA
4131 CAAGTAAAGCGCCGCGACTAGATCATAAATCAGCCATACCACATTTGTAGAGGTTTTACTGTCTTAA
4201 AAAACCTCCACACCTCCCTGAACTGAAACATAAAATGAATGCAATTGTGTTGTTAACTTGTATTAT
4271 TGCAGCTTATAATGGTTACAAATAAAGCAATAGCATCACAATTTCAAAAATAAAGCATTTTTTTCACTG
4341 CATTCTAGTTGTGGTTTTGTCCAAACTCATCAATGTATCTTAAAGCGTAAATTTGTAAGCGTTAATATTTT
4411 TTAATAATTCGCGTTAAATTTTTGTTAAATCAGCTCATTTTTTAACCAATAGGCCGAAATCGGCAAAATCC
4481 CTATAAATCAAAAAGATAGACCGGATAGGTTGAGTGTGTTCCAGTTTGGAAACAAGATGCCACTATT
4551 AAAGAACGTGGACTCCAACGTCAAAGGGCGAAAAACCGTCTATCAGGGCGATGGCCACTACGTGAACCA
4621 TCACCCTAATCAAGTTTTTGGGGTTCGAGGTGCCGTAAGCACTAATCGGAACCTTAAAGGGAGCCCC
4691 GATTTAGAGCTTGACGGGAAAGCCGGCAACGTGGCGAGAAAGGAAGGAAGGAAGCGAAAGGAGCGGG
4761 CGTTAGGGCGCTGGCAAGTGTAGCGGTACCGTGCAGTAAACCAACACCCCGCTTAAATGCGCCG
4831 CTACAGGGCGCTCAGGTGGCACTTTTTCGGGAAATGTGCGCGGAACCCCTATTTGTTTATTTTTCTAAA
4901 TACATTCAAAATATGTATCCGCTCATGAGACAATAACCTGATAAATGCTTCAATAATATTGAAAAAGGAA

```

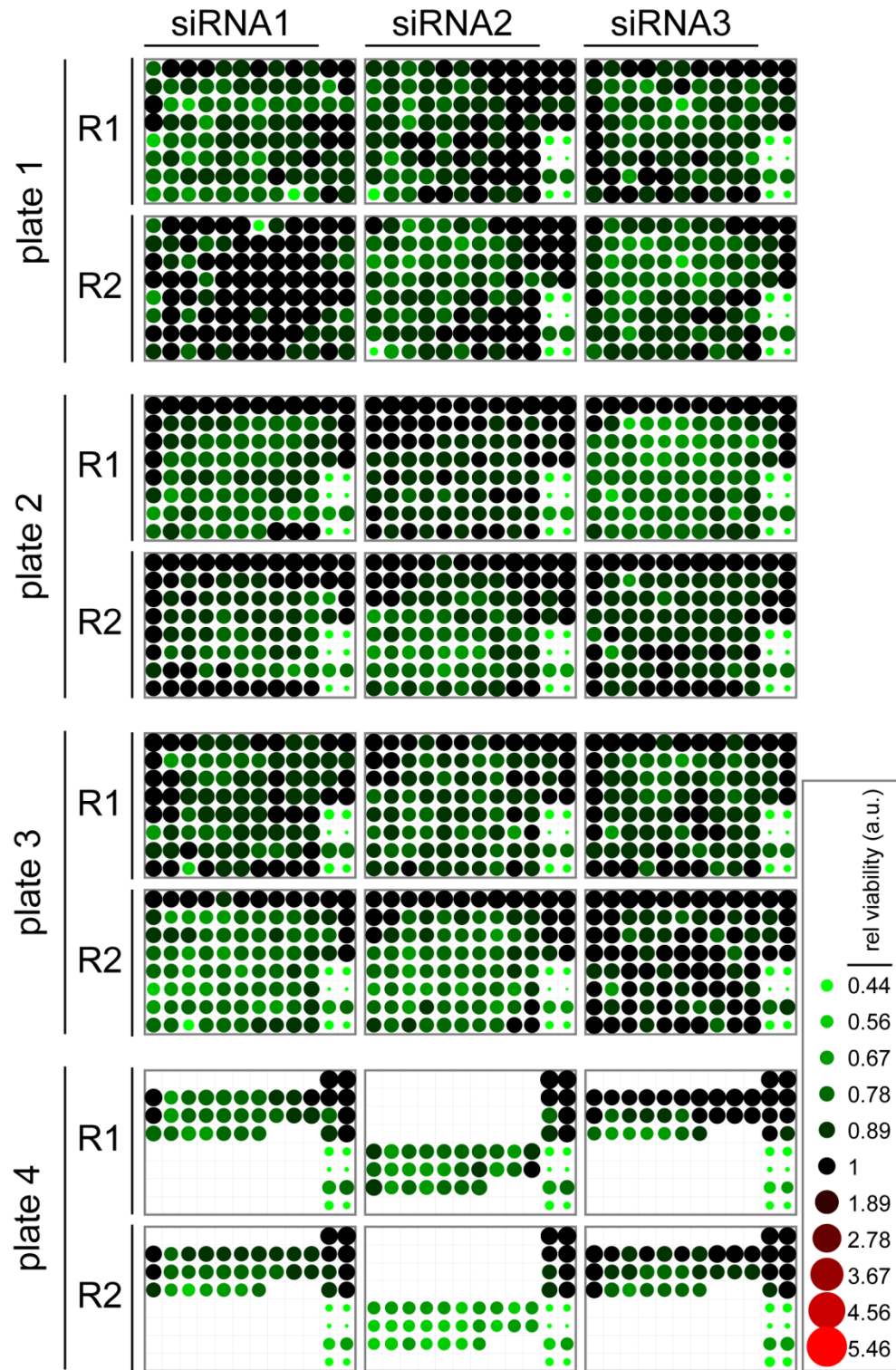
4971 GAGTCCTGAGGCGAAAGAACCAGCTGTGGAATGTGTGTCAGTTAGGGTGTGGAAAGTCCCAGGCTCCC
5041 CAGCAGGCAGAAGTATGCAAAGCATGCATCTCAATTAGTCAGCAACCAGGTGTGGAAAAGTCCCAGGCTC
5111 CCCAGCAGGCAGAAGTATGCAAAGCATGCATCTCAATTAGTCAGCAACCATAGTCCCAGCCCTAACTCCG
5181 CCCATCCCAGCCCTAACTCCGCCAGTTCGCCCATTTCTCCGCCCATGGCTGACTAATTTTTTTTATTT
5251 ATGCAGAGGCCGAGGCCGCTCGGCCTCTGAGCTATTCAGAAGTAGTGAGGAGGCTTTTTTGGAGGCCT
5321 AGGCTTTTGCAAAGATCGATCAAGAGACAGGATGAGGATCGTTTCGCATGATTGAACAAGATGGATTGCA
5391 CGCAGGTTTCCGGCCGCTTGGGTGGAGAGGCTATTCCGGCTATGACTGGGCACAACAGACAATCGGCTGC
5461 TCTGATGCCCGCTGTTCGGCTGTGAGCGCAGGGCGCCCGGTTCTTTTTGTCAAGACCACCTGTCCG
5531 GTGCCCTGAATGAAGTCAAGACGAGGCAGCGCGGCTATCGTGGCTGGCCACGACGGGCGTTCCCTGTCCG
5601 AGCTGTGCTCGACGTTGTCACTGAAGCGGGAAAGGACTGGCTGCTATTGGCGAAGTGCCTGGGCGAGGAT
5671 CTCCTGTCACTCACCTTGCTCCTGCCGAGAAAGTATCCATCATGGCTGATGCAATGCGGGCGGTCATA
5741 CGCTTGATCCGGCTACCTGCCATTTCGACCACCAAGCGAAACATCGCATCGAGCGAGCACGTAAGTCCGAT
5811 GGAAGCCGGTCTTGTGATCAGGATGATCTGGACGAAGAGCATCAGGGGCTCGCGCCAGCCGAAGTTC
5881 GCCAGGCTCAAGGCGAGCATGCCCGACGGCGAGGATCTCGTGTGACCCATGGCGATGCCTGCTTCCGGA
5951 ATATCATGGTGGAAAATGGCCGCTTTTCTGGATTCACTGACTGTGGCCGGCTGGGTGTGGCGGACCCGTA
6021 TCAGGACATAGCGTTGGCTACCCGTGATATTGCTGAAGAGCTTGGCGGCGAATGGGCTGACCGCTTCCCTC
6091 GTGCTTACGGTATCGCCGCTCCCGATTTCGACGCGCATCGCCTTCTATCGCCTTCTTGACGAGTTCCTTCT
6161 GAGCGGGACTCTGGGGTTCGAAATGACCCGACCAAGCGACGCCAACCTGCCATCACGAGATTTTCGATTCC
6231 ACCGCCGCTTCTATGAAAGGTTGGGCTTCGGAATCGTTTTCCGGGACGCCGGCTGGATGATCCTCCAGC
6301 CGGGGATCTCATGCTGGAGTCTTCGCCCCACCTAGGGGGAGGCTAACTGAAACACGGAAGGAGACAAT
6371 ACCGGAAGGAACCCGCGCTATGACGGCAATAAAAAGACAGAATAAAAACGCACGGTGTGGGTGCTTTGTT
6441 CATAAACGCGGGGTTCCGGTCCAGGGCTGGCACTCTGTGATACCCACCGAGACCCCATTTGGGGCCAAT
6511 ACGCCCGCTTTCTTCTTTTCCCCACCCACCCCAAGTTCGGGTGAAGGCCAGGGCTCGCAGCCAA
6581 CGTCGGGCGCGCAGGCCCTGCCATAGCCTCAGGTTACTCATATATACTTTAGATTGATTTAAAACCTCAT
6651 TTTTAATTTAAAAGGATCTAGGTGAAGATCCTTTTTGATAATCTCATGACCAAAATCCCTTAACGTGAGT
6721 TTTCTGTTCCACTGAGCGTCAAGCCCGTAGAAAAGATCAAAGGATCTTCTTGAGATCCTTTTTTTCTGCG
6791 CGTAATCTGCTGCTTGCAAACAAAAAACCACCGCTACCAGCGGTGGTTTGTGTTGCCGGATCAAGAGCTA
6861 CCAACTCTTTTTCCGAAGGTAAGTGGCTTTCAGCAGAGCGCAGATAACCAAACTACTGCTCTTCTAGTGTAGC
6931 CGTAGTTAGGCCACCACTTCAAGAAGTCTGTAGCACCGCTACATACTCGCTCTGCTAATCCTGTTACC
7001 AGTGGCTGCTGCCAGTGGCGATAAAGTCGTGCTTACCAGGGTTGGACTCAAGACGATAGTTACCGGATAAG
7071 GCGCAGCGGTCCGGCTGAACGGGGGTTTCGTGCACACAGCCAGCTTGGAGCGAACGACCTACACCGAAC
7141 TGAGATACCTACAGCGTGAAGTATGAGAAAAGCCACGCTTCCCGAAGGGAGAAAAGCGGACAGGTATCC
7211 GGTAAGCGGCAGGGTTCGGAACAGGAGAGCGCAGGGAGCTTCCAGGGGAAACGCCTGGTATCTTTAT
7281 AGTCCTGTCCGGTTTCGCCACCTCTGACTTGAGCGTCGATTTTGTGATGCTCGTCAGGGGGCGGAGCC
7351 TATGAAAAACGCCAGCAACGCGGCTTTTTACGGTTCCTGGCCTTTTGTGCTGGCCTTTTGTCTCACATGTT
7421 CTTTCTGCGTTATCCCTGATCTGTGGATAACCGTATTACCGCCATGCAT

```

Figure A2.1. DNA sequence of the HK1 expression construct. The pEGFP-N1 expression vector is shown in upper case letters, the insert of HK1 variant 1 in lower case letters, and restriction sites are underlined. Expressed nucleotides inclusive green GFP-encoding nucleotides are shown in bold.

**APPENDIX 3. HEAT MAP REPRESENTATION OF KINASE
AND PHOSPHATASE PLATES IN THE siRNA SCREEN.**

A phosphatases: no TNF or CHX



B phosphatases: TNF+CHX

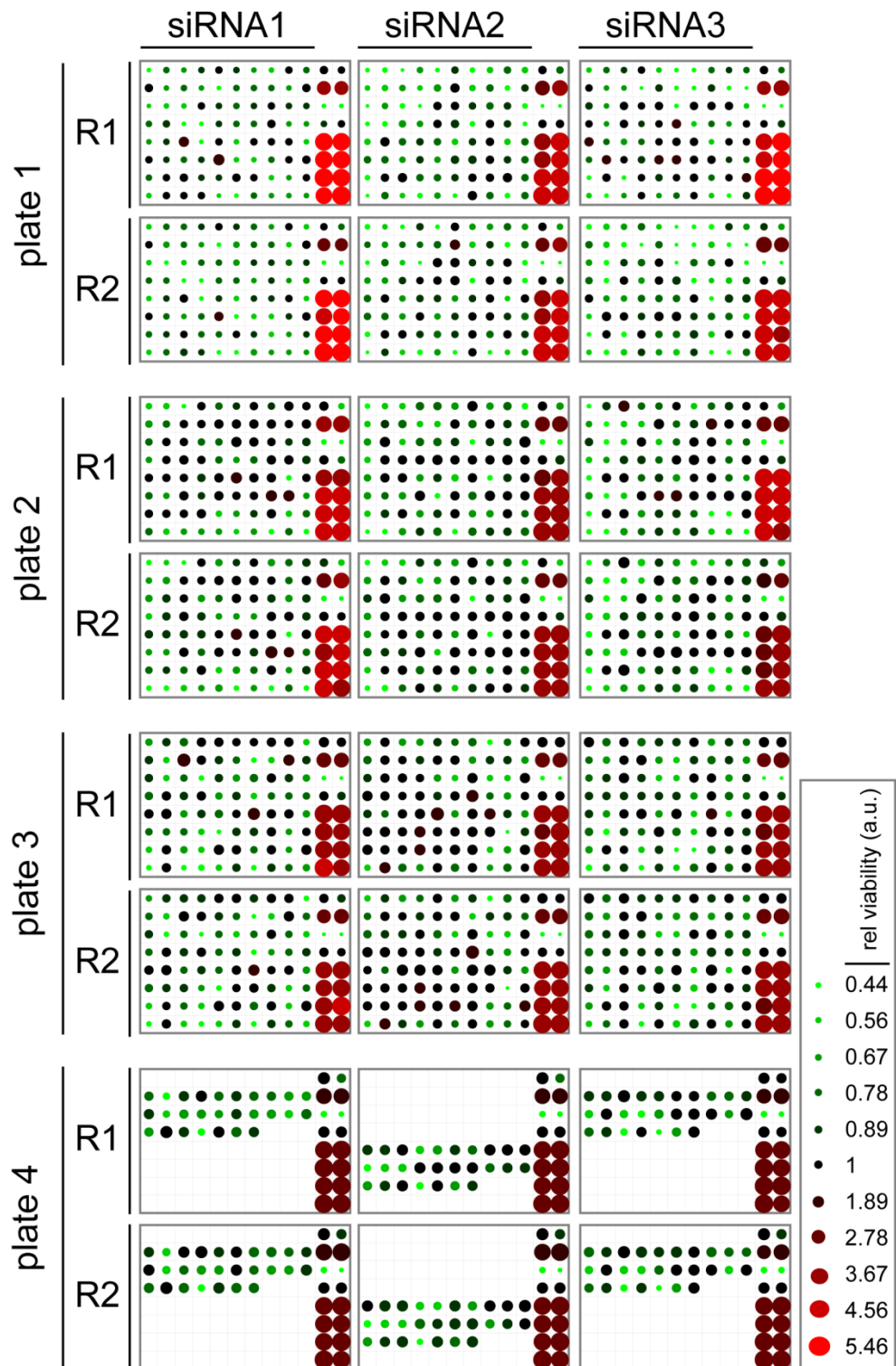
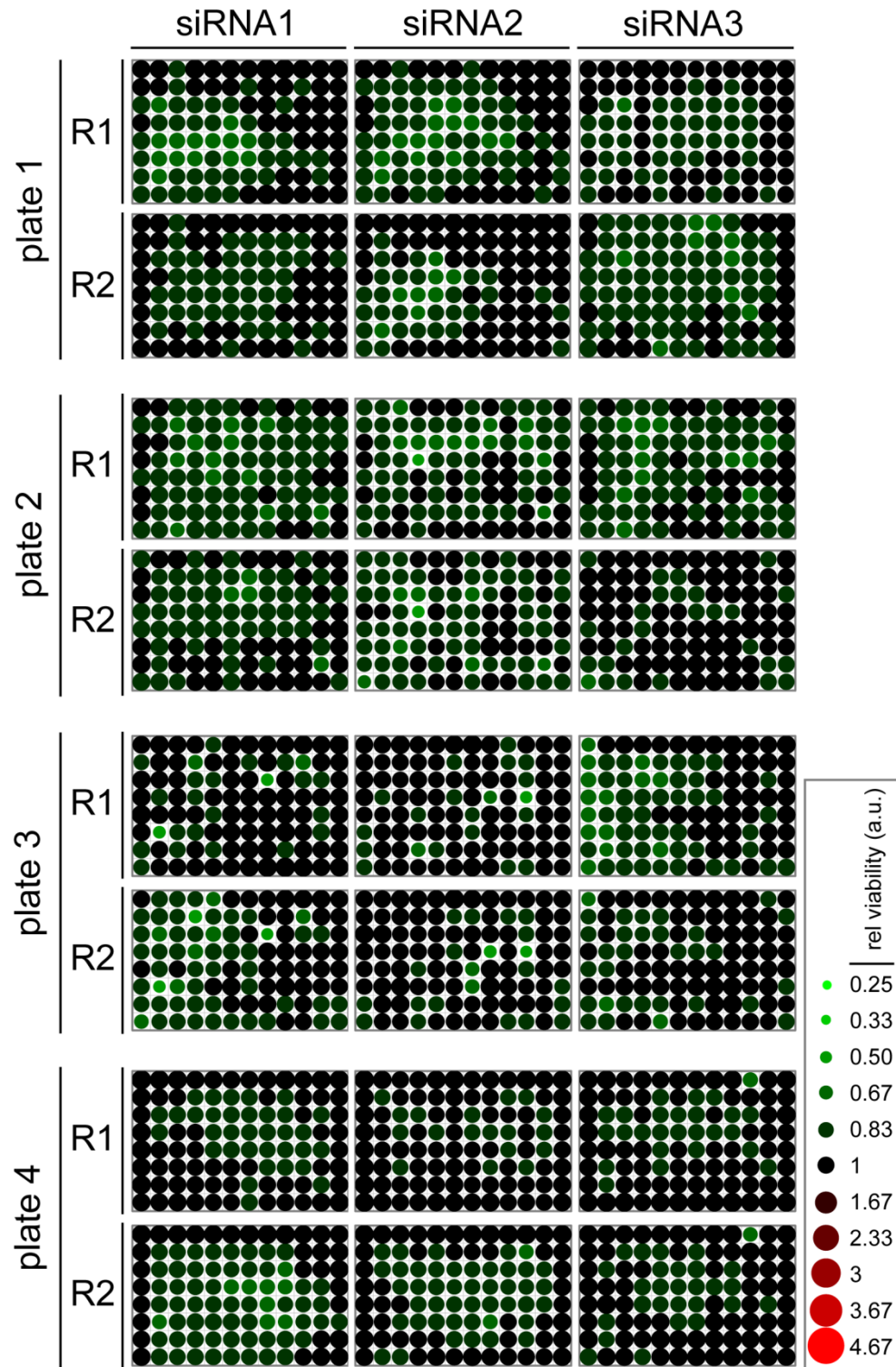


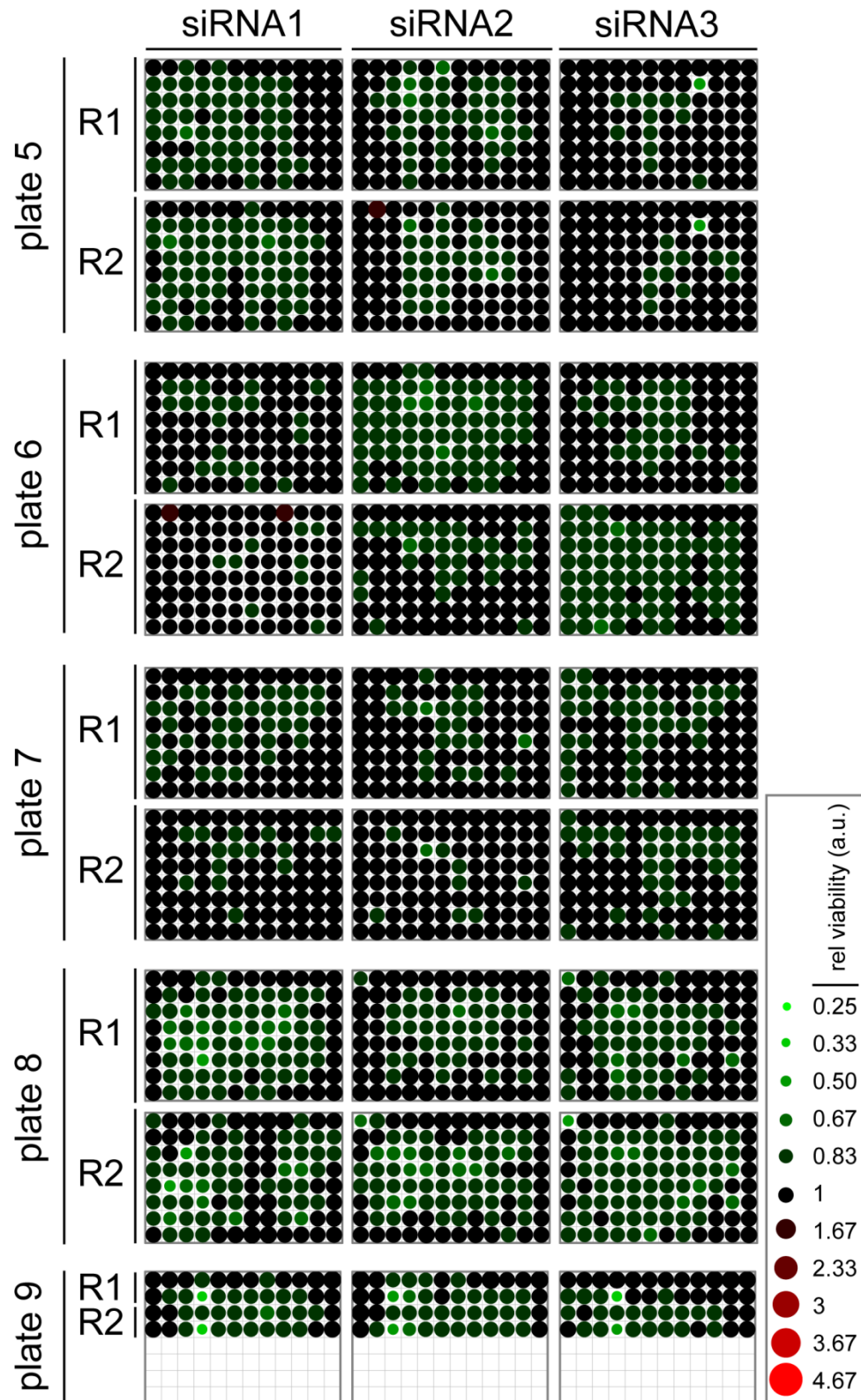
Figure A3.1. Heat map representation of all normalized phosphatase plates.

A: Combination of bubble diagram and heat map to illustrate the spatial distribution of the normalized basal fluorescence/viability values on screened 96-well plates after transfection with siRNAs from the phosphatase library. The four plate sets (plate 1 to 4) of the phosphatase siRNA library with three individual siRNAs for the same gene (siRNA1, 2 and 3) in identical positions were screened in duplicate (replicates R1 and R2). The size of the well decreases with the viability of the cells in the well as indicated on the scale. Viability values in a defined range around the viability of control cells incubated with non-silencing control siRNAs are shown in black. Viability values above that range are presented in tones of red, and viability values below that range are presented in tones of green as indicated on the scale. **B:** As panel A, but normalized fluorescence/viability values of screened ninety six-well plates are presented after incubation with siRNAs from the phosphatase library and treatment with TNF and CHX.

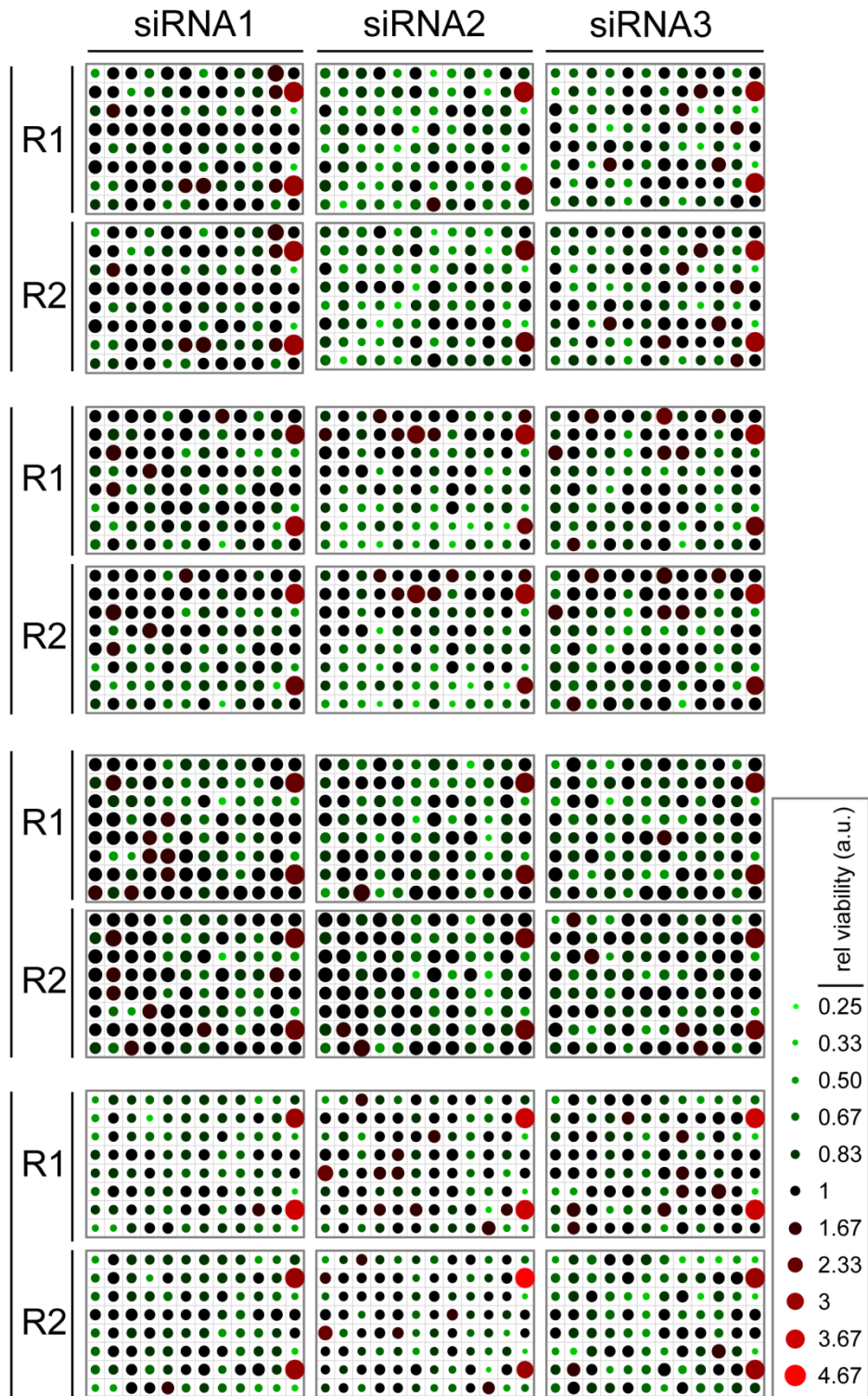
A kinases: no TNF or CHX



B kinases: no TNF or CHX



C kinases: TNF+CHX



D kinases: TNF+CHX

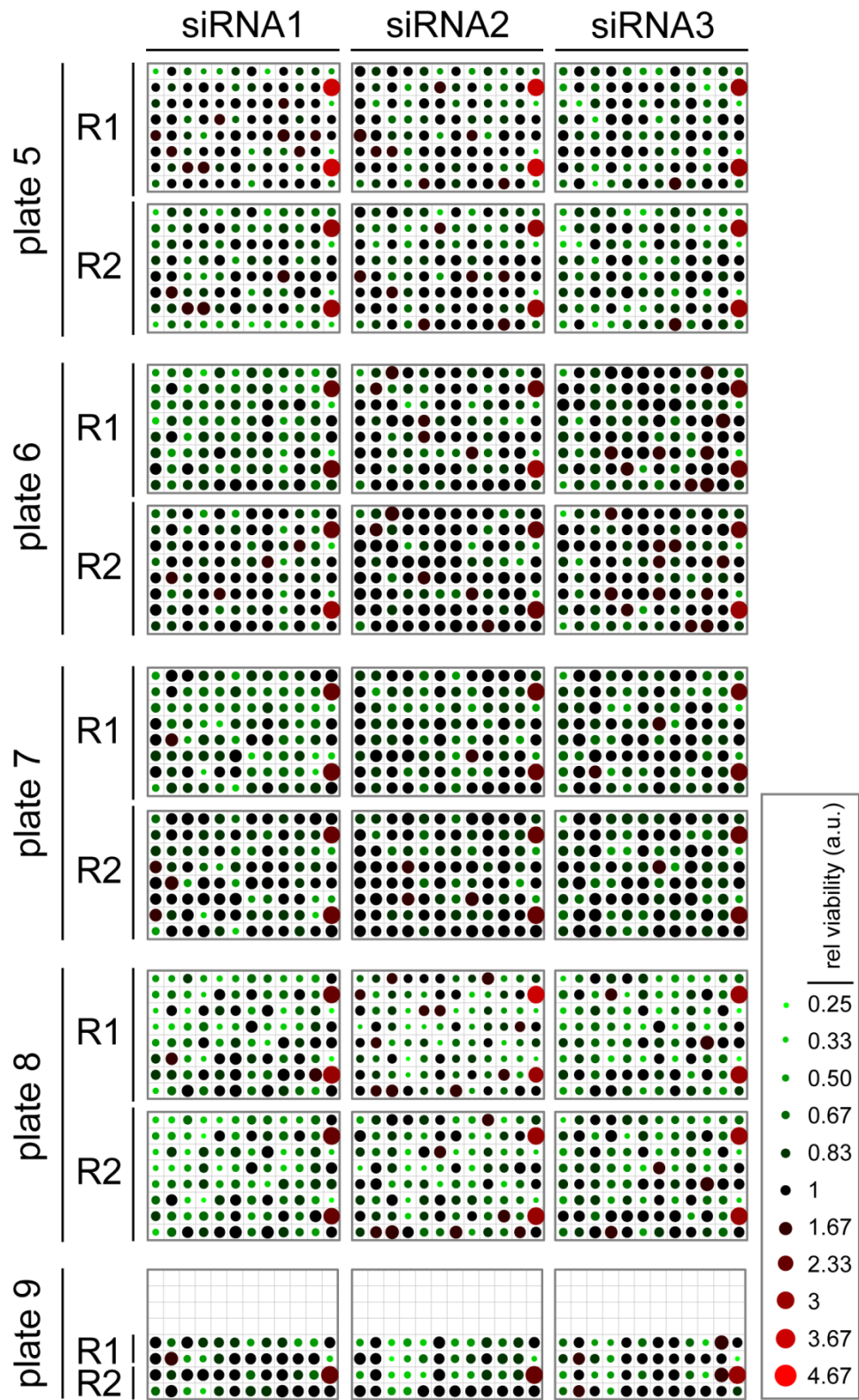


Figure A3.2. Heat map representation of all normalized kinase plates. A, B: Combination of bubble diagram and heatmap to illustrate the spatial distribution of the normalized basal fluorescence/viability values on screened ninety six-well plates after transfection with siRNAs from the kinase library. The nine plate sets (plate one to nine) of the kinase siRNA library with three individual siRNAs for the same gene (siRNA1, 2 and 3) in identical positions were screened in duplicate (replicates R1 and R2). The size of the well decreases with the viability of the cells in the well as indicated on the scale. Viability values in a defined range around the viability of control cells incubated with non-silencing control siRNAs are shown in black. Viability values above that range are presented in tones of red, and viability values below that range are presented in tones of green as indicated on the scale. **C, D:** As panel A and B, but normalized fluorescence/viability values of screened ninety six-well plates are presented after incubation with siRNAs from the kinase library and treatment with TNF and CHX.

**APPENDIX 4. DATA TABLE OF THE VIABILITY VALUES
AND DEATH INDICES FOR EACH siRNA IN THE SCREEN.**

Table A4.1. Viability values and death indices of each siRNA in the screen.

The nine hundred eighty six screened genes are presented with NCBI RefSeq accession number (NCBI RefSeq), gene symbol, three basal relative viability values, three relative viability values in the presence of TNF and CHX, and three death indices corresponding to the three screened siRNAs per gene. All genes are sorted according to the median death index in descending order, and their respective confidence interval (CI) for pro-survival and pro-death phenotype in TNF signaling is indicated. The death index of control cells treated with a non-silencing control siRNA (1) is indicated with a horizontal black line. Kinases are shown in black font and phosphatases in blue font.

CI	rank	NCBI RefSeq	gene symbol	rel. viability untreated			rel. viability TNF and CHX			death index		
				siRNA 1	siRNA 2	siRNA 3	siRNA 1	siRNA 2	siRNA 3	siRNA 1	siRNA 2	siRNA 3
99	1	NM_033497	HK1	0.925	0.918	0.973	0.291	0.274	0.595	3.175	3.355	1.636
	2	XM_496170	NUDT7	1.113	1.129	1.011	0.521	0.378	0.324	2.136	2.985	3.117
	3	NM_145342	MAP3K7IP2	0.916	1.065	1.023	0.310	0.359	0.387	2.953	2.963	2.642
	4	NM_012382	OSRF	0.843	0.750	0.787	0.310	0.297	0.518	2.717	2.523	1.519
	5	NM_002860	ALDH18A1	0.581	0.774	0.708	0.249	0.256	0.446	2.333	3.021	1.587
	6	NM_206876	PPP1CB	0.879	0.915	0.946	0.604	0.339	0.407	1.456	2.697	2.326
	7	NM_138793	ENTPD8	0.920	0.947	0.815	0.631	0.429	0.359	1.456	2.209	2.268
	8	NM_003648	DGKD	1.177	1.118	1.199	0.466	1.653	0.559	2.527	0.676	2.147
	9	NM_052931	SLAMF6	1.140	1.200	1.056	0.470	0.560	0.500	2.426	2.143	2.111
	10	NM_014572	LATS2	0.915	0.795	0.954	1.147	0.378	0.451	0.798	2.104	2.117
	11	NM_020438	DOLPP1	1.145	1.217	1.120	0.537	0.587	0.813	2.133	2.072	1.378
	12	NM_004439	EPHA5	1.179	0.957	0.878	0.569	0.550	0.406	2.072	1.739	2.162
	13	NM_144648	FLJ32786	0.930	0.828	0.921	0.453	0.315	0.683	2.054	2.631	1.348
	14	NM_006035	CDC42BPB	0.923	1.097	1.025	0.452	0.462	0.499	2.040	2.375	2.053
	15	NM_001776	ENTPD1	1.080	0.732	0.948	0.528	0.321	0.768	2.045	2.283	1.234
	16	NM_022737	LPPR2	0.850	0.888	1.045	0.416	0.515	0.516	2.041	1.723	2.024
	17	NM_004760	STK17A	1.018	1.067	1.193	0.473	0.529	0.923	2.152	2.017	1.292
	18	NM_181843	NUDT8	1.150	1.134	1.093	0.293	0.576	1.534	3.924	1.969	0.712
95	19	NM_001106	ACVR2B	0.880	1.122	0.923	0.292	1.016	0.473	3.013	1.105	1.949
	20	NM_003837	FBP2	0.734	0.953	0.990	0.521	0.386	0.512	1.408	2.471	1.933
	21	NM_003639	IKBKG	0.800	0.982	1.132	0.971	0.512	0.350	0.824	1.916	3.231
	22	NM_002480	PPP1R12A	0.885	0.839	0.983	0.770	0.439	0.368	1.150	1.910	2.674
	23	NM_005546	ITK	0.963	0.886	0.905	0.990	0.463	0.475	0.973	1.913	1.905
	24	NM_003681	PDXK	0.940	0.689	0.561	0.411	0.580	0.298	2.288	1.189	1.884
	25	NM_145262	GLYCTK	1.047	1.230	0.682	0.537	0.656	0.516	1.949	1.876	1.322
	26	NM_001247	ENTPD6	0.907	0.987	0.804	0.874	0.439	0.431	1.037	2.248	1.866
	27	NM_033312	CDC14A	1.008	0.981	0.904	0.432	0.830	0.485	2.332	1.182	1.864
	28	NM_206873	PPP1CA	0.985	0.846	0.833	0.470	0.457	0.496	2.094	1.853	1.678
	29	NM_000294	PHKG2	1.090	0.781	1.045	0.863	0.423	0.462	1.263	1.848	2.260
	30	NM_002031	FRK	0.971	1.143	1.131	0.527	0.645	0.587	1.844	1.773	1.926
	31	XM_497574	LOC342853	0.666	0.932	0.943	0.615	0.512	0.333	1.084	1.823	2.828
	32	NM_003713	PPAP2B	0.872	0.846	0.832	0.484	0.710	0.405	1.800	1.192	2.051
	33	NM_025228	T3JAM	0.963	0.901	0.905	0.541	0.497	0.503	1.781	1.813	1.798
	34	NM_182661	CERK	1.000	1.205	1.065	0.368	1.243	0.598	2.719	0.970	1.780
	35	NM_033331	CDC14B	1.121	1.120	1.133	0.632	0.604	1.278	1.774	1.853	0.887
	36	NM_020680	SCYL1	0.895	0.871	0.971	0.746	0.419	0.548	1.201	2.080	1.772
	37	NM_006301	MAP3K12	0.915	1.057	1.129	0.517	0.882	0.604	1.769	1.199	1.868
	38	NM_014840	ARK5	1.046	0.956	1.058	0.554	0.542	0.904	1.889	1.764	1.170
	39	NM_006293	TYRO3	0.840	0.860	0.930	0.970	0.493	0.457	0.866	1.744	2.034
	40	NM_004712	HGS	0.885	0.637	0.766	0.509	0.314	0.448	1.740	2.031	1.710
90	41	NM_017719	SNRK	1.137	1.178	1.003	0.658	0.679	0.652	1.728	1.735	1.539

CI	rank	NCBI RefSeq	gene symbol	rel. viability untreated			rel. viability TNF and CHX			death index		
				siRNA 1	siRNA 2	siRNA 3	siRNA 1	siRNA 2	siRNA 3	siRNA 1	siRNA 2	siRNA 3
80	42	NM_006252	PRKAA2	0.851	0.702	0.802	0.552	0.410	0.403	1.542	1.713	1.990
	43	NM_002651	PIK4CB	0.945	0.780	0.814	1.034	0.457	0.272	0.914	1.706	2.994
	44	NM_080871	ASB10	1.099	1.112	1.025	0.600	0.957	0.608	1.832	1.162	1.688
	45	NM_002627	PFKP	1.087	1.053	0.878	0.715	0.562	0.521	1.520	1.875	1.686
	46	NM_033266	ERN2	0.762	0.795	0.971	0.811	0.474	0.564	0.939	1.678	1.721
	47	NM_005134	PPP4R1	0.870	0.847	0.885	0.504	0.505	0.775	1.727	1.677	1.141
	48	NM_002748	MAPK6	0.980	0.881	0.867	0.501	0.811	0.519	1.955	1.086	1.669
	49	NM_001715	BLK	0.990	0.994	0.816	0.594	0.306	1.141	1.666	3.251	0.715
	50	NM_152572	C9orf98	0.990	1.111	1.043	0.597	0.631	0.688	1.659	1.761	1.517
	51	NM_000289	PFKM	1.083	1.105	1.066	0.660	0.667	0.591	1.641	1.656	1.804
	52	NM_022809	CDC25C	1.078	1.048	1.027	0.683	0.609	0.626	1.579	1.722	1.640
	53	NM_003913	PRPF4B	0.919	0.948	0.939	0.290	0.733	0.573	3.174	1.293	1.639
	54	NM_015112	MAST2	0.984	0.973	0.904	0.427	0.597	0.903	2.303	1.630	1.002
	55	NM_002596	PCTK3	0.891	0.900	0.727	0.547	0.487	0.548	1.629	1.847	1.328
80	56	NM_000151	G6PC	0.714	0.891	0.996	0.738	0.555	0.381	0.967	1.605	2.614
	57	NM_003620	PPM1D	1.124	0.958	0.956	0.446	0.941	0.598	2.522	1.017	1.598
	58	NM_004672	MAP3K6	0.938	0.973	0.853	0.588	0.833	0.440	1.595	1.168	1.940
	59	XM_377594	LOC401954	0.893	0.933	0.837	0.690	0.586	0.471	1.293	1.593	1.775
	60	NM_181093	PACE-1	0.898	0.904	0.815	0.788	0.359	0.518	1.140	2.521	1.575
	61	XM_499479	LOC442731	0.924	0.930	0.876	0.583	0.594	0.944	1.585	1.565	0.927
	62	NM_021176	G6PC2	0.963	0.859	0.887	1.051	0.369	0.567	0.916	2.330	1.565
	63	NM_030662	MAP2K2	1.041	1.028	1.026	0.646	0.657	0.703	1.611	1.565	1.459
	64	NM_014678	KIAA0685	0.880	0.943	0.993	0.482	0.703	0.636	1.828	1.342	1.560
	65	NM_001277	CHKA	0.836	0.774	0.805	0.644	0.460	0.518	1.299	1.680	1.554
	66	NM_007174	CIT	0.659	0.587	0.800	0.426	0.344	0.525	1.548	1.705	1.523
	67	NM_018425	PI4KII	0.997	0.937	0.813	0.545	0.608	0.895	1.830	1.540	0.908
	68	NM_020786	PDP2	0.905	0.943	0.837	0.999	0.613	0.525	0.906	1.540	1.594
	69	NM_022755	C9orf12	0.920	1.050	0.867	0.598	0.603	1.054	1.538	1.741	0.822
	70	NM_014226	RAGE	0.759	0.802	0.800	0.494	0.562	0.372	1.538	1.427	2.154
	71	NM_005026	PIK3CD	0.878	1.079	1.057	0.755	0.707	0.457	1.163	1.526	2.313
	72	XM_372654	LOC390760	0.914	0.943	0.720	0.710	0.452	0.473	1.289	2.084	1.524
	73	NM_004090	DUSP3	1.164	1.069	1.055	0.764	0.722	0.660	1.524	1.480	1.599
	74	NM_006247	PPP5C	0.803	0.856	0.864	0.864	0.562	0.456	0.929	1.524	1.893
	75	NM_178003	PPP2R4	1.004	0.855	0.859	0.878	0.531	0.566	1.144	1.611	1.518
	76	NM_080841	PTPRA	1.015	1.138	1.164	1.080	0.409	0.771	0.940	2.786	1.511
	77	NM_138923	TAF1	0.865	0.813	0.971	0.536	0.821	0.643	1.612	0.990	1.510
	78	XM_374879	PTPMT1	0.849	0.808	0.929	0.608	0.537	0.529	1.397	1.505	1.758
	79	NM_178432	CCRK	0.911	1.178	1.025	1.088	0.783	0.642	0.837	1.504	1.595
	80	NM_021129	PP	0.799	0.785	0.997	0.522	1.868	0.663	1.532	0.420	1.504
	81	NM_013392	NRBP	1.033	1.157	0.925	0.765	0.737	0.617	1.351	1.569	1.499
	82	NM_015967	PTPN22	1.049	0.772	0.846	0.623	0.585	0.567	1.685	1.319	1.493

CI	rank	NCBI RefSeq	gene symbol	rel. viability untreated			rel. viability TNF and CHX			death index		
				siRNA 1	siRNA 2	siRNA 3	siRNA 1	siRNA 2	siRNA 3	siRNA 1	siRNA 2	siRNA 3
80	83	NM_199284	LOC283846	1.014	1.127	0.986	0.464	0.765	0.663	2.186	1.473	1.489
	84	NM_003691	STK16	0.822	0.852	0.771	0.317	0.574	0.706	2.590	1.483	1.091
70	85	NM_006875	PIM2	1.044	1.014	1.023	0.416	0.842	0.692	2.511	1.204	1.478
	86	XM_498243	LOC442350	1.021	0.830	0.903	0.692	0.413	0.839	1.476	2.009	1.076
	87	NM_002712	PPP1R7	0.790	0.374	0.833	0.535	0.270	0.543	1.475	1.384	1.534
	88	NM_012229	NT5C2	0.955	0.836	0.781	0.764	0.569	0.432	1.251	1.468	1.809
	89	NM_001004318	FLJ16165	0.881	0.727	1.000	0.601	0.895	0.581	1.467	0.812	1.722
	90	NM_000269	NME1	1.001	0.849	0.963	1.370	0.581	0.656	0.731	1.461	1.469
	91	NM_016457	PRKD2	1.080	0.838	0.944	0.739	0.892	0.646	1.461	0.939	1.461
	92	XM_497791	LOC391295	1.032	1.111	1.010	0.707	0.933	0.496	1.458	1.191	2.035
	93	NM_016361	ACP6	0.792	0.886	0.881	0.544	1.552	0.576	1.456	0.571	1.528
	94	NM_001261	CDK9	1.095	1.039	1.215	0.774	0.714	0.625	1.414	1.454	1.945
	95	NM_004440	EPHA7	1.085	1.091	1.157	0.740	0.777	0.799	1.465	1.403	1.449
	96	NM_015518	DKFZP434C131	1.039	0.947	1.147	0.907	0.453	0.793	1.146	2.090	1.448
	97	NM_007236	CHP	0.892	1.128	1.082	0.497	0.992	0.748	1.793	1.137	1.447
	98	NM_001033578	SGKL	0.894	0.975	1.006	0.945	0.573	0.698	0.946	1.701	1.443
	99	NM_002745	MAPK1	1.009	1.160	0.877	1.078	0.491	0.610	0.936	2.360	1.437
	100	NM_005028	PIP5K2A	1.013	1.072	0.866	0.371	0.957	0.604	2.732	1.120	1.434
	101	NM_032728	C9orf67	0.650	0.650	0.726	0.454	0.422	0.934	1.432	1.540	0.777
	102	NM_002611	PDK2	0.866	0.856	0.994	0.681	0.598	0.410	1.272	1.431	2.422
	103	NM_004566	PFKFB3	0.853	1.030	0.893	0.634	0.654	0.625	1.346	1.574	1.430
	104	NM_005734	HIPK3	0.999	1.053	0.936	0.554	1.286	0.659	1.803	0.819	1.421
	105	NM_015533	DKFZP586B1621	0.847	0.815	0.886	0.597	0.477	1.161	1.420	1.708	0.763
	106	NM_172207	CAMKK1	0.909	1.080	1.111	0.642	0.689	1.030	1.416	1.568	1.078
	107	NM_014721	C6orf56	0.748	0.754	0.939	0.945	0.533	0.606	0.792	1.414	1.550
108	NM_005990	STK10	0.769	0.976	0.886	0.547	0.814	0.436	1.407	1.199	2.034	
109	NM_001029881	CIB4	1.077	1.110	1.037	0.893	0.760	0.740	1.206	1.461	1.401	
110	XM_498334	LOC442428	1.006	0.727	0.950	0.718	0.285	0.760	1.400	2.551	1.251	
111	NM_144610	FLJ25006	0.829	1.015	1.088	0.731	0.725	0.721	1.134	1.399	1.509	
112	NM_018584	CaMKIIAlpha	0.981	1.033	0.991	0.702	0.734	0.771	1.397	1.407	1.285	
113	NM_003496	TRRAP	1.067	1.038	1.083	0.610	0.744	0.863	1.751	1.395	1.254	
114	NM_001348	DAPK3	0.939	0.997	0.924	0.791	0.698	0.663	1.187	1.428	1.394	
115	NM_001007071	RPS6KB2	0.846	0.923	0.714	0.607	0.557	0.695	1.394	1.656	1.028	
60	116	NM_000945	PPP3R1	0.953	1.141	1.052	0.798	0.778	0.757	1.193	1.467	1.390
	117	NM_012080	HDHD1A	1.028	0.921	0.914	0.740	0.473	0.924	1.389	1.946	0.989
	118	NM_000507	FBP1	1.084	0.909	0.834	0.782	0.487	0.656	1.386	1.865	1.271
	119	NM_001258	CDK3	1.016	0.928	0.843	0.764	0.670	0.597	1.331	1.385	1.413
	120	NM_000020	ACVRL1	0.953	1.073	1.000	0.602	0.776	0.786	1.584	1.384	1.272
	121	NM_033534	CDC2L2	0.893	0.961	1.015	0.646	0.751	0.684	1.383	1.280	1.484
	122	NM_005761	PLXNC1	0.793	0.824	0.882	0.500	0.597	0.705	1.588	1.381	1.252
	123	NM_002645	PIK3C2A	0.943	0.920	0.867	0.684	0.666	1.334	1.379	1.381	0.650

CI	rank	NCBI RefSeq	gene symbol	rel. viability untreated			rel. viability TNF and CHX			death index		
				siRNA 1	siRNA 2	siRNA 3	siRNA 1	siRNA 2	siRNA 3	siRNA 1	siRNA 2	siRNA 3
80	124	NM_002833	PTPN9	0.941	0.996	1.190	0.996	0.723	0.843	0.944	1.377	1.413
	125	NM_007099	ACP1	0.909	0.974	0.775	1.049	0.547	0.563	0.867	1.780	1.376
	126	NM_002741	PKN1	0.872	0.892	0.953	0.998	0.650	0.632	0.873	1.372	1.508
	127	NM_002706	PPM1B	1.191	1.181	1.114	1.005	0.798	0.814	1.185	1.479	1.369
	128	NM_006609	MAP3K2	1.060	0.894	0.933	0.630	1.069	0.682	1.681	0.836	1.368
	129	NM_025130	FLJ22761	0.972	0.964	0.861	0.711	0.442	0.764	1.368	2.179	1.126
	130	NM_015148	PASK	0.881	0.845	0.849	1.179	0.541	0.622	0.748	1.561	1.366
	131	NM_212539	PRKCD	0.798	1.003	0.995	0.502	0.955	0.729	1.592	1.050	1.366
	132	NM_014016	SACM1L	0.981	0.626	1.179	0.952	0.458	0.603	1.030	1.365	1.956
	133	NM_020547	AMHR2	1.069	1.100	0.997	0.642	1.020	0.731	1.665	1.078	1.363
	134	NM_017514	PLXNA3	0.892	0.871	1.009	0.657	0.628	1.156	1.357	1.386	0.873
	135	NM_001767	CD2	0.841	0.874	0.869	0.504	0.832	0.640	1.667	1.051	1.357
	136	NM_014216	ITPK1	0.993	0.992	0.775	1.294	0.731	0.498	0.768	1.357	1.557
	137	NM_014006	SMG1	0.858	1.004	0.987	0.634	0.433	0.956	1.355	2.318	1.032
	138	NM_006212	PFKFB2	0.927	1.048	0.975	0.685	0.621	0.738	1.354	1.690	1.322
	139	NM_019892	INPP5E	0.807	0.702	0.945	0.597	0.192	1.066	1.352	3.648	0.887
	140	NM_001654	ARAF1	0.977	0.894	0.955	0.723	0.638	1.133	1.352	1.401	0.843
	141	NM_033256	PPP1R14A	0.942	1.041	0.800	0.679	1.003	0.592	1.387	1.038	1.351
	142	NM_001259	CDK6	1.091	1.076	1.018	0.491	1.340	0.756	2.222	0.803	1.346
	143	NM_003582	DYRK3	0.952	0.937	1.108	0.779	0.697	0.571	1.223	1.345	1.940
	144	NM_173492	PIP5KL1	1.072	1.141	1.044	0.613	1.274	0.776	1.747	0.896	1.345
	145	NM_003688	CASK	0.996	0.887	0.934	0.639	0.660	0.962	1.558	1.344	0.970
	146	NM_139068	MAPK9	0.962	1.211	1.226	0.940	0.881	0.913	1.023	1.375	1.343
	147	NM_001018046	FLJ23074	1.142	1.030	1.086	0.671	0.767	0.820	1.703	1.342	1.324
	148	NM_145162	MAP2K5	0.857	1.175	1.099	0.842	0.880	0.473	1.019	1.336	2.324
	149	NM_016440	VRK3	1.277	1.044	1.081	0.865	1.104	0.809	1.477	0.946	1.336
	150	NM_032387	PRKWNK4	0.958	0.838	0.990	0.718	0.357	0.863	1.334	2.350	1.147
	151	NM_178510	ANKK1	0.922	0.840	0.956	0.695	0.959	0.628	1.326	0.875	1.524
	152	NM_139209	GRK7	1.145	1.139	1.091	0.865	1.048	0.467	1.324	1.087	2.337
	153	NM_003584	DUSP11	1.148	1.100	1.006	0.973	0.833	0.664	1.180	1.319	1.514
	154	NM_005160	ADRBK2	1.031	1.053	0.945	1.009	0.798	0.695	1.022	1.319	1.360
	155	NM_003463	PTP4A1	1.032	0.935	0.956	0.783	0.945	0.565	1.318	0.989	1.692
156	XM_375150	LOC400301	0.938	0.975	0.917	1.058	0.691	0.697	0.887	1.410	1.315	
50	157	NM_002832	PTPN7	1.095	1.026	1.204	0.833	0.672	1.087	1.315	1.528	1.108
	158	NM_139021	ERK8	0.794	0.878	0.859	0.604	0.756	0.479	1.313	1.161	1.792
	159	XM_497777	LOC441959	0.860	1.053	1.005	0.656	0.762	0.878	1.312	1.382	1.144
	160	NM_032017	MGC4796	0.968	1.008	0.966	1.224	0.771	0.551	0.791	1.307	1.753
	161	NM_014397	NEK6	0.897	1.065	1.069	0.686	0.849	0.736	1.307	1.254	1.452
	162	NM_139062	CSNK1D	0.785	0.794	0.784	1.286	0.591	0.601	0.610	1.343	1.305
	163	XM_042066	MAP3K1	0.848	0.961	1.082	0.650	0.755	0.422	1.304	1.274	2.563
	164	NM_018291	FLJ10986	0.963	1.022	0.946	0.762	0.695	0.726	1.264	1.471	1.303

CI	rank	NCBI RefSeq	gene symbol	rel. viability untreated			rel. viability TNF and CHX			death index		
				siRNA 1	siRNA 2	siRNA 3	siRNA 1	siRNA 2	siRNA 3	siRNA 1	siRNA 2	siRNA 3
50	165	NM_198041	NUDT6	0.975	0.740	0.893	0.749	1.297	0.326	1.302	0.571	2.734
	166	NM_002012	FHIT	0.885	0.875	0.780	0.700	0.611	0.600	1.266	1.431	1.302
	167	NM_203468	ENTPD2	0.773	0.834	0.744	0.511	0.745	0.571	1.512	1.119	1.301
	168	NM_020439	CAMK1G	0.947	1.116	0.891	0.622	1.265	0.685	1.521	0.882	1.301
	169	NM_006888	CALM1	1.038	0.881	0.955	0.490	0.678	0.981	2.118	1.301	0.973
	170	NM_006256	PKN2	0.992	1.024	0.986	0.822	0.787	0.721	1.207	1.301	1.368
	171	NM_004715	CTDP1	0.919	0.936	0.868	0.618	0.719	0.690	1.489	1.301	1.257
	172	NM_020397	CAMK1D	0.836	0.863	0.855	1.147	0.664	0.493	0.729	1.299	1.734
	173	NM_020526	EPHA8	0.948	1.018	0.907	0.831	0.784	0.587	1.141	1.298	1.544
	174	XM_495953	TPTEps1	0.868	0.895	0.975	0.847	0.545	0.751	1.025	1.640	1.298
	175	NM_015981	CAMK2A	0.959	0.931	0.964	1.010	0.718	0.612	0.950	1.297	1.576
	176	NM_152309	PIK3AP1	1.100	1.053	0.961	0.832	1.434	0.742	1.321	0.735	1.296
	177	NM_152327	AK7	1.035	1.184	1.056	0.769	0.914	0.948	1.346	1.295	1.113
	178	NM_006242	PPP1R3D	1.020	0.973	0.918	0.543	0.887	0.709	1.879	1.097	1.295
	179	NM_177951	PPM1A	1.121	1.054	1.052	0.868	0.646	0.822	1.293	1.631	1.280
	180	XM_496720	LOC441047	1.036	1.177	1.048	0.765	0.960	0.812	1.354	1.226	1.291
	181	NM_145259	ACVR1C	1.089	1.131	1.124	0.844	0.969	0.491	1.290	1.167	2.289
	182	NM_019061	PIP3AP	0.766	0.819	0.977	0.594	1.188	0.690	1.289	0.690	1.417
	183	NM_024819	FLJ22955	0.992	1.237	1.092	0.890	0.959	0.652	1.115	1.289	1.675
	184	NM_021158	TRIB3	0.779	0.808	0.786	0.238	0.627	1.328	3.270	1.289	0.592
	185	NM_019884	GSK3A	0.938	0.912	0.998	0.810	0.708	0.420	1.158	1.288	2.379
	186	NM_198973	MKMK1	0.975	0.999	1.083	0.710	0.776	1.249	1.373	1.287	0.867
	187	NM_002972	SBF1	0.911	0.803	1.131	0.459	0.993	0.879	1.983	0.809	1.286
	188	NM_199040	NUDT4	1.032	0.783	1.166	0.802	0.906	0.836	1.286	0.864	1.396
	189	NM_002005	FES	0.768	0.716	0.843	1.227	0.363	0.656	0.626	1.972	1.285
	190	NM_139283	TA-PP2C	0.919	0.807	0.881	0.716	0.759	0.685	1.283	1.063	1.287
	191	NM_005858	AKAP8	0.902	0.919	0.891	0.704	0.680	0.838	1.281	1.352	1.063
	192	NM_002625	PFKFB1	1.007	1.007	1.102	0.974	0.786	0.843	1.033	1.281	1.307
	193	NM_006556	PMVK	0.830	0.855	0.938	0.639	0.744	0.732	1.299	1.150	1.281
	194	NM_018323	PI4K2B	0.914	1.236	1.188	1.181	0.927	0.928	0.774	1.333	1.280
195	NM_002115	HK3	0.810	0.833	0.832	0.903	0.650	0.632	0.898	1.280	1.316	
196	NM_002740	PRKCI	1.013	0.923	0.934	0.804	0.721	0.451	1.261	1.280	2.071	
197	NM_006206	PDGFRA	0.876	1.021	0.947	0.685	0.769	1.027	1.278	1.328	0.923	
198	NM_001003892	DUPD1	1.034	0.829	0.828	0.919	0.649	0.439	1.125	1.277	1.886	
199	XM_498259	LOC442368	0.738	0.780	0.837	0.360	0.612	0.841	2.051	1.275	0.996	
200	NM_145203	CSNK1A1L	1.070	1.152	0.980	0.839	0.656	1.063	1.275	1.757	0.922	
201	NM_147180	PPP3R2	0.657	1.050	0.929	0.516	1.096	0.658	1.273	0.958	1.411	
202	NM_144685	HIPK4	0.866	1.010	0.956	0.877	0.756	0.751	0.988	1.336	1.273	
203	NM_001003656	PPP2R2D	1.071	1.008	0.876	0.724	0.796	0.871	1.479	1.266	1.006	
204	NM_004409	DMPK	0.834	0.858	0.788	0.648	0.678	1.070	1.287	1.266	0.736	
205	NM_005627	SGK	0.954	1.097	0.971	0.989	0.867	0.757	0.964	1.265	1.282	

CI	rank	NCBI RefSeq	gene symbol	rel. viability untreated			rel. viability TNF and CHX			death index			
				siRNA 1	siRNA 2	siRNA 3	siRNA 1	siRNA 2	siRNA 3	siRNA 1	siRNA 2	siRNA 3	
50	206	NM_002749	MAPK7	0.982	0.843	1.203	0.506	0.941	0.951	1.939	0.896	1.265	
	207	NM_015103	PLXND1	1.012	1.002	1.028	0.772	0.793	0.901	1.310	1.263	1.141	
	208	NM_212535	PRKCB1	1.020	0.986	0.927	0.939	0.782	0.506	1.086	1.261	1.833	
	209	NM_002578	PAK3	0.929	0.898	0.985	0.989	0.681	0.782	0.940	1.318	1.260	
	210	NM_002756	MAP2K3	0.707	1.004	1.085	0.693	0.798	0.757	1.020	1.259	1.434	
	211	NM_017762	FLJ20313	0.869	0.640	1.170	0.691	0.984	0.768	1.258	0.651	1.523	
	212	NM_003800	RNGTT	1.135	0.940	0.972	0.748	0.748	0.820	1.517	1.257	1.186	
	213	NM_006255	PRKCH	0.992	0.996	1.035	0.394	1.098	0.824	2.518	0.908	1.256	
	214	NM_021733	TSKS	0.901	0.827	0.912	1.266	0.658	0.724	0.711	1.256	1.261	
	215	NM_015375	RIPK5	0.986	1.179	1.036	0.804	0.855	0.826	1.226	1.379	1.256	
	216	NM_182642	CTDSP1	0.865	0.917	0.921	0.874	0.731	0.696	0.990	1.256	1.323	
	217	NM_021873	CDC25B	0.912	1.029	0.871	0.727	0.948	0.433	1.255	1.085	2.010	
	40	218	NM_020639	RIPK4	0.845	1.060	0.985	0.452	0.968	0.786	1.867	1.096	1.254
		219	NM_144624	KIS	0.750	0.903	0.874	0.372	1.174	0.697	2.018	0.769	1.253
		220	NM_014521	SH3BP4	1.026	1.245	1.117	0.819	0.951	1.125	1.253	1.309	0.992
		221	NM_003831	RIOK3	0.985	0.691	0.861	0.786	0.417	0.963	1.252	1.657	0.894
		222	NM_032593	HINT2	0.801	0.787	0.683	0.671	0.629	0.288	1.194	1.251	2.371
223		NM_002835	PTPN12	0.914	1.020	1.135	1.001	0.714	0.908	0.914	1.429	1.250	
224		NM_001570	IRAK2	0.738	0.719	0.842	0.754	0.373	0.674	0.979	1.927	1.249	
225		NM_005730	CTDSP2	0.837	0.787	0.934	0.575	0.870	0.748	1.455	0.904	1.249	
226		NM_002220	ITPKA	0.933	0.984	1.035	0.641	1.753	0.829	1.455	0.561	1.248	
227		NM_177983	PPM1G	1.180	1.200	1.105	1.000	0.491	0.886	1.181	2.444	1.247	
228		NM_020990	CKMT1	0.898	0.983	0.830	1.117	0.653	0.668	0.804	1.504	1.243	
229		NM_002513	NME3	0.924	0.909	0.853	0.746	0.567	0.930	1.240	1.605	0.917	
230		NM_033379	CDC2	0.979	0.869	0.894	1.157	0.640	0.721	0.846	1.357	1.239	
231		NM_005232	EPHA1	0.846	0.938	0.750	0.683	0.964	0.422	1.238	0.973	1.780	
232		NM_006374	STK25	0.685	0.848	0.794	0.884	0.627	0.641	0.774	1.352	1.237	
233		NM_001587	OCRL	0.897	0.991	0.905	0.742	0.766	0.732	1.209	1.293	1.237	
234		NM_0010244 01	SBK1	0.860	0.936	0.868	0.753	0.758	0.594	1.142	1.235	1.461	
235		NM_000788	DCK	1.056	1.205	1.060	0.490	1.018	0.859	2.156	1.184	1.235	
236		NM_013993	DDR1	1.011	1.132	1.047	1.899	0.917	0.795	0.533	1.234	1.317	
237		NM_153831	PTK2	1.080	0.757	0.911	0.875	0.548	0.789	1.234	1.381	1.154	
238		NM_0010109 38	ACK1	0.952	0.905	0.840	0.443	0.734	0.712	2.148	1.233	1.179	
239		NM_002730	PRKACA	0.770	0.844	0.905	0.611	0.685	0.998	1.261	1.232	0.907	
240		NM_005204	MAP3K8	0.962	1.077	0.908	1.356	0.738	0.737	0.710	1.459	1.232	
241		NM_018401	STK32B	0.919	0.832	0.784	1.205	0.462	0.636	0.763	1.801	1.232	
242		NM_001823	CKB	0.926	1.115	1.232	0.752	1.289	0.853	1.230	0.865	1.445	
243		NM_006343	MERTK	0.854	0.877	1.052	0.768	0.546	0.856	1.112	1.606	1.228	
244		NM_178275	DKFZp434B12 31	0.908	0.963	0.749	1.106	0.728	0.610	0.821	1.323	1.228	
245		NM_207299	PRG-3	0.940	0.794	1.146	0.766	1.134	0.827	1.226	0.700	1.387	
246		XM_058513	LRRK2	1.064	1.031	1.030	0.735	0.843	1.051	1.446	1.223	0.980	

CI	rank	NCBI RefSeq	gene symbol	rel. viability untreated			rel. viability TNF and CHX			death index		
				siRNA 1	siRNA 2	siRNA 3	siRNA 1	siRNA 2	siRNA 3	siRNA 1	siRNA 2	siRNA 3
40	247	NM_007229	PACSIN2	0.926	1.001	1.032	0.758	1.409	0.819	1.222	0.710	1.260
	248	NM_020354	ENTPD7	0.949	0.802	0.740	0.777	0.688	0.583	1.221	1.166	1.271
	249	NM_015978	TNNI3K	0.843	0.825	0.908	0.659	0.676	0.811	1.279	1.220	1.121
	250	NM_004897	MINPP1	0.913	1.011	0.846	1.301	0.830	0.289	0.701	1.218	2.930
	251	NM_001556	IKKBK	0.844	0.833	0.747	0.749	0.684	0.382	1.126	1.218	1.958
	252	NM_003895	SYNJ1	0.869	0.823	0.973	0.691	0.677	1.226	1.258	1.216	0.794
	253	NM_003258	TK1	0.913	0.960	0.960	0.601	0.850	0.789	1.520	1.129	1.216
	254	NM_139078	MAPKAPK5	0.909	1.086	1.066	0.749	0.761	1.111	1.215	1.428	0.960
	255	NM_053030	MYLK	0.917	0.974	1.113	0.755	0.909	0.687	1.215	1.072	1.620
	256	NM_001001329	PRKCSH	1.183	1.048	1.016	0.866	1.678	0.836	1.366	0.625	1.214
	257	NM_002609	PDGFRB	1.033	0.996	0.930	1.023	0.821	0.510	1.010	1.214	1.822
	258	NM_145332	MAP3K7	0.949	0.851	0.979	0.781	0.477	1.595	1.214	1.784	0.614
	259	NM_001014795	ILK	0.856	0.997	0.979	0.732	0.822	0.534	1.169	1.213	1.831
	260	NM_014720	SLK	0.928	0.858	1.013	0.765	0.534	1.150	1.213	1.607	0.881
	261	NM_018638	ETNK1	0.759	1.014	1.138	0.717	0.729	0.940	1.058	1.390	1.211
	262	NM_005246	FER	1.028	0.983	0.968	0.660	1.747	0.801	1.557	0.563	1.209
	263	NM_021972	SPHK1	0.992	0.998	1.032	0.579	0.988	0.854	1.714	1.011	1.208
	264	XM_208887	LOC283871	0.809	0.603	0.850	0.670	0.901	0.538	1.208	0.670	1.579
	265	NM_006282	STK4	1.000	0.980	0.973	0.792	0.846	0.805	1.263	1.159	1.208
	266	NM_198974	PTK9	0.758	0.917	0.955	0.628	0.978	0.701	1.207	0.938	1.362
	267	NM_001012331	NTRK1	0.879	1.002	0.942	1.275	0.746	0.781	0.689	1.343	1.207
	268	NM_018208	ETNK2	0.812	1.021	0.990	0.479	1.252	0.820	1.695	0.816	1.206
	269	NM_197972	NME7	1.010	1.013	1.230	0.838	0.897	0.818	1.205	1.129	1.504
	270	NM_003985	TNK1	0.855	0.860	0.938	0.710	0.917	0.716	1.205	0.938	1.310
	271	NM_001260	CDK8	0.923	0.905	0.883	0.766	0.767	0.521	1.205	1.180	1.694
	272	NM_002436	MPP1	0.831	0.792	0.848	1.233	0.493	0.704	0.674	1.608	1.204
273	NM_054111	IHPK3	1.101	1.129	1.097	0.940	0.752	0.912	1.171	1.501	1.202	
274	NM_002576	PAK1	1.039	1.069	0.939	0.866	1.133	0.729	1.201	0.944	1.288	
275	NM_005255	GAK	0.914	0.894	0.858	0.762	1.188	0.525	1.200	0.752	1.635	
276	NM_152386	SGPP2	0.854	0.750	0.908	0.706	0.687	0.757	1.210	1.092	1.199	
30	277	NM_006213	PHKG1	0.887	0.980	0.900	0.977	0.783	0.751	0.908	1.252	1.198
	278	NM_017572	MKNK2	0.959	0.922	0.967	0.754	0.994	0.808	1.273	0.928	1.197
	279	NM_152542	DKFZp761G058	0.840	0.816	0.831	1.626	0.663	0.694	0.517	1.231	1.197
	280	NM_004225	MFHAS1	0.953	0.926	1.008	0.468	0.775	0.870	2.037	1.196	1.159
	281	NM_016478	NIPA	0.903	0.859	1.029	0.725	0.718	1.052	1.245	1.195	0.979
	282	NM_001018066	NTRK2	0.894	0.851	0.895	0.765	0.712	0.700	1.169	1.194	1.279
	283	NM_001006944	RPS6KA4	0.861	0.958	0.905	0.674	0.804	0.879	1.277	1.192	1.029
	284	NM_014787	DNAJC6	0.879	1.055	1.054	0.996	0.630	0.886	0.883	1.676	1.190
	285	NM_002880	RAF1	0.984	1.065	0.944	0.827	1.046	0.792	1.190	1.018	1.193
	286	NM_004438	EPHA4	0.911	1.031	0.816	1.047	0.807	0.686	0.870	1.278	1.190
	287	NM_005235	ERBB4	0.873	0.815	1.008	0.734	1.458	0.807	1.189	0.559	1.250

CI	rank	NCBI RefSeq	gene symbol	rel. viability untreated			rel. viability TNF and CHX			death index		
				siRNA 1	siRNA 2	siRNA 3	siRNA 1	siRNA 2	siRNA 3	siRNA 1	siRNA 2	siRNA 3
80	288	NM_002401	MAP3K3	1.081	0.995	1.022	0.909	0.844	0.729	1.189	1.178	1.402
	289	NM_004612	TGFBR1	1.044	1.145	1.024	0.975	0.613	0.862	1.071	1.867	1.187
	290	NM_053006	STK22B	1.057	1.054	1.087	0.891	1.012	0.759	1.187	1.042	1.433
	291	NM_198435	STK6	0.983	0.844	1.043	0.767	0.755	0.879	1.282	1.117	1.186
	292	XM_497521	LOC441777	0.919	0.995	0.943	0.776	1.309	0.465	1.185	0.760	2.027
	293	NM_080790	ACPT	0.770	0.718	0.899	1.171	0.599	0.760	0.658	1.200	1.182
	294	NM_015191	SIK2	0.877	0.901	0.877	0.743	0.645	0.918	1.181	1.396	0.955
	295	NM_004567	PFKFB4	1.015	0.898	0.823	0.861	0.968	0.296	1.180	0.928	2.777
	296	NM_004196	CDKL1	0.852	0.955	0.953	0.413	0.880	0.807	2.064	1.084	1.180
	297	NM_021643	TRIB2	0.839	0.912	0.909	0.711	0.363	1.760	1.179	2.515	0.517
	298	NM_016282	AK3L1	0.936	1.218	1.233	1.034	1.034	0.810	0.905	1.179	1.523
	299	NM_014874	MFN2	0.894	0.875	0.546	0.761	1.162	0.314	1.175	0.753	1.738
	300	NM_006721	ADK	0.827	0.454	0.866	0.492	0.388	0.945	1.680	1.171	0.917
	301	NM_002765	PRPS2	0.949	0.820	0.903	0.921	0.701	0.741	1.030	1.170	1.218
	302	NM_003558	PIP5K1B	0.836	0.480	0.824	1.555	0.410	0.633	0.538	1.170	1.302
	303	NM_000476	AK1	1.027	1.048	0.974	0.878	0.797	0.995	1.170	1.315	0.979
	304	NM_020666	CLK4	1.049	0.592	0.858	1.115	0.506	0.603	0.940	1.169	1.423
	305	NM_024594	PANK3	0.859	1.039	0.940	1.432	0.870	0.804	0.600	1.195	1.169
	306	NM_015028	KIAA0551	0.961	0.930	0.859	0.659	0.797	0.878	1.459	1.167	0.979
	307	NM_002717	PPP2R2A	0.800	0.830	0.883	1.105	0.711	0.478	0.725	1.167	1.849
	308	NM_0010318 12	CSNK1G3	0.863	1.016	1.105	0.355	0.947	0.947	2.429	1.074	1.167
	309	NM_013233	STK39	0.849	1.058	0.890	0.728	1.437	0.716	1.165	0.736	1.243
	310	NM_024025	MGC1136	0.834	0.938	0.815	0.707	0.805	1.126	1.179	1.164	0.724
	311	NM_018216	PANK4	0.761	0.951	0.831	0.654	0.783	0.813	1.164	1.214	1.022
	312	NM_021133	RNASEL	0.820	0.806	0.899	0.706	0.487	0.853	1.161	1.656	1.054
	313	NM_007079	PTP4A3	0.919	0.823	0.884	0.672	0.979	0.763	1.367	0.841	1.159
	314	NM_138633	AKAP7	0.860	0.773	0.813	1.027	0.593	0.702	0.838	1.303	1.159
	315	NM_014839	LPPR4	0.788	0.603	0.861	0.664	0.919	0.744	1.188	0.656	1.158
	316	NM_005881	BCKDK	1.024	0.937	1.043	0.861	0.809	0.948	1.189	1.158	1.101
	317	NM_198269	HIPK1	1.304	1.019	0.964	0.724	0.881	0.882	1.801	1.157	1.093
	318	NM_001248	ENTPD3	0.656	0.659	0.839	0.567	0.464	1.042	1.157	1.420	0.805
	319	NM_014911	AAK1	0.684	0.916	0.776	0.772	0.502	0.671	0.886	1.823	1.157
	320	NM_199347	LOC375328	0.937	0.955	1.064	0.990	0.643	0.921	0.947	1.484	1.155
	321	NM_012474	UCK2	0.874	0.912	0.867	0.934	0.789	0.700	0.936	1.155	1.237
	322	NM_025144	LAK	0.950	0.990	0.989	0.708	0.857	0.872	1.341	1.155	1.133
	323	XM_497141	LOC441511	0.799	0.852	0.844	0.474	0.738	0.840	1.685	1.155	1.005
	324	NM_032844	MASTL	0.863	0.925	0.904	0.749	0.836	0.758	1.152	1.107	1.192
	325	NM_020791	KIAA1361	0.931	0.510	0.964	0.917	0.405	0.837	1.016	1.258	1.152
326	NM_002758	MAP2K6	0.712	0.843	0.826	0.663	0.508	0.717	1.074	1.660	1.151	
327	NM_002711	PPP1R3A	0.912	1.077	0.928	0.933	0.874	0.807	0.978	1.233	1.150	
328	NM_003618	MAP4K3	0.994	1.047	0.806	0.510	1.051	0.702	1.951	0.997	1.149	

CI	rank	NCBI RefSeq	gene symbol	rel. viability untreated			rel. viability TNF and CHX			death index		
				siRNA 1	siRNA 2	siRNA 3	siRNA 1	siRNA 2	siRNA 3	siRNA 1	siRNA 2	siRNA 3
30	329	NM_012401	PLXNB2	1.028	1.262	1.021	0.894	0.642	0.922	1.149	1.966	1.106
	330	NM_022748	TENS1	0.928	0.985	1.051	0.877	0.858	0.759	1.059	1.149	1.385
	331	NM_001031715	FLJ12476	1.005	1.190	1.140	1.089	1.037	0.975	0.923	1.148	1.170
	332	NM_002419	MAP3K11	0.759	0.712	0.854	0.719	0.621	0.588	1.057	1.147	1.453
	333	NM_183048	PRKCBP1	0.709	1.115	0.982	0.618	0.828	1.050	1.147	1.347	0.936
	334	NM_014370	STK23	1.018	1.030	0.891	1.030	0.898	0.620	0.989	1.147	1.438
20	335	NM_004217	AURKB	0.874	0.832	0.799	0.708	0.726	1.001	1.234	1.146	0.798
	336	NM_021132	PPP3CB	0.938	0.791	1.126	0.819	1.260	0.838	1.145	0.628	1.343
	337	NM_001014832	PAK4	0.897	0.918	0.950	0.783	0.829	0.824	1.145	1.107	1.153
	338	NM_004717	DGKI	0.777	1.147	1.020	0.680	0.969	0.987	1.143	1.184	1.033
	339	NM_006296	VRK2	0.838	0.977	0.954	1.238	0.641	0.835	0.677	1.523	1.143
	340	NM_020327	ACVR1B	0.992	0.814	0.919	0.817	0.963	0.805	1.214	0.845	1.142
	341	NM_023109	FGFR1	0.919	0.925	0.892	0.978	0.635	0.781	0.940	1.456	1.142
	342	NM_003331	TYK2	0.812	0.855	0.840	0.539	0.806	0.736	1.506	1.061	1.142
	343	NM_003845	DYRK4	0.871	0.814	0.872	0.669	0.750	0.764	1.302	1.086	1.141
	344	NM_000431	MVK	0.890	1.017	0.868	0.727	0.891	0.881	1.223	1.141	0.985
	345	NM_031313	ALPPL2	0.763	0.720	0.838	0.597	1.495	0.736	1.278	0.482	1.139
	346	XM_499423	MGC26484	0.744	0.795	0.647	0.654	0.803	0.542	1.137	0.990	1.193
	347	NM_178130	TXNDC6	0.926	0.944	1.101	0.919	0.780	0.969	1.008	1.209	1.136
	348	NM_006281	STK3	0.825	0.831	0.867	0.522	0.732	0.928	1.581	1.135	0.934
	349	NM_005192	CDKN3	1.150	1.031	1.094	1.015	1.304	0.537	1.133	0.791	2.038
	350	NM_004336	BUB1	0.870	0.973	0.963	0.768	1.271	0.811	1.133	0.766	1.189
	351	NM_003726	SCAP1	0.879	0.731	0.871	0.733	0.646	1.118	1.199	1.132	0.779
	352	XM_372663	LOC390777	0.813	0.825	0.883	0.719	0.641	1.060	1.131	1.287	0.833
	353	NM_016447	MPP6	0.709	0.889	0.964	0.628	0.712	0.910	1.129	1.248	1.059
	354	NM_003674	CDK10	0.857	0.776	0.904	0.865	0.688	0.719	0.990	1.128	1.256
	355	NM_001007155	NTRK3	0.856	0.774	0.982	0.776	0.390	0.872	1.103	1.987	1.127
	356	NM_201278	MTMR2	0.866	0.690	1.030	1.041	0.590	0.915	0.832	1.170	1.126
	357	NM_152282	FLJ23751	0.843	0.812	0.922	0.608	0.722	0.827	1.387	1.125	1.115
	358	XM_497532	LOC441787	0.857	0.988	0.999	0.762	0.986	0.684	1.125	1.002	1.460
	359	NM_172128	CAMK2D	0.925	0.819	0.909	0.658	0.808	0.808	1.407	1.013	1.125
	360	NM_001211	BUB1B	0.972	0.961	1.006	0.334	0.932	0.895	2.909	1.031	1.125
	361	NM_016441	CRIM1	1.019	1.097	0.854	0.703	1.043	0.760	1.448	1.052	1.124
	362	NM_004935	CDK5	0.908	1.003	0.863	0.954	0.892	0.692	0.951	1.124	1.248
	363	NM_152900	MAGI-3	0.893	1.133	1.196	0.795	1.185	0.499	1.124	0.956	2.399
	364	NM_000061	BTK	1.060	1.124	1.013	0.943	0.499	1.154	1.124	2.251	0.878
	365	NM_002834	PTPN11	0.871	1.112	0.973	1.080	0.962	0.866	0.806	1.156	1.123
	366	NM_145001	STK32A	0.761	0.886	0.837	0.678	1.050	0.656	1.123	0.843	1.276
	367	NM_005793	NME6	0.922	0.951	0.858	0.822	0.873	0.696	1.122	1.089	1.232
	368	NM_004442	EPHB2	1.002	1.011	1.030	0.894	1.184	0.878	1.122	0.854	1.173
	369	NM_020126	SPHK2	1.097	1.079	0.950	0.942	1.100	0.847	1.164	0.981	1.122

CI	rank	NCBI RefSeq	gene symbol	rel. viability untreated			rel. viability TNF and CHX			death index		
				siRNA 1	siRNA 2	siRNA 3	siRNA 1	siRNA 2	siRNA 3	siRNA 1	siRNA 2	siRNA 3
20	370	NM_016542	MST4	0.927	1.002	0.785	0.827	1.039	0.593	1.121	0.964	1.323
	371	NM_002577	PAK2	0.945	0.953	0.974	1.019	0.721	0.869	0.928	1.322	1.121
	372	NM_001619	ADRBK1	1.063	1.150	1.114	0.759	1.247	0.994	1.400	0.923	1.121
	373	NM_017813	FLJ20421	0.860	0.708	1.227	0.768	1.030	0.820	1.120	0.688	1.496
	374	NM_001699	AXL	1.073	1.062	0.872	1.156	0.948	0.747	0.928	1.120	1.167
	375	XM_372705	LOC390877	0.833	0.963	0.921	0.744	0.952	0.710	1.120	1.012	1.297
	376	NM_005401	PTPN14	1.036	0.989	1.122	0.951	0.855	1.004	1.090	1.157	1.118
	377	NM_178564	LOC340371	0.763	0.821	0.881	0.691	0.734	0.715	1.104	1.118	1.232
	378	NM_004685	MTMR6	0.946	0.955	1.090	0.601	0.962	0.976	1.575	0.993	1.118
	379	XM_291141	MAST4	1.031	0.933	0.983	0.993	0.657	0.881	1.038	1.420	1.117
	380	NM_152835	LOC149420	0.881	0.938	0.860	0.789	0.987	0.749	1.117	0.950	1.147
	381	NM_017927	MFN1	0.938	0.918	0.829	0.753	0.834	0.742	1.245	1.101	1.117
	382	NM_005009	NME4	0.874	0.835	0.893	0.784	0.689	1.124	1.116	1.212	0.794
	383	NM_182687	PKMYT1	0.761	0.835	0.963	0.683	0.628	1.042	1.115	1.330	0.925
	384	NM_030949	PPP1R14C	0.646	0.848	1.024	0.580	0.694	1.307	1.115	1.222	0.783
	385	NM_015466	PTPN23	0.845	0.861	0.830	0.758	0.872	0.663	1.115	0.988	1.252
	386	NM_080876	DUSP19	0.859	0.852	0.842	0.418	0.965	0.756	2.055	0.883	1.114
	387	NM_032028	STK22D	1.058	0.974	0.802	1.320	0.874	0.589	0.801	1.114	1.362
	388	XM_496112	LOC440332	0.791	0.974	0.960	0.757	0.732	0.861	1.046	1.330	1.114
	389	NM_001005912	IHPK2	1.020	0.994	0.910	0.934	0.715	0.817	1.092	1.390	1.114
	390	NM_138387	G6PC3	1.040	0.868	0.996	0.916	0.780	0.912	1.136	1.112	1.092
	391	NM_031464	RPS6KL1	0.803	1.093	0.854	0.987	0.983	0.486	0.813	1.112	1.758
	392	NM_139158	ALS2CR7	1.022	1.026	0.991	0.658	0.948	0.891	1.553	1.082	1.112
	393	NM_201284	EGFR	1.000	0.894	0.830	0.861	1.234	0.747	1.162	0.724	1.111
	394	NM_032409	PINK1	0.854	0.992	1.142	0.872	0.845	1.028	0.979	1.174	1.111
	395	NM_004687	MTMR4	0.721	0.692	0.952	0.530	0.935	0.857	1.361	0.740	1.111
	396	NM_001012418	LOC340156	0.823	0.828	0.870	0.742	1.342	0.692	1.110	0.616	1.258
	397	NM_016616	TXNDC3	0.796	0.922	0.938	0.790	0.616	0.846	1.008	1.498	1.108
	398	NM_002755	MAP2K1	0.989	0.987	0.932	0.842	1.118	0.841	1.175	0.883	1.108
	399	NM_004721	MAP3K13	0.902	0.847	1.073	1.211	0.765	0.706	0.745	1.108	1.519
	400	NM_182471	PKM2	0.873	0.931	0.829	0.669	0.840	0.756	1.304	1.108	1.096
	401	NM_000252	MTM1	0.881	0.845	0.910	1.330	0.763	0.660	0.662	1.108	1.379
	402	NM_005356	LCK	0.813	0.741	0.868	1.074	0.622	0.783	0.757	1.192	1.108
	403	XM_372749	LOC390975	0.882	0.872	0.922	0.796	0.509	1.035	1.107	1.713	0.891
	404	NM_012224	NEK1	0.895	0.946	0.953	0.808	0.829	1.112	1.107	1.141	0.857
	405	NM_023923	PHACTR4	0.911	0.937	0.932	0.835	0.774	0.842	1.091	1.210	1.107
	406	NM_198291	SRC	1.019	0.869	0.889	1.217	0.785	0.796	0.837	1.107	1.117
	407	NM_005540	INPP5B	0.877	0.890	0.937	0.793	0.956	0.758	1.105	0.931	1.236
	408	NM_001013742	DGKK	0.900	0.921	0.873	0.816	1.113	0.754	1.104	0.828	1.157
409	NM_002497	NEK2	0.927	0.845	0.923	0.841	0.585	1.053	1.103	1.443	0.877	
410	NM_080836	STK35	0.879	0.988	0.812	0.675	0.895	1.143	1.303	1.103	0.710	

CI	rank	NCBI RefSeq	gene symbol	rel. viability untreated			rel. viability TNF and CHX			death index		
				siRNA 1	siRNA 2	siRNA 3	siRNA 1	siRNA 2	siRNA 3	siRNA 1	siRNA 2	siRNA 3
20	411	NM_014142	NUDT5	0.858	0.832	0.946	0.706	0.755	0.954	1.215	1.102	0.992
	412	NM_033346	BMPR2	0.990	1.013	1.022	0.852	1.231	0.927	1.162	0.823	1.102
	413	NM_007181	MAP4K1	0.885	0.675	0.743	0.749	0.629	0.674	1.182	1.074	1.102
	414	NM_021963	NAP1L2	0.679	0.867	0.955	1.087	0.787	0.627	0.624	1.101	1.523
	415	NM_207519	ZAP70	0.769	0.882	0.958	0.661	1.025	0.871	1.163	0.860	1.100
	416	NM_001616	ACVR2	1.083	0.982	1.005	0.402	1.004	0.915	2.691	0.978	1.099
	417	XM_497861	LOC339819	0.732	0.888	0.781	0.460	0.808	0.749	1.589	1.099	1.043
	418	NM_018571	ALS2CR2	0.975	0.968	1.032	0.888	0.972	0.826	1.098	0.997	1.249
10	419	NM_032538	TTBK1	0.901	1.063	1.030	1.114	0.834	0.940	0.809	1.274	1.096
	420	NM_030768	ILKAP	0.838	0.862	0.722	0.765	0.793	0.580	1.095	1.086	1.244
	421	NM_006305	ANP32A	0.857	0.953	0.718	1.587	0.686	0.656	0.540	1.390	1.095
	422	NM_152776	MGC40579	1.028	1.137	1.096	0.938	1.302	0.996	1.095	0.873	1.100
	423	NM_000208	INSR	0.988	1.000	0.919	0.830	1.059	0.839	1.191	0.945	1.095
	424	NM_023018	FLJ13052	0.787	1.008	0.980	0.855	0.921	0.806	0.921	1.095	1.217
	425	XM_496065	ANP32F	0.969	0.986	0.905	0.504	0.900	1.381	1.923	1.095	0.656
	426	NM_003898	SYNJ2	0.832	0.852	0.982	0.898	0.779	0.581	0.927	1.093	1.691
	427	NM_138733	PGK2	1.033	0.994	0.940	1.001	0.909	0.810	1.031	1.093	1.161
	428	NM_018159	NUDT11	0.859	0.705	1.052	0.786	0.717	0.958	1.093	0.984	1.097
	429	NM_000314	PTEN	0.926	0.945	1.006	0.500	0.961	0.921	1.853	0.984	1.093
	430	NM_024779	PIP5K2C	1.068	1.040	0.955	1.166	0.939	0.875	0.916	1.108	1.091
	431	NM_017900	AKIP	0.806	1.002	0.758	0.871	0.919	0.395	0.925	1.090	1.917
	432	NM_001789	CDC25A	0.877	1.011	0.576	1.048	0.826	0.529	0.837	1.225	1.090
	433	NM_025195	TRIB1	0.901	1.015	0.976	0.898	0.859	0.896	1.004	1.182	1.089
	434	NM_020152	C21orf7	0.917	0.986	0.890	0.842	0.843	0.817	1.089	1.170	1.089
	435	NM_152534	FLJ32685	0.899	0.869	0.957	0.827	0.668	0.912	1.087	1.301	1.049
	436	NM_005539	INPP5A	0.867	0.843	0.875	0.798	1.609	0.731	1.087	0.524	1.198
	437	XM_498294	LOC392265	0.927	0.970	0.952	0.854	0.735	1.068	1.086	1.320	0.892
	438	NM_004103	PTK2B	0.996	0.935	0.960	1.088	0.831	0.885	0.916	1.124	1.085
	439	NM_001346	DGKG	0.829	0.795	0.847	0.893	0.698	0.780	0.928	1.138	1.085
	440	NM_052984	CDK4	0.776	0.807	0.867	0.411	1.184	0.799	1.888	0.681	1.085
	441	NM_006207	PDGFRL	0.981	1.003	0.921	0.905	1.285	0.789	1.084	0.781	1.167
	442	NM_000858	GUK1	0.843	0.868	0.903	0.584	1.155	0.833	1.443	0.752	1.084
	443	NM_001626	AKT2	0.800	0.749	0.723	0.873	0.373	0.668	0.917	2.008	1.083
	444	NM_080685	PTPN13	0.984	0.991	1.168	0.909	1.013	0.796	1.083	0.978	1.466
	445	NM_001486	GCKR	0.811	0.689	0.766	0.749	0.465	0.769	1.083	1.483	0.997
	446	NM_001001852	PIM3	0.886	0.950	0.913	1.108	0.878	0.559	0.799	1.082	1.633
	447	NM_005184	CALM3	1.035	0.926	0.971	0.577	0.856	1.055	1.796	1.081	0.920
	448	NM_014920	ICK	1.042	1.078	1.104	0.927	1.089	1.021	1.124	0.990	1.081
	449	NM_177533	NUDT14	0.853	0.911	0.762	0.790	0.635	0.840	1.081	1.434	0.907
	450	NM_032037	SSTK	1.062	1.034	1.069	0.932	0.956	1.256	1.139	1.081	0.851
	451	NM_001014432	AKT1	0.925	0.865	0.918	0.753	0.801	0.968	1.229	1.080	0.949

CI	rank	NCBI RefSeq	gene symbol	rel. viability untreated			rel. viability TNF and CHX			death index		
				siRNA 1	siRNA 2	siRNA 3	siRNA 1	siRNA 2	siRNA 3	siRNA 1	siRNA 2	siRNA 3
10	452	NM_152880	PTK7	0.905	0.617	0.909	0.839	0.626	0.505	1.079	0.986	1.800
	453	NM_017823	DUSP23	0.956	0.985	0.857	0.886	0.882	1.004	1.079	1.117	0.853
	454	NM_203453	LOC403313	0.756	0.617	0.905	0.701	0.597	0.593	1.078	1.033	1.527
	455	NM_031432	UCK1	1.025	0.971	0.951	1.144	0.901	0.755	0.896	1.077	1.261
	456	NM_025194	ITPKC	0.912	0.962	1.048	1.209	0.862	0.974	0.754	1.117	1.076
	457	NM_006712	FASTK	0.912	0.914	0.974	0.931	0.682	0.905	0.979	1.340	1.076
	458	NM_006176	NRGN	0.947	0.993	0.986	0.862	0.923	0.968	1.098	1.075	1.018
	459	NM_002376	MARK3	0.895	1.078	0.965	0.416	1.003	0.936	2.154	1.075	1.031
	460	NM_006201	PCTK1	0.949	0.925	0.989	0.883	1.218	0.671	1.074	0.759	1.473
	461	NM_201554	DGKA	0.923	0.980	0.863	0.487	1.006	0.804	1.895	0.974	1.074
	462	NM_014225	PPP2R1A	0.653	0.903	0.738	0.609	1.064	0.486	1.074	0.848	1.518
	463	NM_002944	ROS1	1.004	1.058	1.097	1.058	0.986	0.584	0.949	1.073	1.880
	464	NM_176789	MTMR1	0.519	0.904	1.067	0.493	0.843	0.944	1.052	1.073	1.130
	465	NM_017988	FLJ10074	0.860	0.962	0.926	0.803	0.950	0.852	1.071	1.013	1.087
	466	NM_005100	AKAP12	0.805	0.883	0.892	0.751	0.479	0.911	1.071	1.843	0.979
	467	NM_004954	MARK2	0.964	0.860	0.859	0.900	0.979	0.756	1.071	0.878	1.138
	468	NM_004383	CSK	0.941	0.922	0.891	0.788	0.862	0.971	1.194	1.070	0.917
	469	NM_153710	C9orf96	0.838	0.858	0.936	0.784	0.962	0.807	1.070	0.892	1.161
	470	NM_007254	PNKP	0.913	0.836	0.864	0.615	0.825	0.807	1.485	1.013	1.070
	471	NM_130435	PTPRE	0.985	1.165	1.018	1.035	0.797	0.952	0.952	1.462	1.070
	472	NM_178170	NEK8	0.771	0.874	0.843	0.936	0.817	0.597	0.824	1.069	1.412
	473	XM_497433	LOC441708	0.878	1.050	0.786	0.821	0.844	1.553	1.069	1.244	0.506
	474	NM_005983	SKP2	0.989	1.032	0.917	0.870	0.966	1.032	1.136	1.069	0.889
	475	NM_006259	PRKG2	0.943	0.873	0.932	0.459	0.817	1.002	2.057	1.069	0.930
	476	NM_172083	CAMK2B	0.945	0.830	0.877	0.930	0.626	0.821	1.017	1.327	1.069
	477	NM_203488	ACYP1	0.770	0.594	0.856	0.508	0.556	0.974	1.514	1.067	0.878
	478	NM_007170	TESK2	0.875	0.880	1.026	1.000	0.825	0.838	0.875	1.067	1.223
	479	NM_0010246 46	CLK1	0.927	0.994	0.766	0.765	0.931	1.595	1.213	1.067	0.480
	480	NM_198452	PNCK	0.819	0.969	0.923	0.414	1.093	0.865	1.978	0.886	1.067
	481	NM_018423	STYK1	0.466	1.077	1.027	0.381	1.119	0.963	1.224	0.962	1.067
	482	NM_007039	PTPN21	0.935	0.927	0.918	0.680	0.869	0.872	1.374	1.067	1.053
	483	NM_003718	CDC2L5	0.901	0.934	0.930	0.845	1.243	0.588	1.066	0.751	1.580
	484	NM_003137	SRPK1	0.979	1.123	0.901	1.161	1.054	0.834	0.843	1.065	1.080
	485	NM_002829	PTPN3	0.792	0.815	0.817	1.257	0.765	0.682	0.630	1.065	1.198
	486	NM_153361	MGC42105	0.909	0.860	0.922	0.806	0.808	1.009	1.128	1.065	0.914
	487	NM_005030	PLK1	0.382	0.624	0.414	0.359	0.493	0.505	1.065	1.264	0.820
	488	NM_016123	IRAK4	1.080	0.843	0.858	0.912	0.793	1.498	1.185	1.064	0.573
	489	NM_145687	MAP4K4	1.071	0.994	0.984	1.009	1.026	0.684	1.062	0.968	1.438
	490	NM_032430	KIAA1811	0.990	1.093	0.855	1.102	1.024	0.806	0.899	1.067	1.061
	491	NM_181677	PPP2R2B	0.775	0.846	0.835	0.808	0.729	0.787	0.960	1.160	1.061
	492	NM_002498	NEK3	0.888	0.799	0.833	0.838	0.675	0.840	1.060	1.183	0.991

CI	rank	NCBI RefSeq	gene symbol	rel. viability untreated			rel. viability TNF and CHX			death index		
				siRNA 1	siRNA 2	siRNA 3	siRNA 1	siRNA 2	siRNA 3	siRNA 1	siRNA 2	siRNA 3
10	493	NM_005393	PLXNB3	0.847	0.941	1.110	0.747	0.888	1.501	1.135	1.060	0.740
	494	NM_014264	PLK4	0.929	1.000	0.980	0.877	0.872	0.985	1.060	1.147	0.995
	495	NM_003390	WEE1	0.842	0.860	0.634	0.716	1.295	0.598	1.176	0.664	1.060
	496	NM_033215	PPP1R3F	1.028	1.051	0.715	1.262	0.803	0.675	0.814	1.309	1.059
	497	NM_022128	RBKS	0.792	1.062	1.012	0.652	1.004	1.018	1.215	1.058	0.994
	498	NM_005108	XYLB	0.837	0.850	1.101	0.877	0.804	0.965	0.954	1.057	1.142
	499	NM_198532	C19orf35	0.852	1.048	0.984	0.852	0.991	0.882	1.000	1.057	1.116
	500	NM_080917	DGUOK	0.737	0.845	0.840	0.332	0.800	0.851	2.221	1.056	0.986
	501	NM_004783	TAO1	0.887	0.854	0.929	0.968	0.645	0.880	0.917	1.323	1.056
	502	NM_022975	FGFR2	0.916	0.786	0.837	1.109	0.585	0.793	0.825	1.345	1.056
	503	NM_005813	PRKCN	0.832	0.983	0.993	0.788	0.740	1.010	1.056	1.329	0.983
	504	NM_001014796	DDR2	0.799	0.684	1.044	1.143	0.549	0.989	0.699	1.246	1.055
	505	NM_030952	SNARK	1.034	1.009	1.117	0.981	1.077	0.916	1.054	0.937	1.220
	506	NM_002350	LYN	0.947	1.084	0.989	0.898	0.942	0.941	1.054	1.150	1.051
	507	NM_172199	AK2	0.929	0.957	0.950	0.957	0.908	0.725	0.971	1.054	1.310
	508	NM_016276	SGK2	0.946	0.807	0.896	0.838	0.798	0.851	1.129	1.012	1.053
	509	NM_153050	MTMR3	0.840	0.693	0.950	0.798	0.614	0.909	1.053	1.128	1.045
	510	NM_001292	CLK3	0.954	0.900	0.899	0.906	1.174	0.703	1.053	0.767	1.279
	511	XM_047355	KIAA1765	0.854	1.017	0.895	0.811	0.939	0.993	1.053	1.083	0.901
	512	NM_018979	PRKWINK1	1.022	1.058	0.884	0.970	0.831	1.106	1.053	1.273	0.799
	513	NM_014413	HRI	0.985	1.171	0.990	1.182	1.112	0.923	0.833	1.053	1.073
	514	NM_001006665	RPS6KA1	0.836	0.953	0.869	0.794	0.742	1.101	1.053	1.283	0.790
	515	NM_002407	SCGB2A1	0.945	1.048	1.002	1.066	0.529	0.952	0.886	1.982	1.052
	516	NM_030948	PHACTR1	0.904	0.969	1.002	0.765	1.105	0.952	1.182	0.877	1.052
	517	NM_002037	FYN	1.003	0.921	0.884	0.508	1.002	0.841	1.972	0.919	1.052
	518	NM_005044	PRKX	0.817	0.805	0.824	0.777	0.356	1.044	1.052	2.265	0.789
	519	NM_177543	PPAP2C	0.836	0.873	0.953	0.531	0.986	0.906	1.574	0.885	1.051
	520	NM_001025105	CSNK1A1	0.939	1.033	0.960	0.789	0.983	0.986	1.190	1.051	0.974
	521	NM_006724	MAP3K4	1.221	0.960	0.986	0.914	0.913	1.114	1.336	1.051	0.885
	522	NM_001024847	TGFBR2	1.011	0.935	0.951	0.817	0.891	1.125	1.237	1.050	0.845
	523	NM_002020	FLT4	0.944	0.864	0.810	0.899	0.516	0.942	1.050	1.676	0.861
	524	NM_006241	PPP1R2	0.855	0.933	0.810	0.451	0.890	0.783	1.897	1.049	1.034
	525	NM_006482	DYRK2	0.975	0.855	0.868	0.929	0.658	1.468	1.049	1.299	0.591
526	NM_005211	CSF1R	0.948	1.039	1.081	0.786	0.990	1.168	1.207	1.049	0.925	
527	NM_006039	MRC2	0.878	0.968	0.940	0.885	0.924	0.896	0.992	1.049	1.049	
528	NM_012403	ANP32C	0.932	0.978	0.950	0.599	0.934	0.968	1.558	1.048	0.982	
529	NM_033508	GCK	0.803	0.827	0.767	0.695	0.789	1.046	1.156	1.047	0.733	
530	NM_006622	PLK2	1.075	0.884	0.905	0.727	0.845	1.050	1.480	1.046	0.862	
531	NM_014634	PPM1F	0.940	0.901	0.909	0.625	0.862	0.871	1.504	1.046	1.044	
532	NM_145059	FUK	0.926	1.031	0.895	1.020	0.925	0.856	0.908	1.115	1.046	
533	NM_005443	PAPSS1	1.002	0.917	1.048	0.655	0.877	1.955	1.530	1.045	0.536	

CI	rank	NCBI RefSeq	gene symbol	rel. viability untreated			rel. viability TNF and CHX			death index		
				siRNA 1	siRNA 2	siRNA 3	siRNA 1	siRNA 2	siRNA 3	siRNA 1	siRNA 2	siRNA 3
10	534	NM_002446	MAP3K10	0.940	0.964	0.949	0.722	1.241	0.908	1.301	0.776	1.045
	535	NM_198527	MGC45386	0.783	0.823	0.898	0.724	0.890	0.859	1.081	0.925	1.045
	536	XM_370939	LOC388221	0.877	0.888	0.843	0.839	1.491	0.739	1.044	0.596	1.140
	537	NM_052827	CDK2	0.979	0.913	0.653	0.964	0.875	0.428	1.016	1.044	1.528
	538	NM_021923	FGFRL1	0.938	1.133	0.773	1.237	1.085	0.592	0.758	1.044	1.306
	539	NM_003557	PIP5K1A	0.943	0.927	0.989	1.115	0.705	0.948	0.846	1.315	1.043
	540	NM_020630	RET	0.792	0.683	0.895	1.116	0.605	0.858	0.709	1.129	1.043
	541	NM_014931	KIAA1115	0.931	0.955	0.914	1.198	0.898	0.877	0.777	1.064	1.043
	542	NM_016281	JIK	0.820	0.972	1.206	1.137	0.933	0.933	0.721	1.042	1.292
	543	NM_001274	CHEK1	0.963	1.030	1.015	0.858	0.989	1.233	1.122	1.042	0.823
	544	NM_001825	CKMT2	0.936	0.884	0.922	0.987	0.498	0.886	0.949	1.774	1.040
	545	NM_006384	CIB1	0.900	0.744	1.014	0.867	0.591	1.050	1.039	1.259	0.965
	546	NM_007314	ABL2	0.834	0.817	0.927	0.523	0.787	1.003	1.596	1.038	0.925
	547	NM_015716	MINK	0.883	1.050	1.057	0.876	1.012	0.323	1.008	1.038	3.272
	548	NM_004329	BMPR1A	0.989	0.998	0.938	0.693	0.963	1.173	1.427	1.037	0.800
	549	NM_004537	NAP1L1	0.880	0.946	0.929	0.841	0.939	0.898	1.047	1.008	1.035
	550	NM_033066	MPP4	0.968	1.105	0.946	1.155	0.948	0.916	0.838	1.165	1.033
	551	NM_001033057	BAIAP1	0.962	0.868	1.006	1.227	0.841	0.874	0.784	1.032	1.151
	552	XM_373298	LOC392347	0.934	0.962	0.933	0.905	0.873	1.128	1.032	1.102	0.827
	553	NM_022485	FLJ22405	0.803	0.886	0.741	0.778	1.126	0.642	1.031	0.787	1.154
	554	NM_017607	PPP1R12C	0.959	0.880	1.011	0.830	0.854	1.032	1.156	1.031	0.979
	555	XM_496862	LOC441215	0.712	0.857	0.798	0.691	0.632	1.093	1.031	1.355	0.730
	556	NM_001025242	IRAK1	0.929	0.905	0.826	0.843	1.156	0.802	1.102	0.782	1.030
	557	XM_375632	LOC400708	0.861	0.793	0.824	0.923	0.770	0.792	0.933	1.030	1.041
	558	NM_001018041	EPM2A	0.787	0.779	0.832	0.835	0.757	0.569	0.942	1.029	1.463
	559	NM_017677	MTMR8	0.905	0.909	0.922	0.880	0.950	0.872	1.028	0.958	1.057
	560	NM_001278	CHUK	0.948	0.896	0.883	0.877	0.872	0.884	1.082	1.027	0.998
	561	NM_024876	ADCK4	0.917	0.942	0.868	0.808	0.918	0.968	1.135	1.027	0.896
	562	NM_001222	CAMK2G	0.996	0.946	1.074	0.886	1.503	1.046	1.124	0.629	1.026
	563	NM_004586	RPS6KA3	1.147	0.998	1.014	0.906	1.017	0.989	1.266	0.982	1.025
	564	NM_014238	XM_290793	0.878	0.924	0.818	0.857	0.957	0.489	1.024	0.965	1.673
	565	NM_004670	PAPSS2	1.007	0.832	1.003	0.790	0.813	0.983	1.274	1.024	1.020
	566	NM_006488	KHK	0.753	0.801	0.837	1.035	0.783	0.448	0.727	1.024	1.868
	567	NM_002044	GALK2	1.059	1.002	1.002	1.035	1.093	0.846	1.024	0.916	1.184
	568	NM_005374	MPP2	0.926	0.817	0.828	0.904	0.821	0.581	1.024	0.996	1.425
	569	NM_001249	ENTPD5	0.906	0.947	0.875	0.813	0.926	1.066	1.115	1.023	0.821
	570	NM_145910	NEK11	0.897	0.760	1.031	0.878	0.756	0.950	1.022	1.006	1.085
	571	NM_004577	PSPH	0.904	0.819	0.762	0.885	0.635	1.153	1.022	1.289	0.661
	572	NM_004690	LATS1	0.853	0.951	1.050	0.835	1.238	0.853	1.021	0.768	1.231
	573	NM_003177	SYK	0.791	0.915	0.912	0.648	0.904	0.894	1.219	1.012	1.020
574	NM_000291	PGK1	0.846	0.880	0.902	0.928	0.863	0.770	0.912	1.020	1.171	

CI	rank	NCBI RefSeq	gene symbol	rel. viability untreated			rel. viability TNF and CHX			death index		
				siRNA 1	siRNA 2	siRNA 3	siRNA 1	siRNA 2	siRNA 3	siRNA 1	siRNA 2	siRNA 3
10	575	NM_020922	PRKWNK3	0.890	1.126	0.942	0.975	0.881	0.924	0.912	1.278	1.020
	576	NM_001001875	NYD-SP25	0.864	0.880	0.935	1.039	0.561	0.917	0.832	1.568	1.019
	577	NM_003629	PIK3R3	0.808	0.844	0.842	1.101	0.828	0.526	0.733	1.019	1.602
	578	NM_173641	FLJ33655	0.948	1.000	1.062	0.454	0.982	1.291	2.087	1.019	0.822
	579	NM_007240	DUSP12	0.838	0.948	0.826	1.215	0.880	0.811	0.690	1.076	1.018
	580	XM_496234	LOC440451	0.845	0.958	0.912	0.848	0.941	0.889	0.996	1.018	1.026
	581	NM_001004056	GRK4	0.744	0.731	0.772	0.731	0.374	0.873	1.018	1.953	0.884
	582	NM_004538	NAP1L3	0.939	0.801	0.887	0.911	0.824	0.871	1.031	0.973	1.018
	583	NM_198465	NRK	0.833	0.866	0.913	0.819	1.364	0.882	1.017	0.635	1.035
	584	NM_001631	ALPI	0.910	0.899	0.891	1.028	0.885	0.590	0.885	1.017	1.510
	585	NM_014586	HUNK	0.962	0.952	0.986	1.045	0.936	0.746	0.921	1.016	1.321
	586	NM_173354	SNF1LK	0.886	0.952	0.912	0.862	0.982	0.898	1.028	0.969	1.016
	587	NM_001203	BMPR1B	0.919	0.965	0.938	1.047	0.951	0.860	0.878	1.015	1.091
	588	NM_199255	TPTE2	0.773	0.857	0.869	0.381	1.010	0.856	2.027	0.849	1.015
	589	NM_139014	MAPK14	1.098	0.808	0.938	1.014	1.153	0.925	1.082	0.701	1.015
	590	NM_006218	PIK3CA	1.000	0.988	1.059	0.987	0.944	1.158	1.013	1.047	0.915
	591	NM_001894	CSNK1E	1.019	1.014	1.010	1.007	1.010	0.932	1.013	1.004	1.084
	592	NM_002646	PIK3C2B	0.927	0.877	0.862	0.971	0.867	0.755	0.955	1.012	1.141
	593	NM_000189	HK2	0.683	0.834	0.828	0.365	0.825	0.824	1.870	1.012	1.004
	594	NM_032960	MAPKAPK2	0.895	0.895	0.994	0.886	0.929	0.560	1.010	0.964	1.774
	595	NM_005424	TIE	0.919	0.873	0.866	0.781	1.000	0.857	1.177	0.873	1.010
	596	NM_004579	MAP4K2	0.863	0.827	1.061	1.711	0.677	1.052	0.504	1.221	1.009
	597	NM_018492	TOPK	0.951	1.030	1.067	0.860	1.050	1.059	1.106	0.981	1.008
	598	NM_007313	ABL1	1.008	1.001	0.974	0.553	1.196	0.967	1.822	0.837	1.008
	599	NM_016508	CDKL3	1.131	1.105	1.089	1.177	0.989	1.081	0.961	1.117	1.007
	600	NM_002082	GRK6	0.770	0.882	1.080	1.075	0.728	1.072	0.717	1.211	1.007
	601	NM_013254	TBK1	0.878	0.935	0.753	0.872	1.303	0.646	1.007	0.718	1.166
	602	NM_016735	LIMK1	0.993	1.115	0.974	0.986	0.875	1.124	1.007	1.275	0.867
	603	NM_001743	CALM2	0.902	1.080	1.048	1.226	1.066	1.040	0.736	1.013	1.007
	604	NM_007284	PTK9L	1.038	0.904	0.968	0.999	1.001	0.962	1.039	0.904	1.007
605	NM_003215	TEC	1.038	0.923	0.929	1.032	0.803	1.081	1.005	1.149	0.859	
606	NM_012093	AK5	1.071	1.081	1.000	1.095	0.885	0.998	0.978	1.220	1.002	
607	NM_014791	MELK	0.900	0.934	0.960	0.899	1.179	0.948	1.002	0.793	1.013	
608	NM_002716	PPP2R1B	0.886	0.786	0.898	0.559	0.948	0.897	1.586	0.829	1.001	
609	NM_170678	ITGB1BP3	0.880	1.032	0.838	0.977	1.031	0.772	0.901	1.001	1.086	
610	NM_001721	BMX	1.098	1.137	0.837	1.188	0.559	0.836	0.924	2.034	1.001	
10	611	NM_014215	INSRR	0.967	0.953	0.869	0.876	0.972	0.870	1.104	0.981	0.999
	612	NM_004560	ROR2	0.954	0.969	1.011	0.972	0.972	0.969	0.982	0.998	1.043
	613	NM_002612	PDK4	0.843	1.084	0.788	0.845	0.351	1.152	0.997	3.090	0.684
	614	NM_003646	DGKZ	0.838	0.952	0.825	0.873	0.955	0.791	0.961	0.997	1.043
	615	NM_207578	PRKACB	0.950	0.777	0.844	0.953	0.674	1.245	0.997	1.152	0.678

CI	rank	NCBI RefSeq	gene symbol	rel. viability untreated			rel. viability TNF and CHX			death index		
				siRNA 1	siRNA 2	siRNA 3	siRNA 1	siRNA 2	siRNA 3	siRNA 1	siRNA 2	siRNA 3
10	616	NM_022474	MPP5	0.911	0.739	1.070	0.650	0.742	1.359	1.401	0.997	0.788
	617	NM_002595	PCCK2	1.022	1.031	0.943	0.686	1.036	1.067	1.490	0.995	0.884
	618	NM_012301	AIP1	0.913	0.909	0.769	1.097	0.914	0.541	0.832	0.995	1.422
	619	NM_001031801	LIMK2	0.884	1.109	1.137	0.889	1.141	0.802	0.994	0.972	1.418
	620	NM_000875	IGF1R	0.882	0.937	1.049	1.393	0.943	0.558	0.633	0.994	1.880
	621	NM_004073	PLK3	0.853	0.934	0.922	0.885	0.349	0.929	0.963	2.677	0.992
	622	NM_006401	ANP32B	0.968	0.864	0.875	0.976	1.015	0.437	0.992	0.851	2.001
	623	NM_006285	TESK1	0.897	0.779	0.923	0.907	0.332	0.979	0.990	2.342	0.944
	624	NM_020778	MIDORI	1.006	0.972	1.053	0.809	1.001	1.064	1.243	0.971	0.990
	625	NM_173588	FLJ37794	0.858	0.862	0.915	1.218	0.679	0.925	0.705	1.270	0.989
	626	XM_495900	LOC399969	1.002	0.756	0.854	0.830	0.764	1.417	1.208	0.989	0.603
	627	NM_004635	MAPKAPK3	1.133	1.073	0.953	0.747	1.357	0.964	1.516	0.791	0.989
	628	NM_024652	LRRK1	0.922	0.758	0.859	1.164	0.767	0.863	0.792	0.989	0.996
	629	NM_173515	MAGI1	0.975	0.798	1.036	0.986	0.769	1.203	0.989	1.039	0.861
	630	NM_003954	MAP3K14	1.043	0.881	0.899	0.935	1.078	0.910	1.115	0.817	0.988
	631	NM_002742	PRKCM	0.924	1.022	1.015	0.758	1.400	1.027	1.218	0.730	0.988
	632	NM_017525	HSMDPKIN	0.874	1.082	0.911	0.640	1.095	0.999	1.366	0.988	0.912
	633	XM_038150	MAST3	1.039	0.919	0.922	0.748	0.931	0.946	1.388	0.988	0.975
	634	NM_024046	MGC8407	0.753	1.133	0.969	0.430	1.147	1.211	1.752	0.987	0.800
	635	NM_005391	PDK3	0.866	0.809	0.795	0.507	0.861	0.807	1.708	0.939	0.985
	636	NM_022740	HIPK2	0.840	0.788	0.929	0.853	0.602	0.989	0.985	1.308	0.940
	637	NM_033141	MAP3K9	0.844	0.870	0.878	0.604	0.883	0.923	1.397	0.985	0.951
	638	NM_001744	CAMK4	0.863	0.975	0.848	0.597	1.036	0.861	1.446	0.941	0.985
	639	NM_030920	ANP32E	0.958	0.993	0.942	0.663	1.009	1.058	1.445	0.984	0.891
	640	NM_183246	PHACTR3	0.884	0.755	0.921	0.899	0.793	0.469	0.983	0.951	1.965
	641	NM_017567	NAGK	0.857	0.982	0.914	1.020	0.999	0.642	0.840	0.983	1.424
	642	XM_498286	LOC392226	0.915	0.893	0.942	1.037	0.880	0.959	0.882	1.015	0.983
	643	NM_031272	TEX14	0.837	0.906	0.778	1.332	0.922	0.731	0.629	0.983	1.064
	644	XM_055866	LMTK3	1.022	0.893	0.960	1.040	0.676	1.040	0.983	1.321	0.923
	645	NM_133646	ZAK	0.860	0.880	0.866	0.801	0.895	0.982	1.074	0.982	0.881
	646	NM_001033581	PRKCZ	0.812	0.825	0.909	0.826	1.063	0.821	0.982	0.776	1.108
	647	NM_145695	DGKB	0.844	0.845	0.735	1.014	0.675	0.749	0.833	1.251	0.981
	648	NM_002526	NT5E	0.924	0.864	0.844	0.942	0.844	0.962	0.981	1.024	0.878
	649	NM_001005862	ERBB2	0.921	1.009	0.991	1.025	1.029	0.850	0.898	0.980	1.165
	650	NM_052947	HAK	0.958	0.991	0.885	1.026	0.579	0.904	0.933	1.711	0.979
	651	NM_153757	NAP1L5	0.788	0.931	0.960	0.554	1.000	0.981	1.424	0.931	0.979
	652	NM_002648	PIM1	0.843	1.147	1.140	0.970	1.172	0.887	0.869	0.979	1.285
	653	NM_004938	DAPK1	0.982	0.847	0.787	1.004	0.936	0.780	0.978	0.905	1.009
	654	NM_153640	PANK2	0.859	0.922	0.933	0.846	1.125	0.954	1.015	0.820	0.978
	655	NM_005969	NAP1L4	0.903	0.848	0.828	0.924	1.069	0.718	0.978	0.793	1.153
	656	NM_002447	MST1R	0.788	0.956	1.049	1.012	0.978	0.939	0.779	0.978	1.117

CI	rank	NCBI RefSeq	gene symbol	rel. viability untreated			rel. viability TNF and CHX			death index		
				siRNA 1	siRNA 2	siRNA 3	siRNA 1	siRNA 2	siRNA 3	siRNA 1	siRNA 2	siRNA 3
10	657	NM_003159	CDKL5	0.944	1.027	0.962	1.217	1.051	0.718	0.776	0.977	1.339
	658	NM_022126	LHPP	0.897	0.752	0.954	0.724	1.070	0.977	1.240	0.703	0.977
	659	XM_293293	BMP2KL	1.057	1.133	0.984	0.718	2.281	1.008	1.471	0.497	0.976
	660	NM_130474	MADD	1.128	0.910	0.912	1.156	1.027	0.839	0.976	0.886	1.088
	661	NM_003328	TXK	0.917	0.962	1.037	0.940	1.045	0.764	0.976	0.921	1.359
	662	NM_002754	MAPK13	0.778	0.717	0.989	0.796	0.743	1.014	0.977	0.965	0.975
	663	NM_182493	LOC91807	0.956	1.138	1.008	0.825	1.167	1.280	1.159	0.975	0.787
	664	NM_198585	UNQ2492	0.923	0.801	0.876	1.197	0.628	0.899	0.771	1.274	0.975
	665	NM_016507	CRK7	1.014	1.069	1.086	1.161	1.097	1.049	0.874	0.975	1.035
	666	NM_003011	SET	0.945	0.977	0.952	1.124	0.561	0.978	0.841	1.744	0.973
	667	NM_002760	PRKY	0.910	0.823	0.816	0.724	1.026	0.839	1.257	0.802	0.972
	668	NM_052853	ADCK2	0.969	0.874	0.876	0.998	1.019	0.831	0.971	0.858	1.054
	669	NM_002110	HCK	0.754	0.913	0.793	0.891	0.854	0.817	0.847	1.070	0.970
	670	NM_014916	LMTK2	1.021	0.865	0.910	1.019	0.892	1.083	1.002	0.970	0.840
	671	NM_003821	RIPK2	0.862	0.942	0.915	0.889	0.741	1.197	0.969	1.271	0.765
	672	NM_005167	MGC19531	0.829	0.754	0.829	1.113	0.778	0.572	0.744	0.969	1.448
	673	XM_370878	KIAA2002	1.001	1.002	0.938	1.386	1.034	0.830	0.722	0.969	1.130
	674	NM_138981	MAPK10	0.821	0.849	0.912	0.847	1.325	0.778	0.969	0.640	1.173
	675	NM_005808	CTDSPL	0.826	0.917	0.829	1.405	0.906	0.858	0.588	1.012	0.966
	676	NM_002019	FLT1	1.011	0.866	0.855	1.047	0.757	0.966	0.966	1.144	0.885
677	NM_014214	IMPA2	0.711	0.730	0.952	0.733	1.243	0.986	0.971	0.587	0.965	
678	NM_005340	HINT1	0.872	0.844	0.818	0.904	0.269	0.860	0.965	3.143	0.950	
679	NM_001319	CSNK1G2	1.035	1.143	1.016	1.075	1.204	0.861	0.963	0.950	1.180	
680	NM_021135	RPS6KA2	0.791	0.933	0.941	0.821	1.074	0.817	0.963	0.869	1.151	
681	NM_001184	ATR	1.000	0.995	1.002	1.149	1.034	1.008	0.870	0.962	0.993	
682	NM_002759	PRKR	0.828	0.883	1.044	0.886	0.919	0.841	0.934	0.962	1.242	
20	683	NM_138687	PIP5K2B	0.809	0.901	0.942	1.123	0.938	0.587	0.720	0.961	1.603
	684	NM_016086	MK-STYX	0.801	0.869	0.784	0.695	1.167	0.817	1.152	0.745	0.959
	685	NM_014975	MAST1	0.923	0.803	0.969	0.963	0.334	1.179	0.959	2.407	0.822
	686	NM_002481	PPP1R12B	1.006	1.026	0.934	0.625	1.070	1.056	1.610	0.959	0.884
	687	NM_004836	EIF2AK3	0.866	0.952	1.095	0.920	0.994	0.802	0.941	0.958	1.366
	688	NM_002710	PPP1CC	0.815	0.909	0.924	0.851	0.770	0.997	0.957	1.180	0.927
	689	NM_015000	STK38L	0.885	0.962	0.858	0.924	0.993	0.913	0.957	0.969	0.939
	690	NM_182398	RPS6KA5	0.944	0.892	0.870	0.900	0.932	1.455	1.049	0.957	0.598
	691	NM_152224	PPEF1	0.823	0.904	0.870	0.628	1.179	0.910	1.310	0.766	0.956
	692	NM_013410	AK3	0.858	0.896	0.893	0.897	1.052	0.568	0.956	0.852	1.572
	693	NM_153499	CAMKK2	0.884	0.836	0.968	0.961	0.328	1.013	0.920	2.546	0.956
	694	NM_002673	PLXNB1	0.994	0.908	1.078	1.137	0.892	1.129	0.874	1.018	0.955
	695	NM_018312	C11orf23	0.860	0.935	0.916	0.953	0.445	0.959	0.902	2.103	0.954
	696	NM_178813	AKAP28	0.882	0.938	0.872	0.927	0.923	0.927	0.951	1.016	0.940
	697	NM_012404	ANP32D	0.931	0.988	0.833	0.980	0.892	1.178	0.950	1.107	0.707

CI	rank	NCBI RefSeq	gene symbol	rel. viability untreated			rel. viability TNF and CHX			death index		
				siRNA 1	siRNA 2	siRNA 3	siRNA 1	siRNA 2	siRNA 3	siRNA 1	siRNA 2	siRNA 3
20	698	NM_004901	ENTPD4	0.856	0.870	0.802	0.901	0.896	0.936	0.950	0.971	0.856
	699	NM_001381	DOK1	0.872	0.858	0.772	0.918	0.517	0.871	0.950	1.658	0.886
	700	NM_024888	FLJ11535	0.795	0.650	0.994	0.670	0.686	1.079	1.186	0.948	0.921
	701	NM_139354	MATK	0.925	0.941	0.934	0.979	0.997	0.932	0.945	0.944	1.002
	702	NM_152619	MGC45428	0.968	0.878	0.869	1.026	1.004	0.804	0.944	0.875	1.081
	703	NM_133494	NEK7	0.976	0.865	0.868	0.920	1.372	0.920	1.061	0.631	0.944
	704	NM_015251	KIAA0431	0.952	1.066	0.636	1.040	1.130	0.460	0.916	0.944	1.384
	705	NM_022158	FN3K	0.824	0.845	0.847	0.873	0.497	1.128	0.943	1.700	0.751
	706	NM_003948	CDKL2	0.806	0.799	0.928	0.983	0.723	0.984	0.820	1.106	0.943
	707	NM_000051	ATM	1.004	0.984	0.964	1.201	0.472	1.023	0.835	2.086	0.943
	708	XM_496125	LOC440345	0.799	0.818	1.010	0.848	0.678	1.725	0.942	1.206	0.585
	709	NM_032902	PPP1R16A	0.875	1.028	0.808	0.928	1.027	1.059	0.942	1.001	0.763
	710	XM_379927	PLXNA4A	0.992	0.976	1.072	1.335	0.844	1.138	0.744	1.156	0.942
	711	NM_005476	GNE	0.955	0.987	0.976	1.055	1.049	0.669	0.905	0.941	1.458
30	712	NM_145862	CHEK2	0.946	0.876	0.886	0.886	0.931	1.028	1.068	0.940	0.862
	713	NM_001030059	PPAPDC1A	0.762	0.849	0.761	0.810	1.296	0.337	0.940	0.655	2.261
	714	NM_004431	EPHA2	0.963	0.981	0.869	1.024	0.752	1.020	0.940	1.305	0.852
	715	NM_003957	STK29	0.837	0.879	0.931	0.985	0.936	0.975	0.850	0.939	0.955
	716	NM_001003786	LYK5	1.012	1.061	0.931	1.114	1.131	0.940	0.908	0.938	0.990
	717	NM_022133	SNX16	1.031	1.010	1.038	1.100	0.776	1.187	0.938	1.301	0.874
	718	NM_002011	FGFR4	0.923	0.987	1.140	1.513	1.053	0.621	0.610	0.937	1.836
	719	NM_004734	DCAMKL1	0.981	1.060	0.985	1.268	0.894	1.051	0.773	1.187	0.937
	720	NM_002650	PIK4CA	0.920	0.953	0.912	0.709	1.017	1.183	1.298	0.937	0.771
	721	NM_020416	PPP2R2C	0.807	0.845	0.837	0.690	0.999	0.894	1.169	0.845	0.936
	722	NM_001105	ACVR1	0.879	0.958	0.966	0.939	0.682	1.104	0.936	1.404	0.875
	723	NM_176865	PPA2	0.846	0.798	0.923	0.904	1.031	0.874	0.935	0.775	1.055
	724	NM_130436	DYRK1A	0.938	0.845	0.821	0.743	0.904	1.342	1.262	0.935	0.612
	725	NM_031965	GSG2	0.921	0.993	0.913	0.985	1.204	0.767	0.935	0.825	1.190
	726	NM_152649	FLJ34389	0.980	0.859	0.883	0.773	1.258	0.944	1.268	0.683	0.935
	727	NM_174922	ADCK5	0.833	0.901	0.811	0.919	0.964	0.472	0.906	0.934	1.718
	728	NM_004614	TK2	0.866	0.918	1.075	0.691	0.998	1.151	1.253	0.920	0.934
	729	NM_144714	FLJ25449	0.829	0.925	0.803	0.696	0.992	1.311	1.191	0.933	0.612
	730	NM_004441	EPHB1	0.876	0.788	0.801	1.065	0.846	0.600	0.822	0.932	1.336
	731	NM_002221	ITPKB	0.812	0.950	0.882	1.005	0.634	0.946	0.807	1.498	0.932
	732	NM_002764	PRPS1	0.969	0.784	0.930	0.752	0.844	1.047	1.289	0.929	0.888
	733	NM_152230	IPMK	0.921	0.933	0.917	0.734	1.005	1.043	1.254	0.928	0.879
	734	NM_173598	KSR2	0.887	0.903	0.882	0.955	1.090	0.751	0.928	0.828	1.175
	735	NM_005012	ROR1	0.985	0.978	0.955	1.000	1.054	1.446	0.985	0.927	0.661
	736	NM_001291	CLK2	1.019	0.917	0.925	1.179	0.989	0.807	0.864	0.927	1.146
	737	XM_372002	LOC389599	0.857	0.892	0.854	0.815	0.963	1.121	1.051	0.926	0.761
	738	NM_004570	PIK3C2G	0.937	0.796	0.996	0.953	1.029	1.076	0.983	0.774	0.926

CI	rank	NCBI RefSeq	gene symbol	rel. viability untreated			rel. viability TNF and CHX			death index		
				siRNA 1	siRNA 2	siRNA 3	siRNA 1	siRNA 2	siRNA 3	siRNA 1	siRNA 2	siRNA 3
30	739	NM_206961	LTK	0.783	0.857	0.879	0.626	0.926	1.278	1.251	0.926	0.688
	740	NM_006648	PRKWINK2	0.486	1.093	0.838	0.570	1.181	0.893	0.852	0.926	0.939
	741	NM_052902	STK11IP	0.886	1.028	0.897	0.998	1.111	0.691	0.888	0.925	1.297
	742	NM_004304	ALK	0.884	0.981	0.870	0.973	0.785	0.941	0.908	1.249	0.925
	743	NM_030906	STK33	0.958	0.881	0.916	0.735	0.987	0.990	1.303	0.892	0.924
	744	NM_031417	MARK4	0.942	1.007	1.034	0.788	1.089	1.508	1.195	0.924	0.686
	745	NM_004119	FLT3	1.010	1.000	0.851	1.092	0.861	1.431	0.924	1.161	0.595
	746	NM_033116	NEK9	0.726	0.942	0.908	0.786	0.825	1.087	0.923	1.141	0.835
	747	NM_005536	IMPA1	0.894	0.837	0.960	1.072	0.907	0.838	0.834	0.923	1.146
	748	NM_002610	PDK1	0.974	1.001	1.131	1.055	1.301	0.920	0.923	0.769	1.229
	749	XM_290923	KIAA1639	1.027	0.936	0.772	1.114	0.846	0.870	0.923	1.106	0.888
	750	NM_015605	DKFZP566K05 24	0.824	0.952	0.804	0.896	1.374	0.843	0.920	0.693	0.954
	751	NM_004972	JAK2	0.967	1.129	0.847	1.051	0.763	0.995	0.920	1.481	0.851
40	752	NM_003503	CDC7	0.940	1.017	1.030	1.024	1.108	0.975	0.918	0.918	1.056
	753	NM_002958	RYK	0.942	1.010	0.956	0.677	1.465	1.041	1.391	0.689	0.918
	754	NM_000298	PKLR	0.886	1.026	1.071	1.370	1.118	0.915	0.647	0.918	1.171
	755	NM_006251	PRKAA1	0.915	0.858	0.939	0.997	0.665	1.134	0.918	1.291	0.828
	756	NM_025164	KIAA0999	1.106	0.933	1.005	0.814	1.085	1.096	1.360	0.859	0.917
	757	NM_0010016 71	FLJ16518	0.802	0.921	0.976	0.589	1.005	1.278	1.361	0.917	0.764
	758	NM_021221	LY6G5B	0.932	0.925	0.799	1.294	1.009	0.785	0.720	0.917	1.019
	759	XM_497470	PRKXP1	0.911	0.994	0.980	1.023	1.085	1.044	0.891	0.916	0.938
	760	NM_016223	PACSIN3	0.909	0.919	0.945	0.833	1.029	1.033	1.091	0.893	0.915
	761	NM_005398	PPP1R3C	0.862	0.985	0.943	0.942	0.835	1.278	0.915	1.180	0.738
	762	NM_006575	MAP4K5	0.565	0.821	0.849	0.327	0.898	0.952	1.730	0.914	0.892
	763	NM_006314	CNKSR1	0.971	0.888	0.893	1.062	1.177	0.862	0.914	0.754	1.037
	764	NM_0010108 61	LOC163404	0.897	0.822	1.024	0.852	0.946	1.122	1.052	0.869	0.913
	765	NM_0010020 21	PFKL	0.964	0.988	0.925	0.895	1.082	1.030	1.077	0.913	0.899
	766	NM_002093	GSK3B	0.817	0.827	0.891	0.921	0.711	0.977	0.887	1.164	0.912
	767	XM_497647	LOC441868	0.851	0.898	0.889	0.934	0.957	1.058	0.911	0.938	0.840
	768	NM_012145	DTYMK	1.051	1.031	1.037	0.515	1.147	1.138	2.041	0.899	0.911
	769	NM_145040	PRKCDBP	1.072	0.858	0.900	1.178	0.814	1.312	0.910	1.054	0.686
	770	NM_001611	ACP5	0.767	0.822	0.680	0.843	1.235	0.514	0.910	0.666	1.323
	771	NM_025233	COASY	1.019	0.954	0.986	0.778	1.143	1.086	1.310	0.835	0.909
	772	NM_148978	PANK1	0.939	0.954	0.912	1.231	1.050	0.860	0.763	0.908	1.060
	773	NM_000245	MET	0.883	0.978	0.870	0.841	1.077	0.982	1.050	0.908	0.887
	774	NM_181690	AKT3	0.813	0.850	0.998	1.079	0.936	1.046	0.753	0.907	0.954
	775	NM_0010095 65	CDKL4	0.909	0.883	0.990	1.128	0.857	1.091	0.806	1.030	0.907
	776	NM_018984	SSH1	0.873	1.000	0.864	0.962	1.205	0.447	0.907	0.830	1.933
	777	NM_001632	ALPP	0.824	0.756	0.807	0.908	0.998	0.827	0.907	0.758	0.975
	778	NM_018276	SSH3	0.853	0.933	0.882	1.197	0.788	0.973	0.713	1.185	0.906
	779	NM_018339	RFK	0.968	1.080	0.798	1.068	1.032	0.923	0.906	1.046	0.865

CI	rank	NCBI RefSeq	gene symbol	rel. viability untreated			rel. viability TNF and CHX			death index		
				siRNA 1	siRNA 2	siRNA 3	siRNA 1	siRNA 2	siRNA 3	siRNA 1	siRNA 2	siRNA 3
40	780	NM_080823	SRMS	0.693	0.735	0.875	0.573	0.811	1.012	1.209	0.905	0.864
	781	NM_014602	PIK3R4	1.046	0.944	1.063	0.953	1.089	1.175	1.098	0.867	0.905
	782	NM_000215	JAK3	0.853	0.884	0.994	1.181	0.978	0.747	0.722	0.904	1.330
	783	NM_014371	AKAP8L	0.798	1.030	0.739	0.884	0.836	0.870	0.903	1.232	0.850
	784	XM_496630	LOC442075	0.886	0.998	0.987	0.984	1.428	0.766	0.901	0.699	1.288
	785	NM_005605	PPP3CC	0.792	0.720	0.980	0.879	1.004	0.903	0.901	0.717	1.085
	786	NM_022445	TPK1	1.015	1.030	0.937	1.128	0.816	1.087	0.900	1.262	0.862
	787	XM_371672	LOC389168	0.966	0.737	0.808	0.476	0.820	1.140	2.028	0.899	0.709
	788	NM_014326	DAPK2	0.871	1.064	0.972	0.984	1.185	0.522	0.885	0.898	1.860
	789	NM_032781	PTPN5	0.824	0.852	0.808	1.215	0.950	0.794	0.678	0.897	1.018
	790	NM_002647	PIK3C3	0.807	0.867	1.002	1.276	0.805	1.117	0.632	1.077	0.897
50	791	NM_002747	MAPK4	0.865	0.934	0.893	0.966	1.137	0.550	0.895	0.822	1.624
	792	NM_173575	STK32C	0.836	0.954	0.913	0.935	1.137	0.954	0.895	0.840	0.958
	793	NM_005109	OSR1	1.024	1.008	0.945	1.145	0.935	1.265	0.894	1.078	0.747
	794	NM_001948	DUT	0.723	0.672	0.775	0.816	0.752	0.696	0.885	0.894	1.113
	795	NM_033118	MYLK2	0.725	0.898	0.763	1.102	0.616	0.855	0.658	1.459	0.893
	796	XM_497921	LOC391533	0.804	1.011	0.847	1.104	1.134	0.450	0.729	0.892	1.884
	797	NM_002737	PRKCA	0.898	0.993	0.869	1.035	1.117	0.548	0.868	0.889	1.585
	798	NM_004226	STK17B	0.971	0.974	0.869	0.869	1.256	0.979	1.117	0.775	0.888
	799	NM_002253	KDR	0.780	0.763	0.844	0.879	0.832	1.101	0.888	0.916	0.767
	800	NM_020168	PAK6	0.765	1.040	0.902	1.164	1.172	0.862	0.658	0.887	1.046
	801	NM_002827	PTPN1	0.912	0.820	0.816	0.898	0.925	1.132	1.016	0.887	0.720
	802	NM_015076	CDK11	0.908	0.910	1.068	1.024	0.834	1.234	0.887	1.092	0.865
	803	NM_017859	UCKL1	0.839	1.126	0.891	0.946	1.110	1.162	0.887	1.015	0.766
	804	NM_018498	PPP4R1L	0.835	0.975	0.911	0.885	1.099	1.079	0.943	0.887	0.845
	805	NM_014431	PALD	0.838	0.899	0.808	0.645	1.014	1.061	1.299	0.887	0.761
	806	NM_005906	MAK	0.872	0.881	0.955	1.234	0.994	1.045	0.707	0.886	0.914
	807	NM_002732	PRKACG	0.946	0.927	0.822	1.068	0.905	1.284	0.886	1.023	0.640
	808	NM_199289	NEK5	0.854	0.898	0.939	1.048	1.014	0.820	0.815	0.886	1.145
	809	NM_0010116 64	CSNK1G1	0.937	0.931	0.854	0.931	1.199	0.964	1.007	0.777	0.885
	810	NM_138689	PPP1R14B	0.984	0.834	0.832	1.112	1.052	0.652	0.885	0.793	1.277
	811	NM_017881	C9orf95	0.895	0.942	0.801	1.013	0.662	1.339	0.884	1.423	0.598
	812	NM_0010040 65	AKAP2	0.945	0.973	0.993	0.895	1.291	1.125	1.056	0.754	0.882
	813	NM_001347	DGKQ	0.862	0.647	0.807	0.977	0.557	1.022	0.882	1.163	0.790
	814	NM_177990	PAK7	0.922	1.015	0.912	1.329	1.151	0.868	0.694	0.881	1.051
	815	NM_016308	UMP-CMPK	0.958	0.810	0.839	1.091	0.462	1.380	0.879	1.753	0.608
	816	NM_006697	CRA	0.834	0.672	1.064	0.949	0.893	0.944	0.879	0.753	1.126
	817	NM_021970	MAP2K1IP1	0.884	0.860	0.921	1.071	0.979	0.748	0.825	0.878	1.231
	818	NM_012395	PFTK1	0.867	0.944	1.092	1.070	1.075	1.091	0.810	0.878	1.001
819	NM_016532	SKIP	0.848	0.791	0.962	0.967	1.274	0.574	0.877	0.621	1.677	
820	NM_020185	DUSP22	0.877	0.938	0.775	1.149	1.069	0.769	0.763	0.877	1.007	

CI	rank	NCBI RefSeq	gene symbol	rel. viability untreated			rel. viability TNF and CHX			death index		
				siRNA 1	siRNA 2	siRNA 3	siRNA 1	siRNA 2	siRNA 3	siRNA 1	siRNA 2	siRNA 3
50	821	NM_024607	PPP1R3B	0.866	0.841	0.929	0.937	0.998	1.060	0.925	0.842	0.877
	822	NM_020804	PACSIN1	0.895	0.977	0.835	0.822	1.115	1.092	1.089	0.876	0.765
	823	NM_001824	CKM	0.932	0.966	0.844	1.064	1.046	1.127	0.875	0.924	0.749
	824	NM_001032296	STK24	0.791	0.847	0.924	0.904	1.076	0.715	0.874	0.787	1.293
	825	NM_007199	IRAK3	0.859	0.885	0.817	0.984	0.563	1.369	0.873	1.573	0.596
60	826	NM_001018137	NME2	0.921	0.933	0.928	1.199	0.740	1.063	0.768	1.260	0.873
	827	NM_002766	PRPSAP1	0.905	0.805	0.868	1.039	1.222	0.649	0.871	0.658	1.337
	828	NM_006871	RIPK3	0.913	0.916	0.959	1.379	0.364	1.101	0.662	2.520	0.871
	829	NM_006852	TLK2	1.041	1.085	1.035	1.095	1.246	1.571	0.950	0.871	0.659
	830	NM_001433	ERN1	0.972	0.938	0.948	1.312	1.079	0.874	0.741	0.870	1.084
	831	NM_199261	TPTE	0.871	0.858	0.861	0.758	0.988	1.274	1.148	0.868	0.676
	832	NM_003647	DGKE	0.837	0.960	0.720	1.038	1.107	0.592	0.806	0.868	1.218
	833	NM_002751	MAPK11	0.750	0.839	0.878	0.865	1.487	1.005	0.867	0.564	0.874
	834	NM_005248	FGR	0.944	0.968	0.824	1.120	1.001	0.953	0.843	0.966	0.865
	835	NM_014826	CDC42BPA	0.863	0.828	0.897	0.589	0.957	1.279	1.466	0.865	0.701
	836	NM_003161	RPS6KB1	0.838	0.860	0.948	1.196	0.996	0.533	0.701	0.863	1.777
	837	NM_138448	ACYP2	0.708	0.728	0.956	0.821	1.046	0.931	0.862	0.696	1.027
	838	NM_176895	PPAP2A	0.886	0.835	0.977	1.029	1.541	0.743	0.861	0.542	1.315
	839	NM_182692	SRPK2	0.990	0.964	0.959	0.963	1.409	1.114	1.028	0.684	0.861
	840	NM_000167	GK	0.801	0.835	0.941	1.072	0.970	0.824	0.747	0.861	1.141
	841	NM_031268	PDPK1	0.868	0.801	0.963	1.017	0.745	1.121	0.853	1.074	0.859
	842	NM_014906	PPM1E	0.846	0.872	0.854	0.987	0.928	1.076	0.857	0.940	0.794
	843	NM_181897	PPP2R3A	0.753	0.927	0.961	0.720	1.082	1.269	1.046	0.857	0.757
	844	NM_006258	PRKG1	0.825	0.813	0.847	0.963	1.098	0.946	0.856	0.741	0.895
	845	XM_291277	DKFZp761P0423	0.963	0.988	0.980	0.877	1.155	1.219	1.098	0.856	0.804
	846	NM_020240	CDC42SE2	0.844	1.000	1.143	1.124	1.170	0.737	0.751	0.855	1.550
	847	NM_153183	NUDT10	0.791	0.752	0.922	0.710	0.967	1.079	1.115	0.777	0.854
	848	NM_002739	PRKCG	0.777	0.831	0.961	0.910	1.239	1.116	0.854	0.671	0.861
	849	NM_001034843	LOC400927	0.859	0.795	0.920	0.778	1.224	1.079	1.104	0.649	0.853
	850	NM_017886	FLJ20574	0.849	0.696	1.001	1.713	0.684	1.175	0.496	1.018	0.852
	851	NM_001932	MPP3	0.904	0.829	0.943	1.347	0.955	1.107	0.671	0.869	0.852
	852	NM_001030313	RP26	0.859	0.921	0.969	1.008	1.388	0.813	0.852	0.664	1.192
	853	NM_003160	AURKC	0.802	0.735	0.907	0.943	0.763	1.417	0.850	0.963	0.640
	854	NM_175886	PRPS1L1	0.821	0.877	0.931	0.966	0.761	1.255	0.850	1.152	0.742
	855	NM_001007272	DUSP13	0.841	0.816	0.773	0.957	1.048	0.910	0.879	0.779	0.850
	856	NM_153273	IHPK1	0.983	1.177	1.012	1.158	1.230	1.198	0.849	0.957	0.845
	857	NM_002227	JAK1	0.785	0.861	0.849	0.924	1.491	0.982	0.849	0.577	0.865
	858	NM_032435	KIAA1804	0.947	0.890	0.833	0.850	1.231	0.981	1.114	0.723	0.849
	859	NM_013302	EEF2K	0.762	0.955	1.001	0.813	1.580	1.179	0.938	0.604	0.849
	860	NM_052841	STK22C	0.876	1.105	0.668	1.133	1.302	0.711	0.773	0.849	0.940
	861	NM_003565	ULK1	0.958	0.873	0.890	1.129	1.423	0.972	0.849	0.613	0.916

CI	rank	NCBI RefSeq	gene symbol	rel. viability untreated			rel. viability TNF and CHX			death index		
				siRNA 1	siRNA 2	siRNA 3	siRNA 1	siRNA 2	siRNA 3	siRNA 1	siRNA 2	siRNA 3
60	862	NM_014937	INPP5F	0.758	0.756	0.822	0.856	0.894	1.052	0.885	0.846	0.781
	863	XM_371701	LOC389217	0.958	0.866	0.752	0.881	1.023	1.030	1.088	0.846	0.730
	864	NM_003384	VRK1	0.912	1.141	1.168	1.447	1.349	0.923	0.631	0.846	1.266
	865	NM_000459	TEK	0.867	0.901	0.954	1.029	0.762	1.173	0.843	1.183	0.813
	866	NM_002194	INPP1	0.821	0.779	0.938	0.933	1.412	1.113	0.879	0.552	0.843
	867	XM_350880	PPM1H	0.826	0.874	0.836	1.141	1.037	0.881	0.724	0.843	0.949
70	868	NM_001896	CSNK2A2	0.938	0.814	0.871	0.931	1.003	1.034	1.008	0.811	0.842
	869	NM_005400	PRKCE	0.937	0.819	0.942	1.113	1.255	0.723	0.842	0.653	1.304
	870	NM_003318	TTK	0.552	0.931	0.989	0.656	1.353	0.870	0.842	0.688	1.137
	871	NM_017771	PXK	0.863	0.893	0.545	1.027	0.688	0.806	0.840	1.297	0.676
	872	NM_005923	MAP3K5	0.934	0.932	0.805	0.723	1.110	1.690	1.291	0.840	0.477
	873	NM_005198	CHKB	0.909	0.984	1.004	1.085	1.172	0.938	0.837	0.840	1.071
	874	NM_022097	LOC63928	0.748	0.828	0.822	0.892	1.090	0.707	0.839	0.759	1.163
	875	NM_000455	STK11	0.754	0.701	0.844	0.900	0.775	1.444	0.838	0.904	0.584
	876	NM_004445	EPHB6	0.802	0.803	0.865	1.153	0.958	0.418	0.696	0.838	2.071
	877	NM_080423	PTPN2	0.916	0.850	0.817	0.885	1.019	1.279	1.035	0.835	0.639
	878	NM_001567	INPL1	0.795	0.855	0.990	1.004	0.704	1.187	0.791	1.216	0.834
	879	NM_006197	PCM1	0.964	0.850	0.875	1.262	1.019	0.517	0.763	0.834	1.692
	880	NM_006244	PPP2R5B	0.816	0.792	0.821	0.979	0.882	1.050	0.834	0.898	0.782
	881	NM_004686	MTMR7	0.820	0.693	0.942	0.940	0.989	1.132	0.872	0.701	0.832
	882	NM_153809	TAF1L	0.916	0.896	0.938	1.101	1.173	0.996	0.832	0.764	0.942
	883	NM_033389	SSH2	0.842	0.844	0.807	1.015	1.019	0.613	0.829	0.828	1.316
	884	NM_181775	DKFZp434G0625	0.886	1.011	0.914	0.923	1.219	1.132	0.959	0.829	0.807
	885	NM_005372	MOS	0.883	0.808	0.926	1.205	0.443	1.118	0.733	1.826	0.828
	886	NM_018650	MARK1	0.815	0.963	0.929	0.985	1.186	0.879	0.827	0.812	1.057
	887	NM_014683	ULK2	0.821	0.900	0.917	1.027	0.792	1.110	0.800	1.136	0.827
	888	NM_018444	PPM2C	0.899	0.921	0.818	1.088	1.035	1.361	0.826	0.890	0.601
	889	NM_012398	PIP5K1C	0.949	1.062	0.975	1.149	0.985	1.360	0.826	1.079	0.717
	890	NM_006246	PPP2R5E	0.741	0.819	0.884	0.846	1.229	1.071	0.876	0.666	0.825
	891	NM_198892	BMP2K	0.909	1.075	0.850	1.247	1.208	1.030	0.729	0.890	0.825
	892	NM_006257	PRKCQ	0.790	0.814	0.859	0.958	0.887	1.067	0.824	0.918	0.806
	893	NM_013276	CARKL	1.034	0.945	0.896	0.720	1.146	1.248	1.437	0.824	0.718
	894	NM_145185	MAP2K7	0.867	0.941	1.005	1.053	1.189	1.046	0.824	0.792	0.961
	895	NM_005433	YES1	0.960	0.837	0.872	0.835	1.213	1.063	1.149	0.690	0.820
	896	NM_024619	FN3KRP	0.891	0.933	0.867	0.524	1.138	1.058	1.701	0.820	0.820
	897	NM_031480	RIOK1	0.842	0.870	0.807	1.304	1.063	0.958	0.646	0.818	0.842
	898	NM_173496	MPP7	0.865	0.926	0.881	0.856	1.135	1.240	1.011	0.816	0.710
	899	NM_001610	ACP2	0.649	0.722	0.979	0.797	1.133	0.824	0.814	0.637	1.188
	900	NM_003010	MAP2K4	0.841	1.010	0.881	0.745	1.241	1.304	1.128	0.814	0.676
	901	NM_014002	IKBKE	0.906	0.924	0.950	1.140	0.926	1.170	0.795	0.997	0.812
	902	XM_497237	LOC441567	0.854	0.874	0.819	0.967	1.077	1.126	0.883	0.812	0.727

CI	rank	NCBI RefSeq	gene symbol	rel. viability untreated			rel. viability TNF and CHX			death index		
				siRNA 1	siRNA 2	siRNA 3	siRNA 1	siRNA 2	siRNA 3	siRNA 1	siRNA 2	siRNA 3
70	903	NM_139245	PPM1L	0.845	0.852	0.874	1.042	1.073	0.586	0.811	0.794	1.492
	904	NM_004850	ROCK2	0.988	0.835	0.825	0.795	1.031	1.192	1.243	0.810	0.692
	905	NM_000154	GALK1	0.818	0.809	0.938	1.196	0.829	1.159	0.684	0.976	0.810
	906	NM_004444	EPHB4	0.891	0.835	0.785	0.668	1.032	1.330	1.335	0.810	0.590
80	907	NM_030962	CMT4B2	0.662	0.675	0.703	0.822	0.927	0.461	0.805	0.728	1.525
	908	NM_022648	TNS	0.900	0.718	0.827	1.121	0.542	1.133	0.803	1.325	0.730
	909	NM_012407	PRKCABP	1.230	0.926	1.021	0.478	1.155	1.335	2.573	0.802	0.765
	910	NM_015568	PPP1R16B	0.936	0.856	0.692	1.167	1.108	0.468	0.802	0.773	1.479
	911	NM_013355	PKN3	0.975	0.912	0.808	0.735	1.139	1.082	1.327	0.801	0.747
	912	NM_004333	BRAF	0.939	0.845	0.860	0.832	1.056	1.307	1.129	0.800	0.658
	913	NM_174944	C14orf20	0.824	0.885	0.861	0.883	1.349	1.078	0.933	0.656	0.799
	914	NM_006219	PIK3CB	0.987	0.755	0.943	1.238	0.856	1.532	0.797	0.881	0.616
	915	NM_030791	SGPP1	0.865	0.807	0.889	1.088	1.409	0.333	0.795	0.573	2.666
	916	NM_002969	MAPK12	0.850	0.800	0.828	1.070	1.164	0.564	0.794	0.687	1.467
	917	NM_000944	PPP3CA	0.887	0.835	0.932	1.120	1.180	0.858	0.792	0.708	1.086
	918	NM_032454	STK19	0.878	0.911	1.039	1.112	1.133	1.313	0.790	0.804	0.791
	919	NM_006703	NUDT3	0.813	0.767	0.877	0.992	1.057	1.111	0.820	0.725	0.789
	920	NM_002649	PIK3CG	0.874	0.965	0.895	1.110	1.450	1.136	0.787	0.665	0.787
	921	NM_003804	RIPK1	0.898	0.754	0.932	1.420	0.642	1.186	0.632	1.174	0.786
	922	NM_001013703	EIF2AK4	0.814	0.765	1.013	1.036	1.147	1.224	0.786	0.667	0.827
	923	NM_005308	GRK5	0.784	0.836	0.823	1.093	0.728	1.047	0.717	1.148	0.786
	924	NM_006484	DYRK1B	0.901	0.867	0.991	1.147	1.300	1.034	0.785	0.667	0.958
	925	NM_025179	PLXNA2	0.971	1.039	0.887	1.332	1.325	0.966	0.729	0.784	0.918
	926	NM_020315	PDXP	0.843	0.856	1.015	1.027	1.205	1.295	0.821	0.710	0.784
	927	NM_012290	TLK1	1.003	1.127	0.871	1.282	0.448	1.127	0.783	2.514	0.772
	928	NM_003157	NEK4	0.857	0.877	0.851	1.150	1.126	0.397	0.745	0.779	2.142
	929	XM_042936	GRIP2	0.852	0.854	0.847	1.100	0.835	1.277	0.775	1.022	0.664
	930	NM_015690	STK36	0.974	0.935	0.914	1.666	1.026	1.183	0.585	0.911	0.773
	931	NM_018238	FLJ10842	0.848	0.783	0.765	1.007	1.014	1.050	0.842	0.772	0.729
	932	NM_173655	DKFZp434C1418	0.809	0.864	0.860	1.119	0.987	1.114	0.723	0.876	0.771
	933	NM_002767	PRPSAP2	0.862	0.907	0.922	0.935	1.248	1.196	0.922	0.727	0.770
	934	NM_178494	FLJ40125	0.892	0.895	0.863	1.158	1.216	0.768	0.770	0.736	1.124
	935	NM_177560	CSNK2A1	0.941	1.224	1.170	1.226	1.698	0.951	0.768	0.721	1.230
	936	NM_005406	ROCK1	0.883	0.901	0.940	0.667	1.175	1.435	1.323	0.767	0.655
	937	NM_152934	PPEF2	0.827	0.819	0.873	1.080	1.131	0.867	0.766	0.724	1.007
	938	NM_144641	FLJ32332	0.861	0.842	0.809	1.198	1.102	1.002	0.718	0.764	0.808
	939	NM_004443	EPHB3	0.836	0.773	0.773	1.118	1.013	0.713	0.748	0.763	1.085
	940	NM_006904	PRKDC	0.944	1.007	0.965	1.478	0.957	1.268	0.639	1.052	0.761
	941	NM_016231	NLK	0.943	0.947	0.881	0.913	1.244	1.221	1.033	0.761	0.722
942	NM_014845	KIAA0274	0.779	0.685	0.777	0.962	0.941	1.021	0.810	0.728	0.761	
943	NM_014369	PTPN18	0.813	0.838	0.808	1.069	0.415	1.158	0.761	2.018	0.698	

CI	rank	NCBI RefSeq	gene symbol	rel. viability untreated			rel. viability TNF and CHX			death index		
				siRNA 1	siRNA 2	siRNA 3	siRNA 1	siRNA 2	siRNA 3	siRNA 1	siRNA 2	siRNA 3
80	944	NM_032483	HTPAP	0.724	0.674	0.719	0.955	0.970	0.269	0.758	0.694	2.671
	945	NM_199326	PR48	0.848	0.835	0.811	1.173	1.102	0.880	0.723	0.757	0.922
	946	NM_000478	ALPL	0.785	0.815	0.944	0.370	1.078	1.331	2.122	0.756	0.709
	947	NM_002929	GRK1	0.762	0.741	0.837	1.099	0.982	0.857	0.694	0.755	0.977
90	948	NM_017726	PPP1R14D	0.988	0.848	0.766	0.761	1.131	1.188	1.298	0.750	0.645
	949	NM_002746	MAPK3	0.811	0.889	0.815	1.083	1.367	0.571	0.749	0.650	1.427
	950	NM_031361	COL4A3BP	0.814	0.884	0.998	1.087	1.383	0.888	0.748	0.639	1.125
	951	NM_006383	CIB2	0.745	0.836	0.822	1.655	0.956	1.098	0.450	0.874	0.748
	952	NM_178009	DGKH	1.060	0.868	0.937	0.932	1.164	1.255	1.137	0.745	0.747
	953	NM_014422	PIB5PA	0.863	0.845	0.980	1.288	1.136	0.863	0.670	0.744	1.136
	954	NM_144688	FLJ32658	0.830	0.857	0.850	1.165	1.152	0.944	0.713	0.744	0.901
	955	NM_003551	NME5	0.692	0.808	0.877	0.935	1.233	0.800	0.740	0.656	1.096
	956	XM_498022	LOC442141	0.876	0.928	0.994	1.187	0.958	1.471	0.738	0.969	0.676
	957	NM_177995	PTPDC1	0.906	0.875	0.846	1.229	0.378	1.176	0.737	2.317	0.720
	958	NM_005975	PTK6	0.887	0.849	0.964	1.730	1.157	1.083	0.513	0.734	0.890
	959	NM_003656	CAMK1	0.869	1.006	0.951	1.186	1.856	1.211	0.732	0.542	0.785
	960	NM_006742	PSKH1	0.947	0.921	1.009	1.092	1.257	1.547	0.867	0.732	0.652
	961	NM_080391	PTP4A2	0.877	0.932	0.802	1.205	0.627	1.273	0.728	1.486	0.630
	962	NM_001982	ERBB3	0.852	0.737	0.801	1.209	1.014	0.684	0.705	0.727	1.170
	963	NM_014496	RPS6KA6	0.617	1.037	0.729	1.267	1.041	1.006	0.487	0.997	0.724
	964	NM_180976	PPP2R5D	0.839	0.895	0.862	1.546	1.171	1.192	0.542	0.764	0.724
	965	NM_001799	CDK7	0.873	0.770	0.834	1.210	0.961	1.361	0.721	0.801	0.613
	966	NM_181493	ITPA	0.879	0.787	0.767	0.825	1.099	1.147	1.065	0.716	0.669
	967	NM_032124	HDHD2	0.698	0.645	0.762	1.083	0.903	0.924	0.645	0.715	0.825
	968	NM_000142	FGFR3	0.823	0.757	0.840	1.194	1.064	1.110	0.690	0.712	0.757
	969	NM_004958	FRAP1	0.737	0.821	0.786	1.039	1.139	1.172	0.709	0.721	0.671
	970	NM_018343	RIOK2	0.958	0.890	0.968	0.772	1.329	1.369	1.241	0.670	0.707
	971	NM_033214	GK2	0.773	0.709	0.875	1.141	0.608	1.239	0.677	1.166	0.706
	972	NM_182644	EPHA3	0.916	0.788	0.787	0.873	1.119	1.156	1.050	0.704	0.681
	973	NM_005592	MUSK	0.844	0.935	0.938	1.638	0.500	1.345	0.515	1.870	0.698
	974	NM_032242	PLXNA1	0.984	0.792	1.001	1.050	1.143	1.931	0.936	0.692	0.519
	975	NM_178588	PPP2R5C	0.872	0.930	0.926	1.822	1.353	1.134	0.478	0.687	0.817
	976	NM_006243	PPP2R5A	0.811	0.779	0.885	1.045	1.138	1.422	0.777	0.685	0.622
	977	NM_001017915	INPP5D	0.880	0.766	0.993	1.050	1.436	1.486	0.838	0.533	0.668
	978	NM_015458	MTMR9	0.908	0.941	0.986	1.365	1.416	1.137	0.665	0.664	0.868
	979	NM_139049	MAPK8	0.752	0.882	0.866	1.131	2.586	1.172	0.664	0.341	0.739
	980	NM_054113	CIB3	0.718	0.826	0.828	1.135	0.850	1.258	0.633	0.973	0.659
	981	NM_007271	STK38	0.901	0.903	0.905	1.369	1.015	1.383	0.658	0.890	0.654
	982	XM_497463	LOC401823	0.958	0.837	0.910	1.852	0.638	1.393	0.518	1.311	0.653
	983	NM_033126	PSKH2	0.891	0.978	0.901	1.396	1.750	0.796	0.638	0.559	1.132
984	NM_080548	PTPN6	0.745	0.691	0.875	1.265	0.476	1.399	0.589	1.451	0.626	

CI	rank	NCBI RefSeq	gene symbol	rel. viability untreated			rel. viability TNF and CHX			death index		
				siRNA 1	siRNA 2	siRNA 3	siRNA 1	siRNA 2	siRNA 3	siRNA 1	siRNA 2	siRNA 3
95	985	NM_000222	KIT	0.752	0.627	0.912	1.247	0.443	1.462	0.603	1.416	0.624
99	986	NM_001099	ACPP	0.833	0.825	1.076	1.750	1.384	0.541	0.476	0.596	1.988

APPENDIX 5. SUPPLEMENTARY DATA.

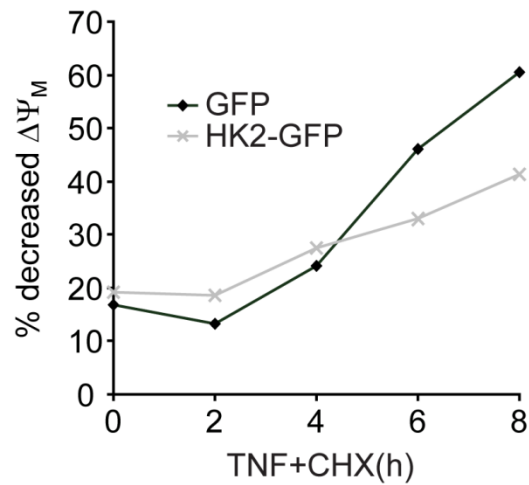


Figure A5.1. HK2 attenuates the TNF-induced decrease of the IMM potential. Time course of the percentage of HeLa cells with a decreased of the inner mitochondrial membrane potential ($\Delta\Psi_M$) after treatment with TNF and CHX. All values are presented as the percentage of GFP-positive cells with reduced TMRE fluorescence in a cell population that was transiently transfected with HK2-GFP or a control GFP expression construct. Data are representative of six independent experiments.

transduction domain of HIV-1 transactivator of transcription. **B:** Western blot of the cellular localization of HK1 and HK2 in HeLa cells treated with 20 μ M control or HK1 peptides in serum-free medium for one hour. Control cells were treated with serum-containing or serum-free medium only. Total lysate, mitochondrial and cytosolic fractions were probed for HK1, HK2, VDAC1 and Tubulin (Tub). Tubulin and VDAC1 served as markers for cytosolic and mitochondrial fractions, respectively. **C:** Fluorescence microscopic images of HeLa cells that were stained with an antibody against endogenous HK1, mitotracker red, and nucleic acid stain Hoechst. All single channel images were false-coloured (HK1 in green, mitotracker red in red, Hoechst in blue) and merged. Note that concentrations of 20 μ M HK1 peptide and higher compromise the viability of HeLa cells. **D:** Western blot of the cellular localization of endogenous HK1 (endog. HK1) and ectopically expressed GFP-tagged wild type HK1 (HK1-GFP), GFP-tagged HK1 lacking the amino-terminal twenty one amino acids (HK1 Δ 21-GFP), and GFP in HeLa cells. Total lysate, mitochondrial and cytosolic fractions were probed for HK1, GFP, VDAC1 and Tubulin (Tub). Tubulin and VDAC1 served as markers for cytosolic and mitochondrial fractions, respectively.